This electronic thesis or dissertation has been downloaded from the King's Research Portal at https://kclpure.kcl.ac.uk/portal/

KING'S College LONDON

Finite element analysis of interfacial failure mechanisms in fibre-reinforced composites.

Nath, Rajat Bushan

The copyright of this thesis rests with the author and no quotation from it or information derived from it may be published without proper acknowledgement.

END USER LICENCE AGREEMENT

Unless another licence is stated on the immediately following page this work is licensed

under a Creative Commons Attribution-NonCommercial-NoDerivatives 4.0 International

licence. https://creativecommons.org/licenses/by-nc-nd/4.0/

You are free to copy, distribute and transmit the work

Under the following conditions:

- Attribution: You must attribute the work in the manner specified by the author (but not in any way that suggests that they endorse you or your use of the work).
- Non Commercial: You may not use this work for commercial purposes.
- No Derivative Works - You may not alter, transform, or build upon this work.

Any of these conditions can be waived if you receive permission from the author. Your fair dealings and other rights are in no way affected by the above.

Take down policy

If you believe that this document breaches copyright please contact librarypure@kcl.ac.uk providing details, and we will remove access to the work immediately and investigate your claim.

Download date: 05. May. 2023

FINITE ELEMENT ANALYSIS OF INTERFACIAL FAILURE MECHANISMS IN FIBRE-REINFORCED COMPOSITES

by

Rajat Bhushan Nath

A thesis submitted for the degree of
Doctor of Philosophy
in the University of London.

King's College London
Department of Mechanical Engineering

March 1998

BIBL.
LONDIN.
UNIV.

ABSTRACT

Finite Element Analysis of Interfacial Failure Mechanisms

in Fibre-Reinforced Composites

The failure of the interfacial bond between a fibre and the surrounding matrix during the tensile loading of a composite is considered as a multi-stage progression, in which each stage is characterised by various key parameters. Non-linear phenomena, such as matrix plasticity, interface crack growth together with the associated frictional stress transfer, and the propagation of matrix cracks are characteristic features of interfacial failure and are key to determining the reinforcement capability of the fibre. Finite element analyses of 2-D single and 3-D multi-fibre systems have been performed for carbon and Kevlar-49 fibre-epoxy matrix composites, incorporating various modes of interfacial failure and the systemic non-linearities. Thermal residual stresses, as well as fibre end fibrillation in Kevlar-49 fibres have also been included in the models. For the multi-fibre analyses, the redistribution of stress in the surrounding intact fibres caused by the fracture of a given fibre has been investigated with a view to establishing its influence on global lamina failure mechanisms. The predicted fibre stress profiles were correlated with experimental Laser Raman Spectroscopy data in order to validate the interfacial failure modes associated with the various composite systems.

Publications Arising From The Research

- Nath, R.B., Fenner, D.N., & Galiotis, C. (1996), Finite Element Modelling of Interfacial Failure in Model Carbon Fibre-Epoxy Composites,
  J. Mat. Sci., **31**, 2879.

- Nath, R.B., Fenner, D.N., & Galiotis, C. (1996), Elasto-Plastic Finite Element Modelling of Interfacial Failure in Model Kevlar-49 Fibre-Epoxy Composites,
  J. Composites, **27A**, 821.

- Nath, R.B., Fenner, D.N., & Galiotis, C. (1995), Finite Element Modelling of Interfacial Failure in Carbon Fibre-Epoxy Composites, *3rd International Conference on Deformation and Fracture of Composites,* The Institute of Materials, London, 606.

- Nath, R.B., Fenner, D.N., & Galiotis, C. (1996), Progression of Interfacial Failure in Kevlar-49 & Carbon Fibre Composites: Elasto-Plastic Finite Element Analysis, *Seventh European Conference on Composite Materials,* The Institute of Materials, London, **I**, 27.

- Nath, R.B., Fenner, D.N., & Galiotis, C. (1998), The Progressional Approach to Interfacial Failure in Composites: Interface Cracks, *in press*.

Acknowledgements

I would like to gratefully thank Dr. David N. Fenner for his guidance, support and unabated interest throughout the course of this research.

Thanks is heartily extended to Dr. Costas C. Galiotis for the successful collaboration that has been instituted between the Mechanical Engineering Department at King's College London and the Materials Department at Queen Mary and Westfield College. Professor George Papanicolaou and Peter di Cara are also thanked for their all their help over the years.

* * *

Equations are more important to me, because politics is for the present, but an equation is something for eternity.

If *A* is success in life, then *A* equals *x* plus *y* plus *z*. Work is *x*; *y* is play; and *z* is keeping your mouth shut.

Albert Einstein 1879-1955, in *Observer* 15 January 1950

Science is built up of facts, as a house is built of stones; but an accumulation of facts is no more a science than a heap of stones is a house.

Henri Poincaré 1854-1912, *Science and Hypothesis* (1905)

I shall certainly admit a system as empirical or scientific only if it is capable of being tested by experience. These considerations suggest that not the verifiability but the falsifiability of a system is to be taken as a criterion of demarcation... It must be possible for an empirical scientific system to be refuted by experience.

Sir Karl Popper 1902-95, *The Logic of Scientific Discovery* (1934)

A statesman is a politician who places himself at the service of the nation. A politician is a statesman who places the nation at his service.

Georges Pompidou 1911-74, in *Observer* 30 December 1973

* * *

CONTENTS

Nomenclature and Abbreviations

Symbol

E	Young's modulus of elasticity
G	shear modulus of elasticity
ν	Poisson ratio
σ	normal stress
τ	shear stress
ε, e	strain
r, θ, z	polar coordinates
v	volume fraction
A	cross-sectional area
μ	coefficient of friction
ϕ	crack angle
a	crack length
$\mathcal{G}$	strain energy release rate
ψ	pressure dependent yield surface angle

Subscript

f	fibre
m	matrix
c	composite
app	applied
cyl, cr	cylinder
I	Mode I
II	Mode II
IC	Mode I interfacial fracture toughness
IR	Mode II interfacial fracture toughness

Superscript

*	failure value
yield	yield value
‘	dilatational component

Abbreviation

FE	finite element
LRS	laser Raman spectroscopy
SEM	scanning electron micrograph
RVE	representative volume element
MMC	metal matrix composite
FEFM	fibrillated fibre end model
ISS	interfacial shear stress
IFSS	interfacial shear strength
SERR	strain energy release rate
SAF	stress amplification factor

Special Notation Used in FemView Figures

S12	in-plane shear stress
E12	in-plane shear strain
S22	axial stress (2D models)
S33	axial stress (3D model)
L*n*, TIME:*n*	load-step *n*
STEP:*m*	increment *m*
DEF, FACTOR	displacement enhancement factor

List of Finite Element Models

Name	Description	Chapter
FIBRE	Plain carbon fibre end	4
KEVAXS	Kevlar fibrillated fibre end (1D-FEFM)	5
KEVAXR	Kevlar fibrillated fibre end (2D-FEFM)	5
CA1	Carbon fibre incorporating interface crack	6
GA05	Carbon fibre incorporating matrix crack	7
3D	Multi- carbon fibre with spontaneous fracture	9

List of Tables

List of Figures

Chapter 1

Introduction

1.1 Composite Materials

The majority of materials found in both nature and the industrialised world are a combination of two or more components, which furnish them with unique and superior properties when compared with homogeneous materials. Muscle, bone, wood, fibre-reinforced plastics, steel-reinforced concrete as well as concrete itself are all examples of composite materials on the macroscopic or microscopic scale. Composites are defined by a bulk material, or matrix, within which are interspersed smaller components, or reinforcers. The combination of two materials to form a new material with optimal properties is a form of synergy, in the sense that the properties of the new whole exceed those of the sum of the individual parts. Composites may be broadly separated into the categories of particulate (e.g. cement) and fibre-reinforced (e.g. carbon fibre-reinforced plastics). The current research is concerned with fibre-reinforced plastics.

In characterising the constituent components of a fibre-reinforced composite, matrix materials tend to be compliant and tough whereas fibres are relatively stiff and brittle, with the ratio of fibre to matrix elastic moduli being of the order of 10 - 1000. Common examples of fibres are carbon, aramid, glass and ceramic, and examples of matrices are polymers, metals and rubbers. Generally, when a matrix is reinforced with fibres, the resultant composite has a stiffness and strength close to that of the fibres, but possesses chemical and crack propagation resistances similar to those of the matrix. It is the combination of these properties that endows composites with superior performance. A composite component part, depending on the intended application, may be designed as to possess exceptional properties in a particular area, such as strength in a particular direction or a high stiffness to weight ratio (i.e. high specific stiffness), with a trade-off of other properties.

Man-made fibre-reinforced composites consist of laminae, or plies, which are sheets of matrix with multiple embedded fibres arranged either in a parallel manner, as in the case of unidirectional laminae, or in a random fashion. A composite laminate is made up of multiple laminae stacked according to a stacking sequence in order to optimise elastic properties in certain directions. Fig. 1.1 shows a $0/90^{\circ}$ cross-ply laminate, which is a fairly common type. Individual laminae consist of either short fibres, usually in a random dispersion in the matrix (Fig. 1.2(a)), or long (continuous) fibres (Fig. 1.2(b)) arranged in a unidirectional manner.

1.2 The Interface

Any reinforcing component in a composite system increases the stiffness and strength of the matrix material in which the reinforcing component is embedded. This is by virtue of the integrity of the bond at the interface that exists between the reinforcer and the matrix. Thus, the fibre-matrix interface is the most critical and complex area in any fibre-reinforced composite material.

The interface is more accurately described as a discrete *interphase* region that divides the reinforcer and the matrix phases. This region, a few nanometers in thickness, is characterised by the presence of voids or microscopic bubbles of trapped gases, as well as other impurities absorbed during the fabrication of the composite. Additionally, there exist micro-cracks produced by the high local shrinkage-stresses induced by the cooling of the composite during the curing stage of fabrication [1].

The carbon fibre-epoxy matrix system interface is additionally complex due to the reactivity of the carbon fibre surface. The surface-reactivity is a major contributor to the strong bonding of carbon fibres. If the fibre is oxidation pre-treated, such as with an acid or other coupling agent, the resulting chemical functional groups form preferentially at the basal plane edges of the fibre surface [1], thus encouraging bonding with the surrounding epoxy matrix. Such pre-teatment effectively increases

the bond strength of the interface and thus suppresses interfacial cracking when the composite specimen is loaded to high levels of applied strain. Furthermore, when macro-molecules of polymer matrix bond to a fibre surface, they show a constraint in their degree of freedom to polymerise [2]. This incomplete polymerisation contributes to the creation of interphasial elastic properties that differ from those of the bulk matrix.

The various physio-chemical flaws endemic to the interphasial region exist at the microscopic level, essentially reducing the ability of the interface to act as a perfect bond between the reinforcer and matrix. Consequently, the macroscopic properties such as the failure strength of the interface is correspondingly reduced. Further, the intricate mechanisms of interfacial failure will be necessarily influenced by the presence of these anomalies.

1.3 Interfacial Failure

Interfacial failure occurs in most fibre-reinforced composite systems after any significant level of loading has been applied to them. The importance of this type of failure is that it is the root stage of macroscopic failure in the system, and hence can lead to catastrophic global failure of the composite component. In order to visualise and obtain an appreciation of the nature of this form of failure, consideration of the mechanical response of a simple composite geometry is necessary.

When a single fibre-reinforced composite specimen is subjected to a given tensile loading the matrix will deform in response to the loading system, but this deformation will be constrained by the stiffer reinforcing component. Throughout this research, consideration will be given to tensile loading which is a common form of loading. During reinforcement, there is stress transfer between fibre and matrix in which the fibre sustains significantly higher stresses than the matrix, thus reinforcing the deforming matrix. As shown in Fig. 1.3, this stress state is created through the

existence of shear stresses induced at the interface. The overall stiffness of the specimen has thus increased due to the presence of the bonded reinforcing fibre.

For the initial low levels of applied strain, a linear-elastic stress transfer regime will prevail across the interface, but as this loading is increased, stresses will be induced at the interface that will exceed the failure stress. The breakdown in linear-elastic stress transfer and the series of events that ensue which reduce the fibre's capability to reinforce the matrix, are collectively known as interfacial failure. This series of events, the commencement of each of which may be specified, form a *progression* of failure of the interface, thus permanently reducing the interfacial bond integrity. Characteristic features of the various stages are localised yielding of the matrix in the interfacial area, the initiation of cracks at the fibre end, and the subsequent propagation of cracks either into the matrix or along the interface. Accounting for such phenomena is key to determining the overall mechanical response and strength of the composite.

In order to facilitate the discussion of interfacial failure modes, three separate Modes have been identified by the author [3-7] from a number of experimental studies [8-13]. These Modes of failure tend to occur in combination during a given loading history of a composite specimen:

- *Mode α :* matrix yielding at the intact interface. This mode has been observed to occur in aramid fibre-epoxy matrix systems [8-9].
- *Mode β :* a crack initiates at the fibre end and propagates along the interface. Frictional stress transfer between the fibre and matrix takes place across the crack faces. This failure mode has been observed to occur in glass and un-sized carbon fibre systems [10-11].
- *Mode γ :* a conical crack initiates at the fibre end and propagates into the matrix at an angle to the axis of the fibre. This failure mode has been observed in carbon fibre systems [12-13].

A high resolution scanning electron micrograph of the fracture surface of the carbon-epoxy specimen is presented in Fig. 1.4 [10]. This shows an interface crack that has developed as a result of the application of high tensile loading on the specimen post-fracture. In another micrograph, Fig. 1.5 [11], both interface and matrix cracks are evident in a short glass fibre-epoxy system.

In the consideration of short fibre composites, the main source of interfacial failure with incremental applied loading is at the multiplicity of fibre ends that exist in this type of composite. When considering the failure at a given fibre location, the effect of surrounding fibres may be considered to be negligible provided the fibre-volume fraction is low. Hence the representative volume element (RVE) of the system is that of a single short fibre surrounded by a finite volume of matrix, Fig. 1.2(a). However, for long fibre composites, the effects of the fibre ends and the associated interfacial failure induced at these locations are of secondary importance, due to the lower fibre-end density. The primary source of failure, which may be catastrophic for the given lamina as a whole, is the interfacial failure induced during the fracture of one of the loaded fibres. In this event, a compensating stress redistribution among the surrounding intact fibres occurs due to the local incapacitation of the fractured fibre. Consequently, for long fibre composite systems, the RVE necessarily includes portions of the intact surrounding fibres Fig. 1.2(b), which play a key role in reinforcement during the fracture of a given fibre.

1.4 Experimental Overview - Data from QMW

Galiotis *et al.* [8-10,13-15], over a number of years at the Department of Materials at Queen Mary and Westfield College, have performed micro-mechanical measurements for a variety of single and multi-fibre composite systems. The stress or strain distributions along an embedded fibre have been measured for tensile-loaded crystalline fibre-matrix systems using the high resolution technique of laser Raman spectroscopy (LRS). This technique relies on the fact that the Raman frequency of the atomic vibrations of crystalline reinforcing fibres, such as aramid or carbon, is a

function of the axial stress in the fibre at that location. Unique Raman frequency versus fibre stress calibration curves, produced for each type of fibre, are used to convert the measured Raman frequency to an axial stress distribution along the length of the fibre. A review of the experimental measurement procedure may be found in Appendix A. LRS is a powerful technique for measuring the stress distribution in embedded fibres with a resolution of 1-2 microns. This enables the stress state in the fibre to be monitored *during* the complete loading-failure history of a composite specimen.

The application of this technique to various single and multi-fibre composite systems has allowed researchers a window into the micro-mechanics of interfacial failure. What is observable by the monitoring of fibre stress during the loading of the composite specimen, is not which failure mode is prevalent for a particular loading level, but its *influence* on the fibre stress distribution. The fibre stress distributions for various fibre-matrix systems have been found to deviate from the linear-elastic predictions, as a direct result of failure mechanisms active at the interface. Thus, inferences as to the failure modes prevalent in various systems have been made *indirectly* by examination of the corresponding influences on the fibre stress profiles [8,13,15]. It should be noted that microscopical investigations, such as SEM's, only reveal the mode of interfacial failure once the specimens have completely failed and thus provide no information as to the type and extent of failure during the regular service loading of the composite component.

For a single carbon fibre-epoxy matrix system subjected to incremental loading, the following general trends have been observed in the experimental fibre stress profiles. The fibre stress distribution has been found to build up from zero at the fibre ends in an S-shape or Ω-shape depending on the type of carbon fibres used, Fig. 1.6. These profiles, which differ fundamentally from their theoretical shapes, are observed to become more pronounced with increased loading, as a result of the increasing size of the zone of interfacial damage [10]. Thus the progressive nature of interfacial failure is exhibited by the observed relaxation of the fibre stress in the region of the fibre

ends, indicating the decreasing reinforcement efficiency of the fibre with applied loading.

The shear stress distribution along the interface has been obtained by applying a balance of forces model [14] to the axial fibre stress distribution. Since the calculated shear stress is a derived quantity, the shear stress distributions will be used only for qualitative purposes and not for quantitative comparison with FE data, thus eliminating any error due to the simplifying assumptions made in the balance of forces model. In the Kevlar-49 fibre-epoxy matrix system, the shear stress distribution has been observed to form plateaus towards the fibre ends which grow in size with applied loading, Fig. 1.7. It was found that the plateau value was approximately equal to the shear yield stress of the matrix [8]. In contrast with the carbon-epoxy system, the shear stress distribution towards the fibre ends exhibits a 'hump' where the shear stress is zero at the fibre end, and whose maximum is at a finite distance from the fibre end [13].

For a carbon-epoxy multi-fibre lamina consisting of several fibres in a planar array, the stress redistribution consequent upon a fibre fracture during the incremental tensile loading has been investigated. Localised stress amplifications in the surrounding intact fibres have been measured indicating that a complex failure mechanism is responsible for this load redistribution.

1.5 Aims and Objectives

The fundamental aim of the current research was to comprehend, define and quantify the intricate failure mechanisms and overall sequence of events that constitute the interfacial failure process. Guided by the experimental evidence from QMW, finite element (FE) models were developed incorporating specific modes of interfacial failure which accounted for the various systemic non-linear phenomena. LRS stress profiles for a variety of composite specimens subjected to a program of incremental tensile loading, obtained by Galiotis *et al.* [8-10,13-15], were used to validate the FE models.

Given the limitations of analyses by other authors, a more rigorous approach to stress transfer and interfacial failure in composite systems, entitled the Progressional Approach, was developed. This approach was applied to a variety of single and multi-fibre specimens subjected to a program of incremental tensile loading.

The following non-linear phenomena have been accounted for in the application of the Progressional Approach with the various FE models:

- Thermal residual stresses induced during curing of the composite.
- Elasto-plastic behaviour of the matrix including localised matrix yielding.
- The initiation and propagation of interface or matrix cracks during the loading history.
- The effects of frictional stress transfer across an interface crack.
- The influence on the failure mode of fibre end fibrillation in Kevlar-49 fibres.
- The importance of pressure dependent yield of matrix during the propagation of matrix cracks.
- Spontaneous fibre fracture during the loading sequence, in multi-fibre systems.

1.6 Structure of The Thesis

- Chapter 2 briefly reviews the more traditional approaches to the analysis of interfacial failure before presenting in detail the Progressional Approach which has been developed by the author.

- Chapter 3 contains a critical literature survey of the more important FE analyses of single and multi-fibre systems that have been performed over the last two decades.

- Chapters 4 presents linear-elastic analyses of a single carbon fibre-epoxy matrix system incorporating a matrix crack-mode of interfacial failure. The characteristic shape of the induced fibre stress profiles is ascertained. Hence the direct influence of a matrix crack interfacial failure mechanism on the fibre stresses may be established.

- Chapter 5 addresses Kevlar fibre-epoxy matrix systems in which the fibre ends are fibrillated. The nature of the fibrillated zone and the importance of this phenomenon with respect to the type of interfacial failure mode supported in this system is thereby investigated.

- Chapter 6 addresses short carbon fibre systems in which interface cracks initiate and propagate during the interfacial failure process. The influence of the crack length and the coefficient of friction is ascertained. The complex interaction between frictional stress transfer and localised yielding interfacial failure mechanisms is also investigated.

- Chapter 7 examines the importance of pressure dependent yield of matrix in the presence of propagating matrix cracks, and the influence of this property on the fibre stress profiles.

- Chapter 8 presents a comparative study which examines the influence of the various modes of interfacial failure on the global modulus of the composite specimen. The reduction in stress transfer efficiency due to the prevalence of the various failure modes is thus ascertained.

- Chapter 9 addresses long fibre unidirectional composite specimens, where the fracturing of a fibre is analysed together with the influence of the surrounding intact fibres. The interfacial failure mechanisms and their progression in single fibre systems is extended to this three-dimensional multi-fibre analysis. The stress redistribution to the adjacent intact fibres is examined along with the local failure phenomena consequent upon fibre fracture.

- Chapter 10 concludes the thesis with a summary of the achievements of the work. The application of the Progressional Approach to complete laminate composite structures and systems incorporating a fibre coating layer are presented as appropriate subjects for future work.

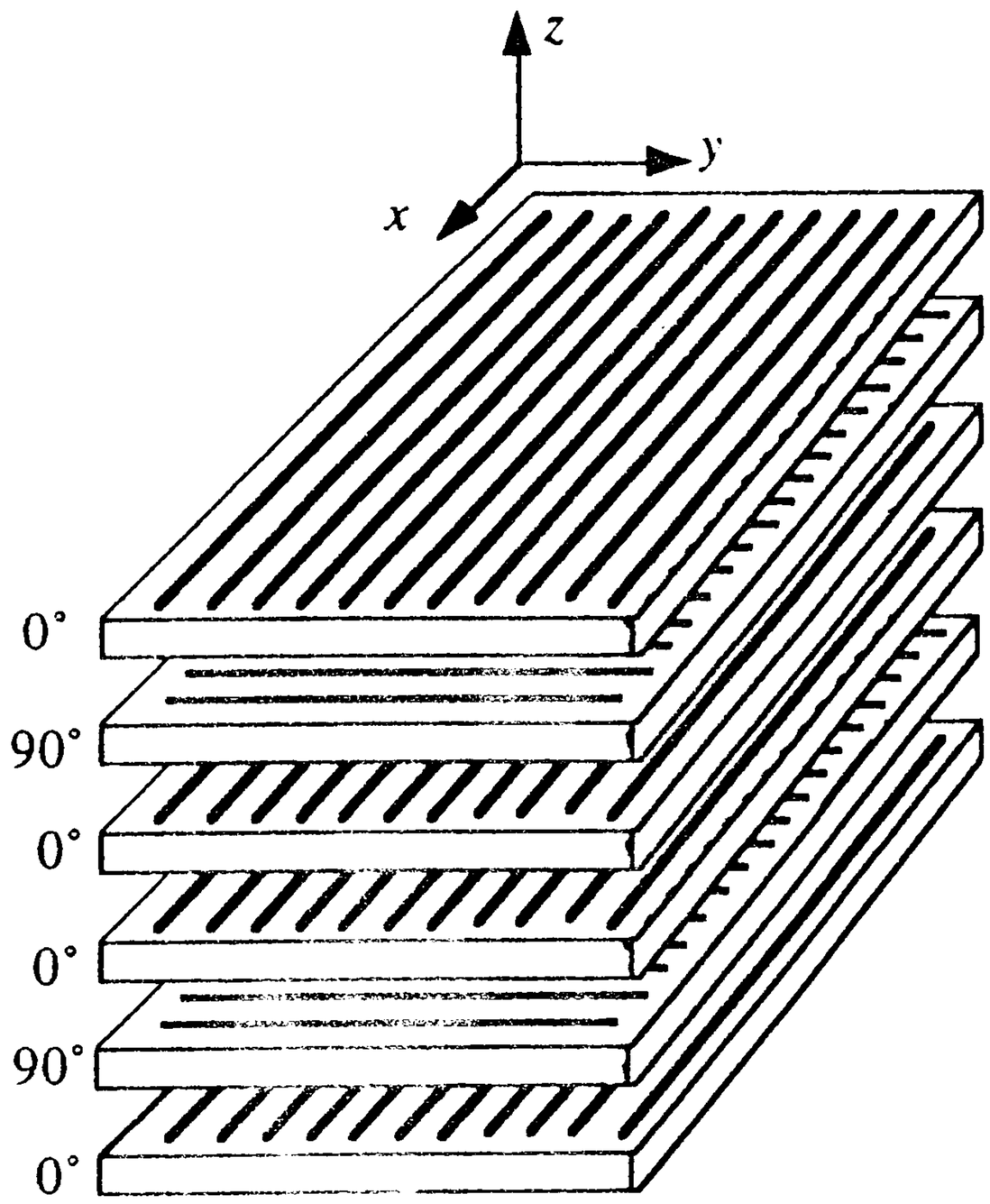

Fig. 1.1 Stacking sequence of unidirectional laminae in a typical 0/90° laminate [1]

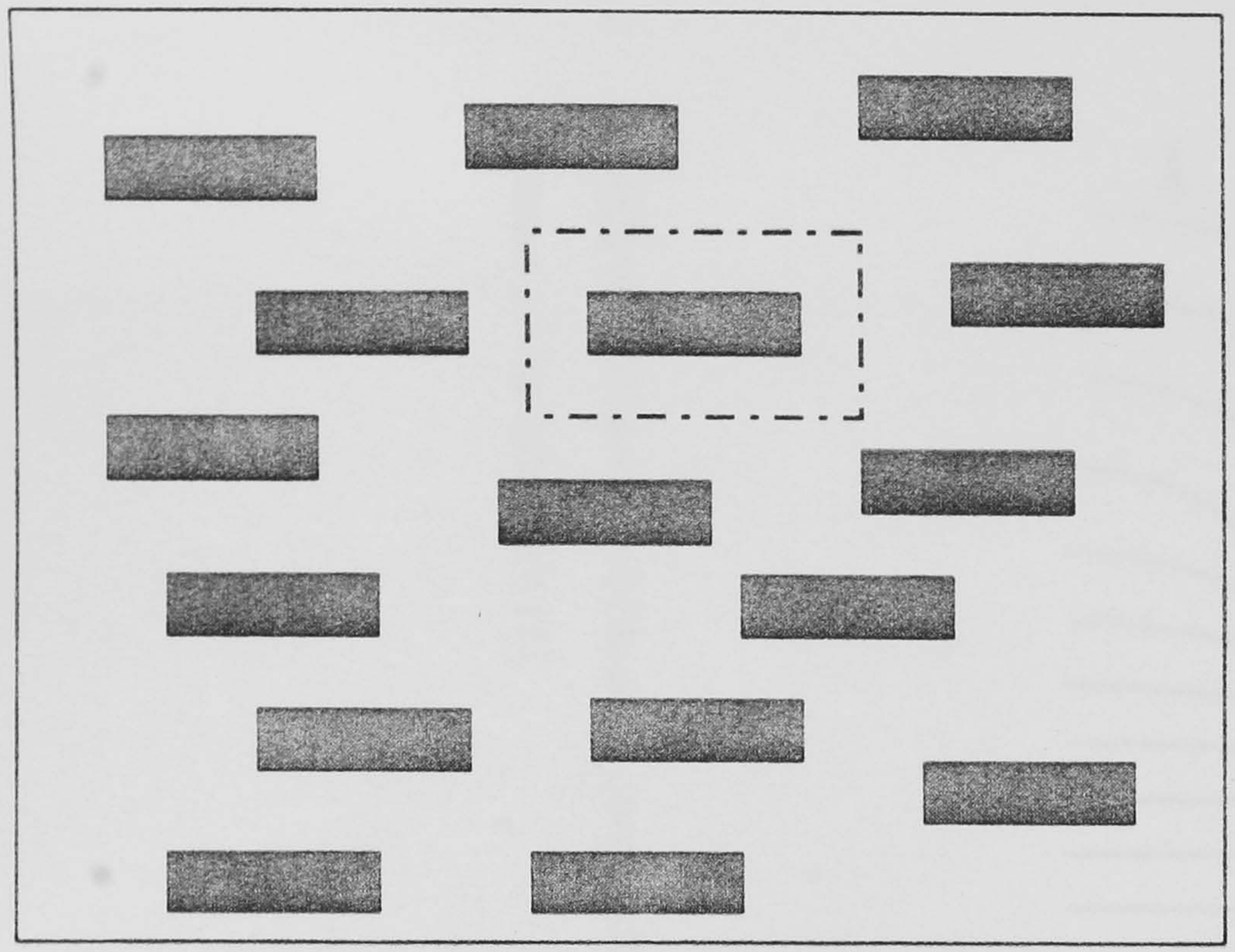

(a)

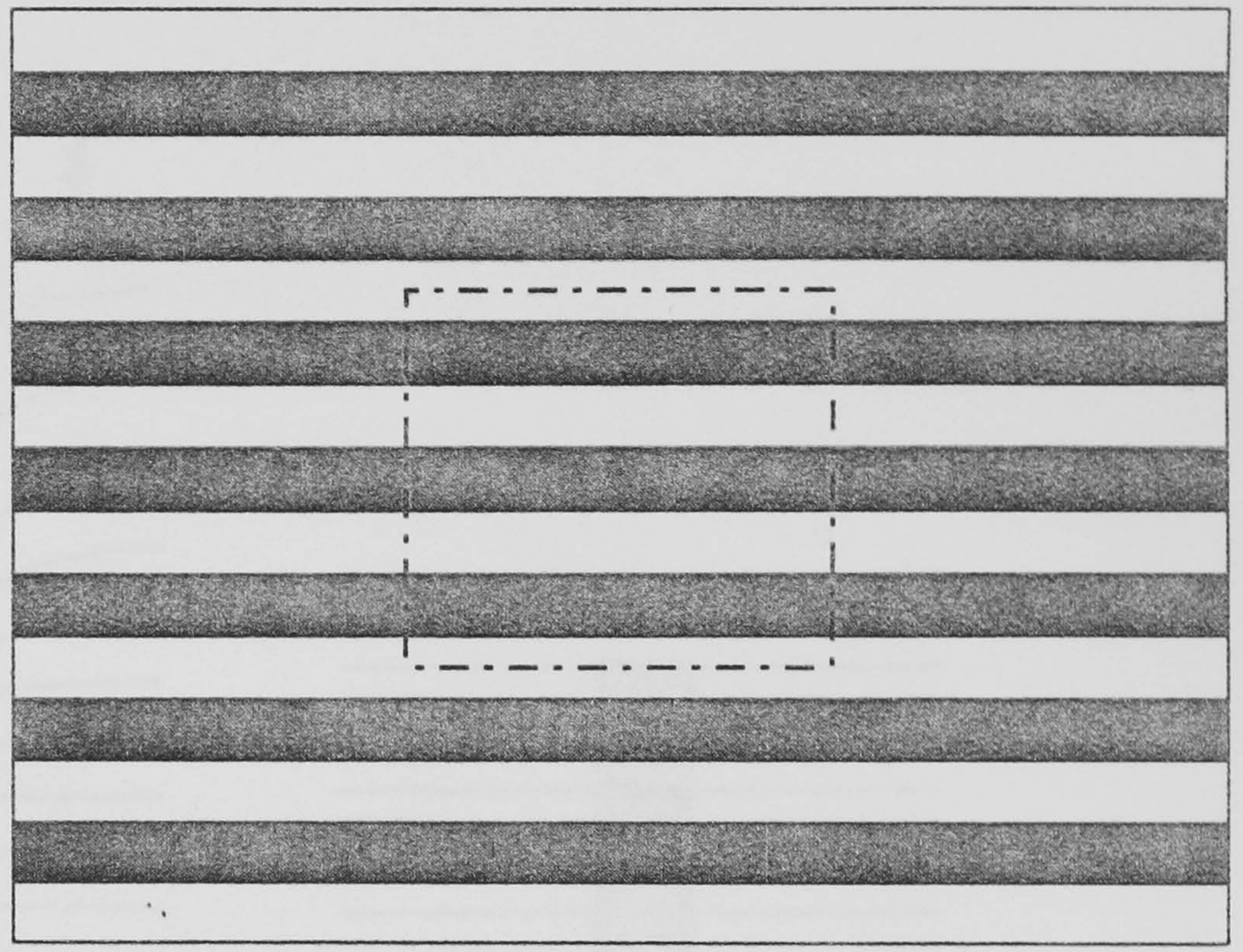

(b)

Fig. 1.2 Composite types showing Representative Volume Elements (dashed areas)
(a) short fibre system, (b) continuous fibre system

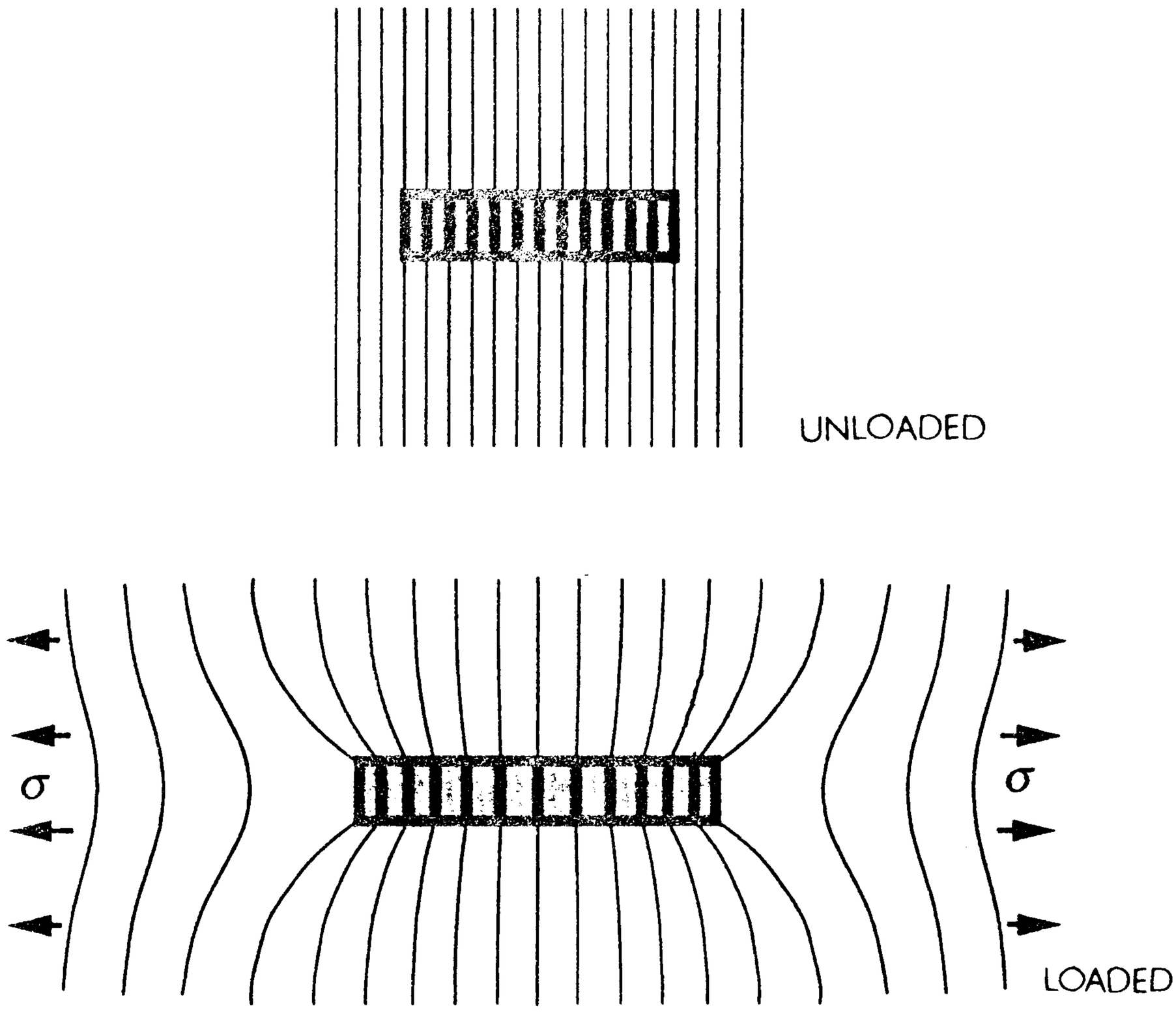

Fig. 1.3 Displacement pattern of loaded composite showing inducement of shear stresses at the interface [1]

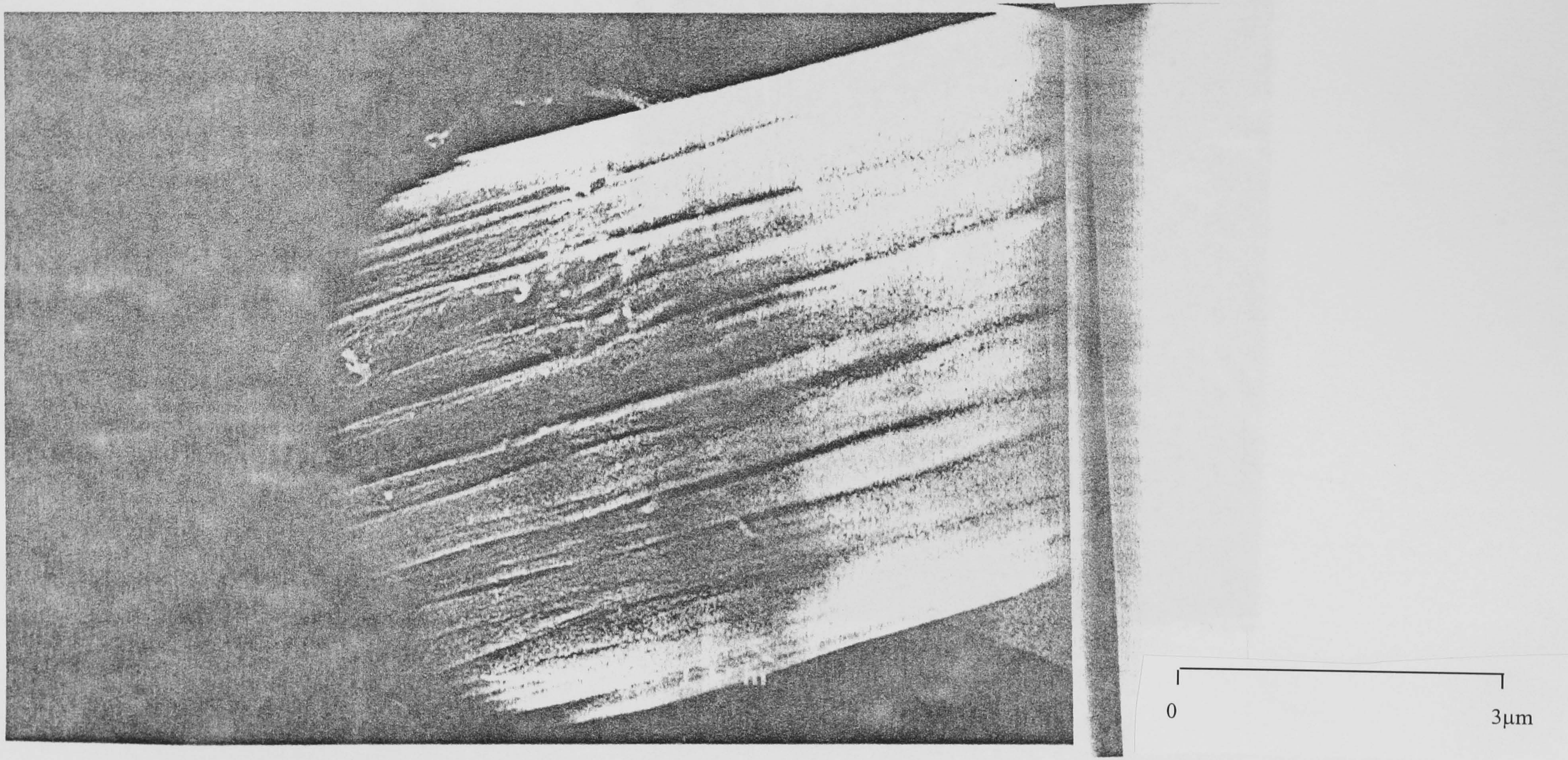

Fig. 1.4 SEM of an interface crack developed in a fractured specimen of carbon-epoxy composite [10]

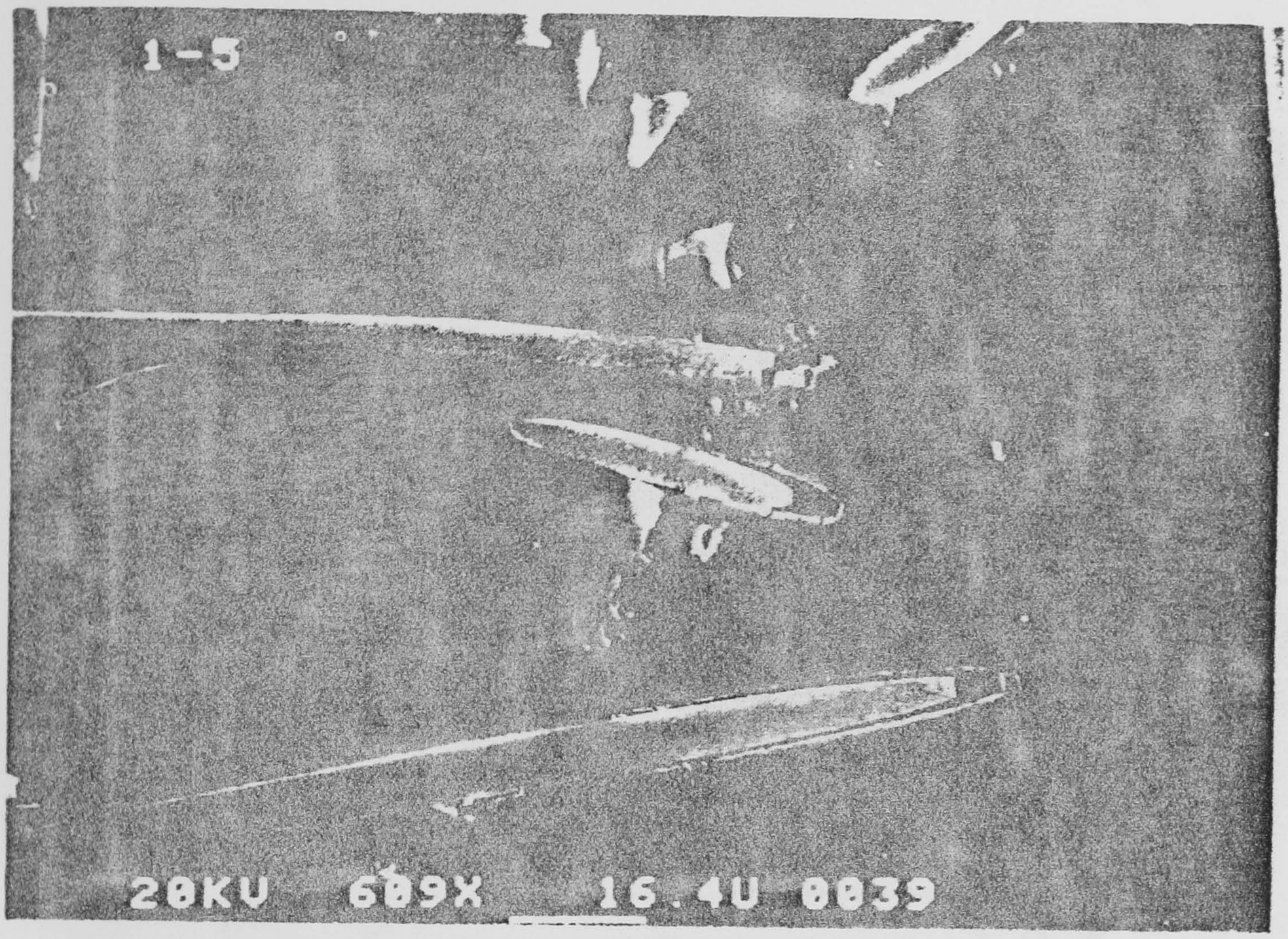

Fig. 1.5 SEM of interface and matrix cracks developed in short glass fibre composite [11]

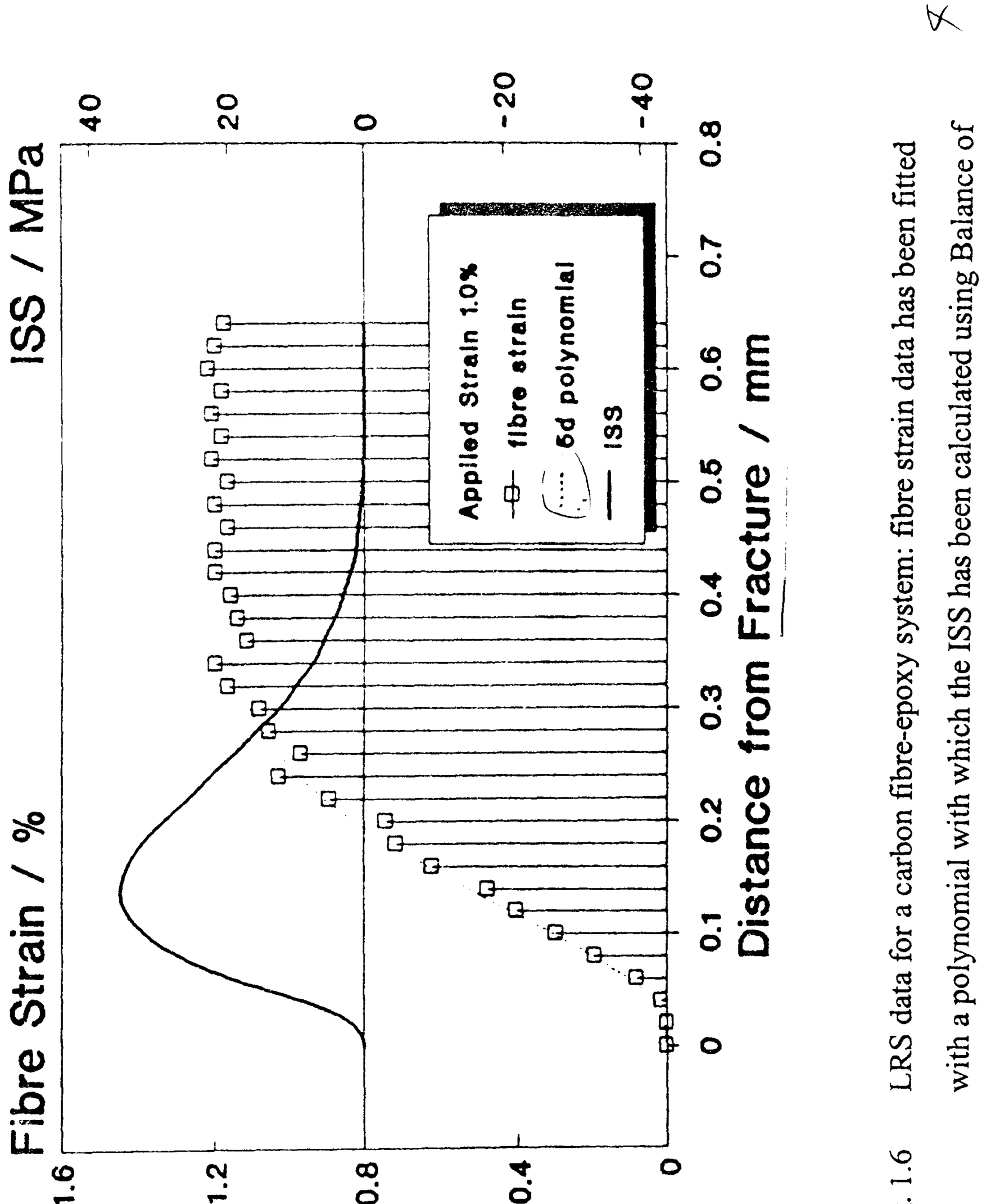

Fig. 1.6 LRS data for a carbon fibre-epoxy system: fibre strain data has been fitted with a polynomial with which the ISS has been calculated using Balance of Forces Model [13]

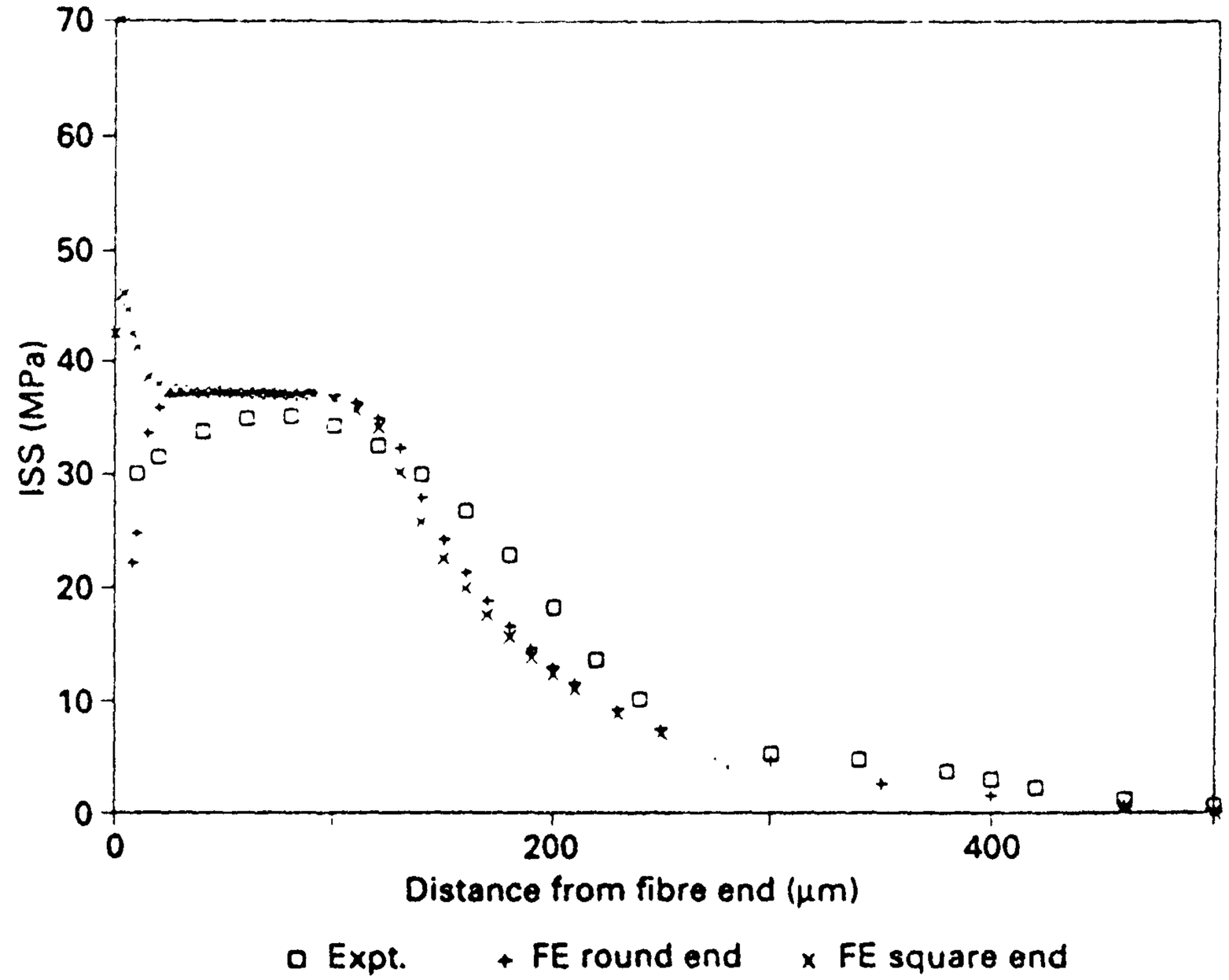

Fig. 1.7 LRS data for a Kevlar-49 fibre-epoxy system: FE predictions by Guild et al. are also shown [9]

Chapter 2

Analysis of Interfacial Failure

Historically, there have been two approaches to the analysis and characterisation of stress transfer and interfacial failure in single fibre composites. Initially there were the traditional mathematical analyses in which a number of restricting assumptions were made regarding the elastic behaviour of both fibre, matrix and their common interface. More recently, there has been the experimentally-based 'Interfacial Shear Strength' approach in which deductions have been made as to the prevalence of interfacial failure phenomena in a generic sense, based on experimental observations of the fibre stress profiles in the loaded composite. Because of the limitations of the restricting assumptions which are inherent in both these approaches, a more rigorous and comprehensive approach which takes into account the major non-linearities that are characteristic of interfacial failure has been developed in the current research. The interfacial failure process is divided up into a series of discrete stages in which the various non-linear phenomena occur, and thus the approach is called the Progressional Approach. The traditional and interfacial shear strength approaches will be reviewed synoptically and then the Progressional Approach will be presented in detail.

2.1 The Traditional Approaches

Cox [16] and Dow [17] have predicted the axial fibre stress and interfacial shear stress distributions along the length of a single fibre composite subject to tensile loading, in a shear-lag analysis, Fig. 2.1(a). The fundamental but restricting assumptions were (i) linear-elastic behaviour of both fibre and matrix, (ii) the fibre supports only axial stresses and the matrix supports only shear stresses, (iii) the interface remains perfectly intact during loading, and (iv) no load transfer through the ends of the fibre. This model predicts a take-up in the fibre stress profile from zero at the fibre ends to a finite constant value towards the centre, over a distance termed the transfer length [1]. Correspondingly, the interfacial shear stress distribution consists of a concentration at

the fibre end, decaying to zero in a hyperbolic manner. As will be shown, this stress field is only valid at very low levels of applied loading in a real composite.

Whitney & Drzal [18], McCartney [19], and Netravali *et al.* [20] have made modifications to the land-mark Cox model to accommodate fibre end debonding. Hence, linear-elastic solutions have been found incorporating the appropriate boundary condition of zero complementary shear stresses at the fibre ends. Thus the interfacial shear stress distribution is zero at the fibre end and increases to its maximum at a finite distance from the fibre end, before decaying to zero in a Cox-type elastic manner, Fig. 2.1(c). These solutions, however, do not incorporate any form of matrix plasticity or crack growth, which are characteristic of interfacial failure.

Piggott [21], addressed one form of interfacial failure consisting of an interface crack of finite length together with the associated frictional stress transfer induced across the cracked interface (also termed debonding). The linear-elastic solution predicts a constant shear stress over the domain of the interface crack, followed by a discontinuity which bridges the Cox-type elastic shear stress decay, Fig. 2.1(b). The crack tip plastic zone is a limiting factor in real failure, which has not been incorporated in the Piggott model. Piggott's predictions, however, do come closest to approximating reality since he considers one of the most complex modes of interfacial failure, Mode β.

2.2 The Interfacial Shear Strength Approach

Galiotis *et al.* [8,13,15] have postulated a criterion for interfacial failure based on experimental observations of the behaviour of shear stress distributions induced during incremental applied loading. It is postulated that there exists an interfacial shear strength (IFSS) threshold limit unique to each composite system, which is defined as the maximum shear stress that can be sustained by the interface, above which interfacial failure is instigated. At very low values of applied loading, the

induced interfacial shear stress, τ, does not exceed the IFSS of the system, so the shear stress maximum occurs at the fibre end as predicted by Cox, Fig. 2.1(a). At progressively higher applied loads, the high shear stresses induced reach the IFSS, thus instigating interfacial failure. It is an inherent limitation that the specification of which particular mode of failure instigated has not been made, but is synoptically described as a 'gradual interfacial yielding and/or partial fracture of the interface' [15]. The shear stress distribution is thus observed to drop to zero at the fibre end and also to exhibit a maximum at a finite distance from the fibre end. The criterion may be explicitly expressed as:

Criterion for interfacial failure: $\tau = \text{IFSS}$ (2.1)

The major drawback of this approach, apart from being incapable of distinguishing which failure modes will be induced, is the fact that the criterion is one-dimensional in stress, whereas the actual stress state at the interface is strongly three-dimensional. Parenthetically, it should also be noted that the vast volume of coupon-type tests (pull-out, shear debond, micro-indentation, and fragmentation tests) developed over the last three decades attempt to estimate the IFSS for various composite systems. However, they make restricting assumptions of the existence of constant and in some cases linear-elastic shear stresses over the interfacial domain, hence predicting inaccurate estimations for the IFSS.

2.3 The Progressional Approach

The approach developed by the author in the current research is that of the Progressional Approach. In order to make the analysis of interfacial failure more realistic, this stage-by-stage analysis considers both the thermal and tensile forms of loading. The approach is more rigorous and comprehensive in that the various phenomena of localised matrix plasticity, crack initiation and subsequent growth, together with any associated frictional stress transfer, are considered as discrete stages. The points at which these stages occur are defined by various crack initiation

and propagation criteria, which are derived from the physical behaviour of the fibre and matrix materials. These phenomena, characteristic of interfacial failure, are fundamentally *non-linear* and are key to determining the *reinforcement capability* of the fibre. The traditional assumptions of linear-elastic stress transfer and the continued intactness of the interface with higher levels of applied loading are invalid. Analyses based on these assumptions, both analytical and numerical, inevitably predict large stresses at the interface which are well in excess of the interfacial failure stress, and consequently yield unnaturally high predictions for the reinforcement capability of the fibre as well as for the strength of the composite.

The Progressional Approach is presented in its component stages (Fig. 2.2). In order to more easily visualise the precise micro-mechanisms involved at each stage of the interfacial failure progression, we may consider a small element of matrix adjacent to the fibre-matrix interface located near the fibre end, as shown in Fig. 2.3. Thus, of the six faces of the element, one is bonded to the fibre surface (strictly speaking it *is* the interface) while the remaining five sides bond with the surrounding continuum of matrix.

2.3.1 Stage A: Thermal Pre-Load

In the initial stage, there are the effects due to the residual stresses that are thermally induced during fabrication of the composite specimen (Fig. 2.2(a)). The fabrication itself, for the composite specimens under consideration, typically consists of the following multi-step process. Matrix resin is heated to approximately 90°C and the correct amount of curing agent or hardener is then added. The material is then poured into a mould and after about 15 minutes, a fibre is then laid onto the surface of the now viscous matrix. The fabrication is then completed by adding another layer of matrix. On cooling of the composite specimen, a *gelation* occurs in the matrix, whereupon it goes from being a viscous fluid to a solid. The temperature at which this gelation occurs is estimated to be 70°C. Since the coefficient of thermal expansion of the matrix is greater than that of the fibre, the compliant matrix contracts around the stiffer fibre thus putting the fibre into slight compression. The matrix element is thus sheared slightly, leading to localised yielding.

2.3.2 Stage B: Elastic Stress Transfer

Subsequently, on application of the far-field tensile loading, the element is sheared in the opposite sense due to the thermally-induced shear stresses at the interface. A Cox-type elastic stress transfer regime is maintained across the interface only for very low applied strains (Fig. 2.2(b)).

2.3.3 Stage C: Elasto-Plastic Stress Transfer

As the loading on the specimen increases, this elastic regime gives way to an elasto-plastic stress transfer regime characterised by localised matrix yielding in the vicinity of the fibre end, Mode α (Fig. 2.2(c)). Effectively the element is now being subjected to a stress state in which the von Mises stress (Appendix C) is equal to the yield stress of the matrix. As loading on the composite continues, yielding continues with the element becoming progressively more plastically deformed. Finally, after a certain amount of yielding has taken place, a limit is reached at which the element debonds from the fibre.

2.3.4 Stage D: Crack Initiation

The fibre end debonding, consequent upon excessive plastic deformation, may be defined by a crack initiation criterion which is based on the material upper bound of the von Mises' equivalent strain in the matrix, ε_m:

$$\textit{Crack initiation :} \qquad \varepsilon_m = \varepsilon_m^{*} \qquad \textit{if } \varepsilon_m' > 0 \qquad (2.2)$$

where ε_m^{*} may be two to three times the bulk matrix fracture strain. This increase is attributable to the lower flaw density in thin films of matrix, which act as failure nucleation sites in the bulk matrix. The above failure criterion is valid only when the dilatational strain component, ε_m', (otherwise known as bulk, volumetric or spherical component of strain (See Appendix C)) is positive, i.e. the overall state of strain is tensile thus promoting rupture of the yielding matrix and hence the creation of a macroscopic interface crack. The reason for the use of the von Mises equivalent strain in the criterion as opposed to any other universal measure of strain, is that ductile

failure through a void-growth mechanism has been established to be dependent on the von Mises equivalent strain [22].

2.3.5 Stage E: Fibre End Debonding

Due to the geometry of the fibre end, crack initiation occurs at the fibre corner thus creating a small crack, Mode β (Fig. 2.2 (d)), with one tip oriented towards the interface and the other one towards the fibre end. In order to determine which of the two crack tips propagates first, the problem may be viewed as two competing crack propagation criteria. The traditional fracture mechanics energy criterion [23] may be applied to both crack tips giving:

$$\begin{aligned} & \textit{Fibre-end crack propagation}: && \mathcal{G}_{\mathrm{I}} = \mathcal{G}_{IC} \\ \textbf{versus} \quad & \textit{Interface crack propagation}: && \mathcal{G}_{\mathrm{II}} = \mathcal{G}_{IR} \end{aligned} \tag{2.3}$$

where $\mathcal{G}_{\mathrm{I}}$ and $\mathcal{G}_{\mathrm{II}}$ represent the strain energy release rates (SERR) in Mode I opening mode and Mode II shearing mode, respectively, given the loading geometry on the two crack tips. Similarly, $\mathcal{G}_{IC}$ is the interfacial fracture toughness in Mode I, while $\mathcal{G}_{IR}$ is the interfacial fracture toughness in Mode II. As an approximation, both interfacial fracture toughnesses will be considered to be equal. It will be shown that the fibre-end crack tip propagates first thus leading to complete debonding of the fibre end (Fig. 2.2(e)).

2.3.6 Stage F: Crack Propagation

The interfacial failure process continues, on additional loading, in the form of interface crack extension, Mode β (Fig. 2.2(f)) *or* a crack propagating at an angle into the matrix, Mode γ. The preferred failure mode for the particular composite system will be dependent on the relative fracture toughnesses of the interface versus that of the matrix, for the given induced stress field. Post-failure optical techniques such as SEM, provide information as to *which* interfacial failure mode was prevalent for a given composite system, but only at the most advanced stage of failure when the specimen has globally failed.

A fundamental feature of the interface crack is that frictional stress transfer occurs across the cracked interface, due to the surface roughness of the contacting crack faces. This stress transfer by a frictional mechanism in Mode β is supported due to the significant normal compressive stresses that exist across the interface due to the Poisson's ratio differential between fibre and matrix, and also due to the thermally induced fabrication stresses. Frictional stress transfer is not present in the matrix crack propagation mode, since the crack is predominantly in an opening mode, due to the orientation of the crack.

In summary, the constituent stages of the Progressional Approach to the interfacial failure process are:

- Thermal residual stress state induced during fabrication.
- *Very low level loading:* linear-elastic Cox-type stress transfer.
- *Low level loading:* elasto-plastic stress transfer with localised matrix yielding, Mode α failure.
- *Medium level loading:* crack initiation at fibre end, Mode β failure.
- *Higher level loading:* interface crack propagation with frictional stress transfer, Mode β failure; **or** matrix crack propagation, Mode γ failure.

In conclusion, the Progressional Approach is designed to be comprehensive and rigorous in that it attempts to account for the main systemic non-linear phenomena that are characteristic of the interfacial failure process.

Judicious finite element analyses of single and multi-fibre composite systems based on the Progressional Approach will allow realistic predictions of the various stages of the failure process and their influence on the overall composite behaviour. Important stages such as the initiation and propagation of cracks consequent upon excessive interfacial yielding will be investigated in the finite element models that incorporate these complex mechanisms of interfacial failure. The widely used commercial software package ABAQUS 5.4 [See Appendix B] was used to solve various FE models that were generated using the Femgen pre-processor

2.4 Solution Evaluation Criteria

The stress and strain fields predicted by any given finite element model for loaded composite specimens must conform to certain criteria if they are to be meaningful. These criteria are based on the physical upper bounds of the elasto-plastic material behaviour of the fibre and matrix:

I At any point in the fibre, the axial stress, σ_f, must be lower than the fracture stress of the fibre, σ_f^* :

$$\sigma_f < \sigma_f^*$$

II At any point in the matrix, the von Mises equivalent stress, σ_m, must be lower than or equal to the tensile yield stress of the matrix, σ_m^{yield}, for the given applied strain rate:

$$\sigma_m \leq \sigma_m^{yield}$$

III At any point in the matrix, the von Mises equivalent strain, ε_m, must be lower than the tensile fracture strain of the matrix, ε_m^* :

$$\varepsilon_m < \varepsilon_m^*$$

In addition to these material property based criteria, there are also established criteria which an FE mesh must satisfy in order to ensure that the solution is suitably converged. These consist of various element quality tests regarding element corner angles and aspect ratios. Sufficient mesh refinement must also be imposed in areas of high stress/strain gradients, to minimise the discretisation error of the model [24].

The Progressional Approach automatically satisfies criteria II and III. For the range of loading considered in the analyses of the current research, criterion I is also satisfied,

except in the case where fibre fracture during the loading sequence is defined explicitly during the analysis, as in the case of the multi-fibre analysis of Chapter 9.

The solution evaluation criteria will be useful in the evaluation of the results predicted by the various analyses to be presented in the Literature Survey.

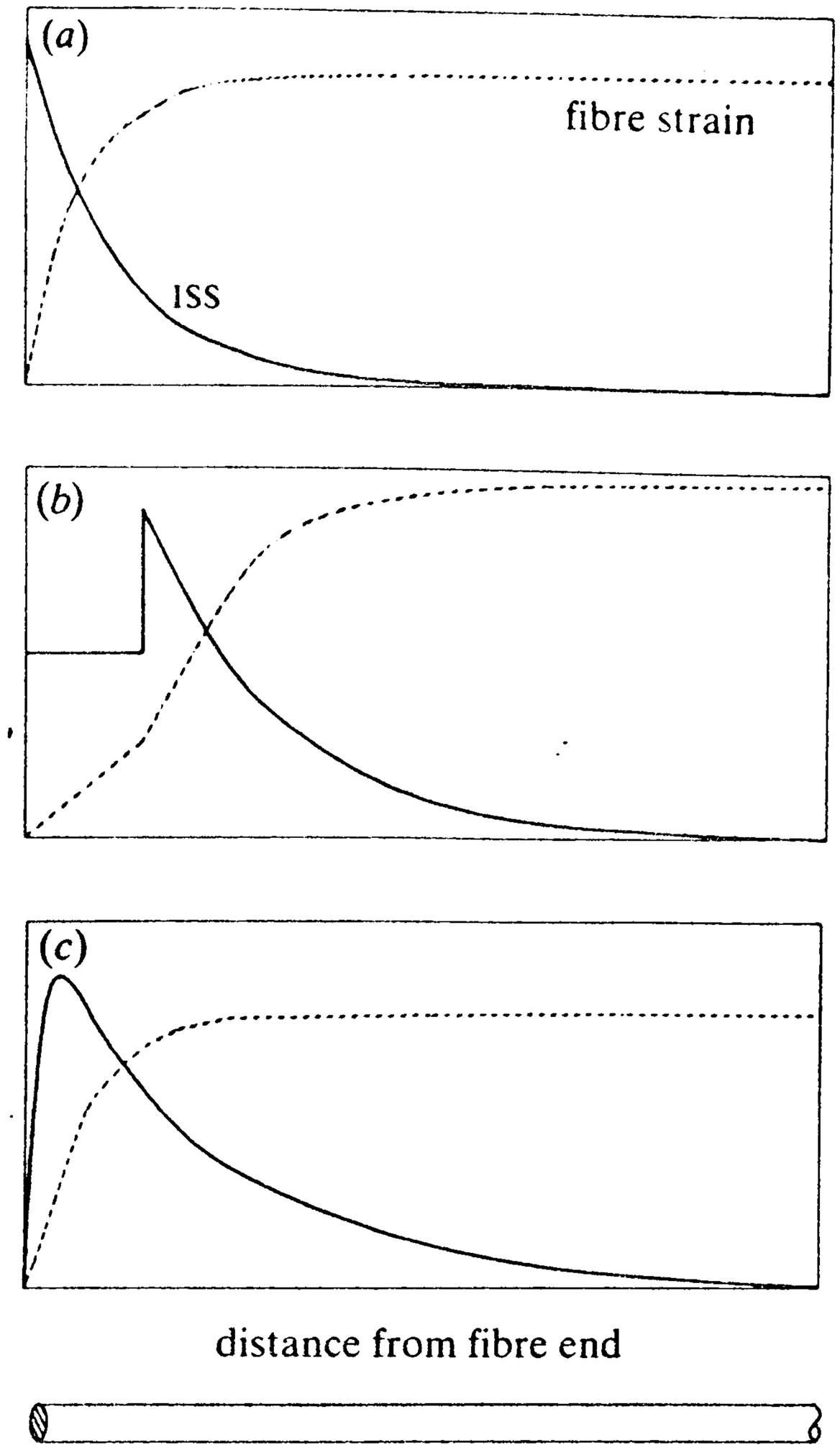

Fig. 2.1 Schematic fibre strain (dashed line) and ISS (thick line) distributions according to (a) classical shear-lag theories, (b) frictional-slip model, and (c) elastic transfer models requiring zero shear stress at fibre end.

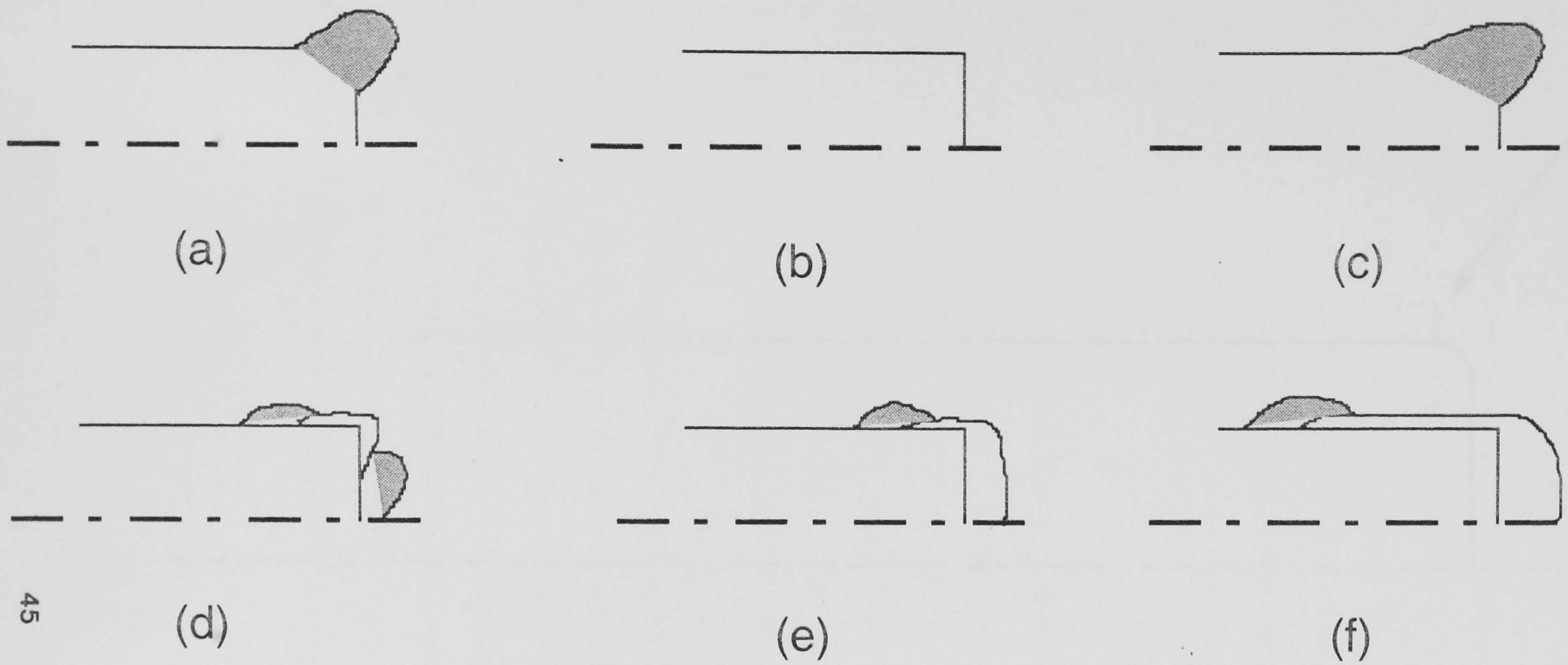

Fig. 2.2 Stages of Progressional Approach of the Interfacial Failure Process: (a) localised yielding due to thermal pre-load, (b) linear-elastic stress transfer due to tensile loading, (c) localised yielding, (d) initiation of interface crack, (e) full debonding of fibre end, and (f) propagation of interface crack (or matrix crack - not shown)

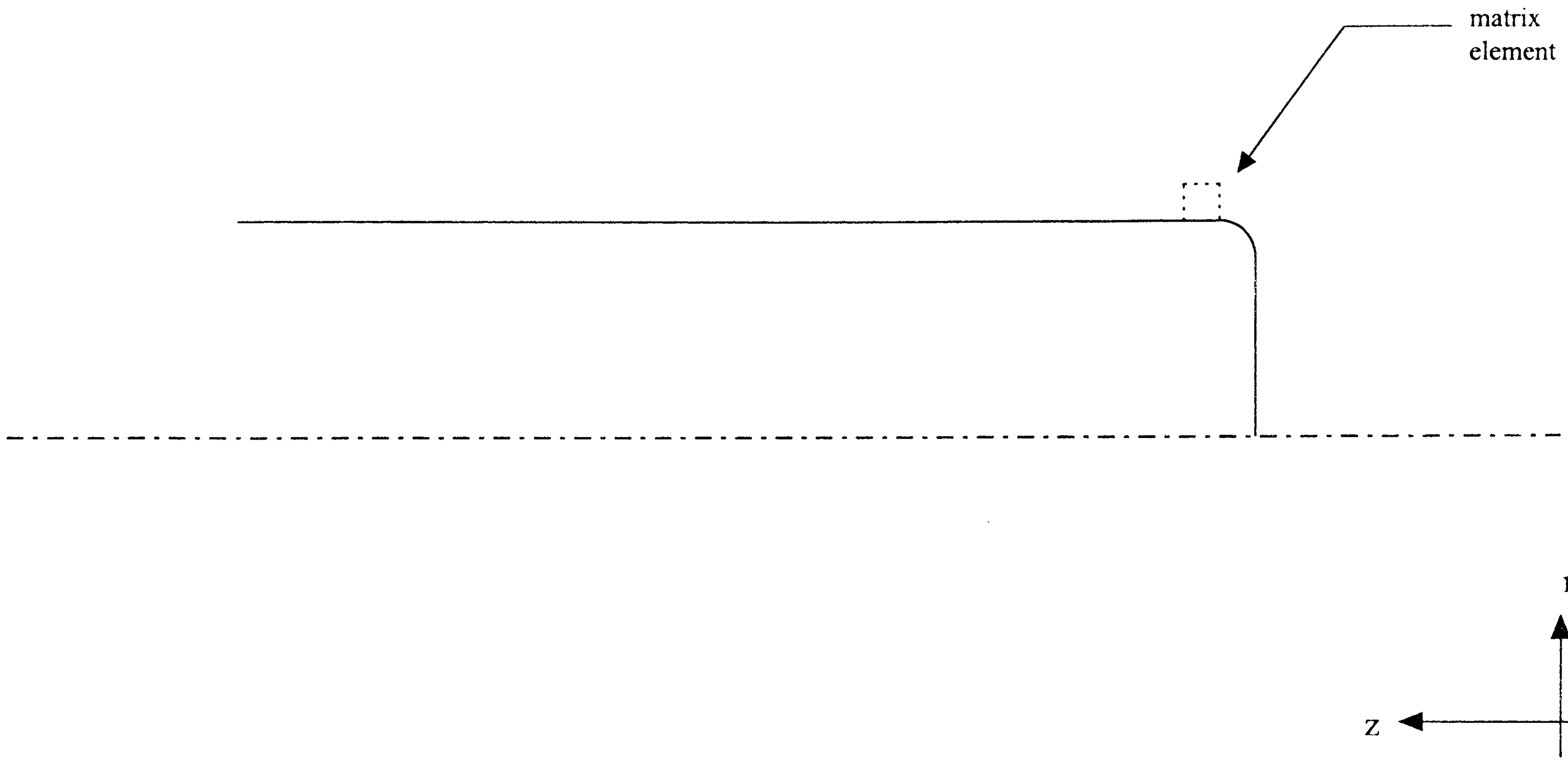

Fig. 2.3 Fibre end geometry showing small matrix element at the interface

Chapter 3

Finite Element Analysis Literature Survey

3.1 Prologue

Finite element analysis is an established modelling technique for furthering the understanding of the stress transfer characteristics and interfacial failure in fibre-reinforced composites. The majority of the analyses to date, are linear-elastic and based on the traditional theoretical considerations such as those of Cox. Highly limited in their scope, such analyses only confirm their underlying theoretical models and provide minimal insight into the non-linear phenomena that are characteristic of real systems.

Some more recent non-linear analyses, however, have produced generic conclusions pertaining to the influence of yielding and interface/matrix cracking at, or in the region of, the interface. These analyses are non-rigorous in their approach, since only specific phenomena are taken into consideration such as exclusively yielding or matrix cracking mechanisms. Consequently, the *progressive* nature of the failure mechanisms and their complex *interaction* have not been investigated.

All the finite element research to date may be categorised into two broad classes. The majority of work pertains to the analysis of single fibre rather than multi-fibre systems. Single fibre systems may be analysed axisymmetrically in a 2D model, whereas multi-fibre systems require the additional complexity of 3D modelling. Both classes may be further subdivided into linear-elastic or elasto-plastic analyses. The majority of analyses are linear-elastic since the importance of the elasto-plastic behaviour of matrix *as an interfacial failure mechanism* is not well understood.

This literature survey will present, in chronological order, the more pertinent FE analyses that have been performed for both single and multi-fibre systems. The linear-elastic analyses will precede the elasto-plastic analyses.

3.2 Single Fibre Analyses

The majority of finite element analyses concern the stress distribution around a single short fibre embedded in matrix, loaded in tension. The analyses are axisymmetric and thus two dimensional. In the majority of analyses, particular attention has been given to the nature of the interfacial shear stresses in the region of the fibre ends. If the analyses are linear-elastic, these stresses have been found to be singular if the geometry of the fibre corner is sharp. Some of the more realistic analyses consider the local stress field in the presence of a matrix/interface crack which is assumed to be pre-existent in the model.

3.2.1 Linear-elastic Analyses

Termonia 1987 [25], Berthelot *et al.* 1993 [26], Fan and Hsu 1992 [27], and Liou 1997 [28] have all studied the linear-elastic case of a single fibre embedded in a finite volume of matrix in which perfect adhesion of the interface is assumed. In all the analyses, the thermal fabrication stresses were not considered and no form of interfacial cracking was present. All of the analyses predict fibre stress and interfacial shear stress (ISS) profiles *similar* to those of the Cox shear-lag analysis. Since the analyses assume linear-elastic behaviour of both matrix and fibre, the magnitudes of the stresses are commonly normalised with respect to the applied stress on the composite.

Termonia's analysis uses the finite-difference method and is one of the first analyses to seriously tackle the fibre end stress concentration phenomenon induced in a glass fibre embedded in epoxy matrix. The ISS is found to increase to a maximum at the fibre end and the value is dependent on the fibre-matrix elastic modulus ratio. For a system whose ratio is 20, an ISS concentration of 1.4 is predicted. These results

would be physically reasonable only if the ISS were significantly lower than the shear yield stress of the matrix, which would be well below the operational applied loads that a composite specimen would be subjected to. Hence violations of Criteria II and III (see Section 2.4) would inevitably occur when the applied stress on the composite reached a significant level. Such violations are characteristic of linear-elastic analyses thus making the assumption of linear-elasticity inadequate for the realistic analysis of composites.

Berthelot *et al.* have performed an FE analysis of a system similar to that of Termonia in which the elastic modulus ratio is 24. The model employs in excess of 2500 elements and possesses satisfactory mesh refinement. The ISS concentration is found to be 1.6 and the profile almost identical to that of Termonia.

Fan and Hsu have analysed a polydiacetlyene fibre embedded in epoxy matrix where the elastic modulus ratio is 11. The model employs 1580 elements and possesses satisfactory mesh refinement with the smallest element in the region of the fibre end being of the order of one tenth of the fibre radius. The matrix strain near the fibre corner is found to be 2.5 times the applied strain and 'judged a likely candidate for failure'. The ISS increases to a maximum of 50MPa at the fibre end, which is acceptable (according to Criterion II, Section 2.4) given the low elastic modulus ratio of the system. A wedge-shaped fibre end geometry is also analysed and is found to reduce the stress concentration that would otherwise exist in a square fibre end. It is concluded, however, that the fibre end geometry effect was negligible for systems in which the aspect ratio of the fibre (length/diameter) is large.

Liou has performed a similar analysis to Fan and Hsu, but for three different fibre end geometries. These were square, wedge-shaped and round fibre end geometries. The system under investigation is a carbon fibre-epoxy matrix composite in which the elastic modulus ratio is 64. The FE model has only 112 elements which was considerably fewer elements than the analyses of Fan and Hsu. Consequently, the stress distributions were only indicative of the underlying trends which were similar to those of the Cox type profiles. The ISS concentrations are 1.3 for the square end

BIBL. LONDIN.

and in the range 2.0 - 4.2 for the wedge-shaped fibre end depending on the angle of inclination of the wedge geometry. For the rounded fibre end, the ISS concentration is substantially lower at 0.4. It is concluded that the fibre end geometry had a significant influence on the local linear-elastic stress concentration.

A work that distinguishes itself from the rest, is the boundary element analysis of Selvadurai and ten Busschen 1995 [29], in which a glass fibre-polyester resin composite is modelled incorporating a matrix crack. The crack is defined to commence at the fibre end and propagate at an angle to the fibre axis determined by a fracture mechanics-based criterion. The elastic modulus ratio is 47. The matrix crack is pre-existent in the model and is allowed to propagate conditional upon the satisfaction of a criterion based on the mixed-mode stress intensity factors. A variety of matrix crack orientations are thus predicted which correlate satisfactorily with the experimentally observed crack geometries. Stress distributions along the fibre are not predicted but the analysis is prototypical in that interfacial failure involving matrix cracks (that are normally induced *during* the loading history) have been explicitly examined. The limitations of the analysis are that the crack is *pre-existent* in the model and the matrix does not exhibit plasticity.

A very similar FE analysis is that of Brockmuller *et al.* 1995 [30], in which a matrix crack is modelled to propagate in a pseudo-conical manner. The aim of the analysis was to ascertain the influence of a propagating matrix crack on the global composite properties, such as composite modulus and failure stress. Simulation of a propagating pseudo-matrix crack was achieved by the definition of an interface crack kinking to become a transverse crack, such that the crack geometry was L-shaped. The resultant stress-strain curve for the composite exhibited a 45% decrease in the modulus. The inadequacies of the model are numerous and include non-account of matrix plasticity and the gross errors associated with the pseudo-matrix crack propagation. The analysis does, however, explicitly evaluate the effect of crack propagation on the global composite modulus.

3.2.2 Elasto-plastic Analyses

Levy and Papazian 1991 [31], Shi *et al.* 1992 [32], Guild *et al.* 1994 [9], and Tripathi *et al.* 1996 [33] have performed elasto-plastic analyses of a single fibre composite in which the interfacial failure mode is defined to be exclusively yielding; hence the initiation and propagation of cracks within the system have not been incorporated.

Levy and Papazian study a SiC fibre metal-matrix composite (MMC) in which the elastic modulus ratio is 7, loaded in both tension and compression. The analysis is 3D in order to investigate the influence of multiple fibre end interactions and includes the thermal fabrication-induced residual load. Approximately 150 elements are used which is far less than would be necessary for satisfactory modelling of the strain gradients induced in the yielding zones. The thermal load induces plastic deformations of 2% in the region of the fibre corner. Tensile loading subsequently induces plastic deformation over the majority of the interfacial region whereas compressive loading induces plastic deformation only in the fibre end regions. The influence of the matrix yielding mechanism on the global composite mechanical response is represented by a stress-strain curve which exhibits substantial non-linearity above 0.4% applied strain. It was concluded that for MMC's, localised plastic deformation due to both the thermal pre-load and the subsequent tensile/compressive loading are significant factors that determine the mechanical response of the composite.

Shi *et al.* have also analysed the same system as Levy and Papazian but using a simplified 2D plane strain model. The number of elements in the model totals only 65 which is of the same order of mesh refinement employed in the Levy and Papazian analysis. The thermal pre-load is included and the subsequent tensile loading is applied incrementally, so as to obtain an accurate *global* composite mechanical response. The thermal load induces a plastic zone in the region of the fibre corner, which is found to increase the global composite modulus and strength significantly once subsequent tensile loading is applied. This is because large amounts of work are dissipated in the thermally-induced plastic region, during the tensile loading. During

the tensile loading phase, the plastic zone evolves outwards from the interfacial area until the entire matrix region is yielding, in a similar manner as with the Levy and Papazian analysis.

Guild *et al.* have performed an elasto-plastic analysis for a Kevlar-49 fibre epoxy matrix system whose elastic modulus ratio is 47. The axisymmetric model employs in excess of 1000 elements and possesses satisfactory mesh refinement. The interfacial shear stress and strain profiles are obtained for various levels of applied strain on the composite. It was found that as the loading was increased, the area of matrix yielding in the fibre corner region evolved in the same way as the analysis of Shi *et al.*. The interfacial plastic strain was found to far exceed any meaningful value. For instance, a von Mises strain maximum of 180% was predicted for an applied strain of 1.8%. This is inevitably due to the fact that fibre end fibrillation, characteristic of Kevlar fibres, has not been accounted for. An analysis incorporating such a phenomeneon would reduce the induced strain concentration considerably. However, this is the only elasto-plastic analysis which explicitly investigates the nature of the strain concentration induced under an elasto-plastic matrix regime.

Tripathi *et al.* investigate the extent of the interfacial plastic zone induced in a glass fibre-epoxy matrix system. Large-scale interfacial yielding instigated at the fibre end is predicted but evaluation of the magnitude of the plastic strain has been omitted. Hence, the development of interfacial cracking consequent upon yielding and subsequent propagation along the interface is not investigated. Thus the effects of these failure mechanisms upon the local stress and strain fields, as well as the global composite properties, have not been established.

Ho and Drzal 1995 [34] perform a non-linear analysis of a single fibre composite incorporating an interface crack. The AS4 carbon fibre-epoxy matrix system has an elastic modulus ratio of 55 and the model employs 3400 axisymmetric elements. The efficiency of stress transfer across the interface was found to be suppressed by matrix plasticity, especially for high levels of applied strain. The thermal residual stresses are also found to reduce the stress transfer efficiency. The fibre stress profile in the

presence of an interface crack is similar to the Ω-shape profile predicted by Piggott [21], (see Fig. 2.1(b)). The major shortcoming of the analysis is the assumption of a pre-existing interface crack together with a pre-existing fibre fracture. It is clear that the analysis for a fibre that fractures creating interface cracks *during* the loading history is fundamentally different to the analysis which assumes that the fibre and interface are fractured from the *beginning* of the loading history, in a non-linear analysis.

King *et al.* 1992 [35] analyse a carbon fibre-epoxy matrix system subjected to thermal and *transverse* loading. This analysis is the only one which employs matrix cracking initiated upon excessive matrix yielding in a *progressive* manner. The transverse loading is applied incrementally until yielding is predicted initially in the interfacial region and then in the entire matrix region. Matrix cracking then occurs near the interface, according to the maximum normal stress failure criterion that was used. The analysis, although fully non-linear in its approach, considers the relatively simple case of transverse loading, in which the significant discontinuities at the fibre ends are not relevant. More importantly, the implications of reinforcement efficiency of the composite in the main axial direction is also not relevant. Hence the implications of the analysis for global stiffness, strength and failure mechanisms of composite components are limited, due to the transverse nature of the loading.

3.3 Multi-Fibre Analyses

There are few multi-fibre composite FE analyses which investigate the effects of *spontaneous* fibre fracture during the loading program, and the interaction between the fibres consequent upon fracture. Particularly of interest is the redistribution of stress among the surrounding intact fibres and the nature of the damage in the zone of the fibre fracture. The analyses to be cited assume a *pre-existent* fibre fracture, which is a fundamental simplification of the problem, as discussed earlier. This assumption is especially erroneous if the surrounding matrix behaves elasto-plastically.

3.3.1 Linear-elastic Analyses

Wang *et al.* 1991 [36] have performed a 2D axisymmetric simplified analysis of a 7-fibre glass/epoxy system, in which the central fibre is fractured. The six adjacent intact fibres are simulated using equivalent concentric cylinders whose thicknesses are defined so as to maintain the fibre volume fraction equal to that of the real composite. When the system is loaded in tension, the stress amplification in the intact adjacent fibre is found to be more than twice the far-field fibre stress, which would thus increase the probability of successive fibre fractures. This stress amplification was found to increase with the fibre volume fraction as the inter-fibre spacing was decreased. A shear stress concentration was predicted in the fracture zone of approximately 30% the value of the far-field fibre stress. For an applied strain of 1%, the ISS value would be 250MPa which is far in excess of the matrix yield stress. The analysis is highly simplified since through-the-thickness effects in the fibres have not been considered by virtue of the two-dimensional nature of the model. Furthermore, non-linear effects such as matrix plasticity, crack initiation/propagation and thermal pre-load have not been comsidered.

Nedele and Wisnom 1994 [37] have performed a 3D analysis of a carbon fractured fibre surrounded by six equally-spaced fibres in a hexagonal array. The model of a dodecatant section consisted one twelfth of the fractured fibre and one half of the adjacent intact fibre separated by a thin layer of matrix, subjected to an applied strain. Only 40 elements have been used with the minimum element size being half the fibre radius. An *abnormally low* stress amplification factor of 1.025 is predicted in the adjacent fibre. This is inevitably due to the existence of a sharp singularity at the fracture tip where the adjacent matrix, behaving linear-elastically, sustains excessive levels of strain energy due to the large shearing action of the fractured fibre. The predicted shear stresses are found to be well in excess of the matrix shear yield stress over a distance of several fibre radii from the fracture location.

The analysis is fundamentally inadequate from a number of aspects. The results indicate that the mesh refinement is not sufficient to cope with the high stress gradients induced at the fibre fracture location. Furthermore, the inclusion of matrix

elasto-plasticity would lead to a larger zone of stress redistribution corresponding to an enlarged crack-tip plastic zone. Consequently, significantly more of the load originally supported by the fractured fibre would be distributed to the adjacent fibres, and not absorbed by the *abnormally stiff* matrix which is behaving linear-elastically. The analysis of a pre-existent fibre fracture in the model leads to substantial error since, in reality, fracture occurs after a composite strain of about 0.3% has been sustained. The combination of all these factors highlight the inadequacies of the simplified model, and consequently lead to *significantly erroneous* predictions of the stress amplification factors for the adjacent fibres. It was concluded by Nedele and Wisnom that certain established analytical predictions that have been made by a number of authors [38-39] severely over-estimate the stress amplification factors based on this analysis.

3.3.2 Elasto-plastic Analysis

Xu and Weitsman 1996 [40] have analysed a carbon-epoxy system subjected to *compressive* loading in which there is included a sinusoidal transverse component to simulate micro-buckling effects. A large mesh employing 12,800 elements was subjected to the compressive loading and revealed 'high non-uniformities and localisations' especially near fibre-matrix interfaces. It is broadly concluded that these localisations would lead to compressive failure of the composite, which is not accounted for by the model. This analysis is the only fully 3D FE analysis that has been found by the author.

3.4 Epilogue

The majority of analyses, to date, consider only one of the many aspects of the interfacial failure process. For instance, either yielding at the interface or the existence of a matrix crack have been modelled as isolated failure mechanisms. A consistent and thorough analysis, in which all the various phenomena are accounted for, is required if realistic modelling of interfacial failure is to be achieved.

Chapter 4

Matrix Crack Analyses

4.1 Introduction

Linear-elastic FE analyses are presented for a continuous (long) carbon fibre embedded in epoxy matrix subjected to the incremental tensile loading, employed in a fragmentation test [1]. The test involves a single fibre subjected to loading so that successive fractures occur along the length of the fibre, at gradually higher levels of applied load. The test is commonly used in the estimation of the IFSS as discussed in Section 2.2. Carbon fibres fracturing in such a manner induce mode γ interfacial failure which involves the initiation and propagation of matrix cracks. Short carbon fibres, however, are more likely to fail in a Mode β interface crack manner, as will be investigated in Chapter 6. Experimental observation of conical cracks in carbon fibre-reinforced systems is generally very difficult to perform optically, but SEM evidence of conical cracks in this type of system are reported elsewhere [10,12].

The analyses presented here are a simplified version of the Progressional Approach, since the matrix is considered to behave linear-elastically and the effect of the thermal residual stress state induced during the fabrication of the specimen has not been included. Furthermore, the non-linear stage of matrix crack initiation is not considered, and hence the crack is assumed to be pre-existent in the model. The central aim of these simplified analyses was to demonstrate that the existence of a matrix crack influences the fibre stress or strain distributions in a way that significantly *reduces* the stress transfer efficiency in the fibre end regions. The influence of the crack dimensions on the fibre strain profiles was investigated using a FE model of a single carbon fibre-epoxy matrix composite incorporating a Mode γ conical crack of various geometries. Hence the fibre strain characteristics of Mode γ failure were ascertained, and the results obtained were compared with experimental data obtained using the LRS technique [13]. The crack geometries for which the

predicted fibre strain distributions correlated best with the experimental data were thereby established.

It should be noted that a rigorous analysis of Mode γ matrix cracks, based on the Progressional Approach, in which all the non-linear stages of the failure process are considered is presented in Chapter 7.

4.2 Experimental Measurements at QMW

The model composite which has been tested by Galiotis *et al.* [13], comprised a single continuous high modulus carbon fibre embedded in an epoxy resin. The fibres, supplied by Courtaulds Graphil plc, were approximately 6.5μm in diameter and a Ciba Geigy MY750/HY951 epoxy resin was used. Full details of the manufacturing procedure are given in [13]. The elastic modulus of the fibres, measured in the axial direction, was 390GPa and that of the matrix was 2.6GPa. Complete material property data are presented in Table 4.1.

The composite specimen was subjected to a program of incremental tensile loading. Using the LRS technique, the fibre strain distribution along the fibre was monitored at each level of applied strain, e_{app}, until full fragmentation occurred [13], where the long fibre had fractured successively to form several smaller fragments. The FE predictions were matched to the experimental fibre strain profiles for various applied strain levels. It should be noted that the resolution of the technique was 2μm, whereas for the more recently produced experimental data employed in the later chapters, the resolution was increased to 1μm. Furthermore, in these tests the LRS measurement probe was calibrated with axial fibre strain, whereas in the rest of the research calibration was made with axial fibre stress. This distinction is of no importance since the fibre behaves linear-elastically throughout the loading program. Further details of the experimental set up are given in Appendix A.

Optical studies of fragmented test specimens have shown that, of the three possible modes of interfacial failure described in Chapter 1, Mode γ failure is the most likely to occur in high modulus continuous carbon-epoxy systems [10,12]. There are several arguments to support this ascertion, in addition to the SEM evidence. Mode α localised yielding may be ruled out since the experimental shear stress distributions along the interface have been observed to be zero in the regions of the fibre ends. The shear stress would otherwise necessarily be equal to the shear yield stress of the matrix, if a predominantly yielding failure mechanism was prevalent. By a similar argument, Mode β is also eliminated since the interfacial shear stresses are not equal to a constant frictional value that has been observed in short carbon fibre systems [10]. More fundamentally, however, the interfacial failure mode is unlikely to be the same for a long carbon fibre fragmenting as for the case of a single short carbon fibre system, since during the fragmentation process, large amounts of strain energy are released from the fracturing fibre resulting in the dynamic formation of matrix cracks. In the case of short carbon fibres subjected to incremental tensile loading, the process is much less dramatic resulting in the formation of interface cracks, as will be discussed in Chapter 6.

4.3 Finite Element Models

The axisymmetric FE model incorporating Mode γ type failure (see Fig. 4.1(a)) included a conical-shaped matrix crack and covered one quarter of the diametral section, due to the symmetry of the problem (Fig. 4.1(b)). The matrix was assumed to be linear-elastic and isotropic and the fibre was assumed to be linear-elastic and transversely isotropic. The mesh consisted of approximately 400 6-noded triangular and 2,200 8-noded quadrilateral axisymmetric elements, (Fig. 4.2). The loading took the form of a uniform displacement imposed on those nodal points lying on the end face of the composite. The level of mesh refinement employed was found to be sufficient with respect to the convergence of the local solution, as shown in the mesh of Fig. 4.3, where fibre elements are represented shaded. The geometry of the matrix crack was defined in terms of its orientation with respect to the fibre axis, ϕ, and its

length, *a*. The aim was to find the crack geometry for which the corresponding fibre strain distribution correlated best with the experimental data, for levels of applied strain on the composite specimen of 1.05%, 1.15% and 1.35%.

For comparison purposes, an FE model which did not incorporate any mode of interfacial failure was analysed, in which the interface was defined as perfectly bonded and the applied strain on the composite was 1.0%. The mesh for this model is shown in Fig. 4.4.

4.4 Results and Discussion

The FE model not incorporating any failure mode produced fibre stress (S22) and interfacial shear stress (S12) profiles along the fibre length as shown in Figs. 4.5-6. Since the interface remains perfectly bonded and both fibre and matrix are linear-elastic, the distributions of Figs. 4.5-6 are similar to those predicted by the Cox shear-lag analysis (Section 2.1). The high fibre-matrix stiffness ratio induces large interfacial shear stresses towards the fibre end with the maximum occurring at the fibre end. The shear yield stress of the matrix is also indicated in Fig. 4.6 thus demonstrating that the stresses induced significantly *exceed* the material yield stress and consequently that the analysis along with similar analyses is inadequate, as has been discussed in Chapters 2 and 3. Fig. 4.7 shows the displacement field in which may be observed the large shearing effect induced at the interface towards the fibre ends.

The fibre strain distribution obtained from the FE model of the Mode γ interfacial failure (see Fig. 4.8), exhibits a characteristic S-shape in the take-up region. This S-shape has been observed in the experimental (LRS) fibre strain data, and has been found to become more pronounced as the applied loading on the composite was increased [13]. More specifically, as the matrix crack propagates, it was observed that the fibre strain S-curve moves forward leaving behind it an increasing portion of unloaded fibre. It is clear that in this region where the fibre is becoming progressively

unloaded, that the reinforcement efficiency is dropping. In Chapter 7, it will be demonstrated that the effective composite modulus correspondingly reduces for a propagating matrix crack. This S-shape, characteristic of the induced fibre strain profile, may be considered to be the *fingerprint* of interfacial failure by matrix crack propagation, Mode γ. It was also found that the interfacial shear stress reaches a maximum value at a finite distance from the fibre end (see Fig. 4.9), a feature also observed in the experimental data. This is in contrast with the Cox-type profile of Fig. 4.6, since the shear stress maximum is no longer at the fibre end but at a finite distance away. More importantly, this maximum is much less than the Cox shear stress maximum.

The FE predictions for the displacements in the model reveal that the crack opens up under the influence of the tensile loading, which is expected due to the opening nature of the crack. It follows that there cannot be any frictional stress transfer across the crack faces for this mode of interfacial failure. Load transfer by a frictional mechanism across an interface crack, as is characteristic of Mode β type failure, would necessarily require a closing-up of the crack in order that the crack faces may come into sliding contact with one another.

To investigate the influence of the stress concentration at the crack tip on the fibre strain profiles, the crack tip was blunted. The fibre strain distribution for the modified FE model was found to be unchanged showing that the interfacial stress transfer mechanism is insensitive to events local to the matrix crack tip. In the present analysis, the matrix has been modelled as linear-elastic, and therefore account of the crack tip plastic zone has not been taken. In Chapter 7, localised yielding in the model will be shown to occur in the vicinity of the fibre end and at the crack tips, when all the stages of the Progressional Approach are accounted for.

The geometric parameters that were found to influence the fibre strain and interfacial shear stress distributions, were the angle of crack orientation, ϕ, and the crack length, a. In order to establish the geometry of the matrix crack prevalent in the actual composite specimen, the combination of these two crack geometry parameters was

found that yielded a fibre strain distribution that correlated best with that measured experimentally, for a given level of applied strain. The method used to ascertain the crack dimensions entailed analysing a series of FE models in which the crack geometry was varied. The predicted strain distributions revealed that the crack length and angle influenced the fibre strain profiles in particular ways. It was found that the S-shape became steeper with larger crack angle and more elongated with larger crack length. Examination of these trends allowed the crack dimensions for the current experimental data to be ascertained. For e_{app} = 1.05%, these parameters were found to be $\phi = 20^{\circ}$ and a = 100μm. When the length of the matrix crack was increased, whilst keeping the crack angle constant, good correlation with the experimental fibre strain data was achieved for applied strain levels of 1.05%, 1.15% and 1.35% (see Figs. 4.10-12). This supported evidence that the matrix crack propagates in a self-similar manner in response to the incremental loading on the composite. For e_{app} = 1.05%, there was fair correlation between the FE and experimental results for the interfacial shear stress distribution, as shown in Fig. 4.13.

It has been observed in numerous studies of the propagation of interface and matrix cracks, in various composite systems, that they initiate at a certain angle to the fibre axis, but subsequently turn towards the interfacial region [10]. Matrix cracks have also been observed to bifurcate or even trifurcate at certain critical points during the loading history, thus making the problem even more complex.

	Carbon fibre	MY750/HY951 Epoxy matrix
Axial Tensile Modulus, GPa	390	2.6
Transverse Modulus, GPa	20	2.6
Axial Tensile Strength, GPa	3.2	78×10^{-3}
Axial Fracture Strain, %	0.8	4.2
Axial Poissons Ratio	0.22	0.36
Transverse Poissons Ratio	0.03	0.36

Table 4.1. Material Properties of Carbon Fibre and Epoxy Matrix

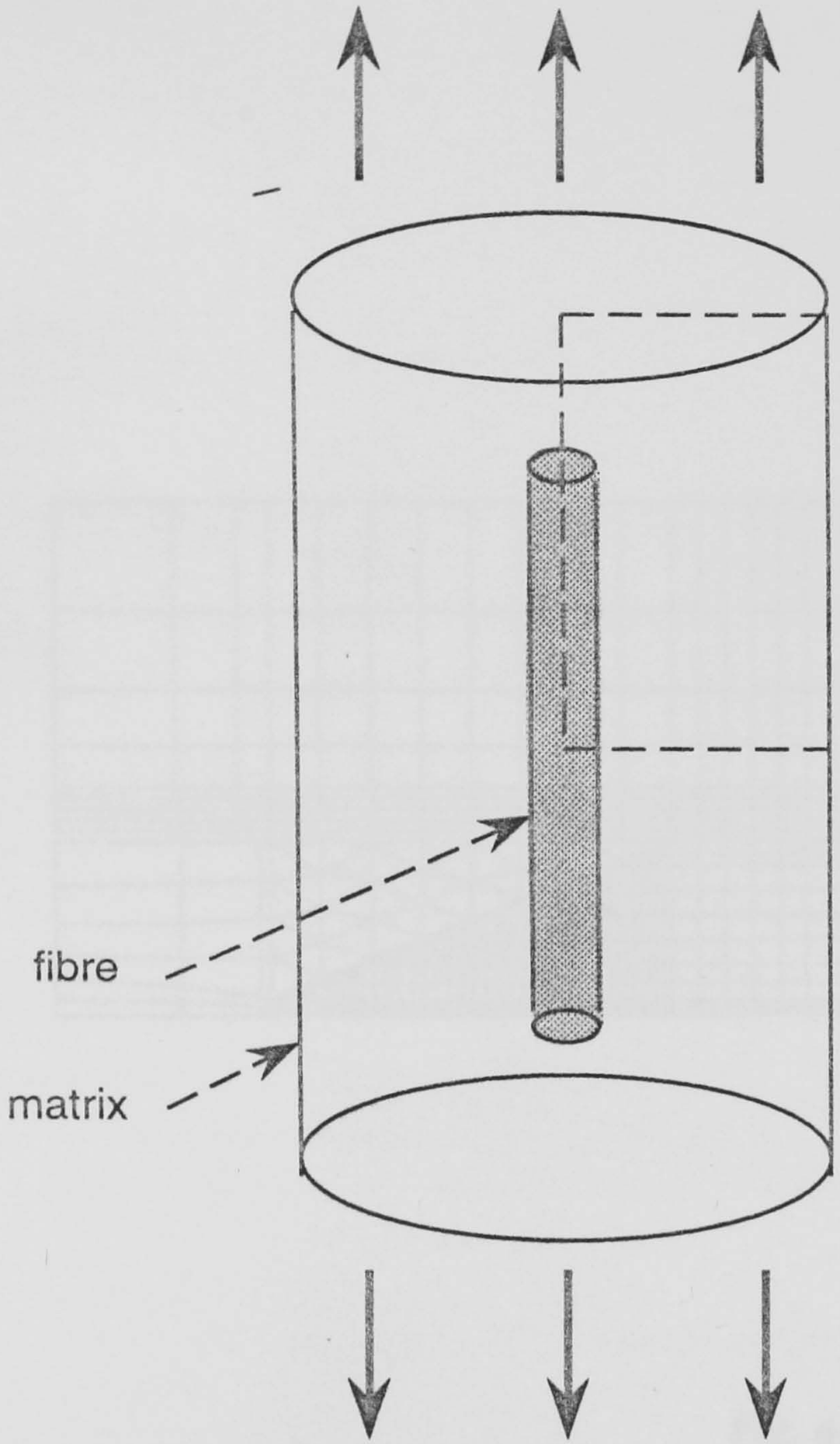

(a) Specimen Geometry

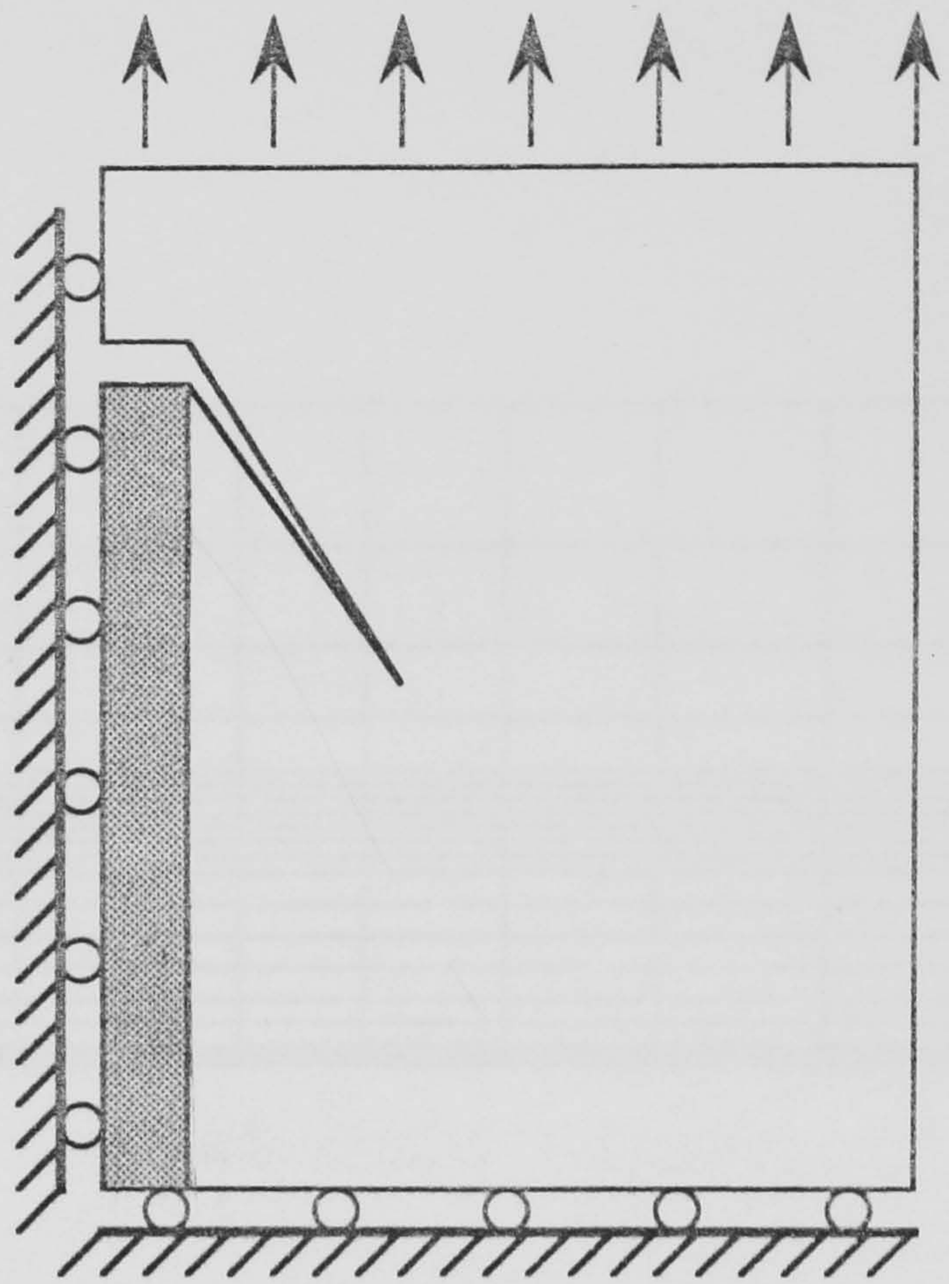

(b) Axi-symmetric Section showing Mode γ Interfacial Failure

(model represents one fragment)

Fig. 4.1 FE model geometry

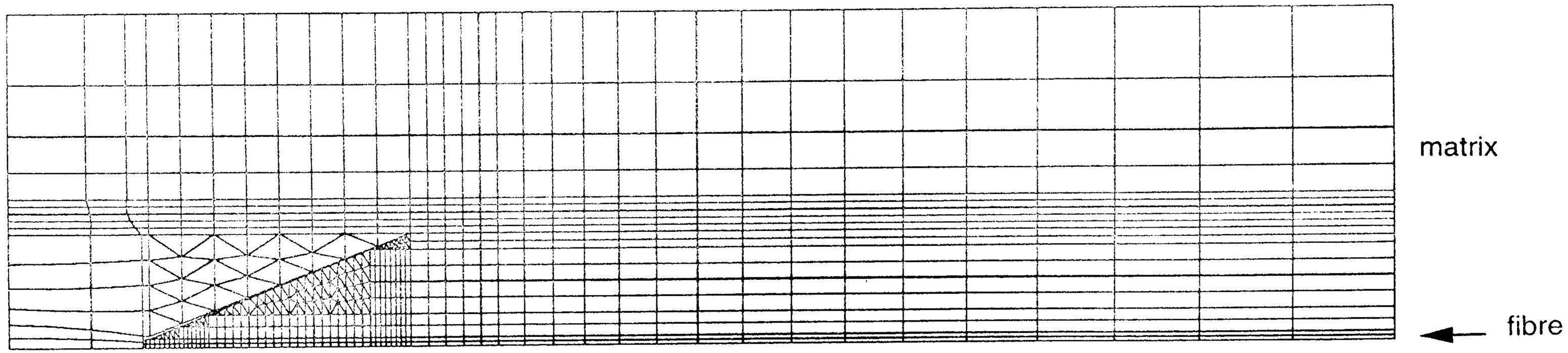

Fig. 4.2 FE mesh

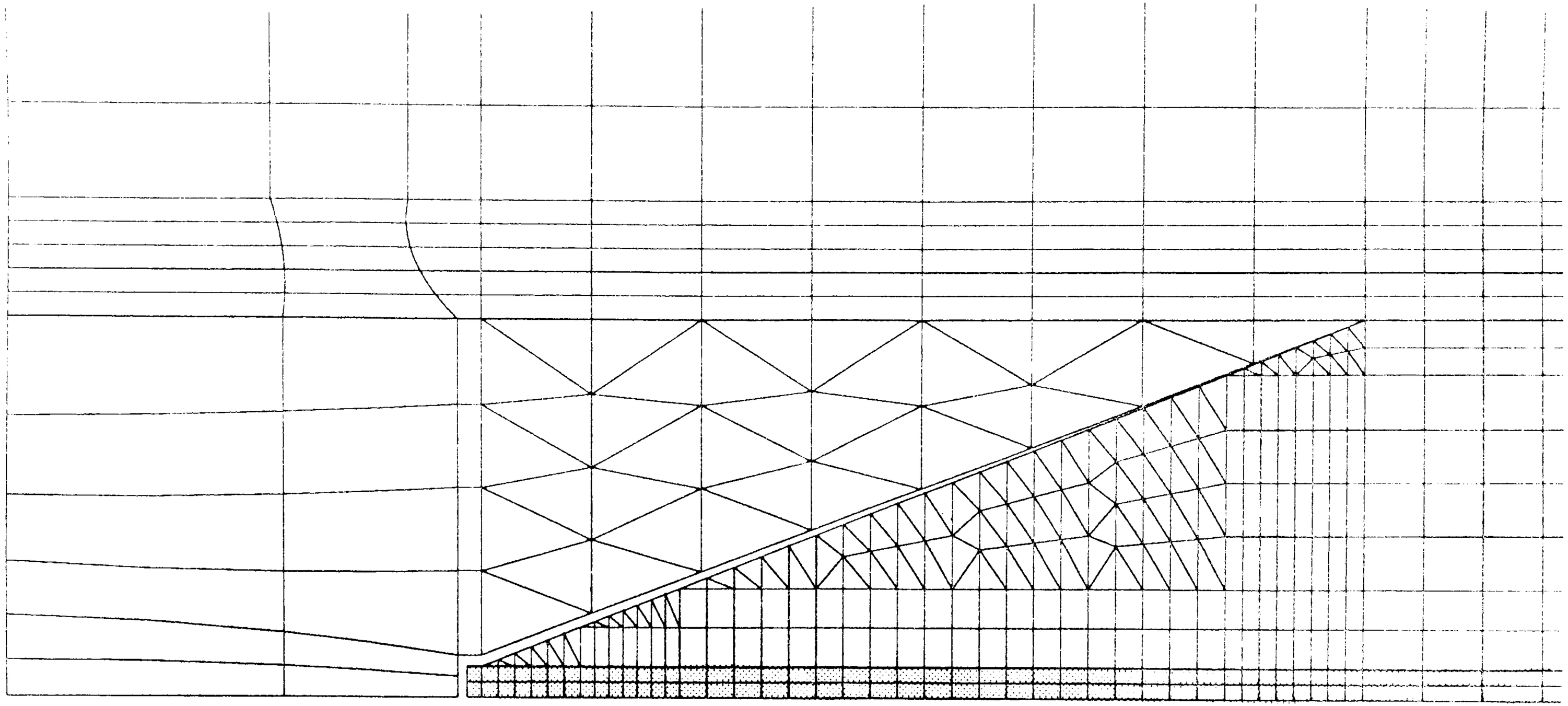

Fig. 4.3 FE mesh in region of fibre end showing matrix crack

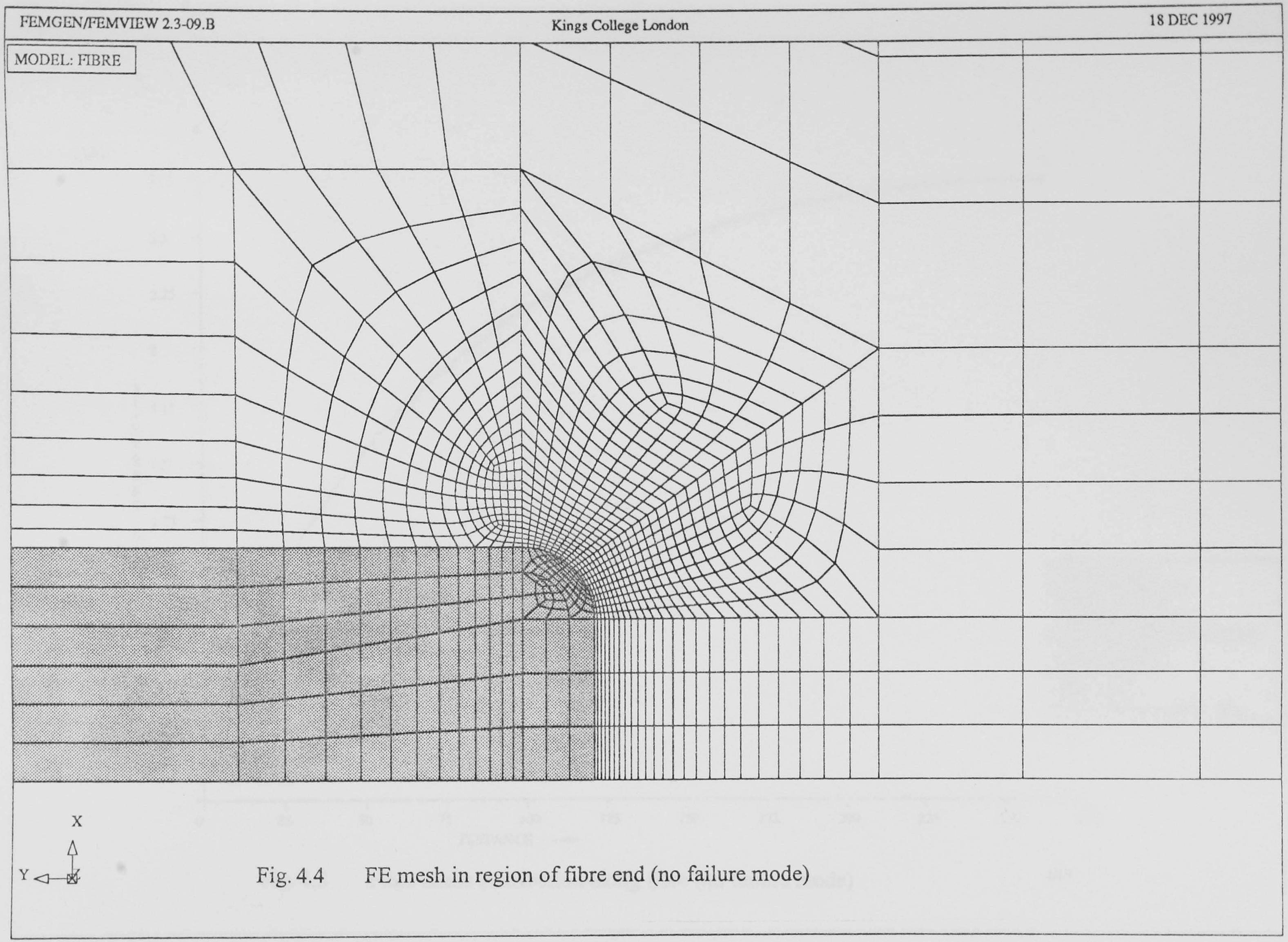

Fig. 4.4 FE mesh in region of fibre end (no failure mode)

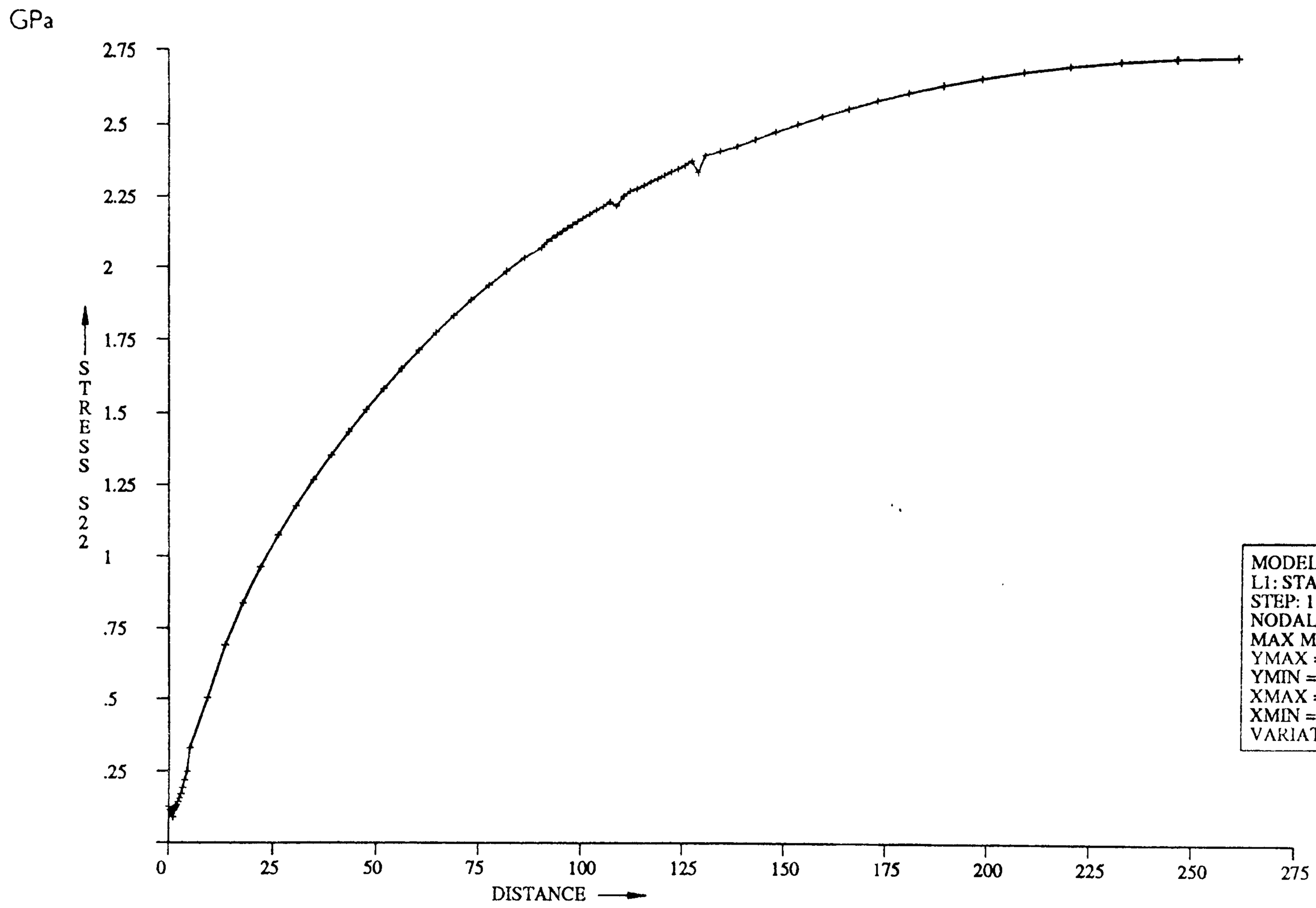

Fig. 4.5 Fibre stress distribution along fibre (no failure mode)

μm

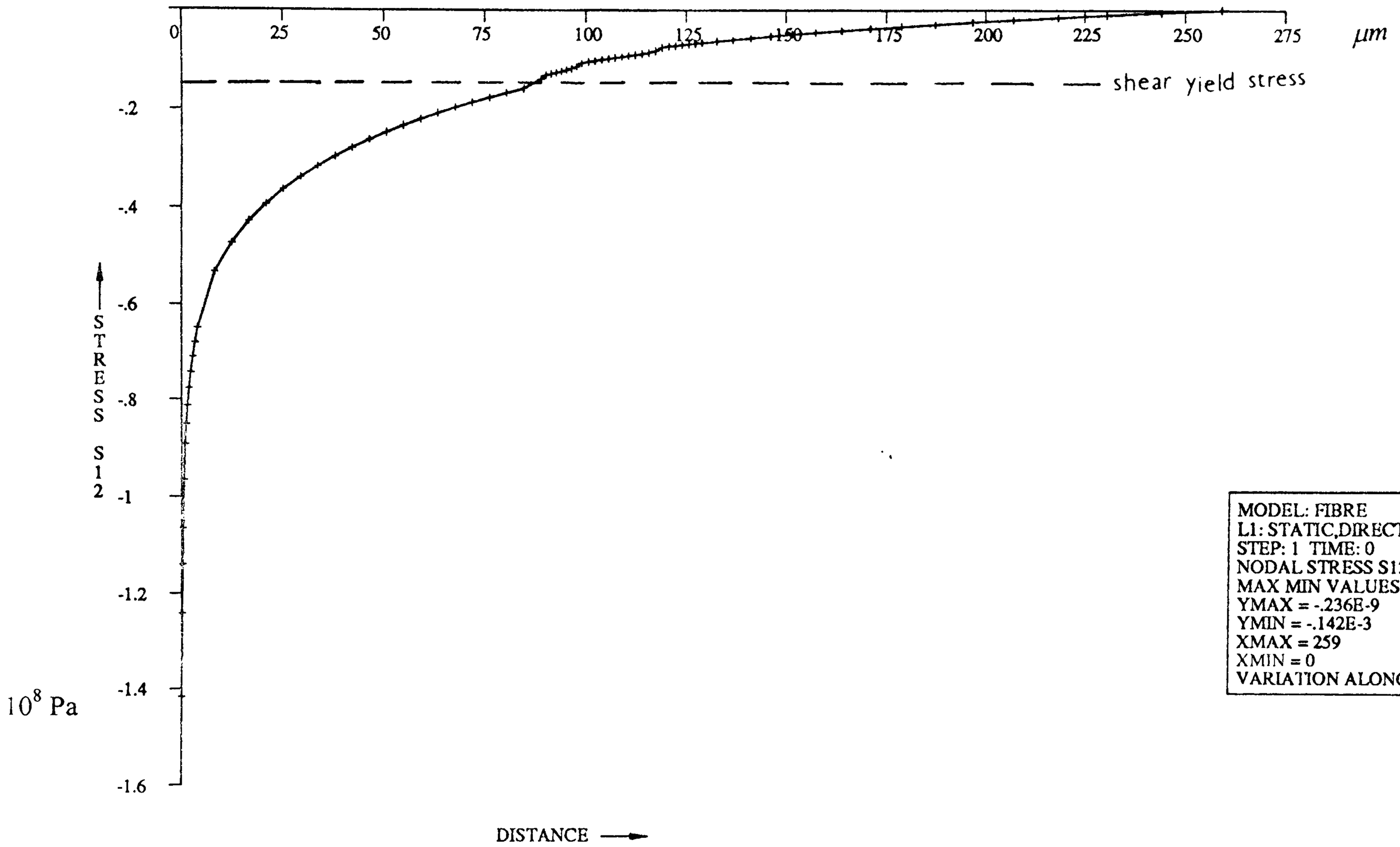

Fig.4.6 ISS distribution along interface (no failure mode)

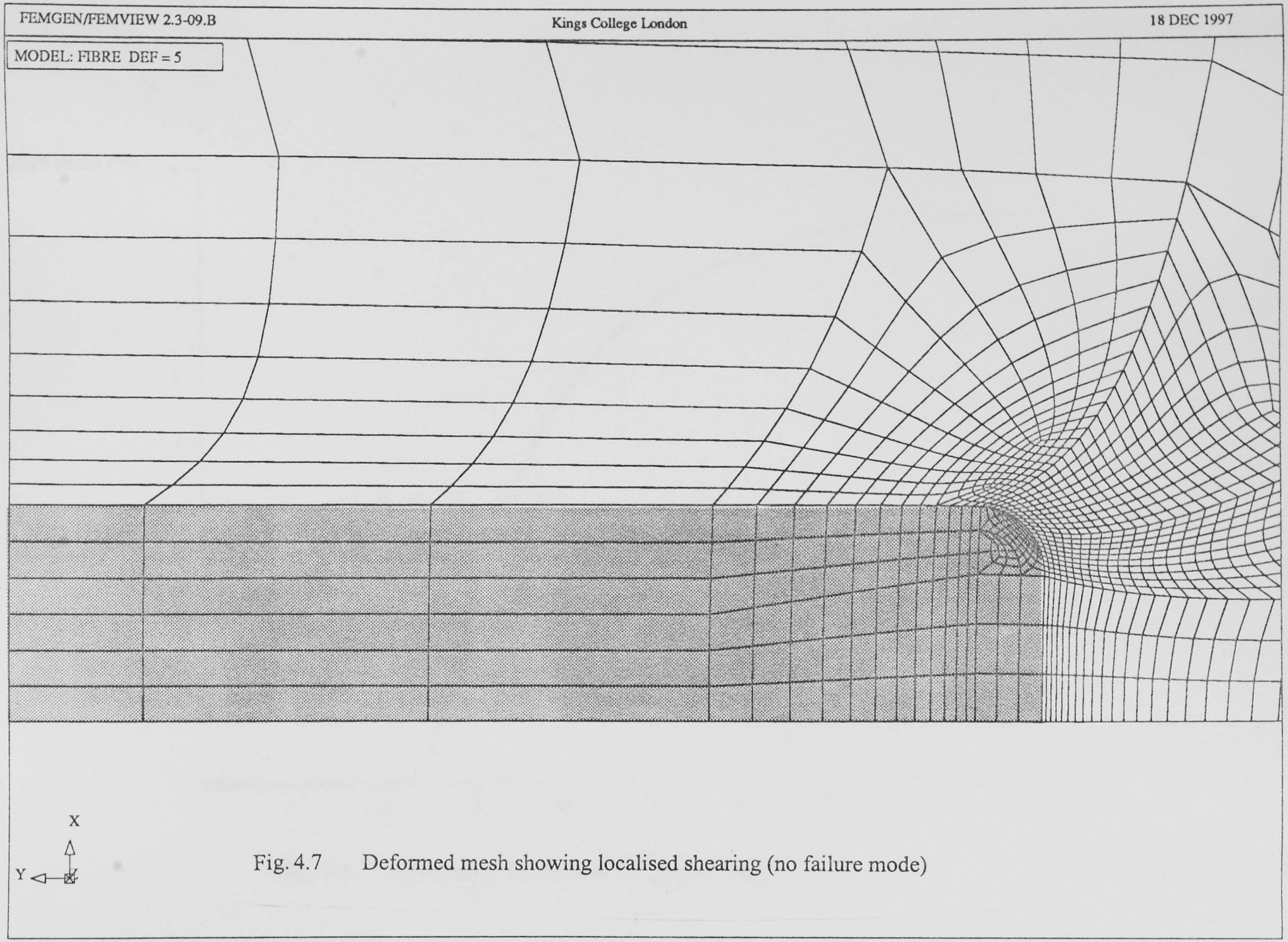

Fig. 4.7 Deformed mesh showing localised shearing (no failure mode)

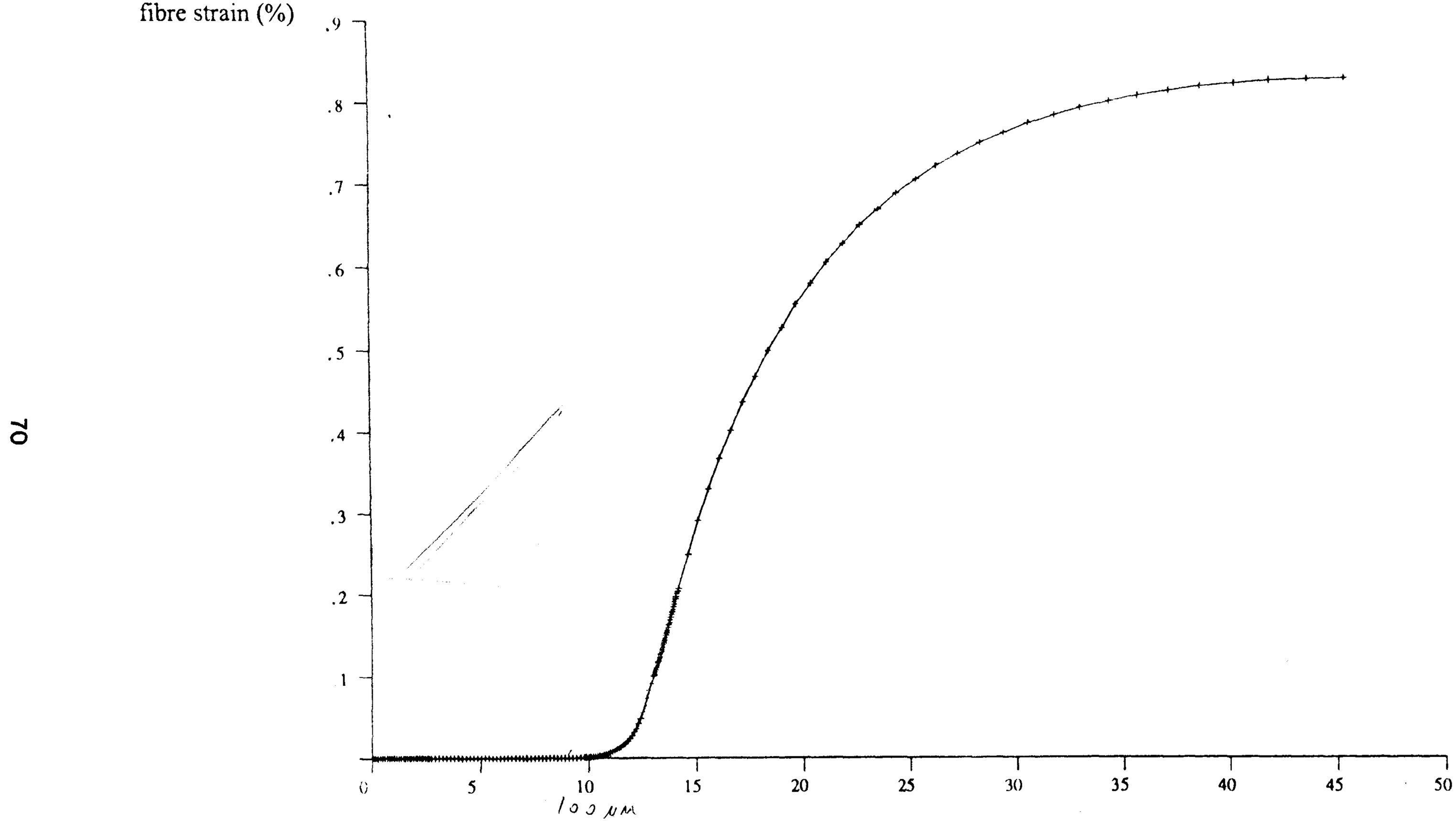

Fig. 4.8 Fibre strain distribution (37° matrix crack)

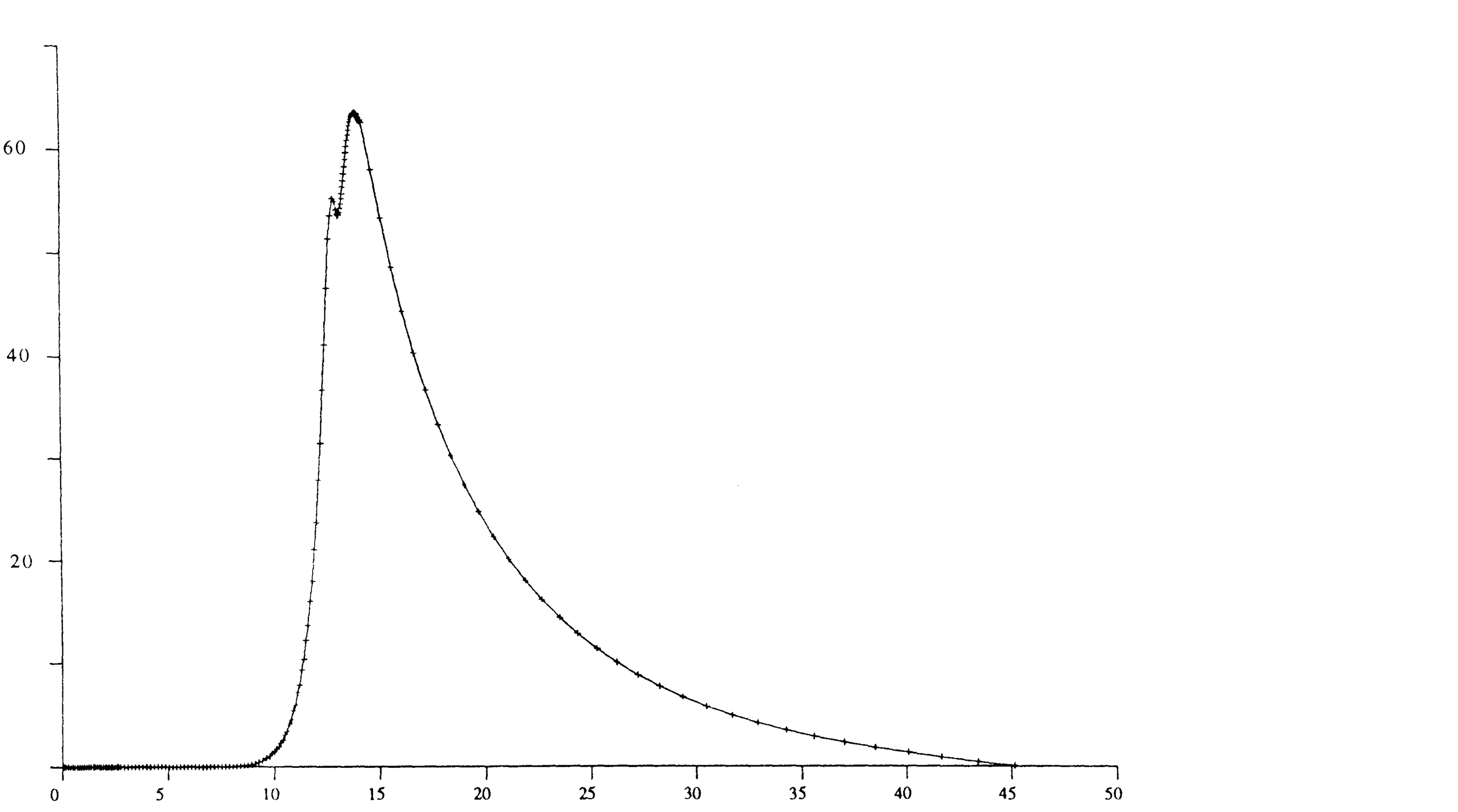

Fig. 4.9 ISS distribution (37° matrix crack)

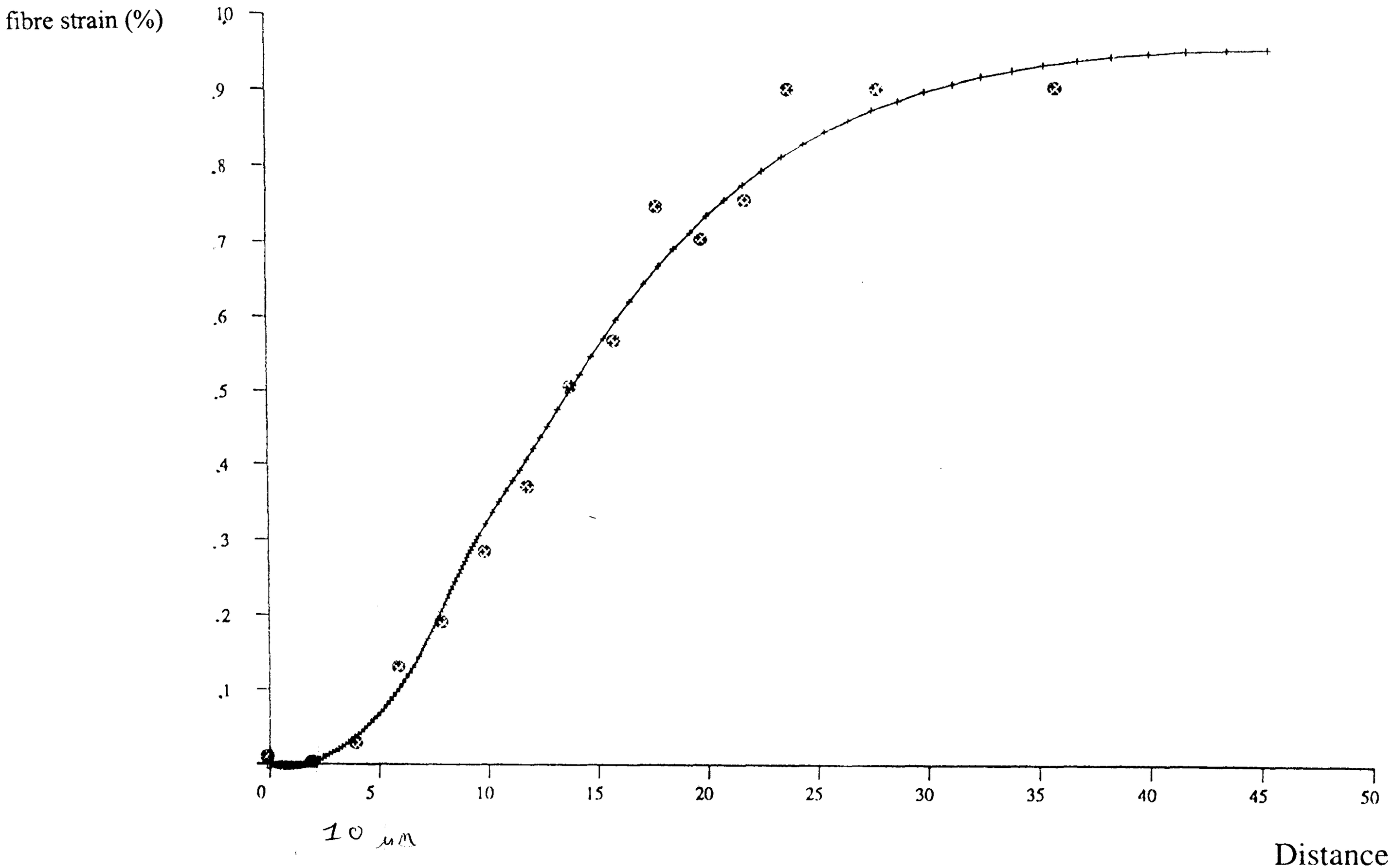

Fig. 4.10 Fibre strain distribution with LRS data (20° matrix crack; e_{app}=1.05%)

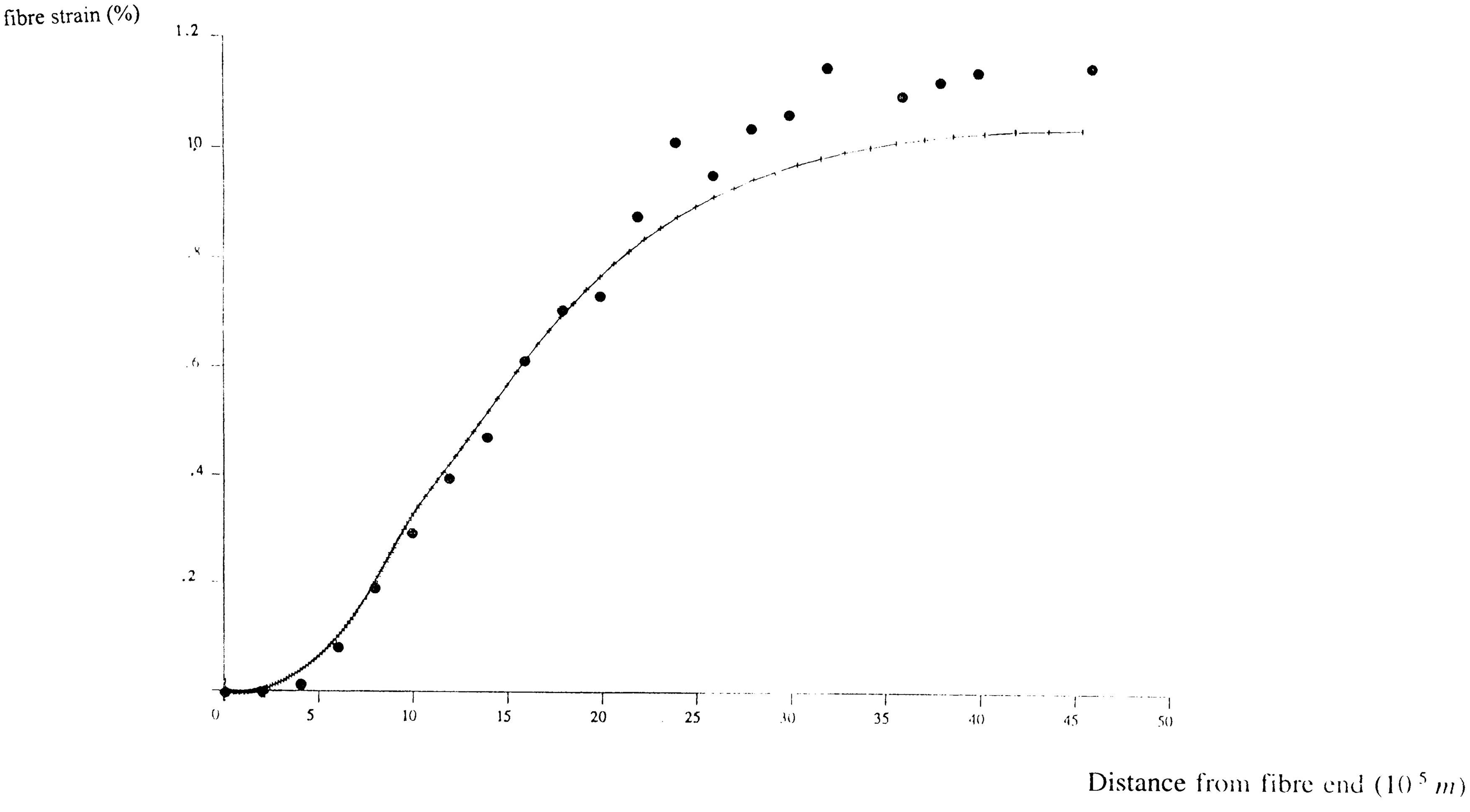

Fig. 4.11 Fibre strain distribution with LRS data (20^{o} matrix crack; e_{app}=1.15%)

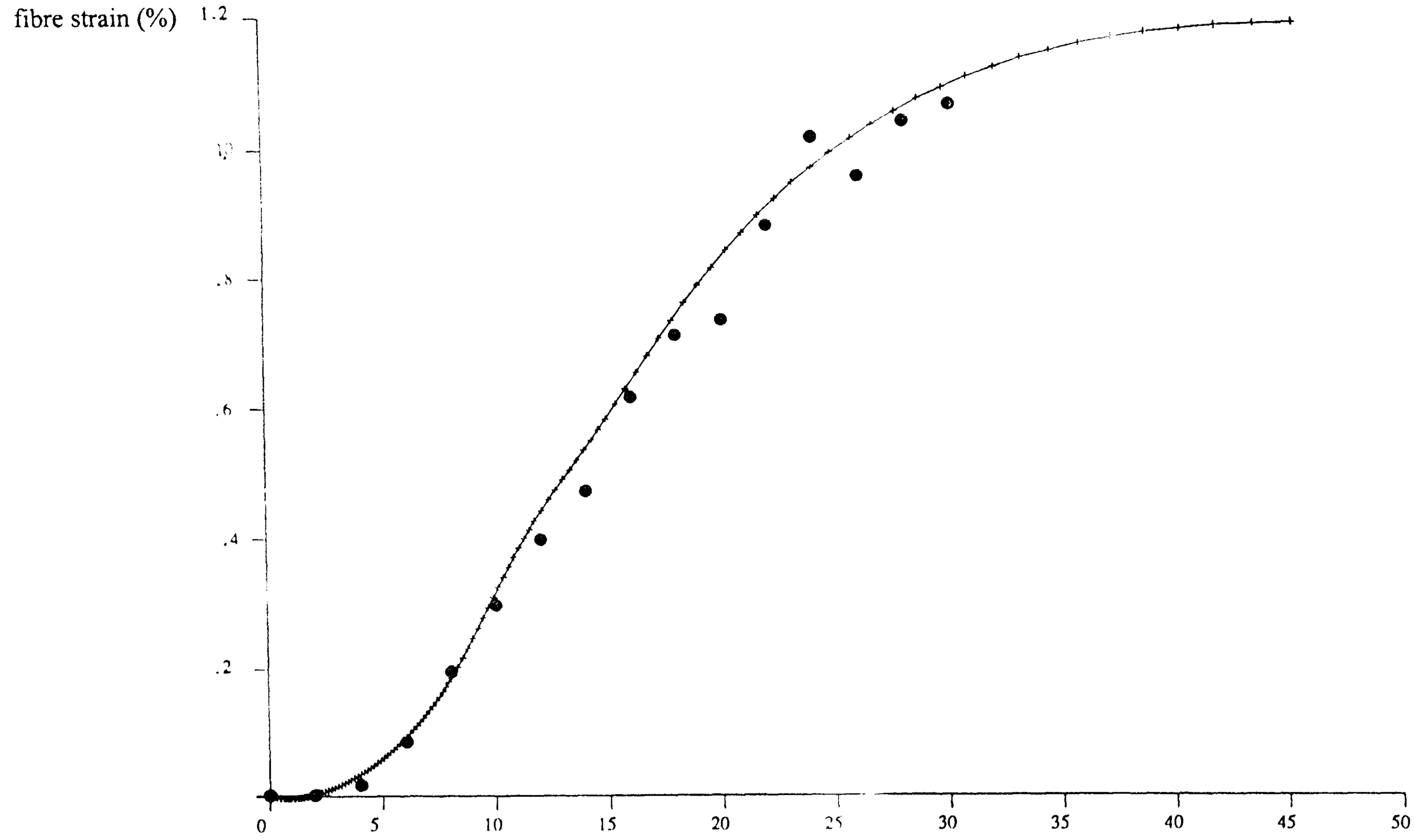

Fig. 4.12 Fibre strain distribution with LRS data (20° matrix crack; e_{app}=1.35%)

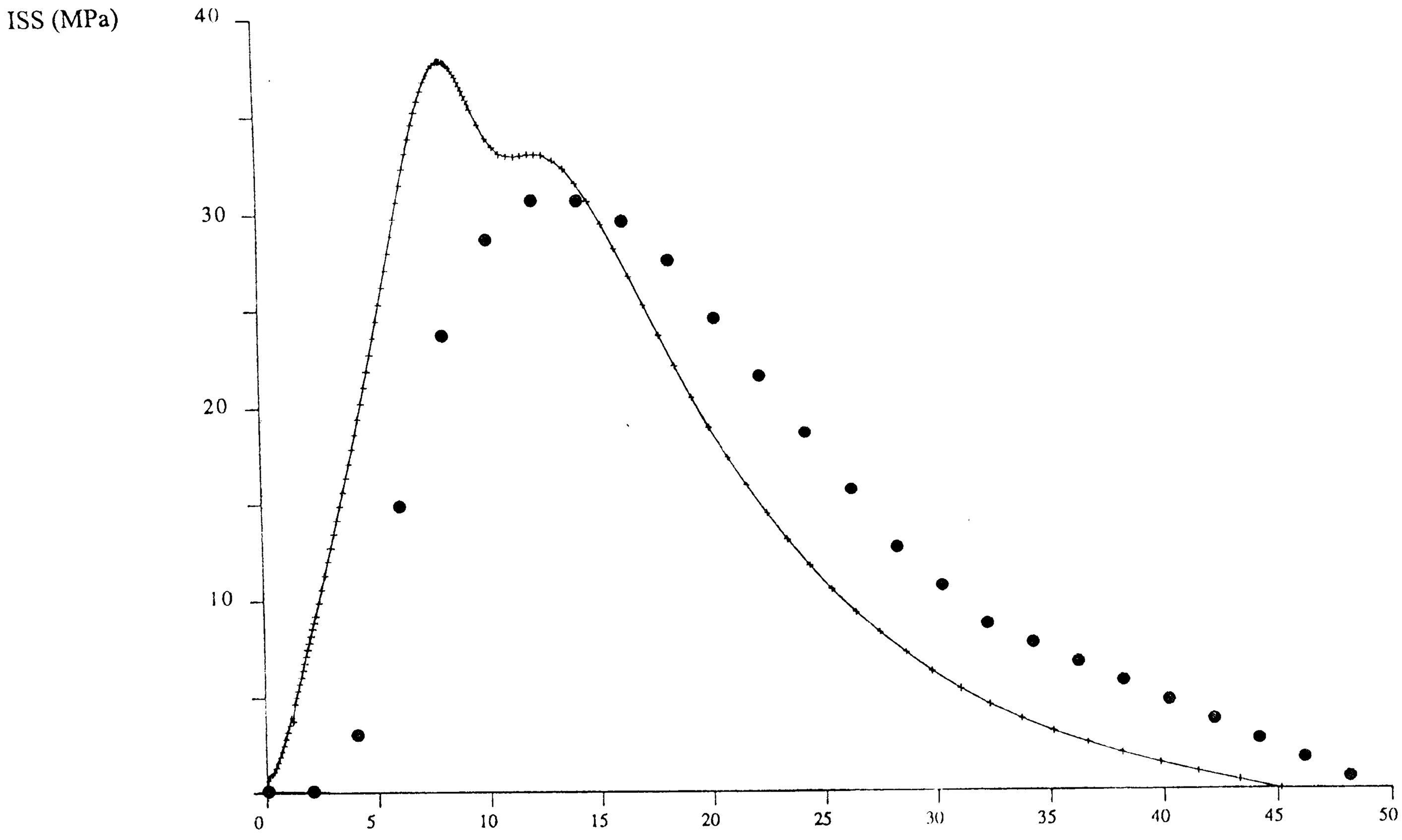

Fig. 4.13 ISS distribution with LRS data (20° matrix crack; e_{app}=1.05%)

Chapter 5

Kevlar-49 System and Fibre End Fibrillation

5.1 Introduction

In the consideration of short fibre composites reinforced with Kevlar 49 fibres, there is a fundamental property possessed by the fibres which is salient to the interfacial failure process. This property is the fibrillation of the fibre ends and occurs when Kevlar fibres are cut either with scissors or in an industrial chopping process. A Kevlar fibre cut in this manner has ends which are splayed out (Fig. 5.1), and not cleanly cut as in the case of a carbon fibre. The cutting process itself applies greatest shear stresses to the surface layers of the fibre, which in the case of Kevlar, causes extensive fibrillation of the fibre end [9]. The resultant *fibrillated zone* consists of numerous Kevlar fibrils interspersed with matrix, where the effective radius of the fibre is now larger whilst there is a corresponding *dilution* of the material properties of the fibre by those of the matrix. It will be shown that in short Kevlar fibre composites, fibrillation is responsible for localised matrix yielding at the fibre end (Mode α) as the chief interfacial failure mode, and that this mode is prevalent until significantly high levels of applied strain on the composite are reached. Consequently, the failure Modes β and γ which involve cracking of the interface at later stages of the failure progression, are suppressed until very high load levels are reached.

Guild *et al.* [9] have modelled a short Kevlar 49 fibre embedded in an elasto-plastic epoxy matrix, using FE analysis. Fair correlation between FE and experimental fibre stress data was achieved, but exceptionally high von Mises interfacial strains were predicted in the vicinity of the fibre end. These von Mises matrix strains were found to be much higher than is reasonable in a real composite specimen. For example, for an applied strain of 1.2%, a von Mises strain of 60% was predicted. A strain concentration was found to occur for both a rounded fibre end and a sharp corner, indicating that the geometric singularity inherent to the sharp corner was not the cause

of the von Mises strain concentration. The reason for such a high strain concentration was that account had not been taken of the real fibrillated nature of the fibre end geometry.

To account for this complex fibre-matrix interaction in the current study, two analytical fibre end fibrillation models (FEFM) have been developed in which the material properties are inhomogeneous. They are a one dimensional model, 1-D FEFM, in which the material properties of the fibrillated zone are considered to vary with axial coordinate, *z,* and a two dimensional model, 2-D FEFM, where the variation is both a function of axial and radial, *r,* coordinates.

5.2 Experimental Measurements at QMW

A short Kevlar 49 fibre-epoxy composite has been subjected to an incremental loading program and the fibre stress profile monitored using the LRS technique for various levels of applied strain [8-9]. The axial stress distribution after the instigation of interfacial failure, was found to be trapezoidal in shape until a relatively high value of applied strain on the composite. In Fig. 5.2, the applied strain is 1.0% and there is no significant deviation in the fibre stress profiles from the initial Cox type, indicating the absence of cracking at the interface. The interfacial shear stress was found to exhibit a plateau with a value of approximately 45MPa in the region of the fibre ends, and then decay to zero away from the fibre ends in a Cox type elastic manner (see section 1.4). The value of 45MPa corresponds to the shear yield stress of the bulk matrix, so support is given to the micrographic evidence which indicates that interfacial plastic deformation occurs as the applied strain on the composite is increased [8]. This suggests a *Mode* α interfacial failure is prevalent for the Kevlar 49-epoxy composite system. The fibres, supplied by Du Pont, were approximately 12μm in diameter and a Ciba Geigy LY5052/LY1927 epoxy resin was used. Full details of the manufacturing procedure are given in [8] and material properties are given in Table 5.1.

In this test, the composite was subjected to incremental tensile applied strains of 0.5%, 0.7%, 1.0% and 1.3%. The axial stress distribution along the length of the fibre was obtained for various levels of the applied strain, e_{app}. Values of axial stress in the fibre were considered for each point along one half of the fibre length, by averaging the experimental data at both ends of the fibre.

5.3 Finite Element Analysis

The axisymmetric FE model of the composite specimen covers one quarter of the diametral section, due to the symmetry of the problem (Fig. 5.3). The length of the fibre considered was 500μm and was chosen to be greater than the transfer length of the system [8]. The mesh consisted of approximately 4,200 3-noded triangular and 4-noded quadrilateral axisymmetric linear elements. The tensile loading took the form of a uniform displacement imposed on those nodal points lying on the end face of the composite.

Only the initial stages of the Progressional Approach were considered, since the experimental observations indicated a yielding mechanism of failure for the Kevlar system for applied strains below 1.0%. Thus the more advanced crack initiation and propagation stages of the Progressional Approach were not considered. The thermally induced fabrication stresses were modelled by a uniform temperature drop of 50°C applied to all nodes in the FE model in the initial load step. The tensile loading was subsequently applied in incremental steps corresponding to the experimental applied strain levels (Section 5.2).

The material properties for both fibre and matrix are given in table 5.1. The matrix is assumed to exhibit perfect plasticity after a von Mises equivalent strain of 4.2% has been reached. The corresponding tensile yield stress at this value of strain was 78MPa. The matrix was modelled as isotropic and the fibre was assumed to be elastic and transversely isotropic. Since polymers exhibit substantial viscoelasto-plastic behaviour, the *relaxed* stress-strain behaviour was modelled. The matrix, over the

duration of the experiment, undergoes stress relaxation, thus reducing its effective elastic modulus at room temperature. The final relaxed tensile yield stress was taken to be 31MPa [41], as shown in Fig. 5.4, corresponding to 40% of the unrelaxed value, which is thought to be representative of the extent of matrix relaxation.

An initial confirmation of the plain (unfibrillated) fibre end, as modelled by Guild *et al.*, was made. The fibre was modelled with a rounded corner, as shown in Fig. 5.5.

A four finite-size cylinder discretisation of the fibrillated zone was made according to the 1-D FEFM (see equations D.1, Appendix D). Each cylinder was assigned elastic moduli calculated using a mean r_{cyl} for the respective cylinder. A five by four discretization of the fibrillated zone was subsequently modelled, according to the 2-D FEFM (see equations D.2, Appendix D). In this analysis, the modelling of the radial variation of the elastic moduli was achieved by each of the four cylinders used in the 1-D FEFM model being subdivided into five concentric rings. The assignment of elastic moduli to each ring was then based on the mean radius for the respective ring. All cylinders and rings were modelled as transversely isotropic, in line with the assumptions of the FEFM which account for the transverse isotropy of the fibre component. The calculated elastic moduli for the cylinders and rings are given in Appendix D.

5.4 Results and Discussion

5.4.1 Plain fibre end model

The von Mises strain concentration which occurs in the interfacial matrix adjacent to the fibre corner is 200% for e_{app} of 1.0%, as shown by the von Mises strain distribution along the interface (Fig. 5.6). The reason for the substantial increase in this value, in comparison with the Guild *et al.* result of 30% for the same model, is probably due to the higher degree of mesh refinement in this area of high strain gradients. A typical mesh element dimension in this region was 2μm in the Guild model, whereas it is 0.4μm in the current analysis.

Due to this high von Mises strain concentration, a violation of criterion III (see section 2.4) has occurred, thus invalidating these FE stress and strain fields as being a solution to the interfacial failure problem, for the Kevlar-epoxy system. This result confirms the inadequacy of the plain fibre end model in predicting the state of stress and strain in the real loaded Kevlar fibre composite undergoing interfacial failure.

5.4.2 One-dimensional FEFM

The initial thermal pre-load results in the matrix contracting around the stiff fibre, by virtue of the large thermal expansion coefficient differential between the matrix and fibre. This matrix contraction induces minor localised matrix yielding at the fibre corner, as shown by the contour map of von Mises strain, Fig. 5.7. The fibre is consequently put into slight compression. The induced von Mises strain maximum at the fibre corner was 4%.

The subsequent tensile loading on the composite results in the deformed mesh as shown in Fig. 5.8, where the gradual non-uniform deformation of the fibrillated fibre end is clearly observed. A von Mises strain map, (Fig. 5.9), exhibits a maximum in the matrix near the fibre corner of 7%, for an e_{app} of 0.5%. This is more clearly observed in the interfacial von Mises strain distributions along the fibre (Fig. 5.10).

The importance of the thermal pre-load in reducing von Mises strain concentrations, may be understood with reference to Fig. 5.11, where the interfacial shear strain distributions are presented (E12 being the in-plane shear strain). The thermal pre-load induces a shear strain in the matrix at the interface (Fig. 5.11), in a direction opposite to the mesh deformations of Fig. 5.8. When subsequent applied strains are imposed on the thermally prestrained composite, shear strains opposite to the thermal shear strains are observed. Thus, a shear strain *reversal* has occurred. This effectively means that the thermal pre-load reduces the von Mises strain concentration of any subsequent tensile loading, by an amount approximately equal to that generated by the thermal pre-load alone. This result has also been found by other authors [31].

5.4.3 Two-dimensional FEFM

The von Mises strain map of the fibre end region after the application of thermal pre-load and a subsequent applied strain of 0.5% (Fig. 5.12), exhibits a similar pattern as in the 1-D FEFM model except that the von Mises strain concentration has reduced in value from 7% to 6%. There is also marginally more yielding within the fibrillated zone than before. The stress and strain fields are indicative of a Mode α interfacial failure mechanism. Since little difference is observed between the stress and strain fields predicted by the 1-D and 2-D models, it may be concluded that the precise radial variation of elastic modulus within the fibrillated zone is a non-essential parameter. Thus the sensitivity of the overall solution with respect to the radial discretisation of the fibrillated zone will be minimal.

The axial stress distributions for e_{app} of 0.5% and 0.7% (Fig. 5.13), show very good correlation with the experimental data along the fibre length. For the higher levels of e_{app} of 1.0% and 1.3% (Fig. 5.14), however, there is a substantial discrepancy between the experimental data and the FE predicted profiles. The reason for this discrepancy is due to the fact that a more advanced stage of the interfacial failure process has been reached which involves interfacial cracking. This may be appreciated with reference to the values of maximum von Mises strains induced at the fibre end. For the four levels of applied strain of 0.5, 0.7, 1.0 and 1.3%, the values of the maximum von Mises matrix strain (see Fig. 5.10) are 6% 10%, 37% and 72%, respectively. By substituting these values into the crack initiation criterion (Equation 2.2), it is clear that the last two values fail the criterion by a significant margin, thus indicating the initiation of an interface crack at the location of the fibre corner, since the matrix will effectively rupture at this level of applied loading on the composite. Thus, Mode α failure is prevalent for applied strain levels below 1.0% whereas it is more complex for applied strains in excess of 1%.

The way in which fibrillation reduces the fibre end strain concentration may be ascertained by the consideration of a small element of matrix adjacent to the interface near the fibre corner, refer Fig. 2.3. This element is being sheared by the action of the tensile loading and the stiff fibre resisting the load. Since the fibrillated fibre end

modulus is comparable to that of the matrix, the fibre end itself deforms significantly in a non-uniform manner (Fig. 5.8), effectively reducing the amount of shearing on the matrix element than would otherwise be induced without the existence of such fibrillation. This is evident as observed by the reduction in the strain concentration from 200% in the plain fibre end model, to 37% in the fibrillated fibre model, for the same level of applied strain (1.0%). By comparison with the carbon fibre system in which fibrillation does not exist, the same element of matrix would be subjected to substantially higher levels of shear, which would lead to the early onset of crack initiation, as will be the subject of Chapter 6. Thus fibrillation, in reducing the strain concentration at the fibre end that would otherwise exist, effectively *delays* the onset of interfacial fracture during incremental tensile loading.

It may be concluded that at the higher levels of applied strain, an *interfacial failure Mode transition* is occurring from pure Mode α to a mixture of Mode α with Mode β or γ. This transition is suppressed and occurs at a higher applied strain level than in the carbon fibre system, due to the existence of Kevlar fibre-end fibrillation. Thus, purely Mode α interfacial failure is prevalent in the Kevlar system for applied strains of up to 1%, which are representative of the normal service loads that a composite is likely to be subjected to. The failure modes involving interface fracture are not observed within this loading range for Kevlar fibre systems, but are characteristic of carbon fibre systems for the same loading range.

	Kevlar 49 fibre	LY5052/1927 Matrix (relaxed properties)
Axial Tensile Modulus, GPa	115	1.78
Transverse Modulus, GPa	7	1.78
Axial Tensile Strength, GPa	3.6 *(fracture)*	31×10^{-3} *(yield)*
Axial Fracture Strain, %	2.9	4.2
Axial Poissons Ratio	0.40	0.36
Transverse Poissons Ratio	0.33	0.36
Axial CTE*, /K	-5.2×10^{-6}	58×10^{-6}
Transverse CTE*, /K	41.4×10^{-6}	58×10^{-6}

* Coefficient of Thermal Expansion

Table 5.1. Material Properties of Kevlar-49 Fibre and Epoxy Matrix

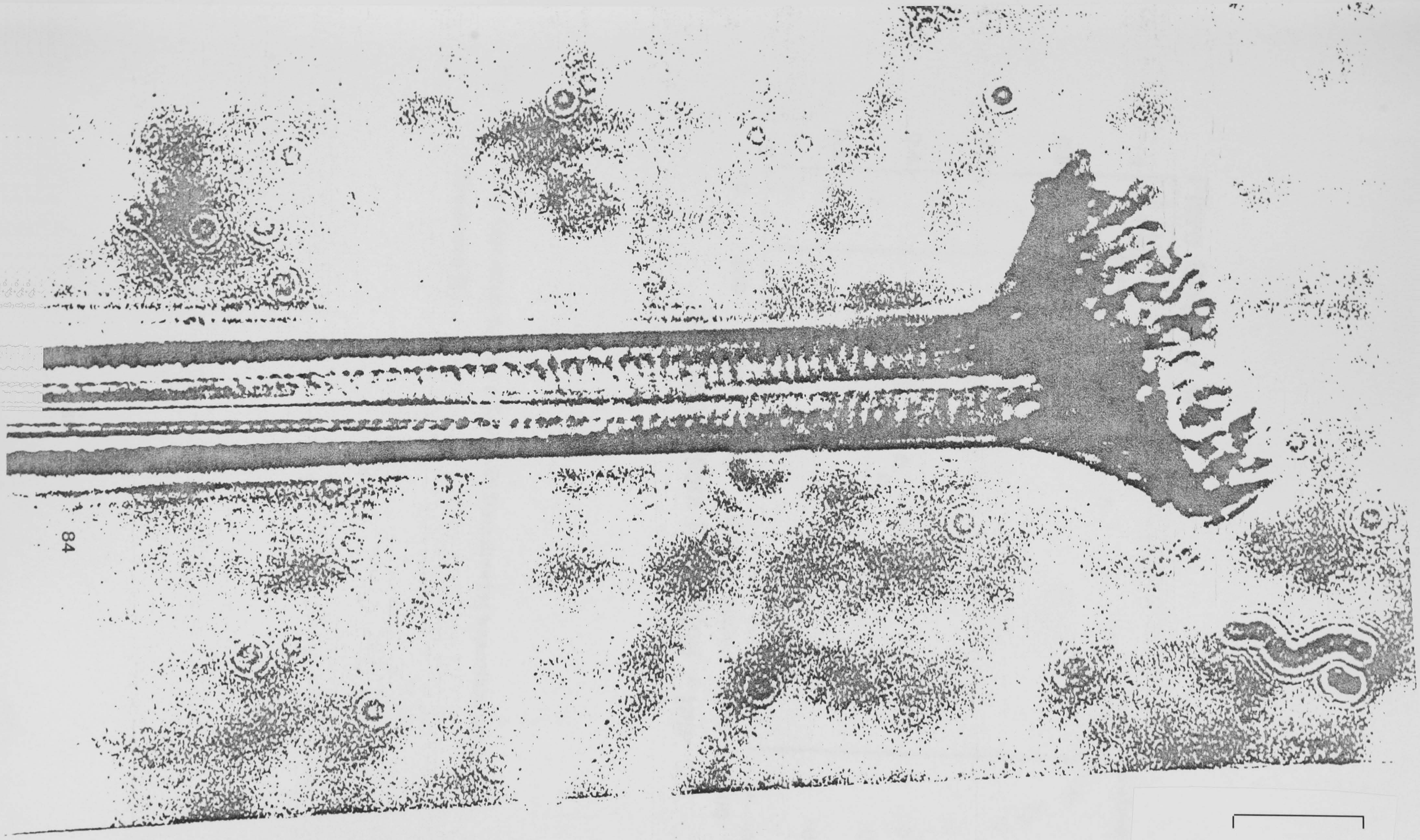

Fig. 5.1 Micrograph of Kevlar-49 fibre end showing extent of fibrillation [courtesy C. Galiotis]

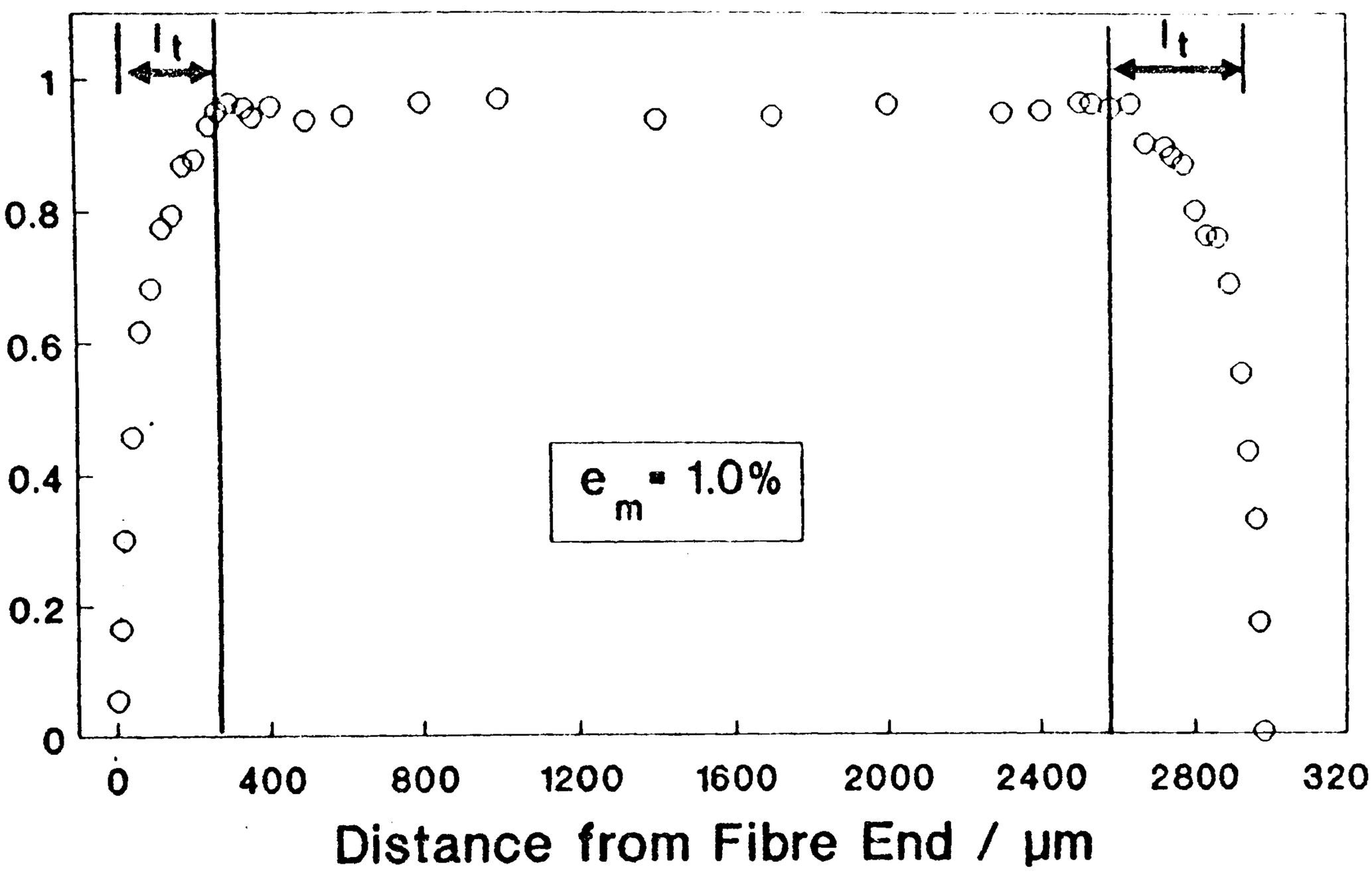

Fig. 5.2 LRS fibre strain data for a Kevlar-49 fibre showing trapezoidal nature of distribution [8]

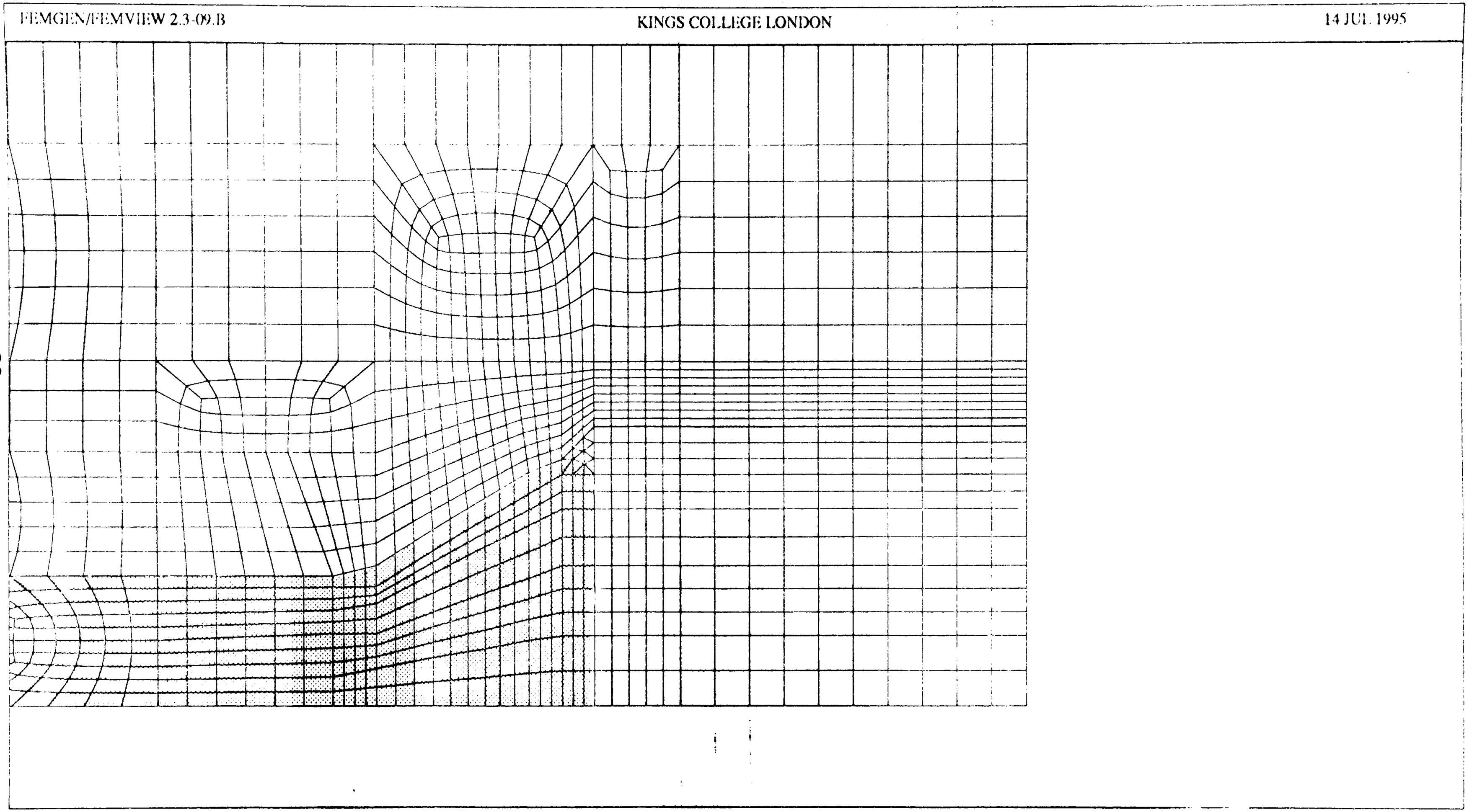

Fig. 5.3 FE mesh of fibrillated fibre end modelled according to 1D-FEFM and 2D-FEFM models

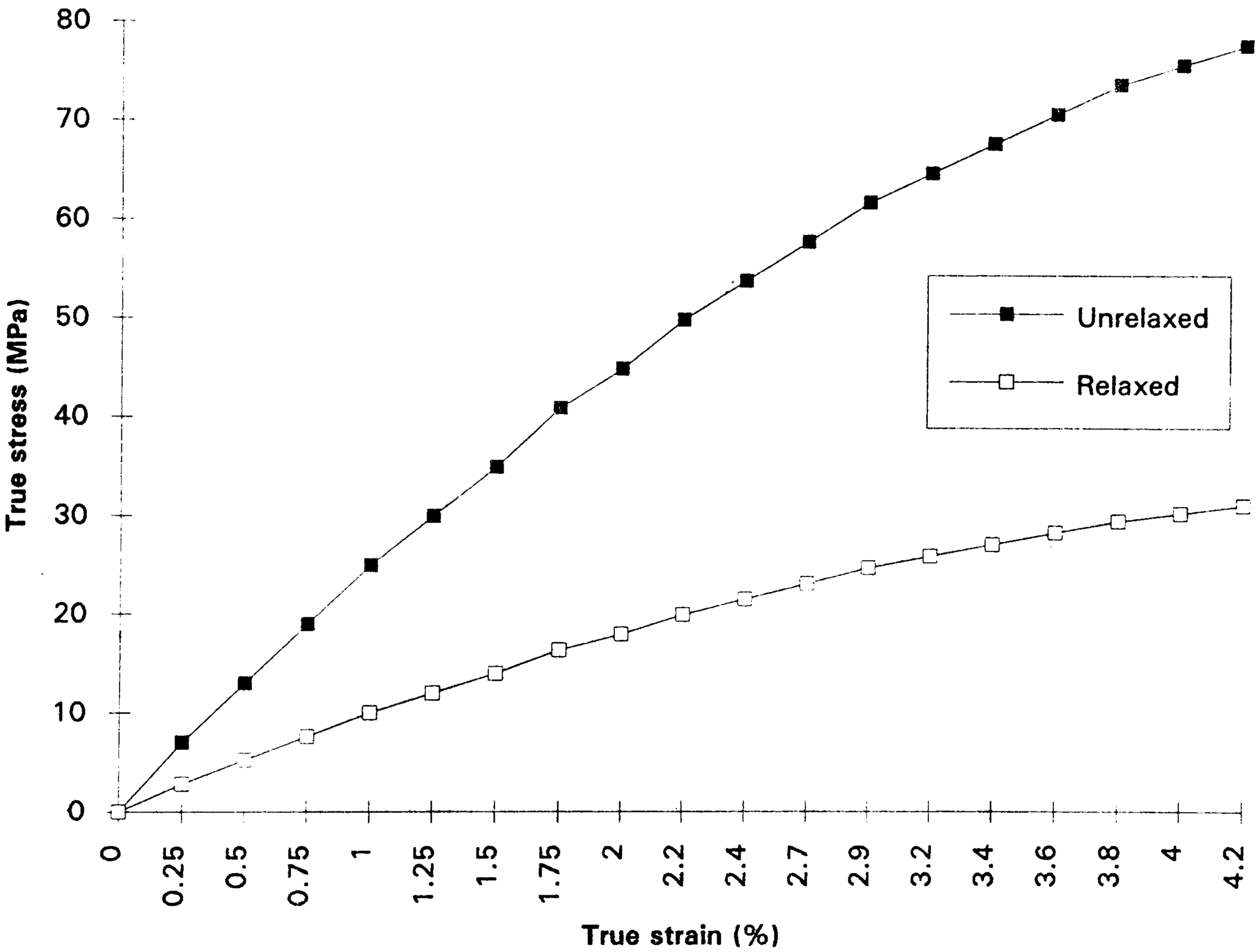

Fig. 5.4 Measured unrelaxed stress-strain curve for epoxy matrix; the derived relaxed response is also shown

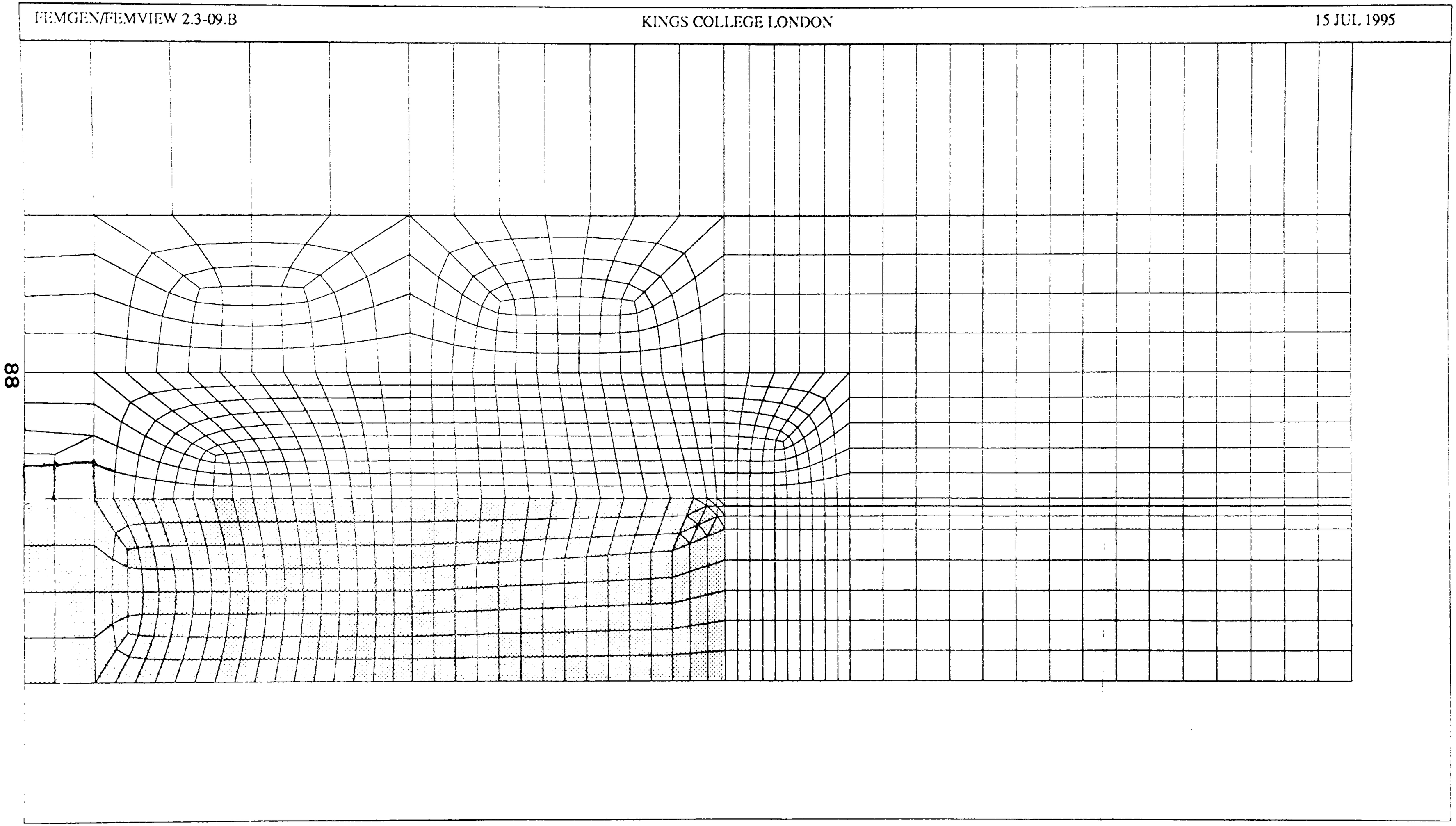

Fig. 5.5 FE mesh of plain fibre end model

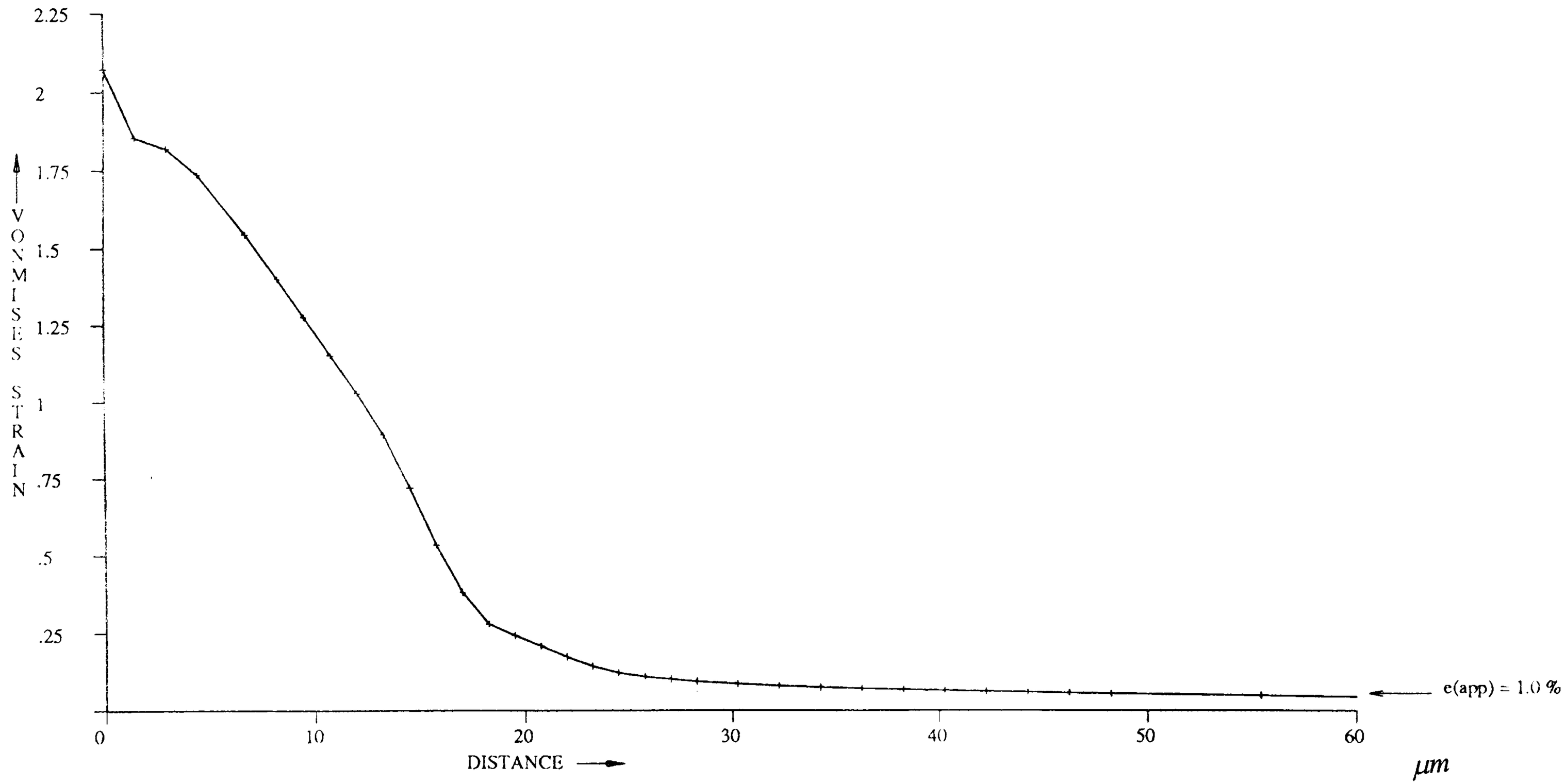

Fig. 5.6 von Mises strain distribution along interface showing strain concentration (Plain fibre end model)

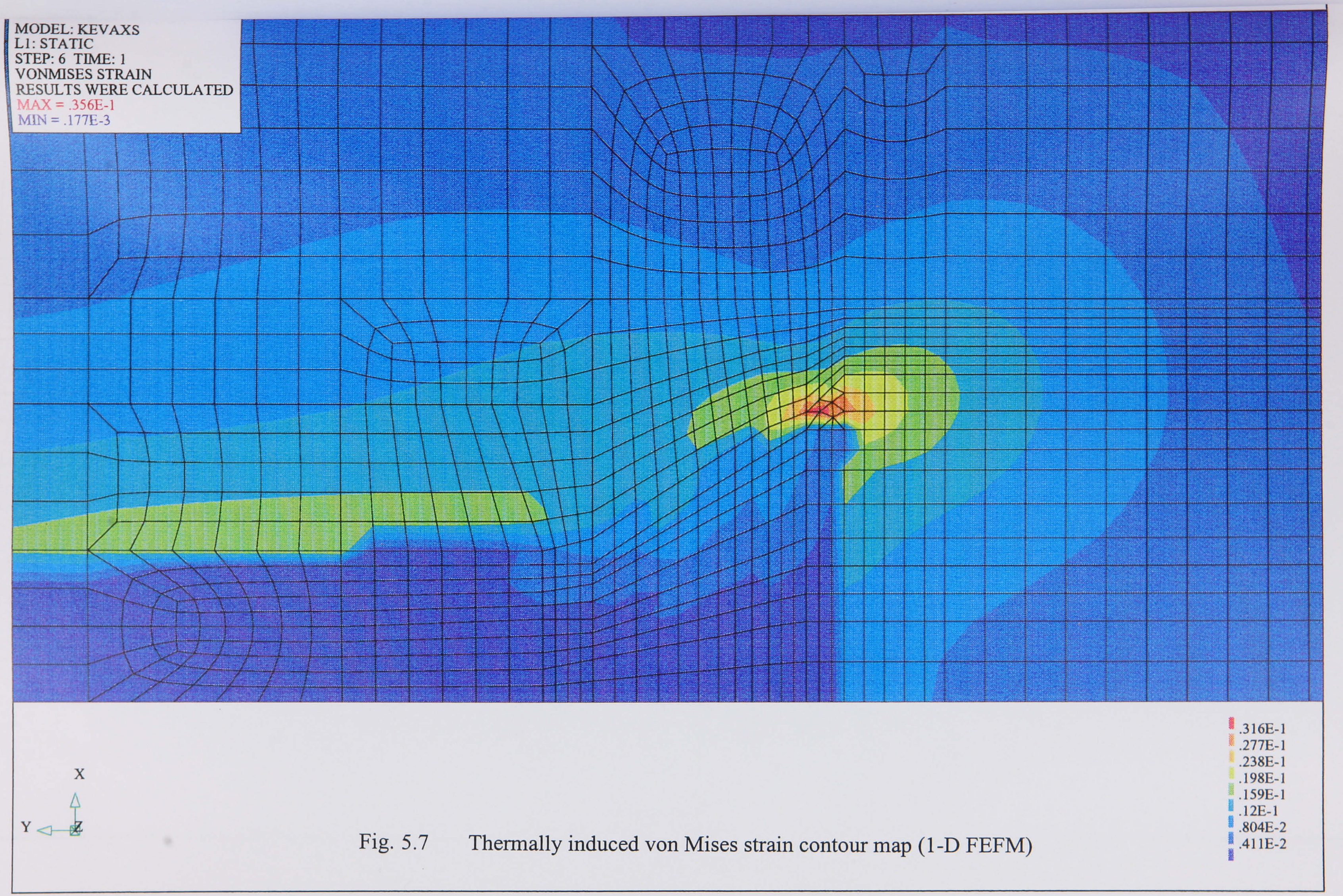

Fig. 5.7 Thermally induced von Mises strain contour map (1-D FEFM)

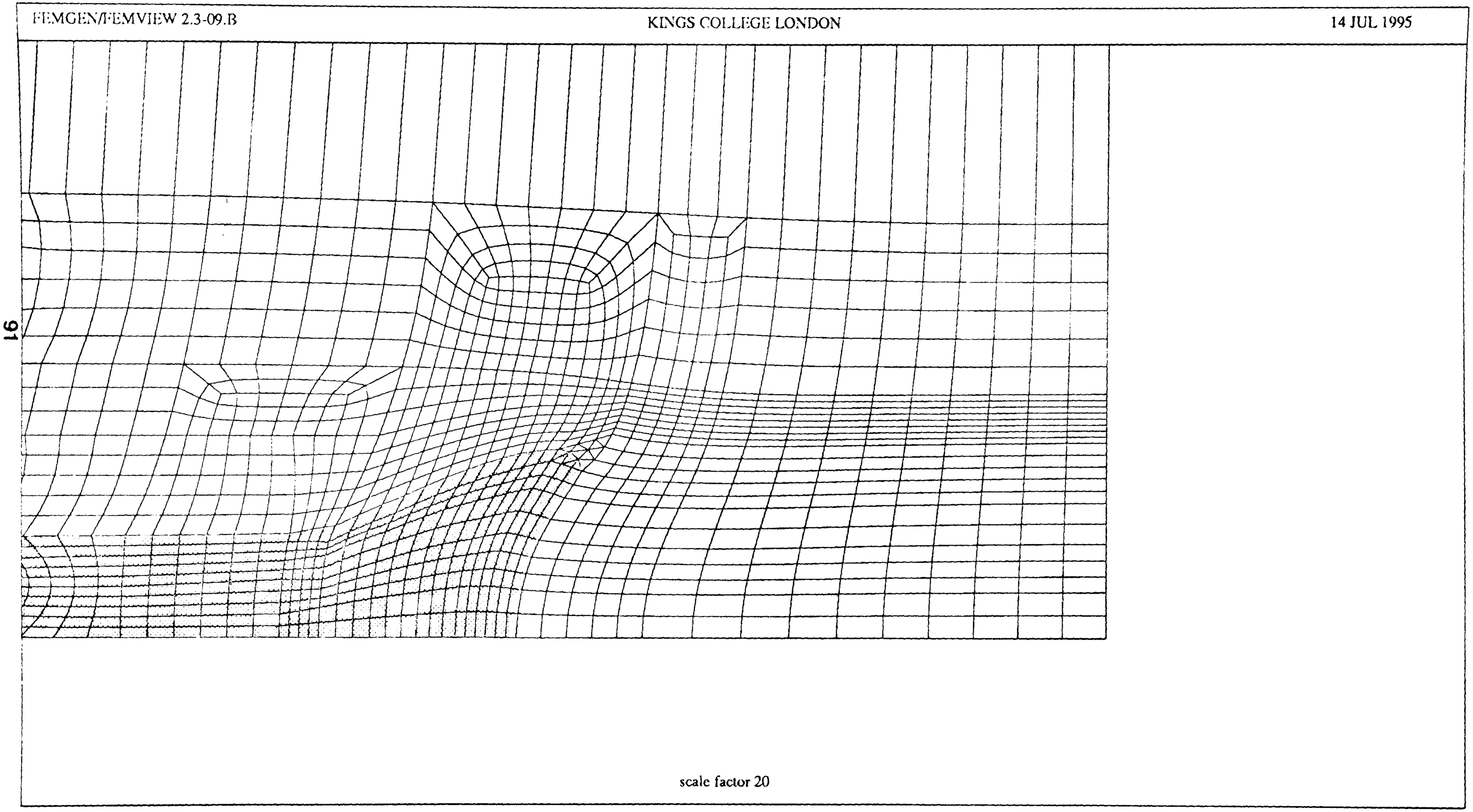

Fig. 5.8 Deformed mesh with applied tensile strain of 0.5%(1-D FEFM)

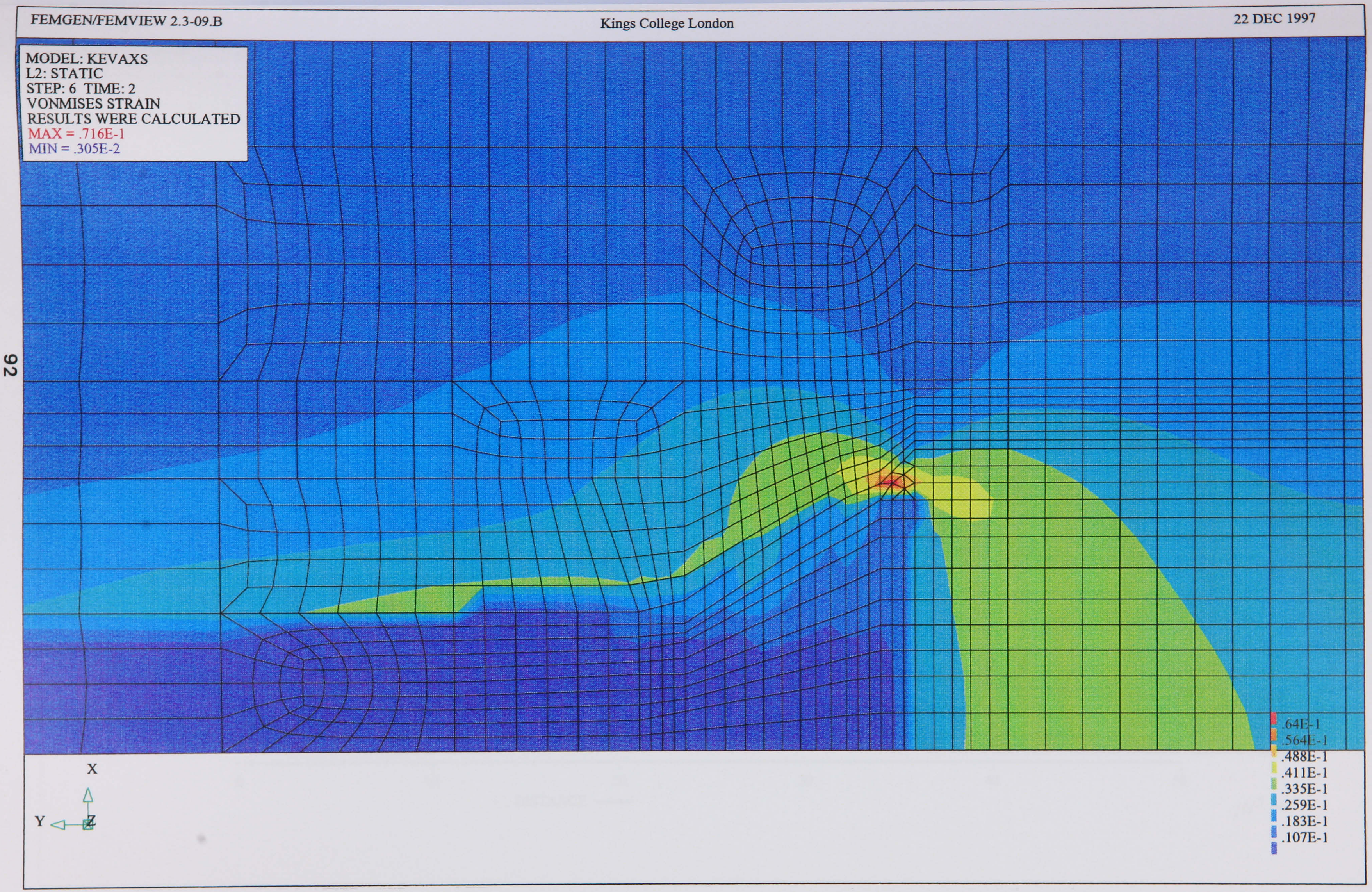

Fig. 5.9 von Mises contour map with applied tensile strain of 0.5% (1-D FEFM)

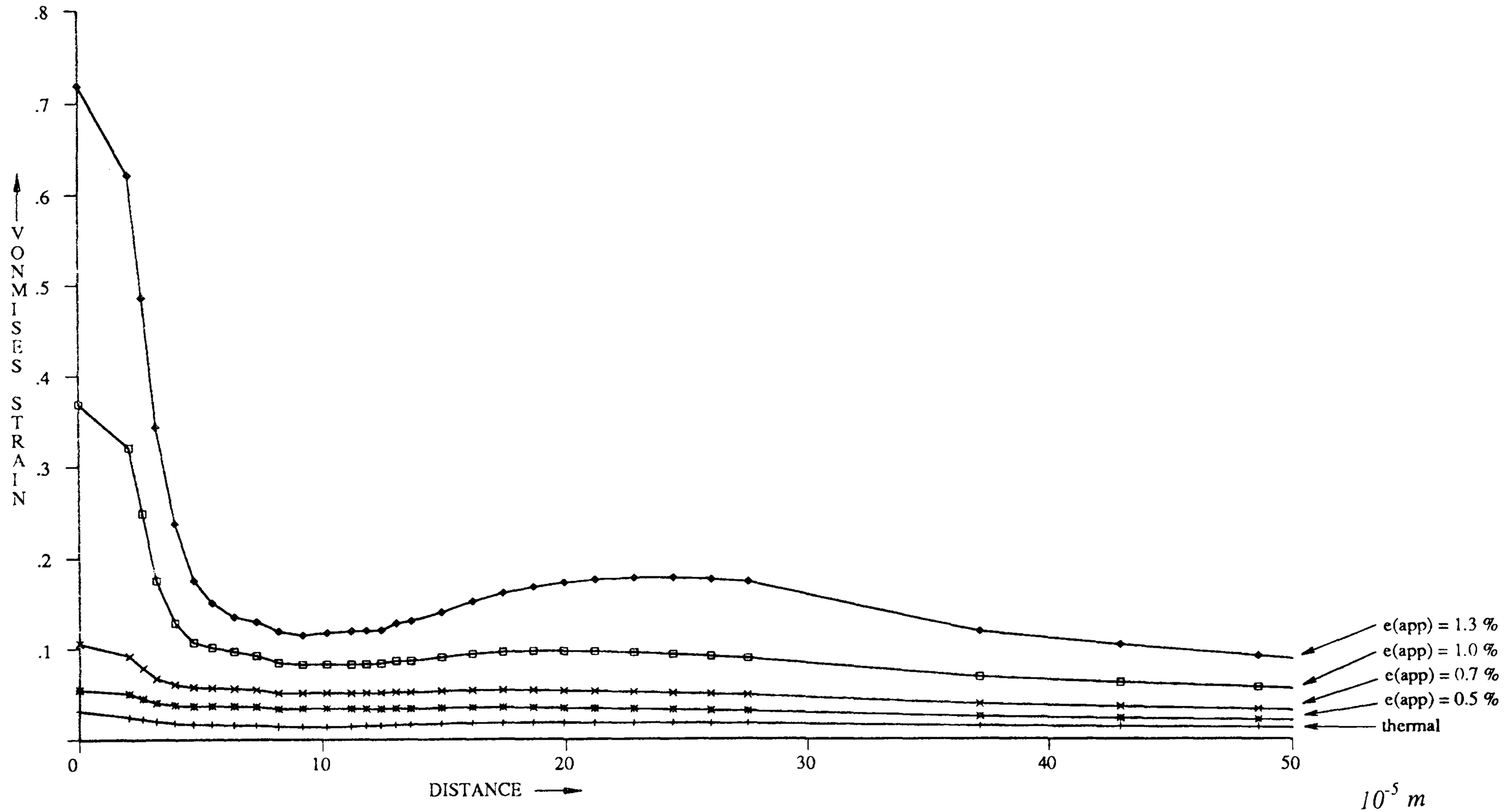

Fig. 5.10 von Mises strain distributions along interface for multiple applied strains

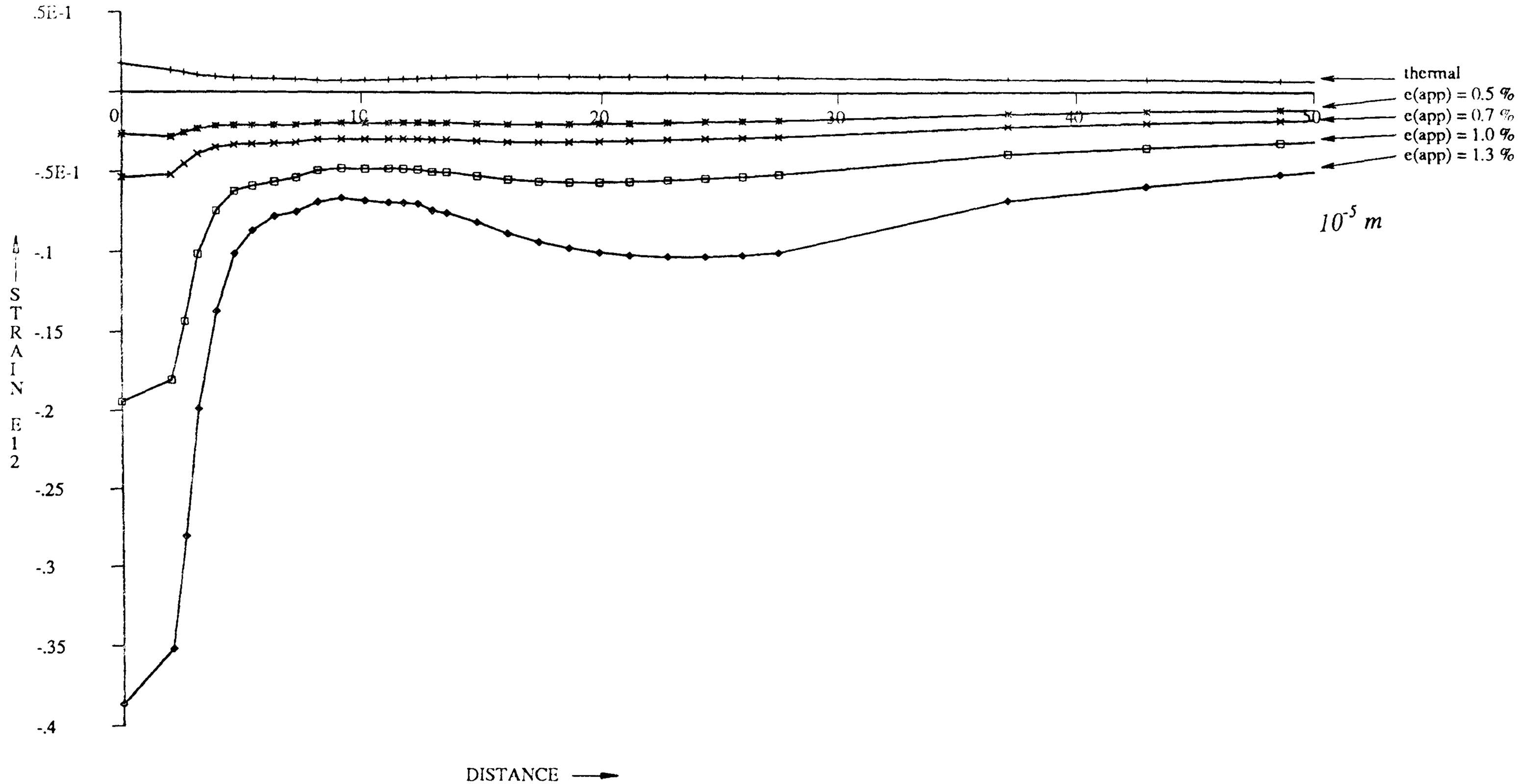

Fig. 5.11 shear strain distributions along interface for multiple applied strains

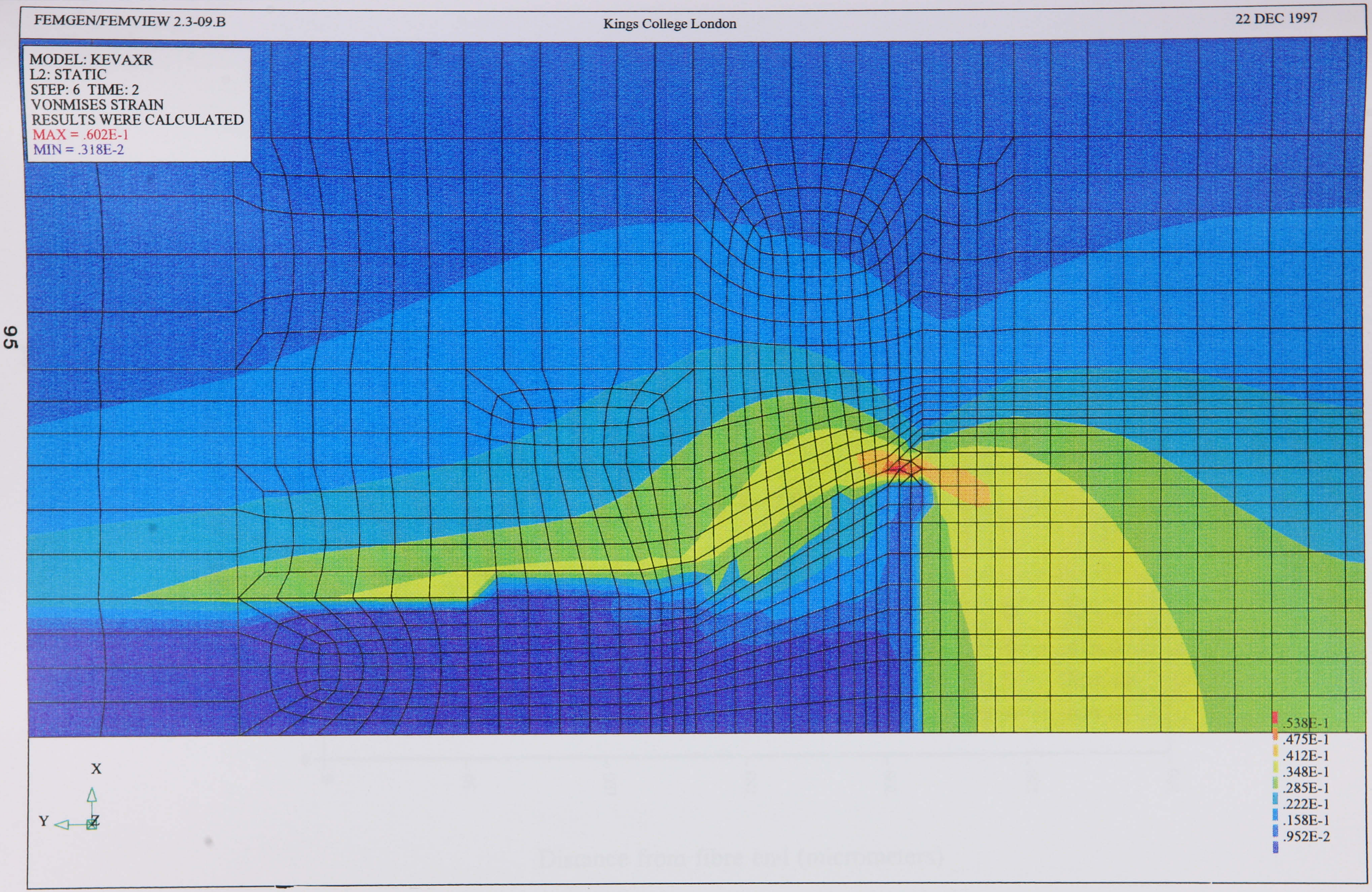

Fig. 5.12 von Mises contour map with applied tensile load of 0.5% (2-D FEFM)

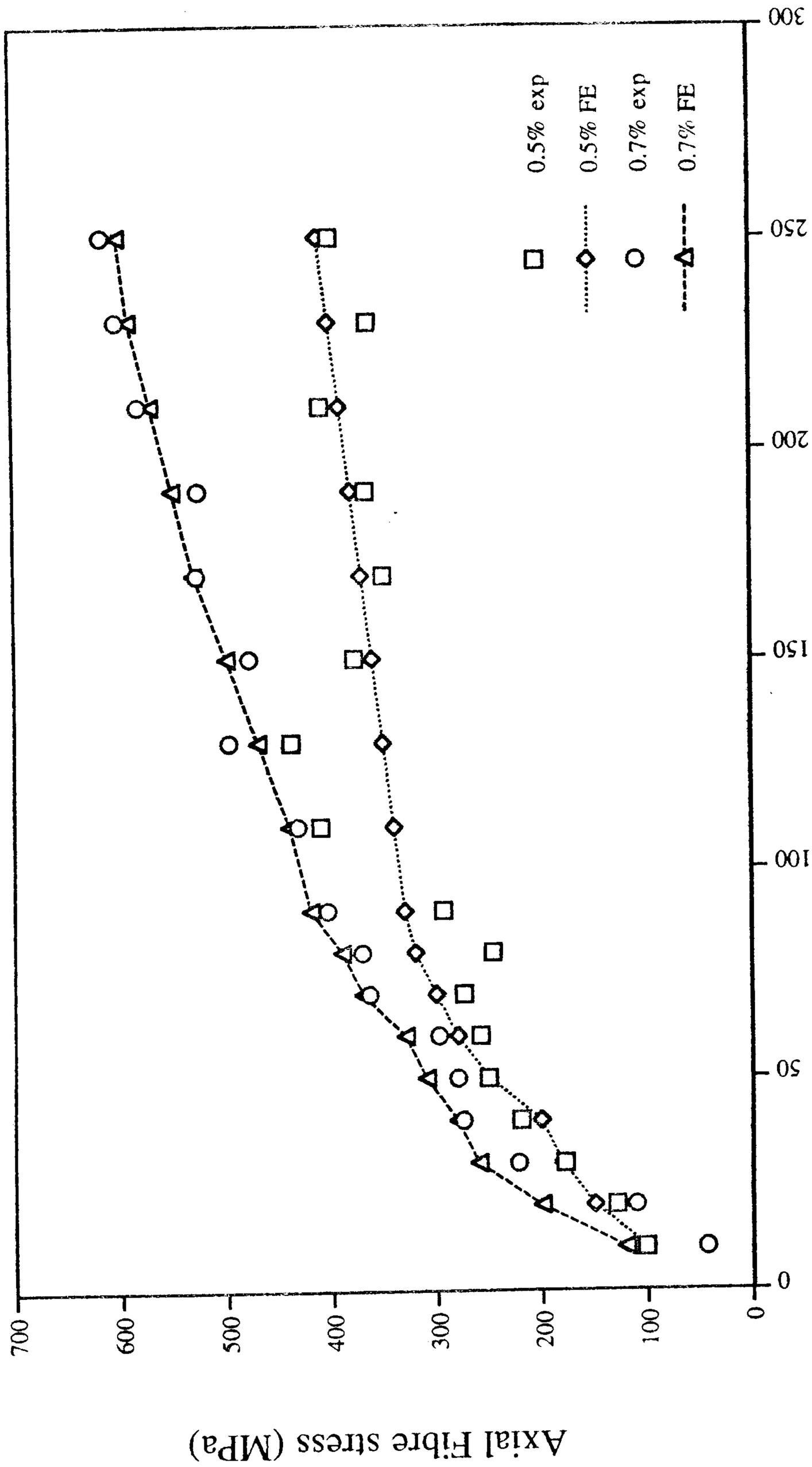

Fig. 5.13 FE and LRS fibre stress distributions along fibre for applied strains of 0.5% and 0.7%

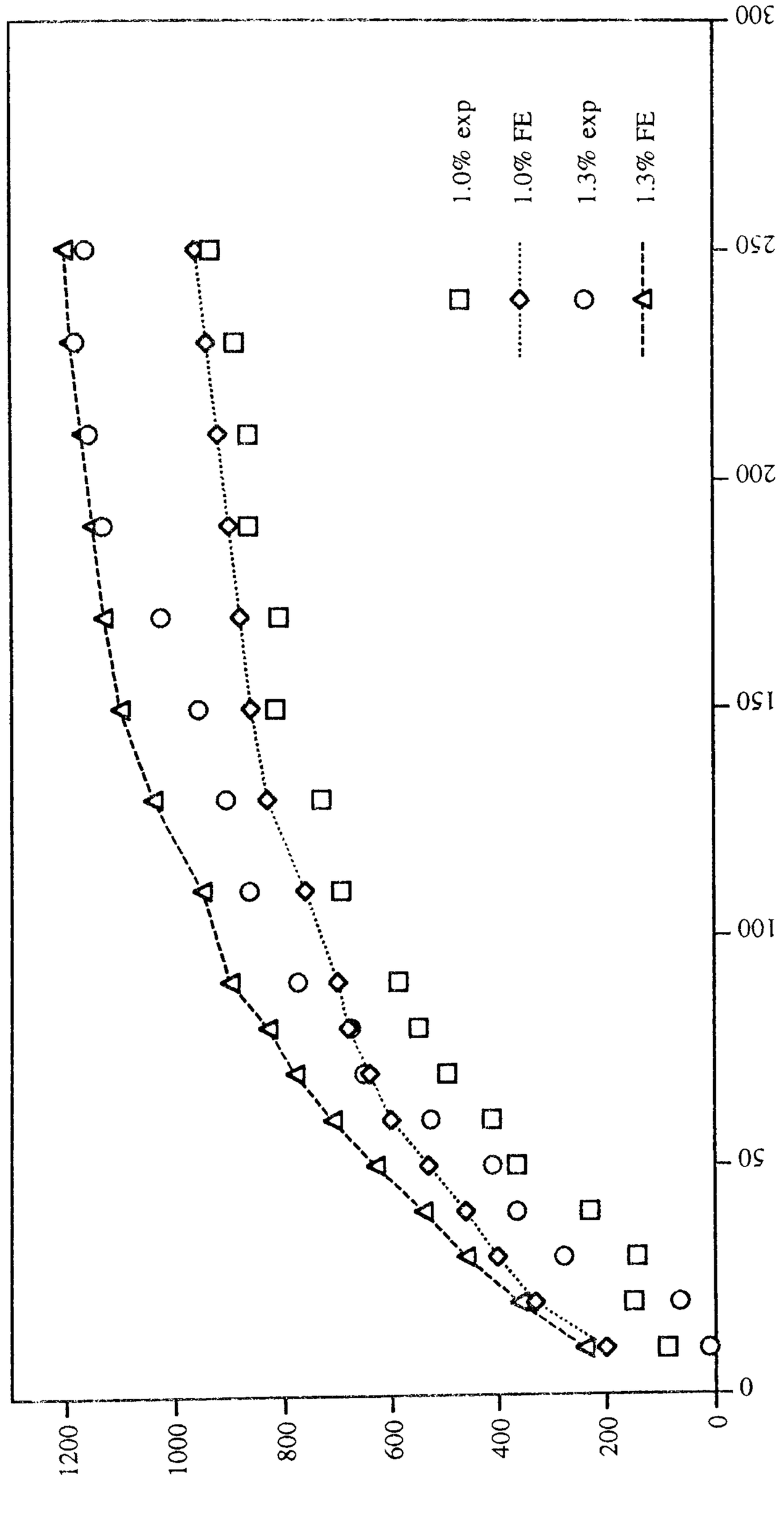

Fig. 5.14 FE and LRS fibre stress distributions along fibre for applied strains of 1.0% and 1.3%

Chapter 6

Interface Crack Propagation

6.1 Introduction

The analysis of the interfacial failure progression in a short carbon fibre composite system subjected to tensile loading is complex in that all the stages of the interfacial failure progression must be considered. The analysis presented in this chapter will demonstrate that the stages of the Progressional Approach consist of the following stages: The thermal residual stress state is followed by the application of tensile loading in which a linear elastic stress transfer regime across the interface is prevalent. As the tensile loading on the composite continues, localised matrix yielding (Mode α) at the fibre end is induced until a point is reached at which an interface crack initiates, Mode β. This crack subsequently propagates along the interface in tandem with the incremental applied loading that is driving it. An experimental scanning-electron microscope micrograph of the fractured surface of a carbon fibre, whose interface has not been pre-treated with a sizing that would otherwise have increased the interfacial bond strength, is shown in Fig. 1.4. This clearly shows the interface crack that has developed as a result of the application of high tensile loading on the specimen.

During propagation of the crack, the cracked interface will be subjected to significant compressive stresses across it, arising from both the thermal stresses and as a consequence of the Poisson ratio differential between fibre and matrix. Due to the rough surface morphology of the cracked interface, frictional stresses will be induced where the fibre will attempt to recoil into its unloaded shape. There will hence be continued reinforcement of the matrix but through a frictional mechanism. Thus, under a frictional stress transfer regime, the fibre's reinforcement capability will be shown to be reduced but not eliminated, as the interface crack propagates. This is in direct contrast to a matrix crack, Mode γ, in which frictional stress transfer does not exist due to the opening mode of the matrix crack.

6.2 Finite Element Model

Approximately 4,500 four-noded quadrilateral axisymmetric elements were used to construct the model. The selection of linear 4-noded as opposed to quadratic 8-noded elements is due to their superior modelling of contact and interface problems [42]. The area of the FE mesh in the vicinity of the fibre end is shown in Fig. 6.1. Interface elements are defined along the fibre-matrix interface and, during the initial stages of loading, the interface is defined as perfectly bonded. However, during crack initiation and propagation along the interface, the interface element nodes become debonded and the two resultant crack faces are now able to interfere with each other, if the crack is 'closed', thus permitting the transmission of normal stresses. Furthermore, depending on the value of the coefficient of friction specified, shear stresses will be supported across the cracked interface and relative slipping may occur between the two crack faces. The Coulomb stick-slip friction model [43] is employed in this analysis.

The fibre is modelled as transversely isotropic linear-elastic, and the matrix as isotropic elasto-plastic. A table of the material properties is given in Table 6.1. The stress-strain curve for the epoxy matrix is given in Fig. 5.4, and corresponds to the low strain rate at which the LRS experimental measurements were made, which was of the order 10^{-7} s^{-1}. For such strain rates, the matrix undergoes viscoelastic stress relaxation and consequently the effective modulus for any given value of strain is substantially reduced [44, 45]. The FE analysis in this study therefore applies to elasto-plastic behaviour at low strain rates, since the relaxed matrix stress-strain curve has been employed. Additionally, given the geometry of the interface crack and the loading on the specimen, there are no areas of matrix in which the dilatational component of the stress tensor is compressive, thus the pressure dependency of matrix yield [46] is not significant in Mode β interfacial failure. This is not the case, however, in Mode γ failure where the geometry of the matrix crack creates large volumes of matrix in dilatational compression.

The FE loading history is highly non-linear in nature and consists of multiple load steps. An example of the ABAQUS input data file showing the various load-step definitions, is given in Appendix B. Initially, a uniform 50°C temperature drop is applied to all the nodes in the mesh to simulate the thermal curing effects induced during fabrication of the composite specimen. The subsequent tensile loading takes the form of a uniform displacement imposed on the nodes on the end-face of the model. After the application of a given level of applied strain, interface element nodes are then debonded at the fibre corner in the subsequent load step, thus simulating the initiation of a crack. During the debonding of interface nodes, a new solution for the stress and strain fields is found by the iterative solution procedure in ABAQUS which takes into account the fact that shear stress transfer across the interface is now only permissible through friction. Thus, a new displacement field is also iterated for, which accounts for the resultant relative slipping that occurs between the crack faces. Strain energy release rate calculations are then made at the two crack tips, using the well-known fracture mechanics path-independent contour J-integral developed by Rice [47].

The latter part of the loading history consists of alternate load steps of increments in the applied loading, followed by extensions of the crack length, which are achieved by specifying a new length of interface nodes to be debonded ahead of the existing crack. This type of procedure thus simulates crack propagation due to the increases in applied loading that precedes it.

Parenthetically, we may note that special crack tip elements, such as the ones designed by Barsoum [48-49], are not applicable to a bi-material interface crack. These elements are formed by either moving the mid-side nodes to the quarter points [48], or preferably by collapsing one side of a quadrilateral element [49], thus imposing a $(1/\sqrt{r})$ singular stress field for the linear elastic case (Westergaard-Irwin solution [50]), or a $(1/r)$ singularity for the elastic-perfectly plastic case (Rice-Rosengren solution [51]). Such crack tip elements are intended for use in the case of a crack in a homogeneous material.

6.3 Results and Discussion

6.3.1 Thermal and initial tensile loading stages

The initial thermal loading, caused by the temperature drop during the fabrication process, puts the fibre into compression, since the matrix has a higher coefficient of thermal expansion than the fibre. The contraction of the matrix around the fibre also induces localised yielding at the fibre end (Mode α), as shown by the contour map of von Mises strain in Fig. 6.2. The maximum von Mises strain is about 15% occuring at the fibre corner, but this does *not* lead to crack initiation in accordance with the crack initiation criterion of Section 2.3.4. This is because the dilatational component of the strain tensor is compressive throughout the matrix, as shown by the contour map of the pressure strain component (negative dilatational strain) in Fig. 6.3. Subsequent tensile loading of the specimen puts the fibre into tension, and at an applied strain of about 0.3% on the composite, the localised yielding in the matrix reaches a value of strain that violates the crack initiation criterion (equation 2.2). A von Mises strain map for this situation is shown in Fig. 6.4(a) in which a maximum strain of 8.5% is observed in the matrix adjacent to the fibre corner. Fig. 6.4(b) shows the pressure component of strain, which is revealed to be tensile in the matrix region adjacent to the fibre end, thus supporting conditions for local matrix rupture due to the yielding. Thus, until this point in the failure process, a Mode α interfacial failure regime has been prevalent.

6.3.2 Crack initiation and propagation stages

Initiation of an interface crack is modelled by the debonding of interface element nodes in the vicinity of the fibre corner. The consequent strain concentrations, as expected, occur at the two crack tips (Fig. 6.5), one of which is oriented towards the interface and the other towards the fibre end. Strain energy release rate evaluations were made at both crack tips using the J-Integral facility in ABAQUS [42]. The crack tip at the fibre end was found to have a SERR of about five times that of the interface tip. In accordance with the crack propagation criterion (equation 2.3), we conclude that the end tip propagates first thus completely debonding the fibre end, as shown by

the deformed mesh of Fig. 6.6. It may be considered that the fibre-corner crack is therefore a *transitional* state, and hence that the fibre end *instantaneously* debonds when a given amount of matrix yielding occurs in the fibre end vicinity. Thus we have an *interfacial failure mode transition* in which the Mode α regime has developed into a mixture of Mode α and β.

The interface crack, propagating in tandem with the applied load incrementations that are driving it, may be observed in the deformed mesh of Fig. 6.7, where the crack shown is of length 10μm. The shearing effect of the fibre on the more compliant matrix at the cracked interface is also evident. The matrix elements immediately adjacent to the fibre are observed to possess a significant shear strain, if the deformed mesh (solid lines) is compared with the undeformed mesh (dashed lines). Also, from the relative displacements of the matrix and fibre elements at the interface, relative slipping of the cracked interface is clearly observed, highlighting the 'stick-slip' nature of frictional stress transfer.

The choice of the value of coefficient of friction was based on FE-predicted fibre stress distributions obtained during a parametric analysis. In this preliminary analysis, the influence of a propagating interface crack on the fibre stress distribution was investigated for various values of the coefficient of friction. The interface crack was initiated and propagated according to the same non-linear loading history as in the main analysis. The interface crack lengths considered were 10, 20, 30, 40 and 50 μm. The applied tensile load was kept constant throughout the crack propagation stage. Separate analyses were carried out for four values of the coefficient of friction specified at the cracked interface, which were 0.2, 0.4, 0.6 and 0.8. The analyses produced fibre stress profiles for the five crack lengths, as shown in Figs. 6.8-11. Two distinct regions were observed. The region of interfacially cracked fibre had a linear fibre stress take-up profile, whereas the rest of the intact fibre had a Cox-type elastic stress profile. Additionally, the location of the interface crack tip (i.e. distance along the fibre) was found to manifest itself in the stress profile as a *point of inflection*. Since this relationship held irrespective of the value of coefficient of friction, it was

concluded that the point of inflection had an exclusive dependency on the crack length. Thus the actual crack lengths were inferred directly from the LRS data.

The *gradient* of the linear region was found to be a positive function of the coefficient of friction specified for the crack faces. The relatively steep gradient of the linear regions in the experimental stress profiles indicate a value for the coefficient of friction in the range 0.8-0.9. Such a high value is not unexpected given the rough surface morphology of the fibre and the chemical reactivity of the carbon basal planes at the surface [1]. The experimental stress profiles that were used for comparison with the FE predicted profiles, were those having far-field fibre stress values of 1.0, 2.5 and 3.0 GPa. The distances from the fibre end of the points of inflection were measured directly from these experimental profiles as being 4μm, 15μm and 25μm, respectively. FE predictions of fibre stress distributions for interface cracks having these lengths, with a coefficient of friction of 0.9, are presented together with the corresponding experimental data superimposed in Figs. 6.12-14. Very good correlation is obtained between the experimental and FE profiles, thus confirming the *Mode β interfacial failure regime* as being the *dominant* one in this carbon-epoxy system.

Analytical solutions for the fibre stress profiles induced in the presence of an interface crack in a single fibre tensile-loaded composite, have been made by Piggott [21]. A fundamental difference between the stress profiles found in this study and those predicted by Piggott is the shape of the transition region between the linear take-up region and the Cox-type intact region. According to Piggott, this transition is abrupt and is a point of mathematical discontinuity, Fig. 2.1(b), whereas the transition has been found in this analysis to be smooth. The discrepancy arises due to the assumption of linear elasticity in Piggott's analysis, which induces the singularity in stresses at the crack tip thus creating the discontinuity in the fibre stress profile. Thus, the crack tip plastic zone manifests itself as a smooth transition in the fibre stress profile. The characteristic *Ω-shape* fibre stress profile is therefore the *fingerprint* of Mode β interfacial failure, since indirect evidence of such a failure mechanism is revealed by observation of the fibre stress profiles.

6.3.3 Friction and interfacial fracture toughness

The nature of the crack surfaces and the stress regime that is supported across the crack, will almost certainly influence the value of the coefficient of friction that exists between the cracked fibre and matrix. The coefficient of friction between a soft epoxy polymer surface and the series of hard asperities on the surface of the fibre is, in general, sensitive to a number of parameters [43]. The visco-elasticity of the matrix will influence the deformation component of friction. Additionally, increasing normal stresses on the interface crack will affect the true area of contact through the mechanisms of junction growth and formation of transfer films, thus influencing the adhesion component of friction. Hence the coefficient of friction itself becomes an implicit function of the normal stresses and the effective area of contact. This phenomenon is a second-order effect, and consequently does not significantly affect the fundamental analysis of frictional stress transfer across the interface.

The interfacial fracture toughness employed in the crack propagation criterion was considered to be the same as that of the opening Mode I. This is a non-essential assumption and requires elaboration. Fracture toughnesses of any given bi-material interface depend strongly on the *mode mixity* ahead of the crack tip [52-53]. This is in contrast to the case of an isotropic homogeneous material whose fracture toughness is approximately equal to the Mode I toughness and is insensitive to the mode mixity of the loading. The interfacial fracture resistance for a given interface is more accurately specified by a toughness curve which is an empirical function of the mode mixity or phase angle at a given distance ahead of the crack tip [52-53]. Such an approach would allow a more exacting evaluation of the crack propagation criterion in a fracture mechanics environment.

	Carbon fibre	Matrix LY5052/1927 (relaxed properties)
Axial Tensile Modulus, GPa	392	1.78
Transverse Modulus, GPa	20	1.78
Axial Tensile Strength, GPa	3.2 *(fracture)*	31×10^{-3} *(yield)*
Axial Fracture Strain, %	0.8	4.2
Axial Poissons Ratio	0.27	0.36
Transverse Poissons Ratio	0.03	0.36
Axial CTE*, /K	-0.25×10^{-6}	58×10^{-6}
Transverse CTE*, /K	25.0×10^{-6}	58×10^{-6}

* Coefficient of Thermal Expansion

Table 6.1. Material Properties of Carbon Fibre and Epoxy Matrix

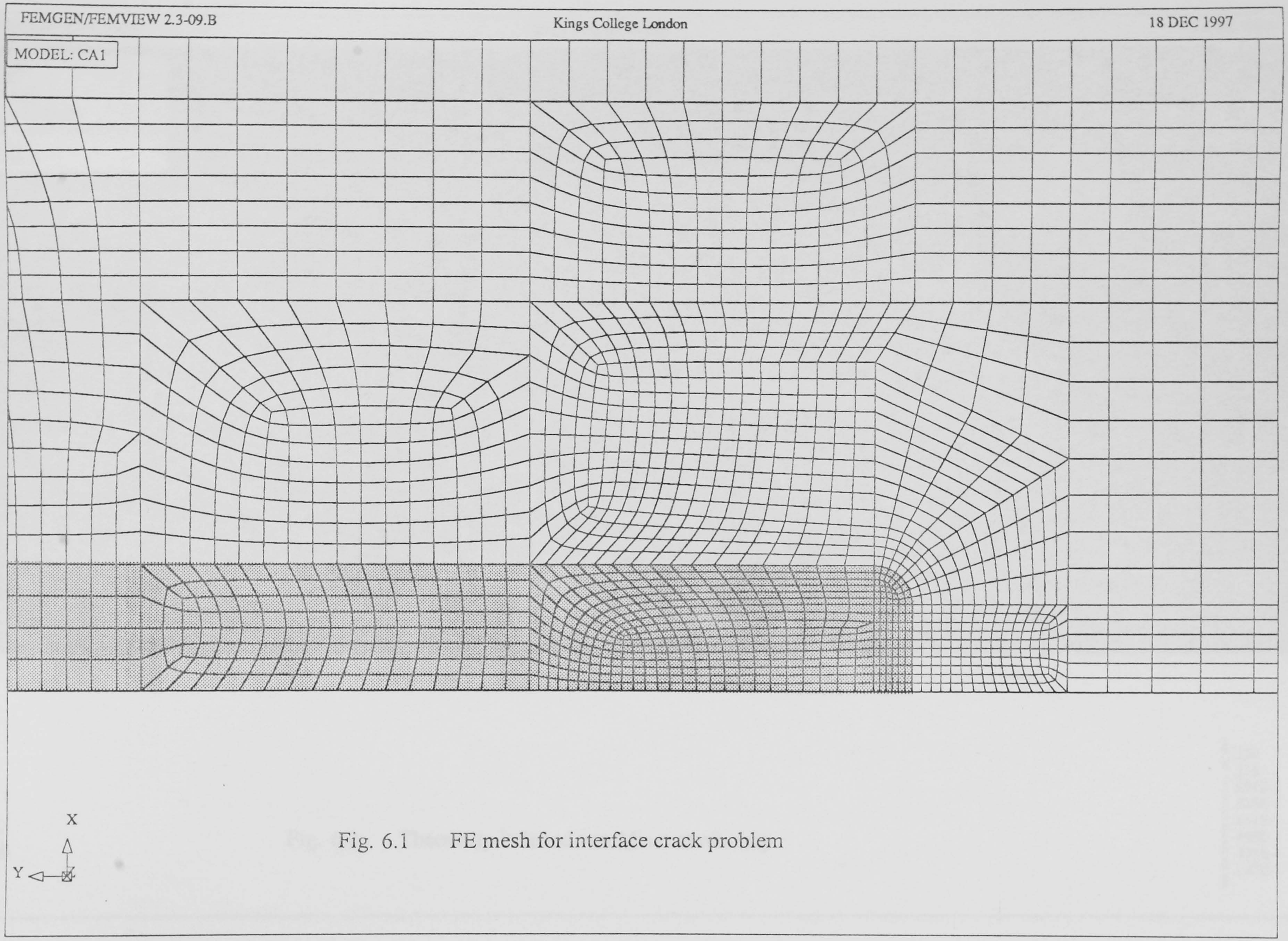

Fig. 6.1 FE mesh for interface crack problem

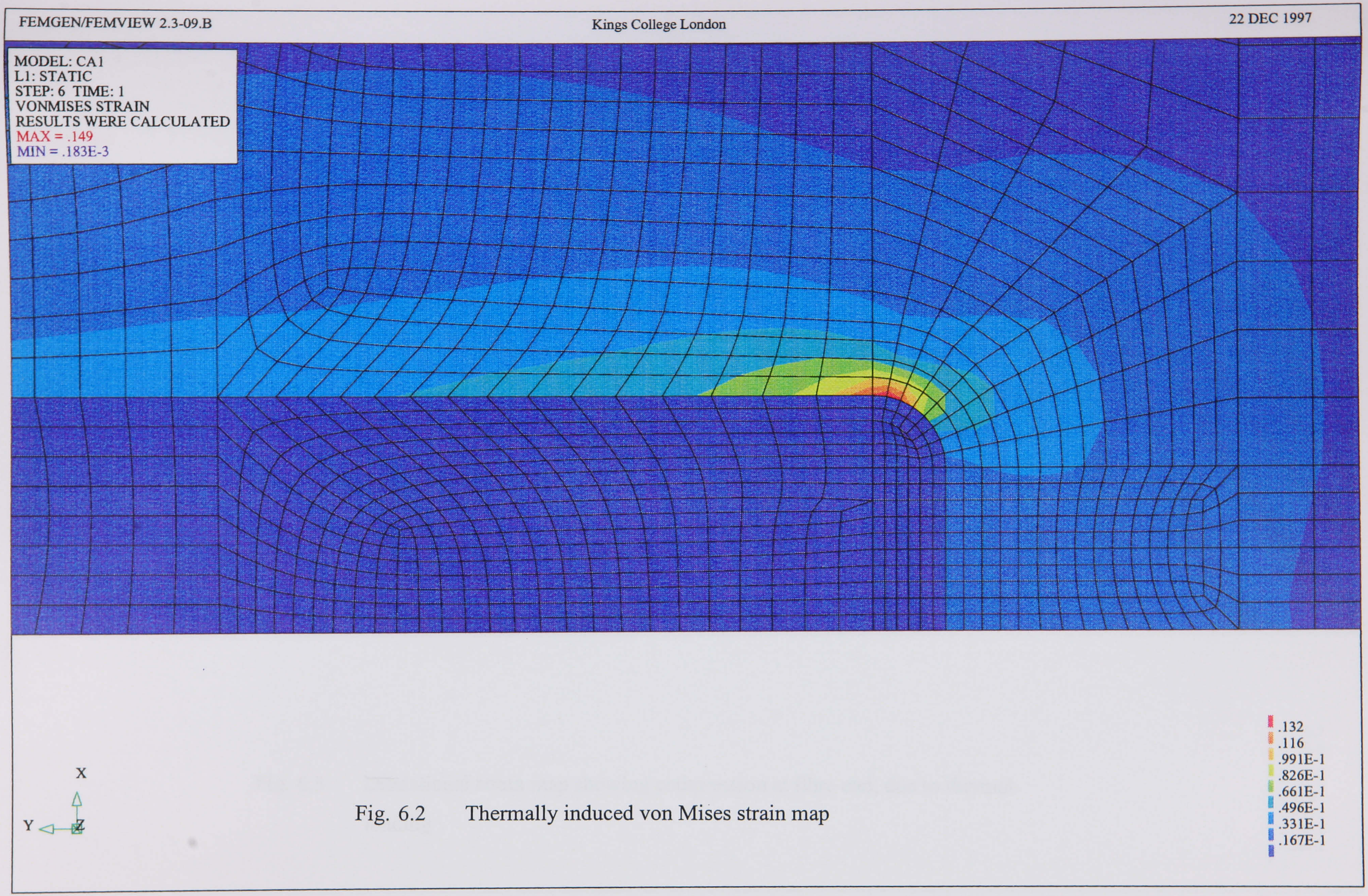

Fig. 6.2 Thermally induced von Mises strain map

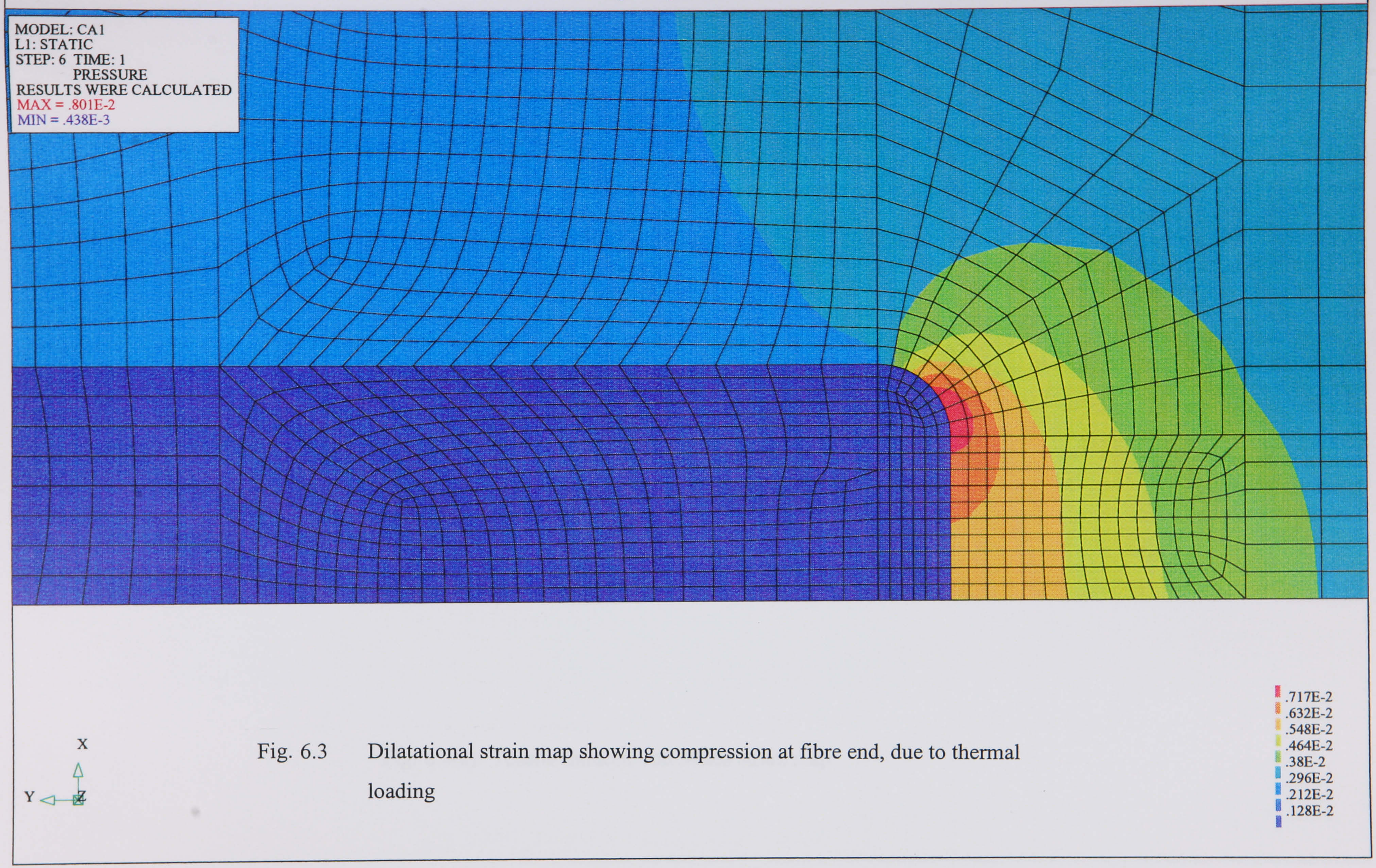

Fig. 6.3 Dilatational strain map showing compression at fibre end, due to thermal loading

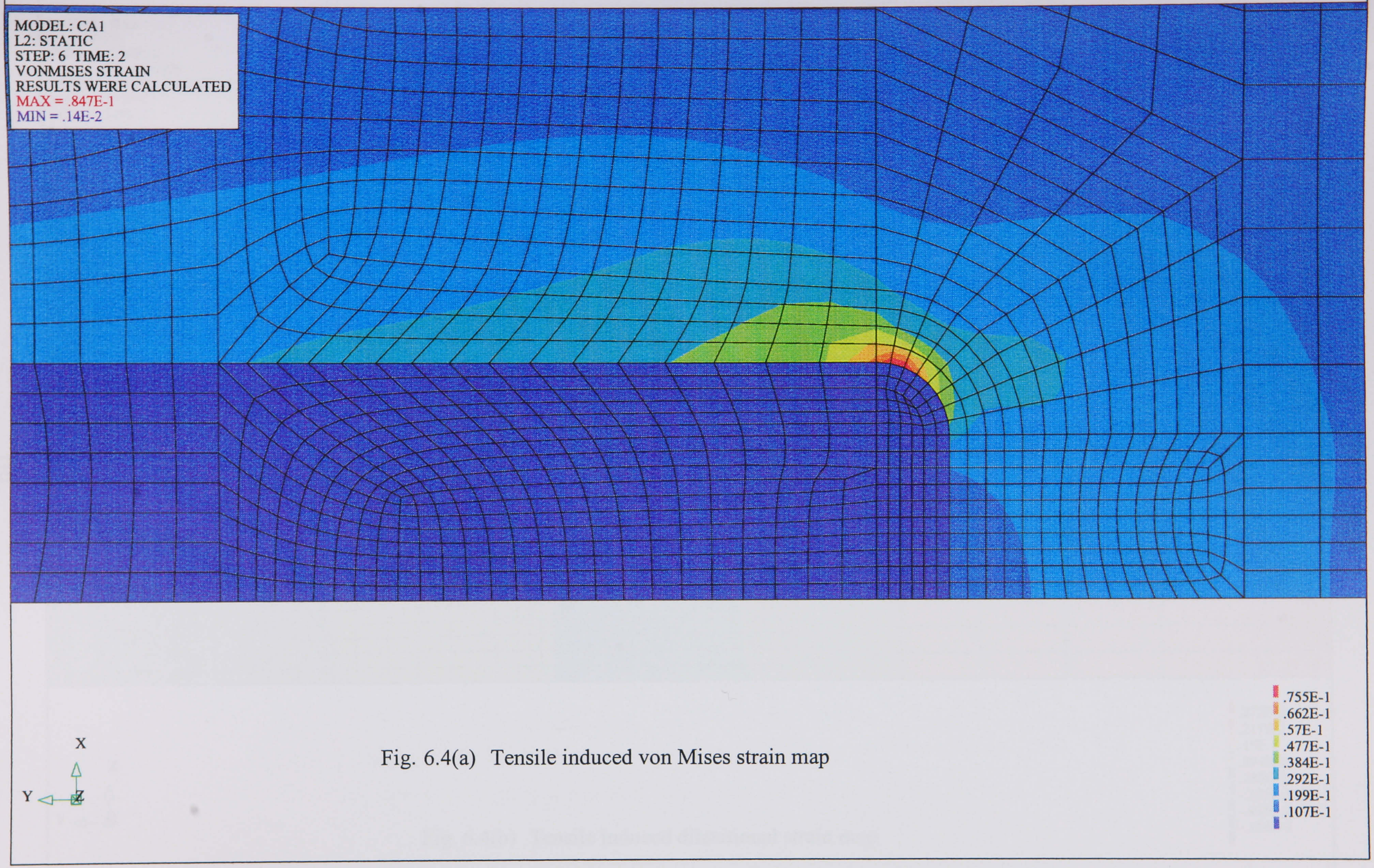

Fig. 6.4(a) Tensile induced von Mises strain map

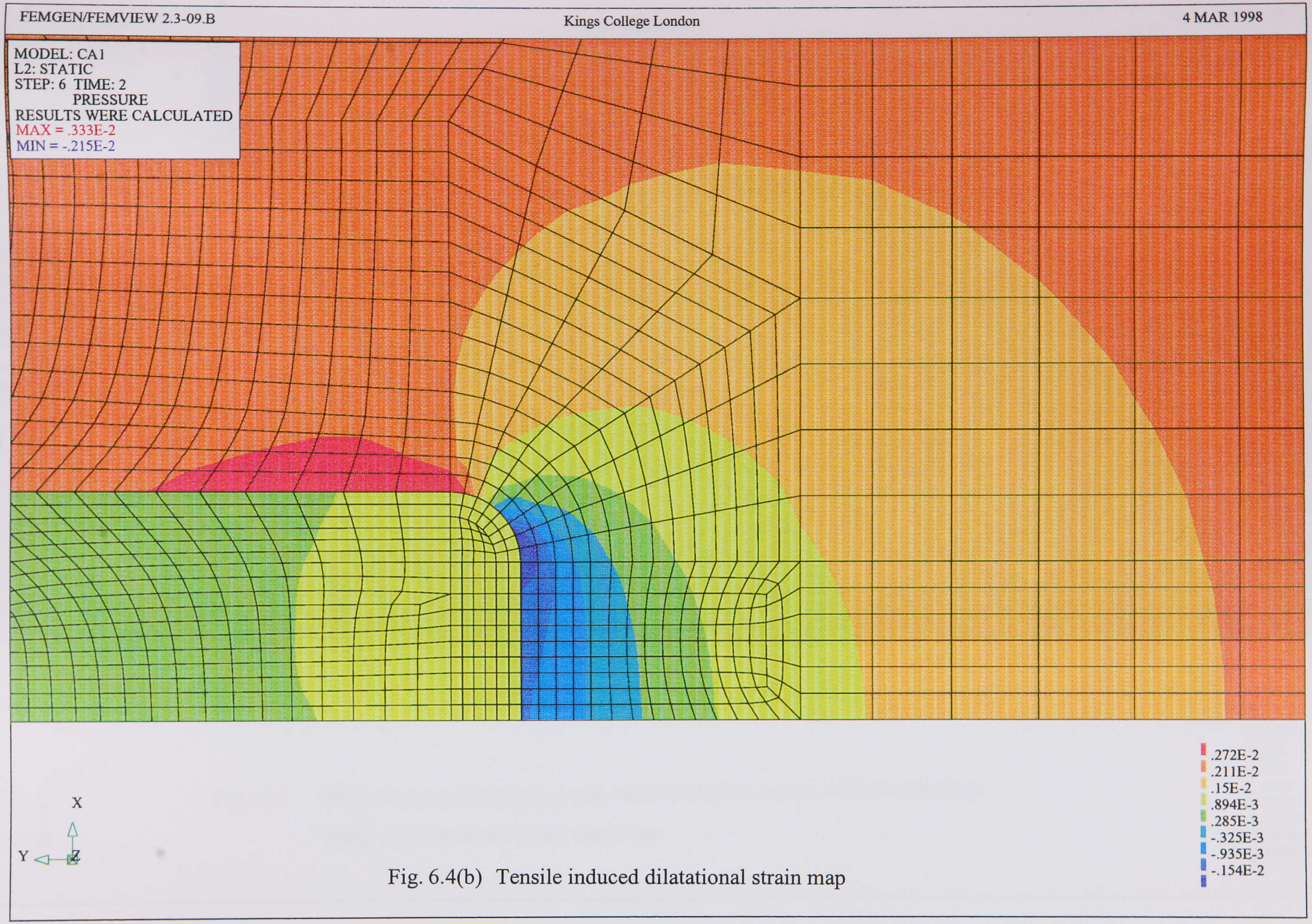

Fig. 6.4(b) Tensile induced dilatational strain map

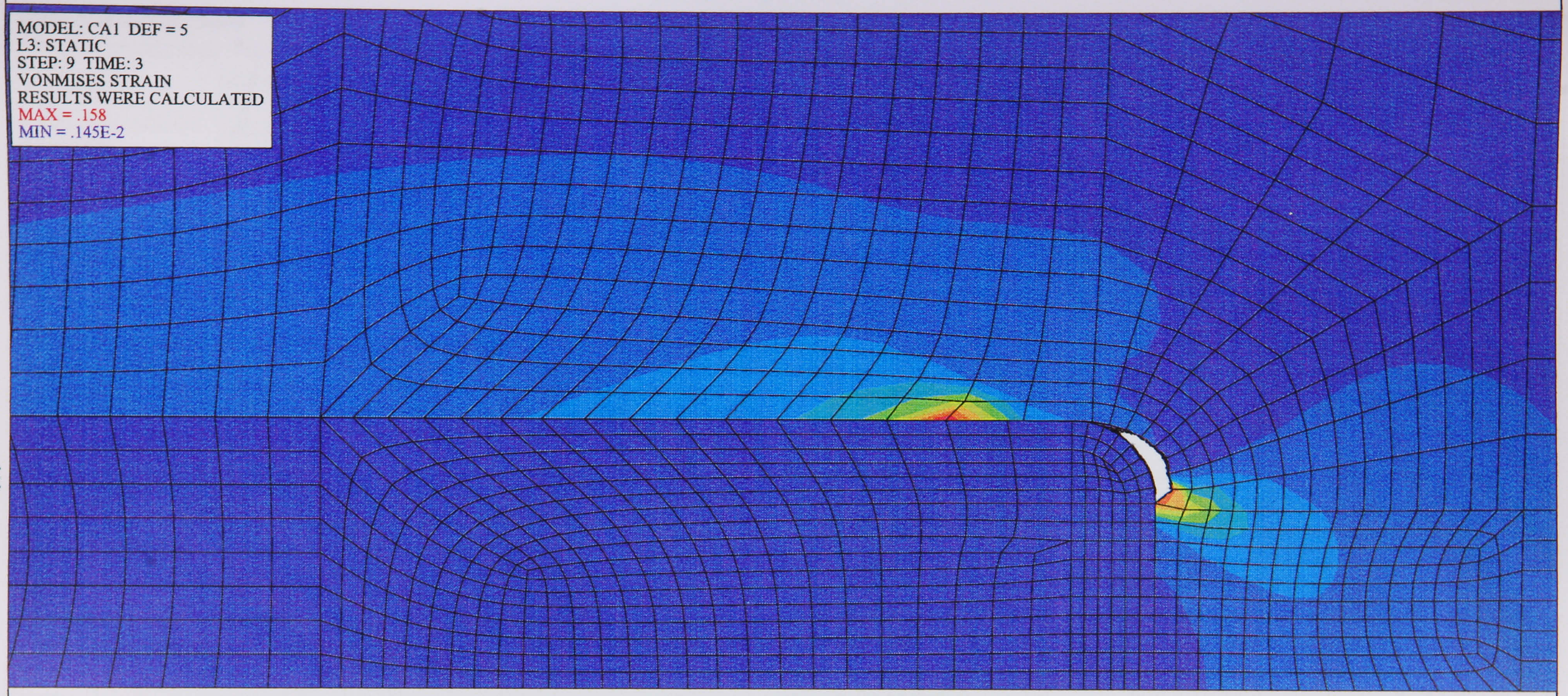

Fig. 6.5 Deformed mesh showing crack initiated at fibre corner, with the resultant strain concentrations at the crack tips

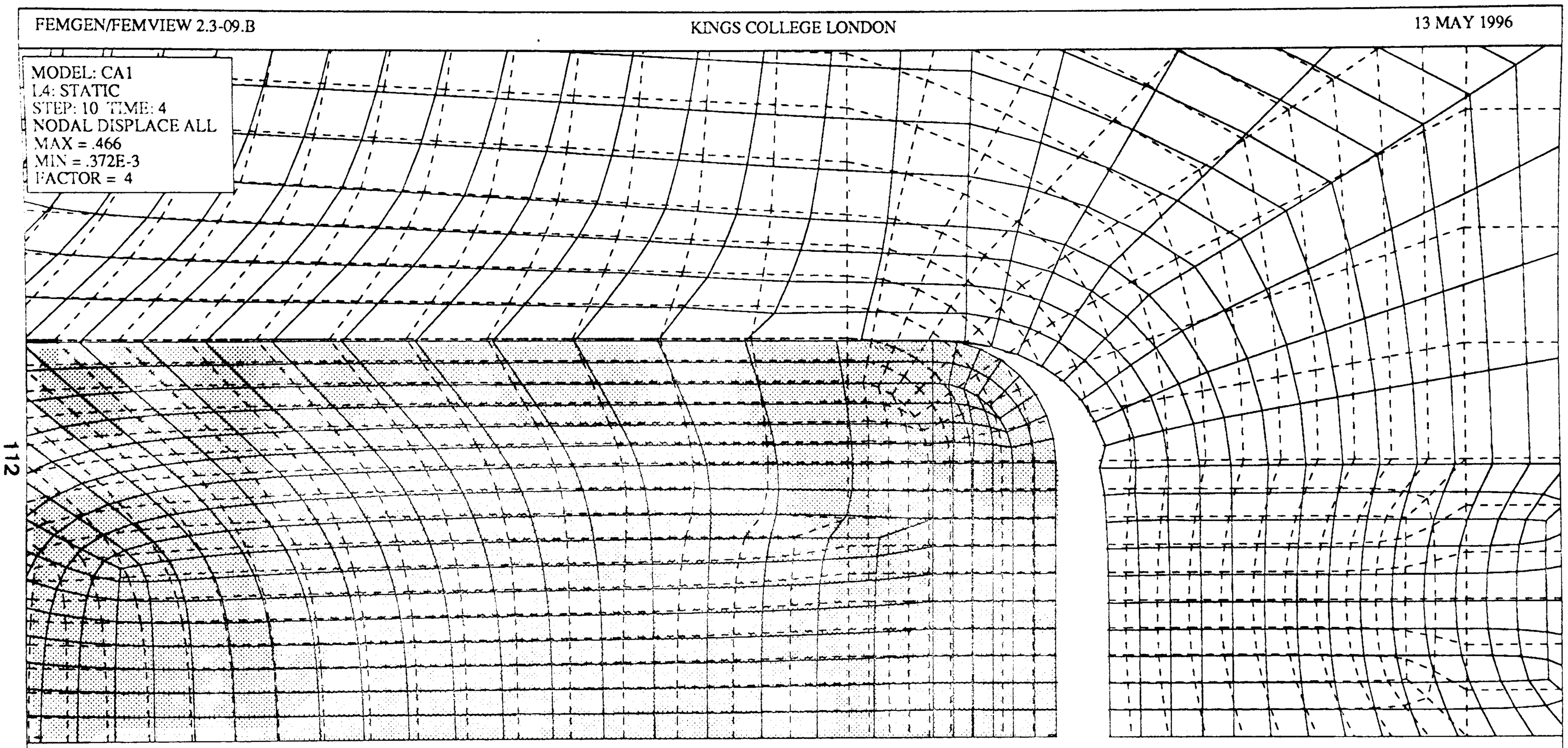

Fig. 6.6 Deformed mesh (solid lines) once fibre end is fully debonded

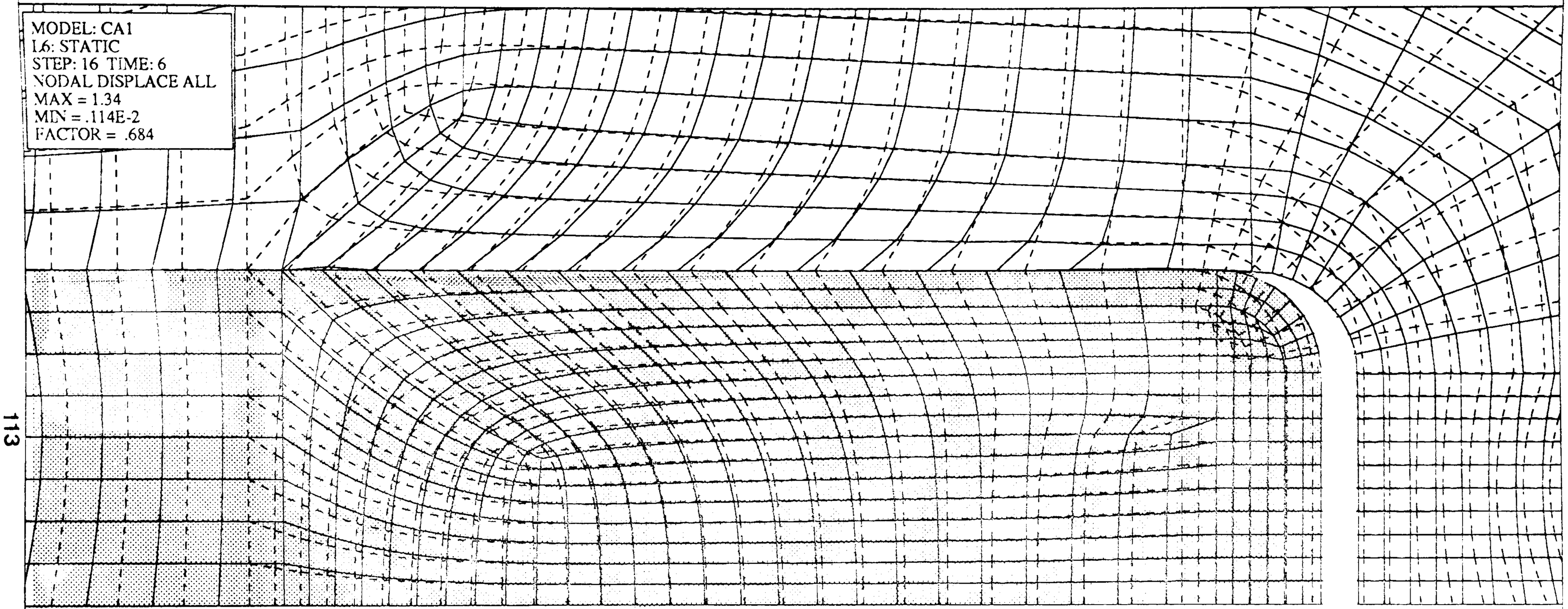

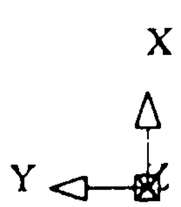

Fig. 6.7 Deformed mesh once interface crack is 10μm in length

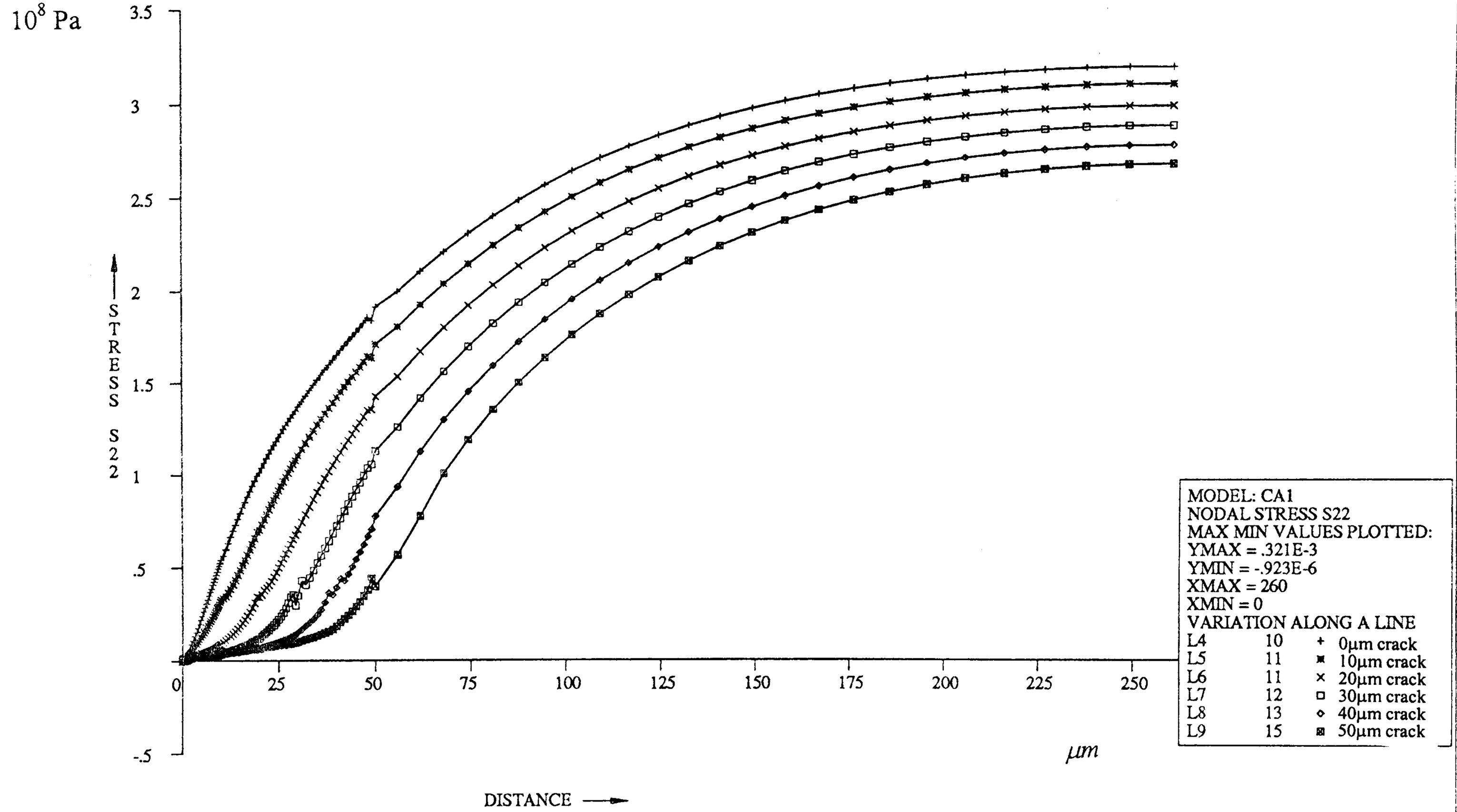

Fig. 6.8 Fibre stress distributions along fibre for interface crack lengths of 0μm, 10μm, 20μm, 30μm, 40μm, and 50μm; (coefficient of friction=0.2)

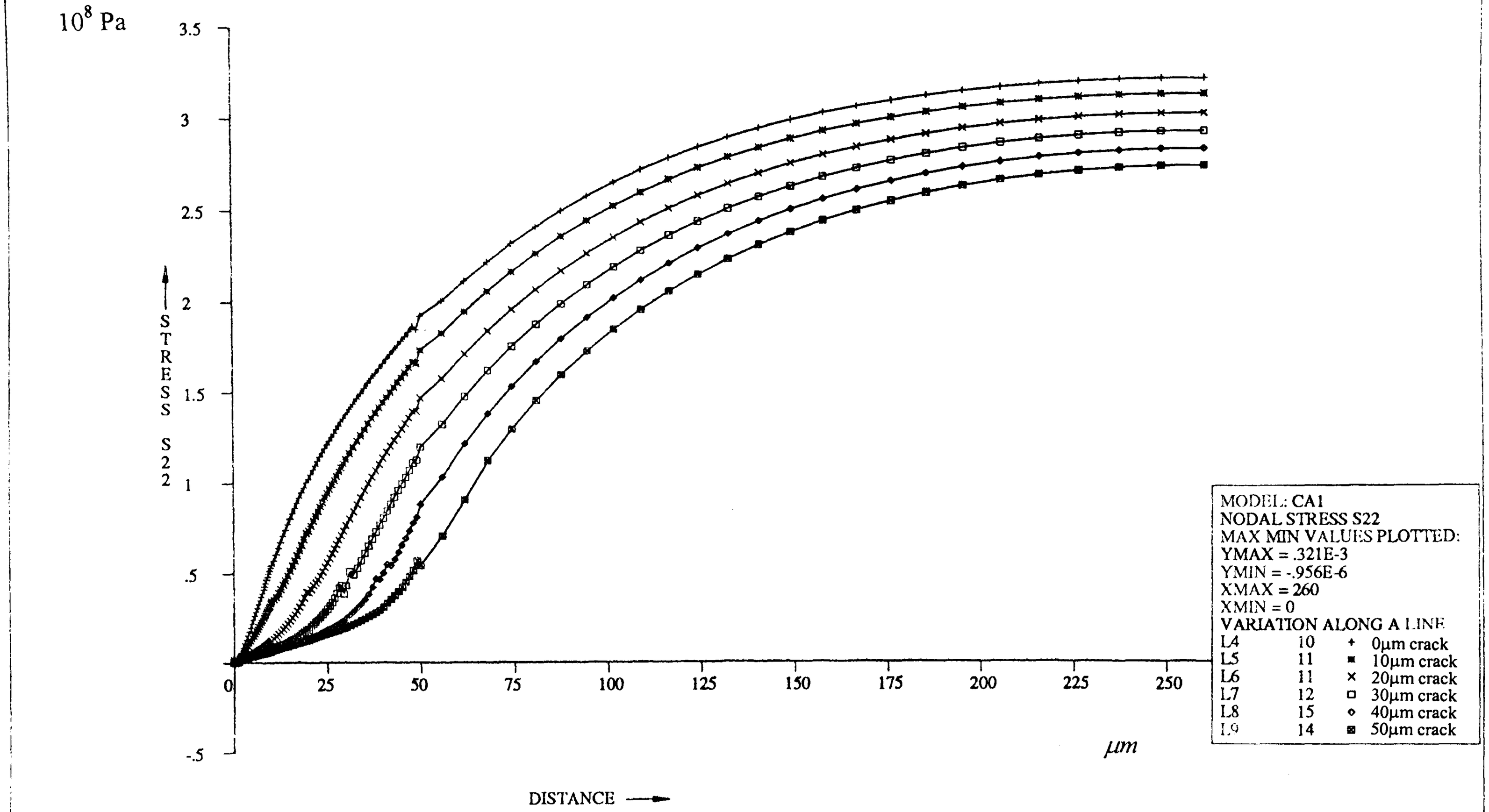

Fig. 6.9 Fibre stress distributions along fibre for interface crack lengths of 0μm, 10μm, 20μm, 30μm, 40μm, and 50μm; (coefficient of friction=0.4)

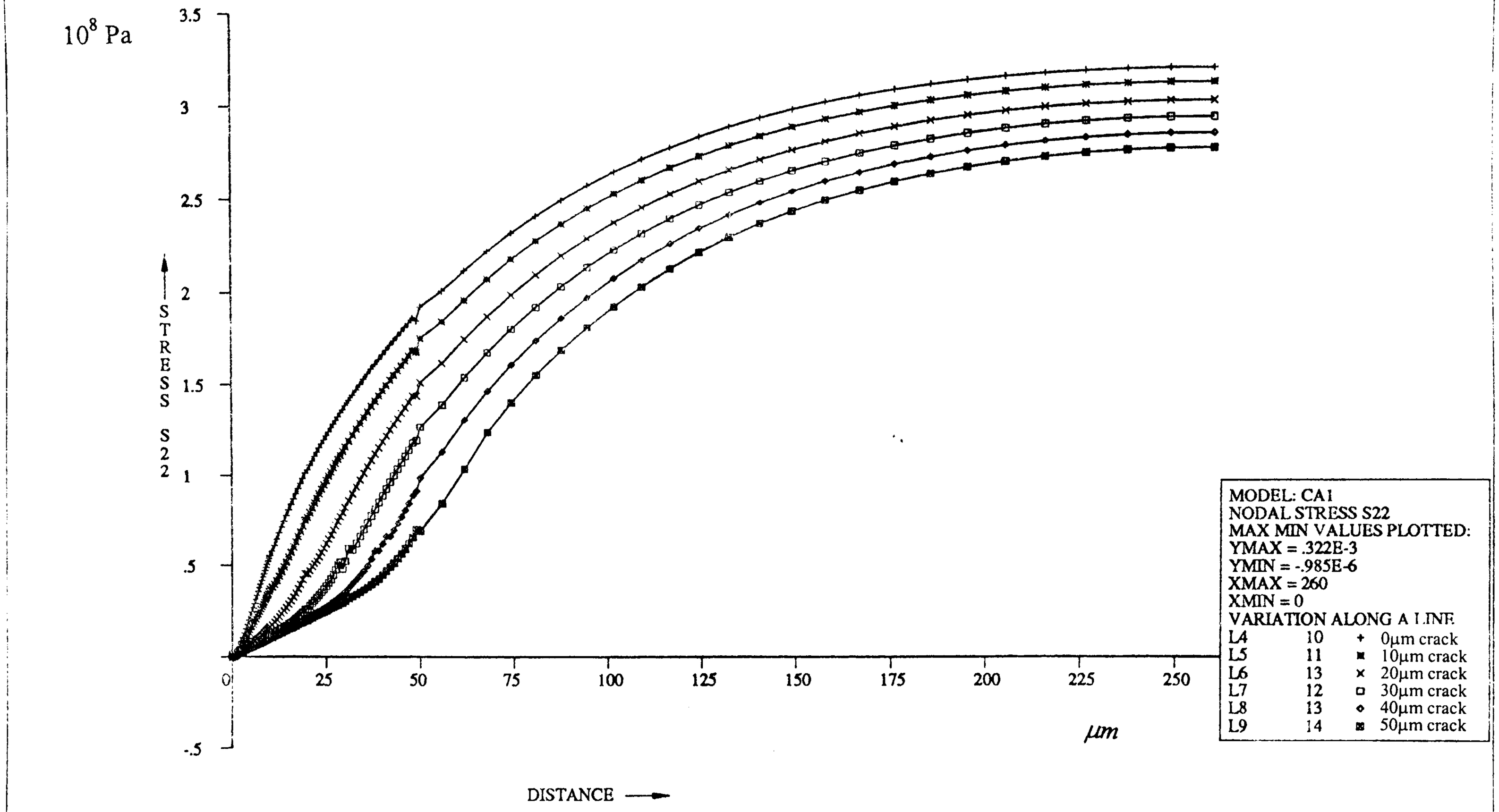

Fig. 6.10 Fibre stress distributions along fibre for interface crack lengths of 0μm, 10μm, 20μm, 30μm, 40μm, and 50μm; (coefficient of friction=0.6)

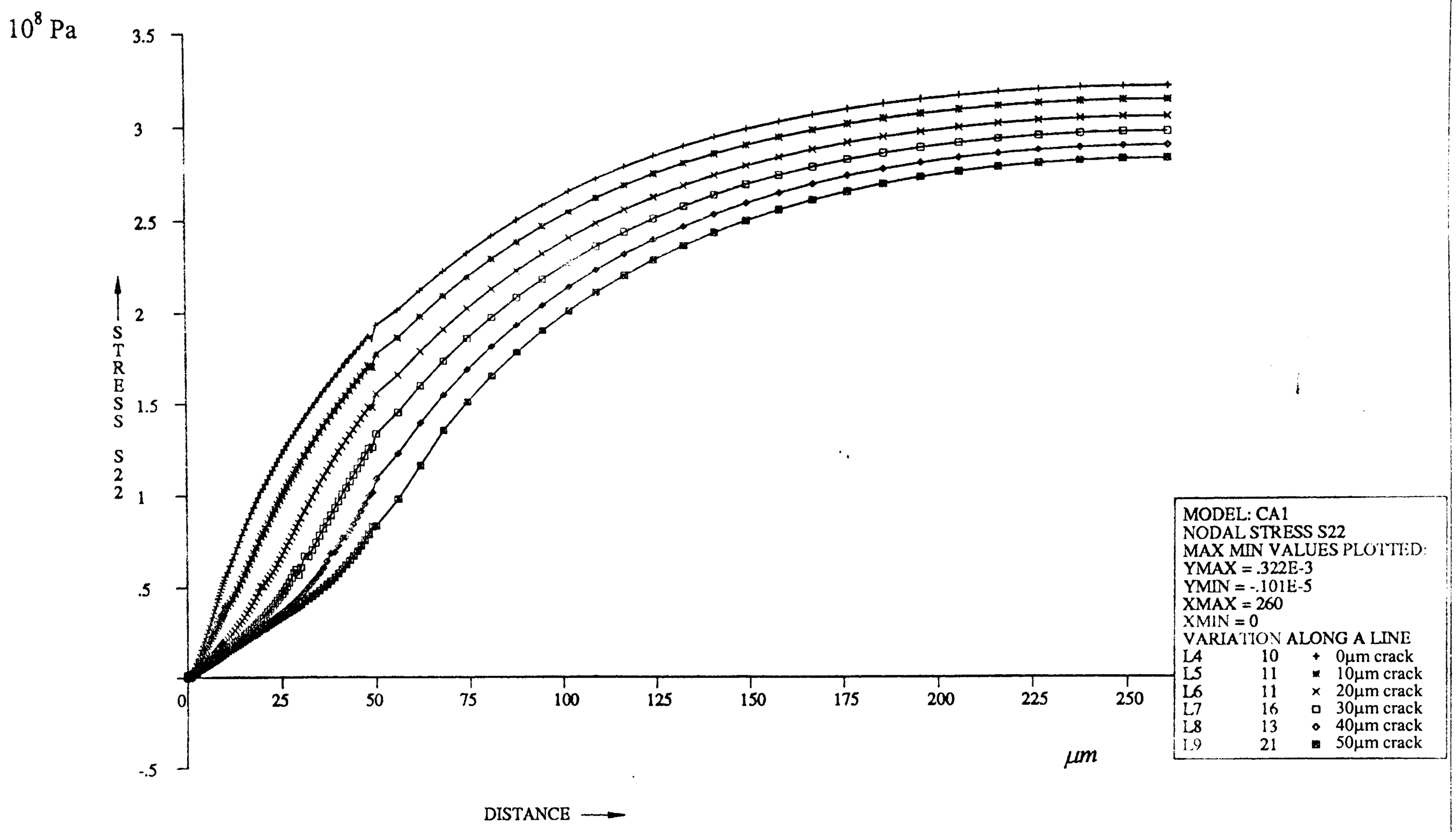

Fig. 6.11 Fibre stress distributions along fibre for interface crack lengths of 0μm, 10μm, 20μm, 30μm, 40μm, and 50μm; (coefficient of friction=0.8)

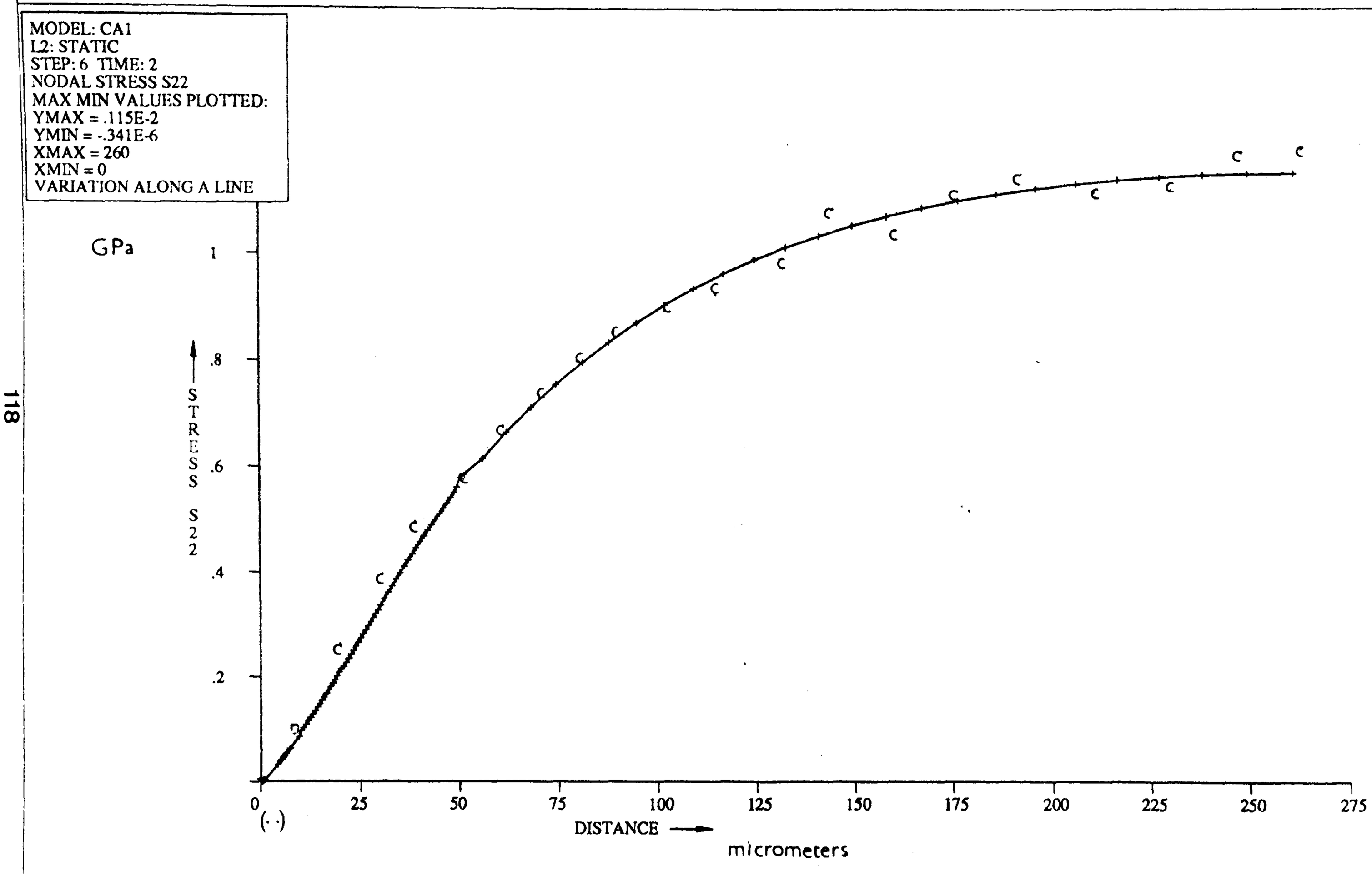

Fig. 6.12 FE and LRS fibre stress data for interface crack length 4μm; (coefficient of friction=0.9)

MODEL: CA1
L2: STATIC
STEP: 8 TIME: 2
NODAL STRESS S22
MAX MIN VALUES PLOTTED:
YMAX = .237E-2
YMIN = -.175E-6
XMAX = 260
XMIN = 0
VARIATION ALONG A LINE

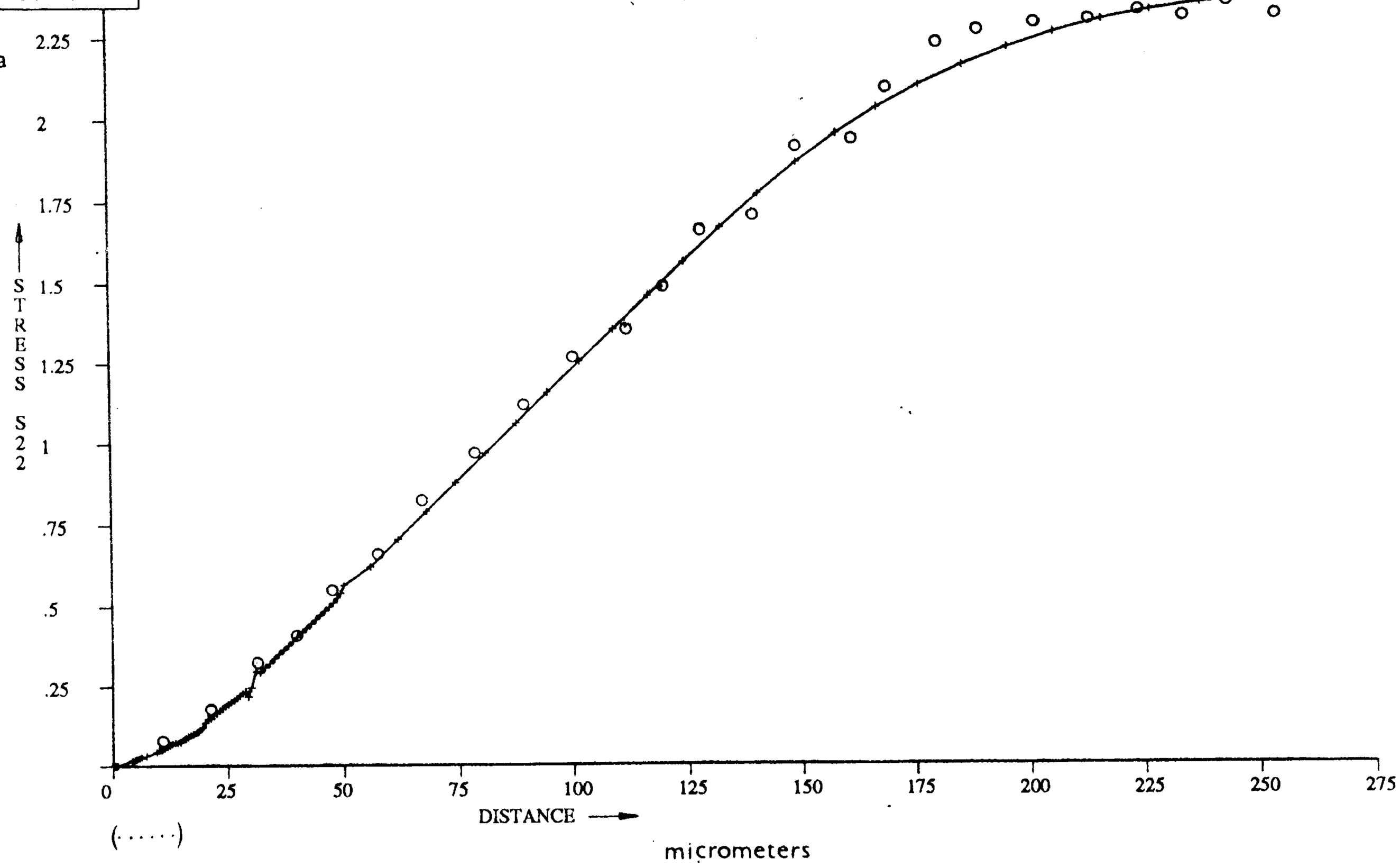

Fig. 6.13 FE and LRS fibre stress data for interface crack length 15μm; (coefficient of friction=0.9)

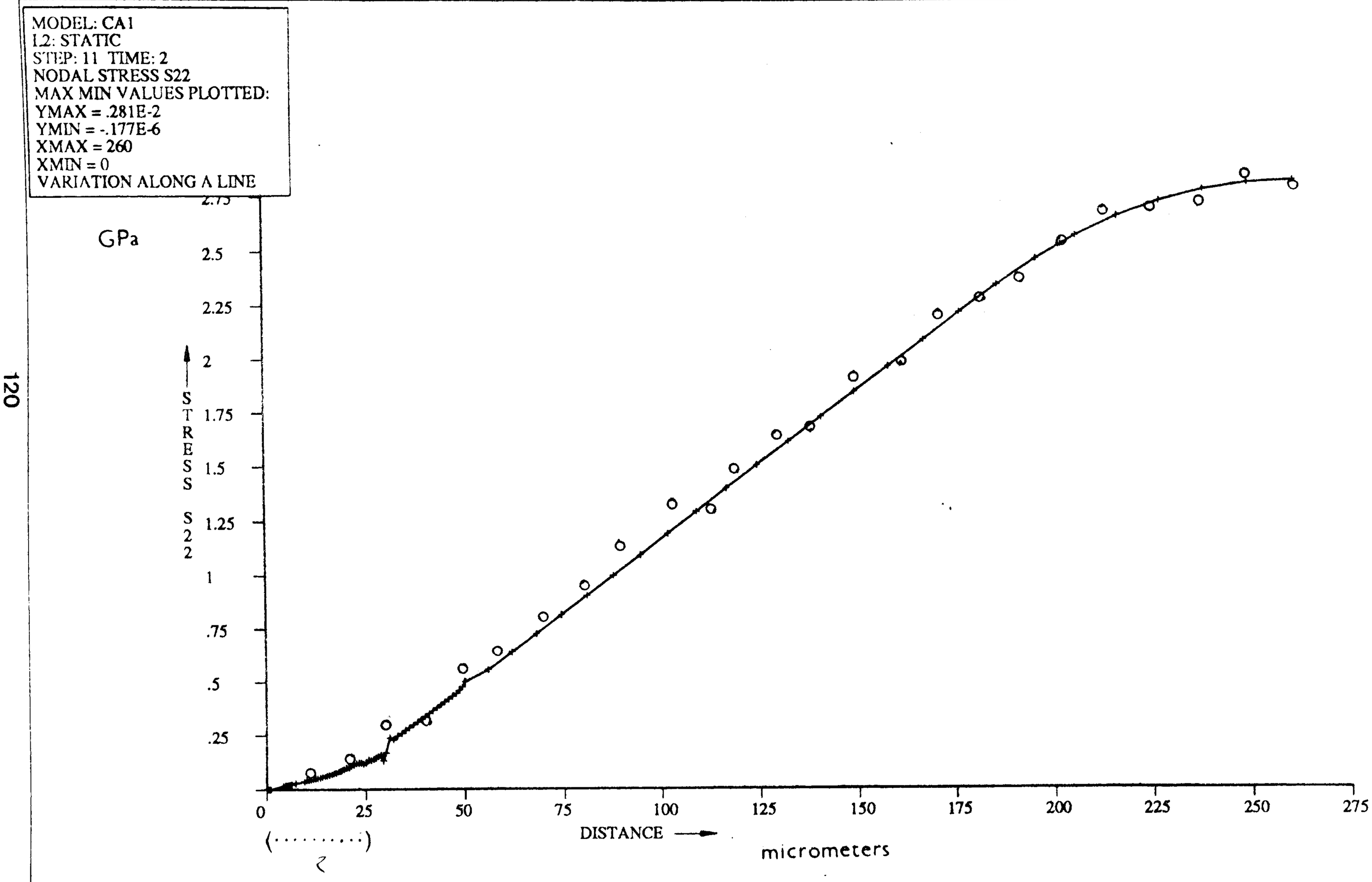

Fig. 6.14 FE and LRS fibre stress data for interface crack length 25μm; (coefficient of friction=0.9)

Chapter 7

Pressure Dependent Yield and Matrix Cracks

7.1 Introduction

The pressure dependent yield property of thermosetting polymer matrix materials is one that affects their fundamental yield behaviour [46]. One of the basic postulates of general three-dimensional plasticity theory is that the yield function is independent of the dilatational component of stress [45]. This is not the case for certain materials whose yield function exhibits a significant dependency on the dilatational stress component [46]. A modified yield surface that is commonly employed in place of the regular von Mises or Tresca yield surfaces is the Drucker-Prager yield surface [see Appendix E]. Because of the nature of the modified yield surface, pressure dependency is only significant for composite systems which contain areas of matrix in dilatational compression, or are subjected to dilatational compression at some point during their loading history. This typically occurs during the propagation of matrix cracks in Mode γ interfacial failure. Hence pressure dependent yield is pertinent to Mode γ failure and not to Mode β, as described in Section 6.2.

The objective of the analyses presented in this chapter was to investigate the influence of pressure dependent yield on the induced fibre stress profiles under a mode γ interfacial failure regime.

7.2 Model Details

The mesh used in the analysis was similar to that containing the interface crack (Chapter 6), except that interface elements were defined at the fibre end and then into the matrix along a line of length 90μm at an angle of 20^{o} to the fibre axis, simulating a conical matrix crack geometry in three dimensions. The line was defined as being

perfectly bonded during the initial stages of the analysis, as with the interface crack analysis, but no coefficient of friction was defined for the cracked surfaces post-fracture since the matrix crack was subjected to an opening mode and thus no interference between the crack faces would be possible (see section 4.4).

The fibre and matrix behaviour were defined as in previous non-linear analyses except for the yield function of the matrix being defined as that of the Drucker-Prager model. The yield surface cone angle was varied from 0° to 70° and the mesh subjected to a non-linear multi-stage loading history based on the Progressional Approach. This consisted of a thermal pre-load of $-50^{\circ}C$, a subsequent tensile applied strain of 0.3% followed by fibre end debonding. The latter part of the loading history consisted of a tensile applied strain of 1.0% followed by crack extensions to form matrix cracks of 20μm, 40μm, 60μm and 90μm, which was achieved by the incremental debonding of the interface element nodes along the pre-defined 20° matrix crack line. An example of the ABAQUS input data file for this non-linear analysis is given in Appendix B. The values of the yield surface cone angle, ψ, for which the analysis was performed were 0° (corresponding to the regular von Mises yield surface [Appendix E]), 13°, 25°, 37°, 50° and 70°.

7.3 Results and Discussion

The thermal pre-load, the subsequent 0.3% tensile loading and fibre end debonding stages (crack initiation) of the interfacial failure process produced results identical to those of the interface crack analysis, since the loading history was correspondingly identical. This applied in all cases for all values of the yield surface cone angle that were considered. The reason for this was that the dilatational component of stress throughout the matrix for these early stages of the loading history was tensile, and hence the pressure dependency of yield did not play a major role.

7.3.1 Pressure independent yield (ψ=0)

Once a tensile strain of 1.0% has been applied and the matrix crack has propagated to a length of 20μm, the deformed mesh of the fibre end region Fig. 7.1 reveals gross shear deformation in the interfacial matrix (matrix adjacent to the interface). This deformation remains once the crack had further extended to 40μm as shown in Fig. 7.2. In the von Mises strain map for the 20μm crack, Fig. 7.3, the darker areas indicate areas of matrix that have yielded in excess of 20%. This is apparent at the crack tip plastic zone, and also at the interface due to the induced gross shear deformation. There is also permanent deformation at the fibre end that has been previously induced during the crack initiation stage of the failure process.

The fibre stress distributions for the four crack lengths are presented superimposed in Fig. 7.4. The characteristic *S-shape fingerprint* observed in the linear-elastic matrix crack analyses of Chapter 4 is again observed in the profiles. This S-shape is fairly pronounced especially when compared with the Ω-type fibre stress distributions associated with Mode β failure (Figs. 6.8-14). Also, a zone of compressive stress is observed to have been induced in the region of the fibre end. Detailed comparisons between the modes of failure and the implications for the global composite properties will be the subject of Chapter 8.

7.3.2 Pressure dependent yield (ψ>0)

For the extreme case of the yield surface cone angle of 70°, the previously observed gross shear deformation of the interfacial matrix is not seen in the deformed meshes incorporating 20μm and 40μm cracks of Figs. 7.5-6. The 20% yield boundaries consequently only appear at the crack tip and fibre end, as shown by the von Mises strain map for the 20μm crack, Fig. 7.7. The fibre stress distributions of Fig. 7.8, however, do not exhibit the minor compression zones previously observed in the case of pressure independent yield. More fundamentally, the fibre stress profiles are substantially higher in the take-up regions than their pressure independent counterparts.

For intermediate values of ψ, the extent of matrix yielding at the interface is less, as shown by the variation of the maximum yield strain with ψ, Fig. 7.9.

7.3.3 Development of fibre compression zones

In order to explain the phenomenon of the development of compressive zones in the fibre end region, and its interaction with the pressure dependency of yield, the response of a small element of interfacial matrix located at 40μm from the fibre end, will be considered during the latter stages of the loading history on the composite specimen (refer Fig. 2.3).

On application of the 1.0% applied strain to the composite containing the fibre end crack, the matrix element undergoes large-scale yielding at a yield stress of 31MPa and reaches a final von Mises strain of 80%. Subsequently, as the matrix crack propagates, the region of matrix under the crack is released from its loaded state. With the exception of the interfacial matrix sub-region, the remainder of this matrix region is elastic and thus returns to zero strain on unloading. The interfacial matrix sub-region, however, is permanently deformed and thus the plastic strain component is residual on unloading, due to the significant hysteresis in the loading-unloading curve (Fig. 7.10). The profiles represented in Fig. 7.10 depict the behaviour of the matrix element during the entire loading history for both pressure independent and dependent yield regimes. Since the primary component of the von Mises strain is the in-plane shear strain, the interfacial matrix posseses a significant residual shear strain. Thus the elastic remainder of the matrix region under the crack returns to zero strain, acting on the residual shear strain in the interfacial matrix subregion (Fig. 7.11), which in turn compresses the fibre end. The interfacial matrix subregion is in a state of dilatational compression and thus will not rupture forming cracks.

For the case of the 70° cone angle, the interfacial matrix element undergoes virtually no yielding on application of the 1.0% applied strain, due to the existence of significant dilatational stresses (averaging -15MPa) induced during the loading of the composite containing the fibre end crack. It should be noted that the dilatational stresses would otherwise have been tensile in the absence of the fibre end crack, as

has been demonstrated in the tensile load step (immediately *before* crack initiation) in the interface crack analysis (see section 6.3.1). Thus loading of the composite specimen containing a fibre end crack that has been initiated *during* the analysis, produces different results than if the crack was pre-existent in the model, or if there was no crack at all, as is commonly assumed in numerous analyses by other authors (see literature survey). Hence *interaction* of the non-linear phenomena of yielding and crack initiation according to the Progressional Approach is observed, which lead to important conclusions as regards the progression of failure. The yield stress for the level of pressure induced is greater than the value of 55MPa obtained by the interfacial matrix element (see Fig. 7.10). Thus the response of the entire region of matrix under the crack, *including* the interfacial matrix sub-region, is elastic. Consequently as the crack propagates, the entire matrix region returns to zero strain on unloading. Due to the absence of residual shear strain in the interfacial matrix subregion, the fibre end zone is not put into compression on unloading.

7.3.4 Fibre stress variation with ψ

The sensitivity of the fibre stress take-up profiles to the angle ψ is emphasized by the graph showing the variation of the nominal fibre stress with ψ, once the matrix crack has propagated to a length of 90μm, Fig. 7.12. The nominal fibre stress value was taken to be that at a distance of 100μm from the fibre end. It is evident that the fibre stress profiles are substantially influenced by the amount of pressure dependency exhibited by the matrix. The stress value is increased by approximately 90%, when comparing that induced under the pressure independent yield regime, $\psi = 0^{\circ}$, with that of $\psi = 70^{\circ}$. This confirms that the pressure dependency of yield is not a secondary parameter with regard to Mode γ failure but, on the contrary, plays a significant role with regard to the level of stress supported by the fibre. This would have important implications for the *reinforcement efficiency* of the fibre during the interfacial failure process.

7.3.5 Crack retardation analogy

The development of compressive zones near the fibre ends may be considered analogous to the phenomenon of crack retardation in fatigue crack growth in fracture

mechanics [23]. In this case, the crack tip plastic zone that has been formed during cyclic loading is compressed by the remainder of the elastic body containing the crack during the unloading phase of the cycle, thus creating residual compressive stresses at the crack tip. Subsequent cycling of the specimen thus results in retarded crack growth reponse due to the existence of the residual stress state at the crack tip.

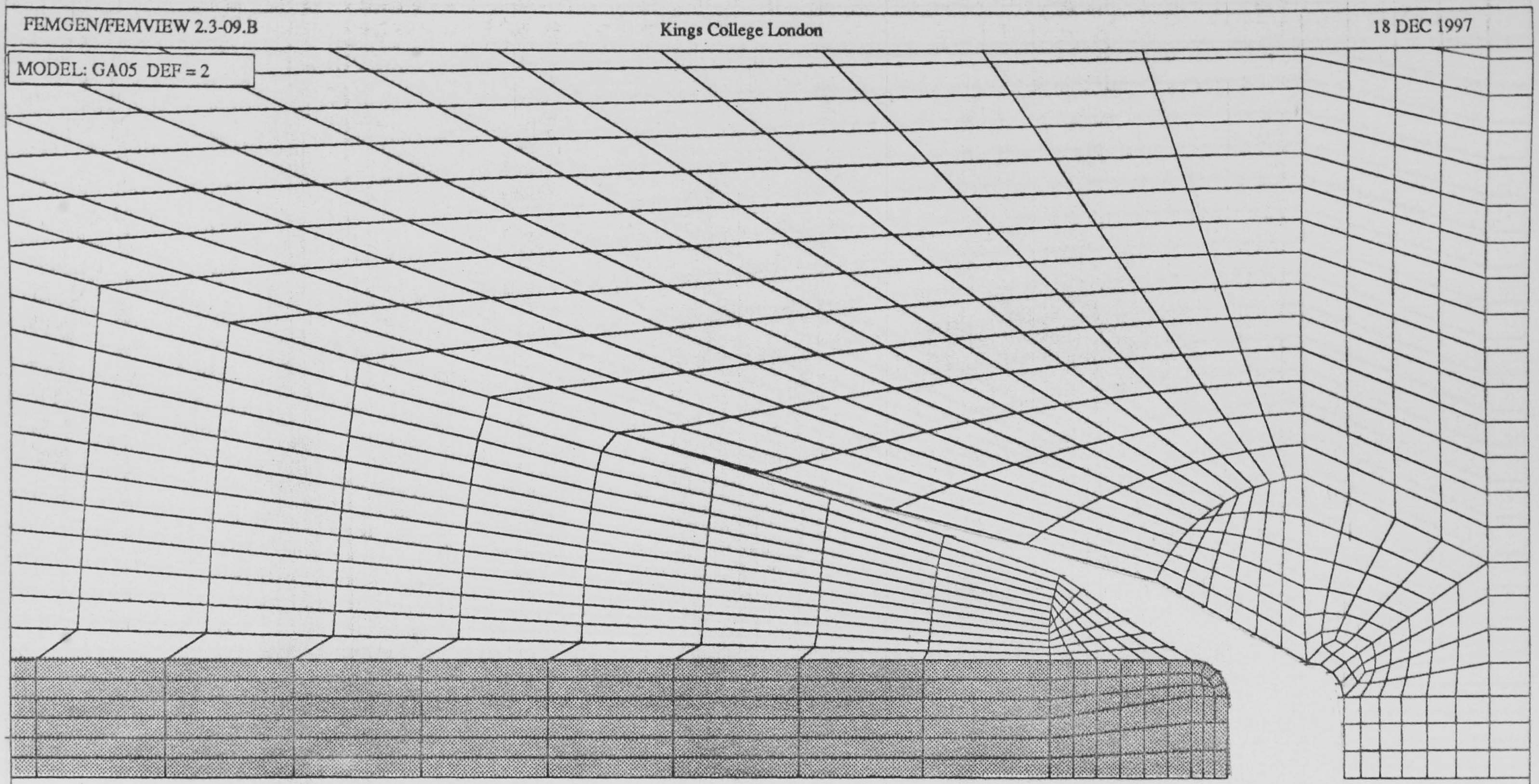

Fig. 7.1 Deformed mesh for matrix crack of length 20μm ($\psi=0^{o}$)

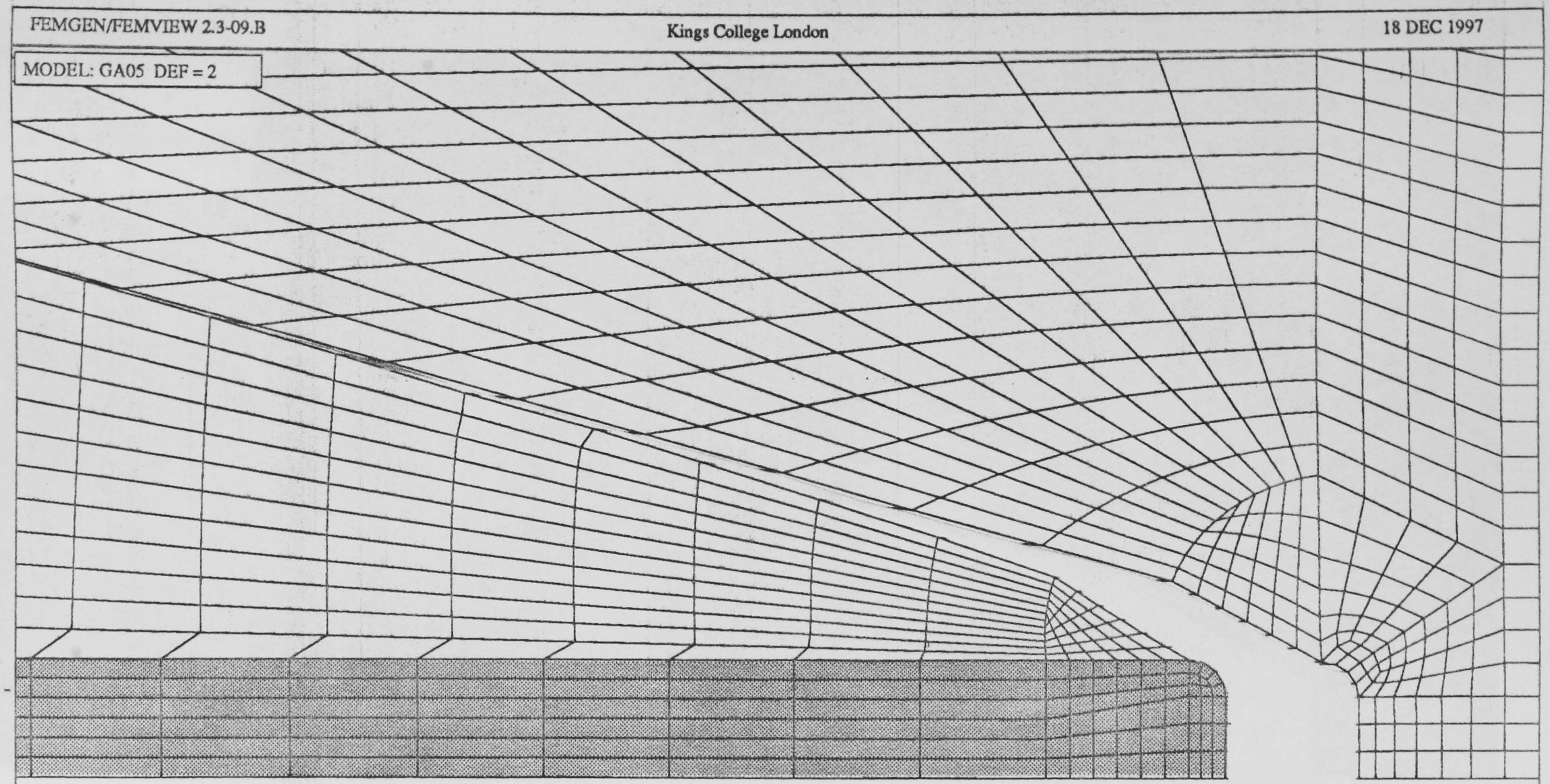

Fig.7.2 Deformed mesh for matrix crack of length 40μm ($\psi=0^{o}$)

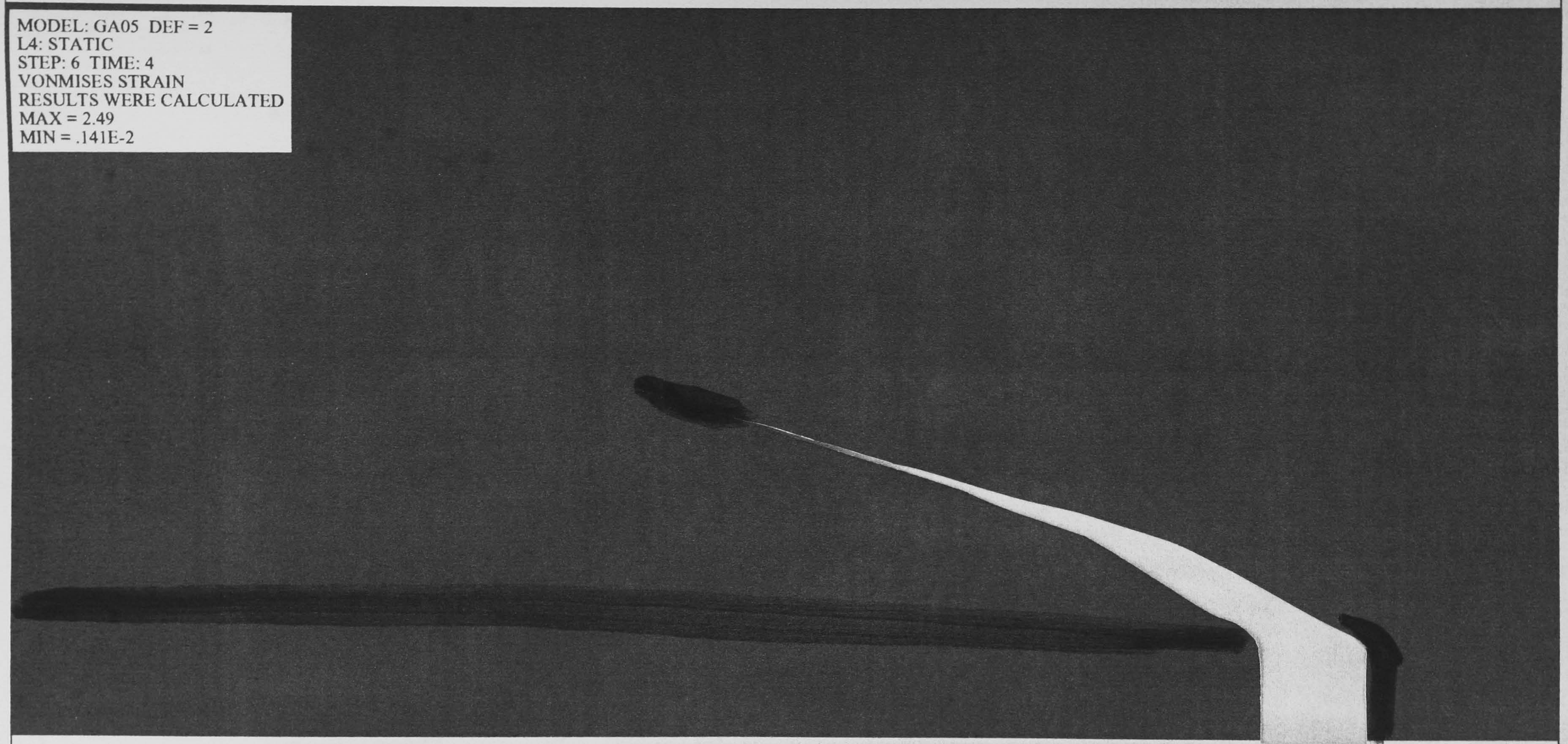

Fig. 7.3 Contour map showing areas of matrix in excess of 20% yield strain (darker areas) ($\psi=0^{o}$)

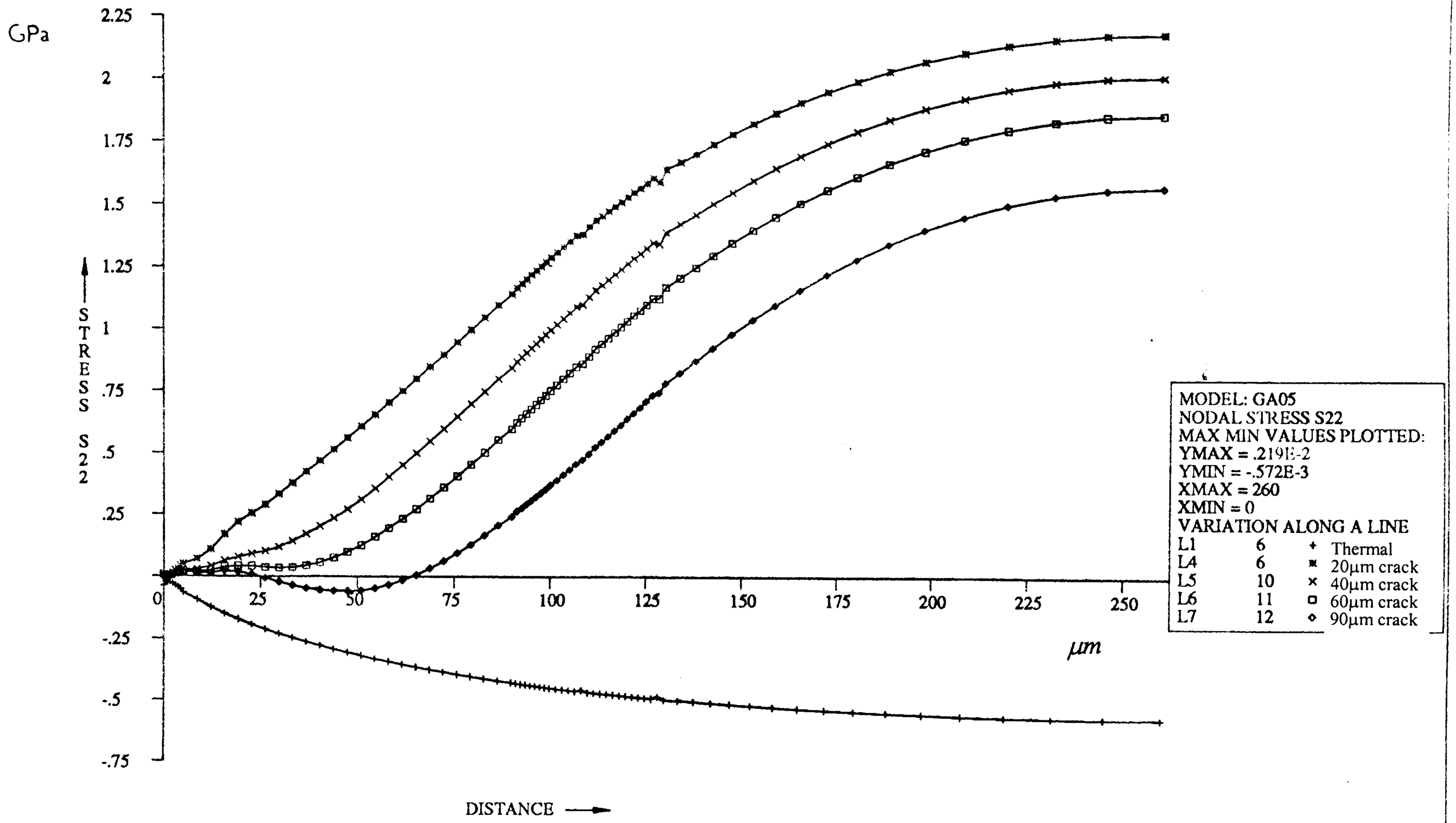

Fig. 7.4 Fibre stress distributions along fibre for matrix crack lengths 20μm, 40μm, 60μm and 90μm ($\psi=0^{o}$)

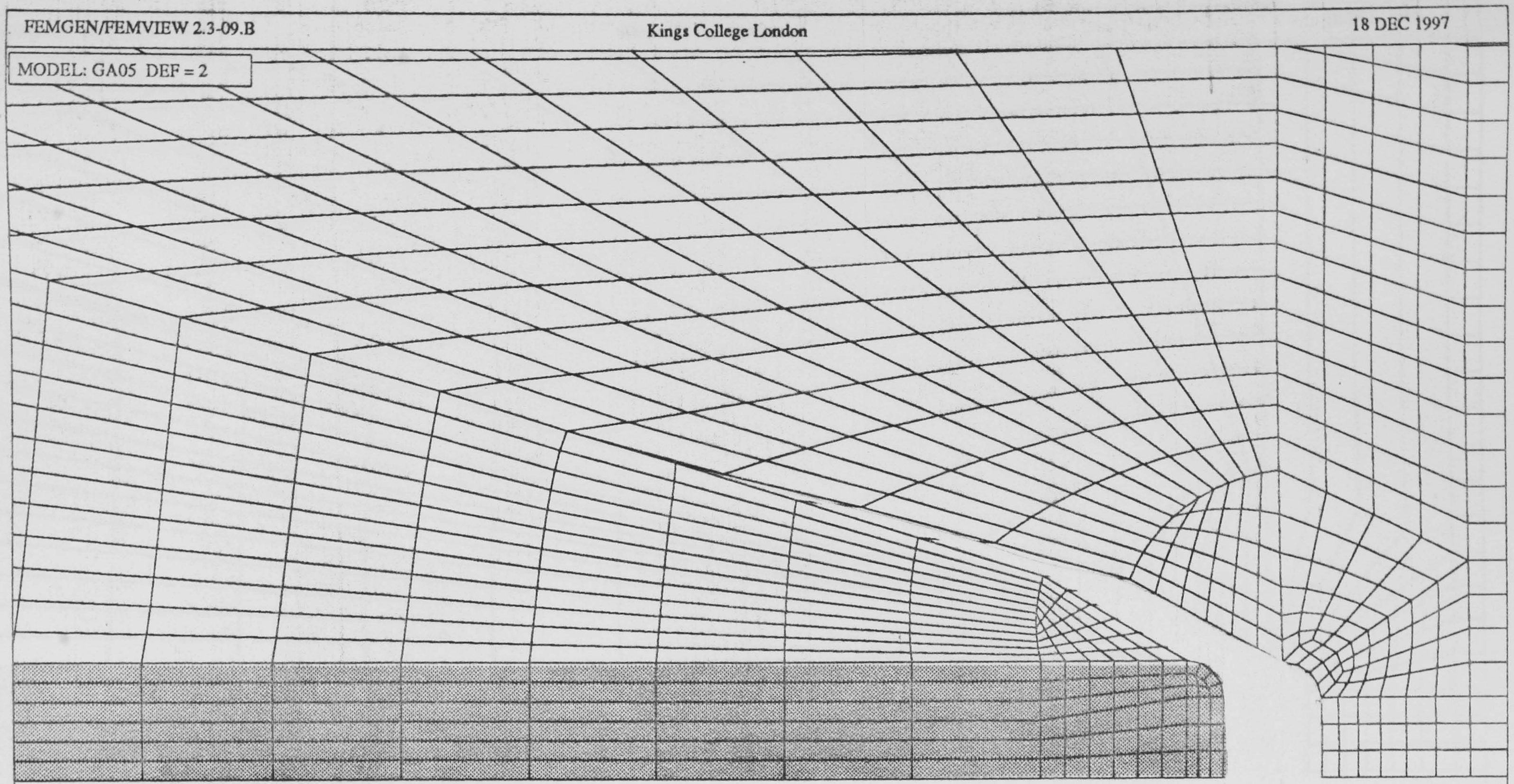

Fig. 7.5 Deformed mesh for matrix crack of length 20μm (ψ=70°)

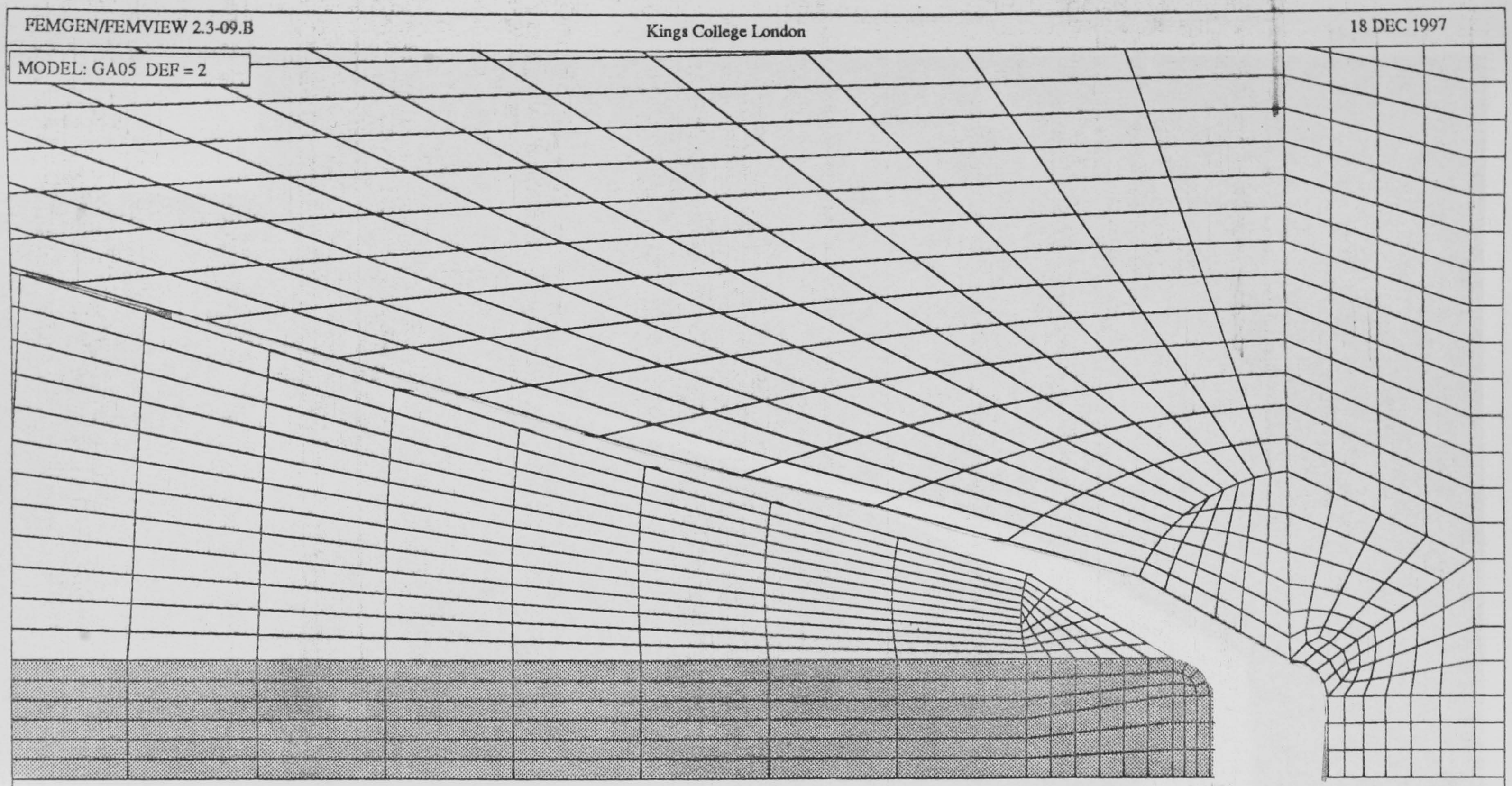

Fig. 7.6 Deformed mesh for matrix crack of length 40μm (ψ=70°)

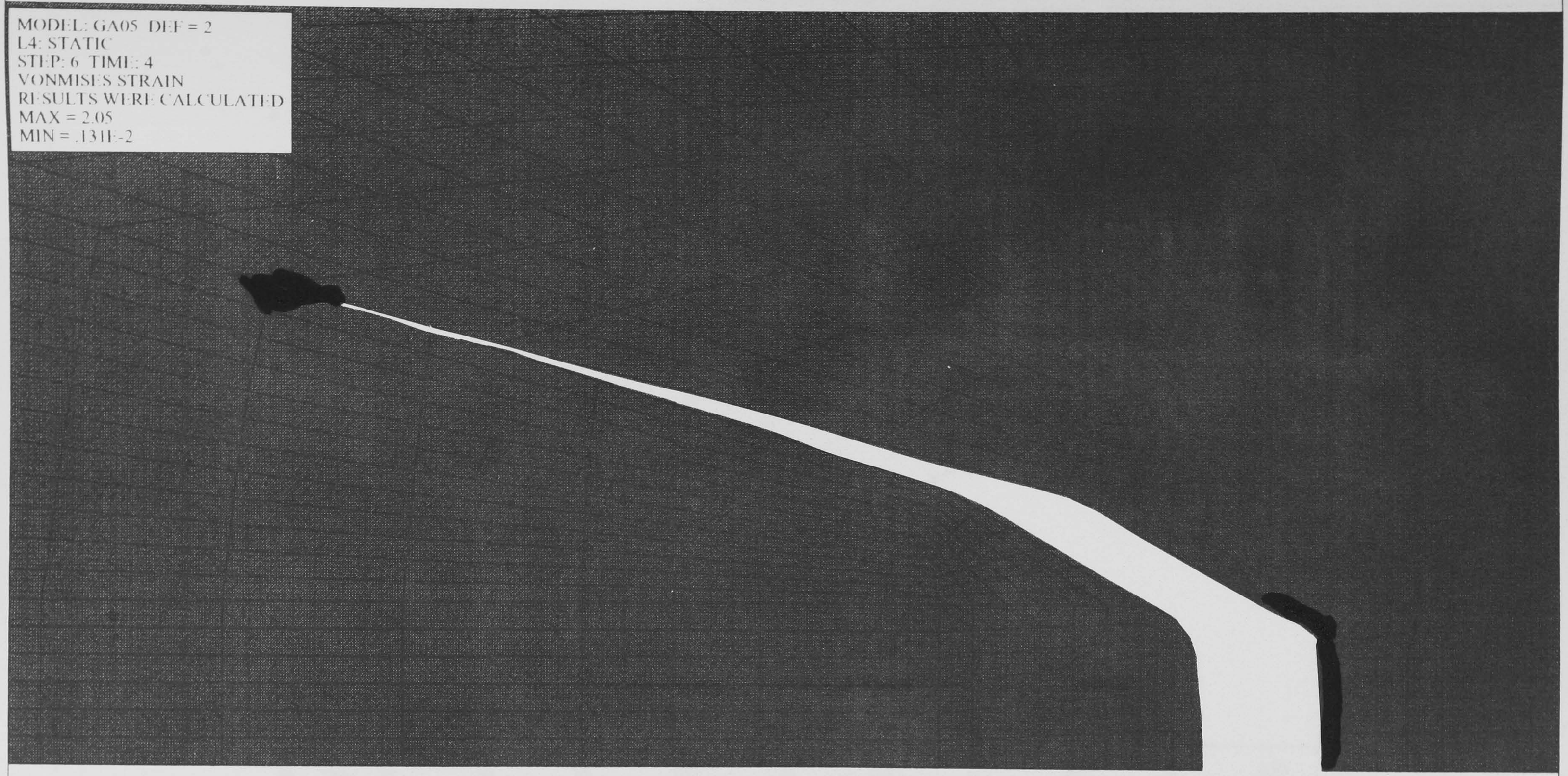

Fig. 7.7 Contour map showing areas of matrix in excess of 20% yield strain (darker areas) ($\psi=70^{o}$)

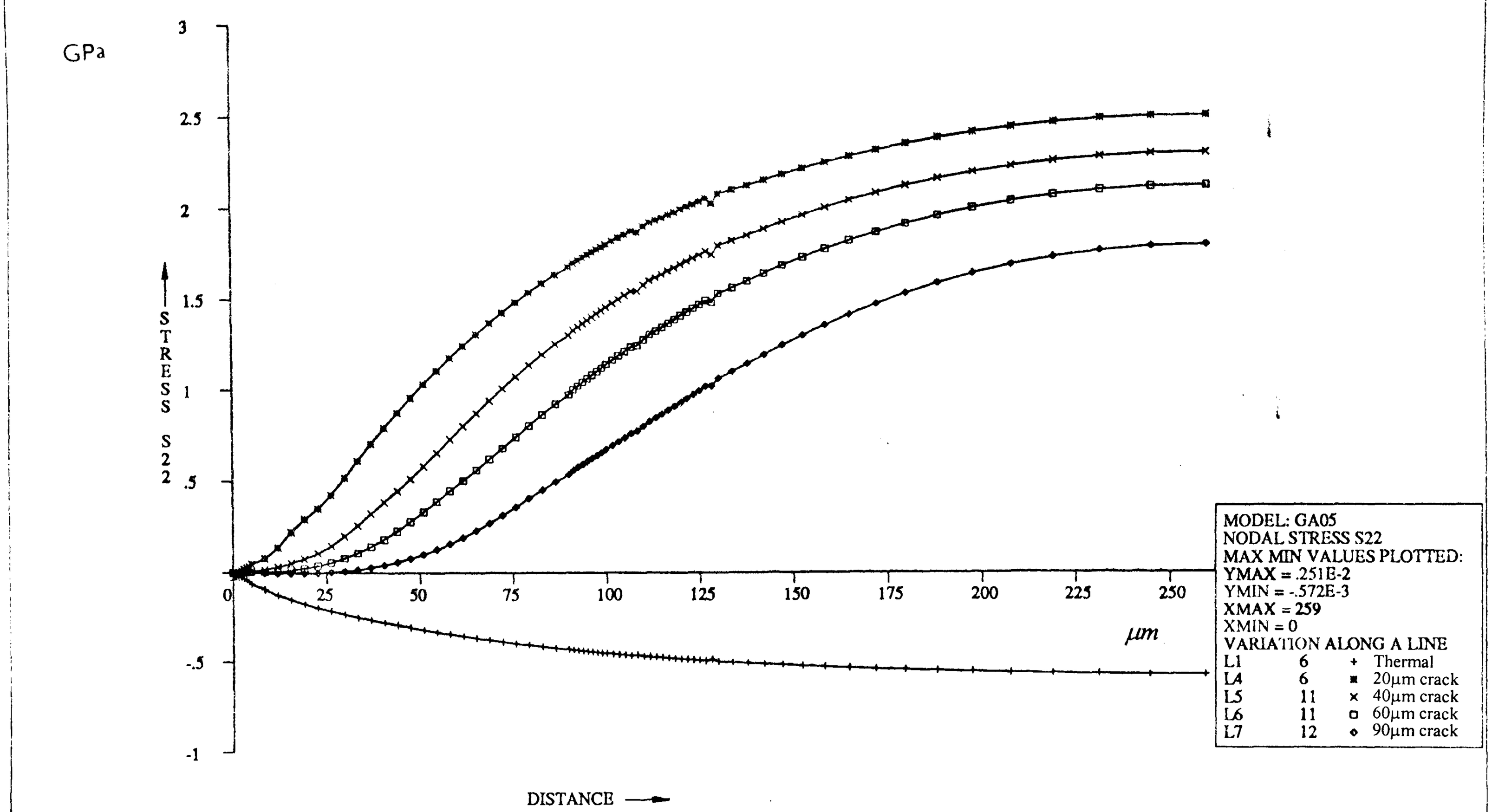

Fig. 7.8 Fibre stress distributions along fibre for matrix crack lengths 20μm, 40μm, 60μm and 90μm (ψ=70°)

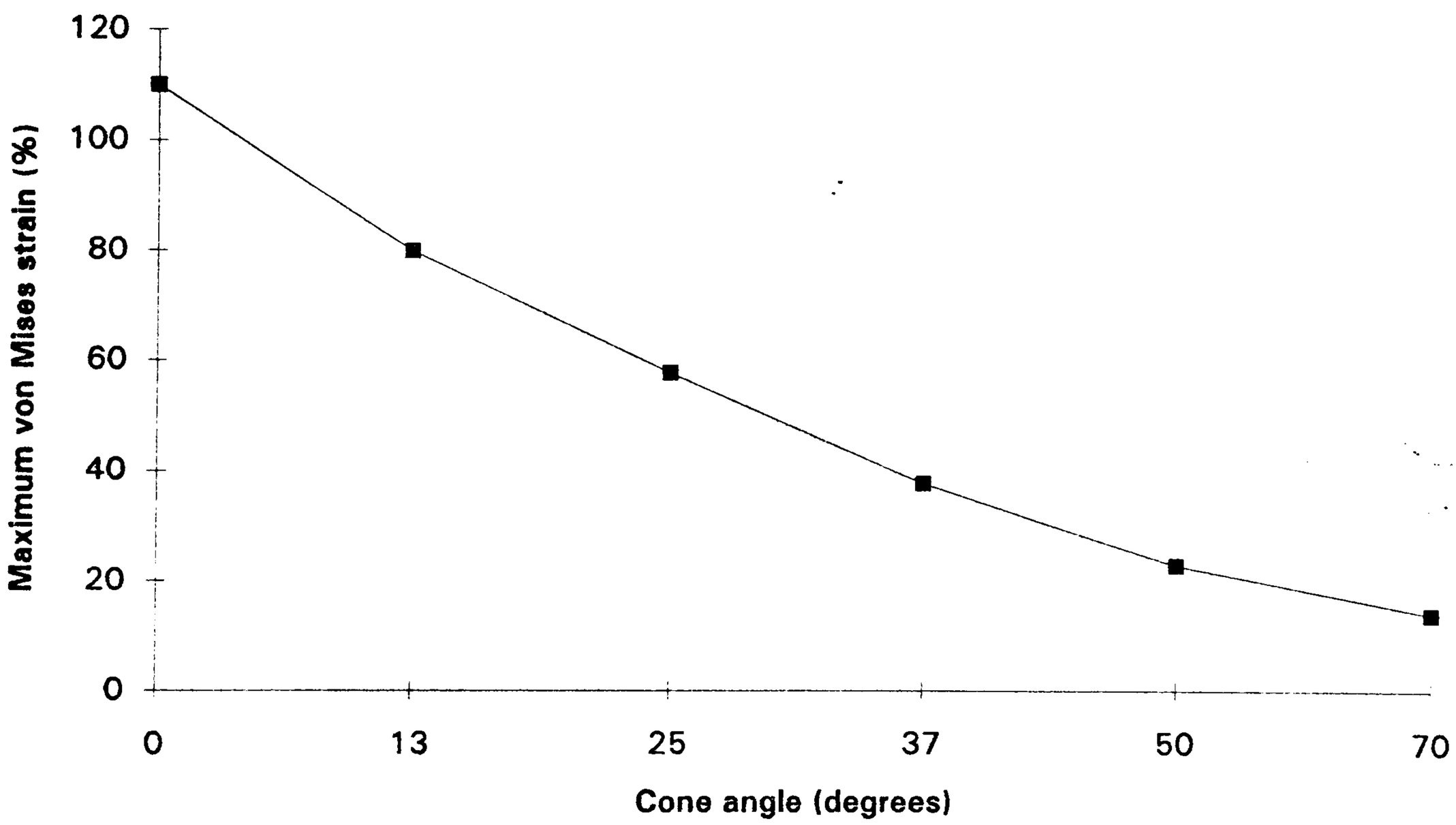

Fig. 7.9 Variation of maximum von Mises strain at the interface versus ψ

23

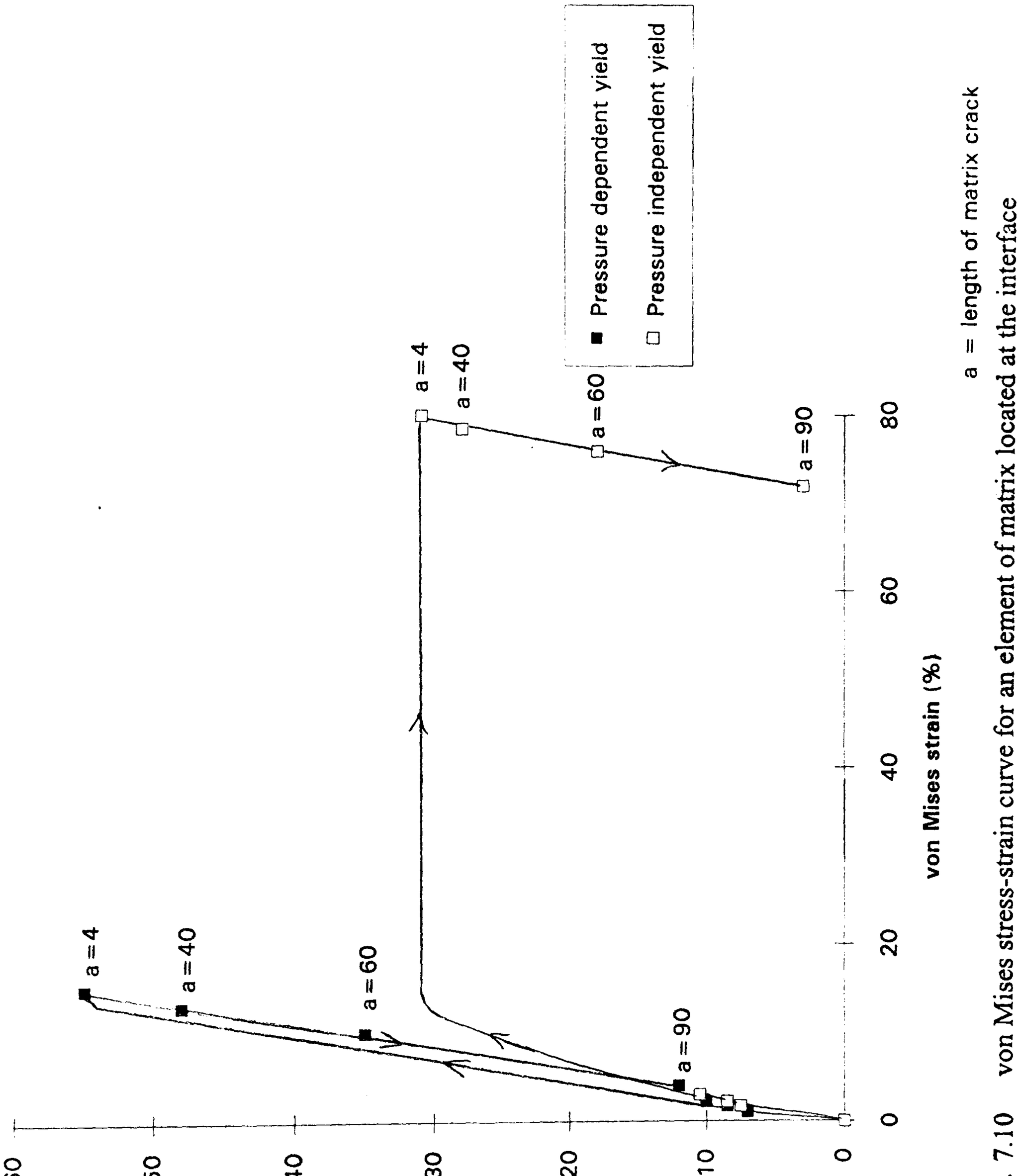

a = length of matrix crack

Fig. 7.10 von Mises stress-strain curve for an element of matrix located at the interface undergoing the non-linear load history; substantial hysteresis is observed for $\psi=0^{\circ}$

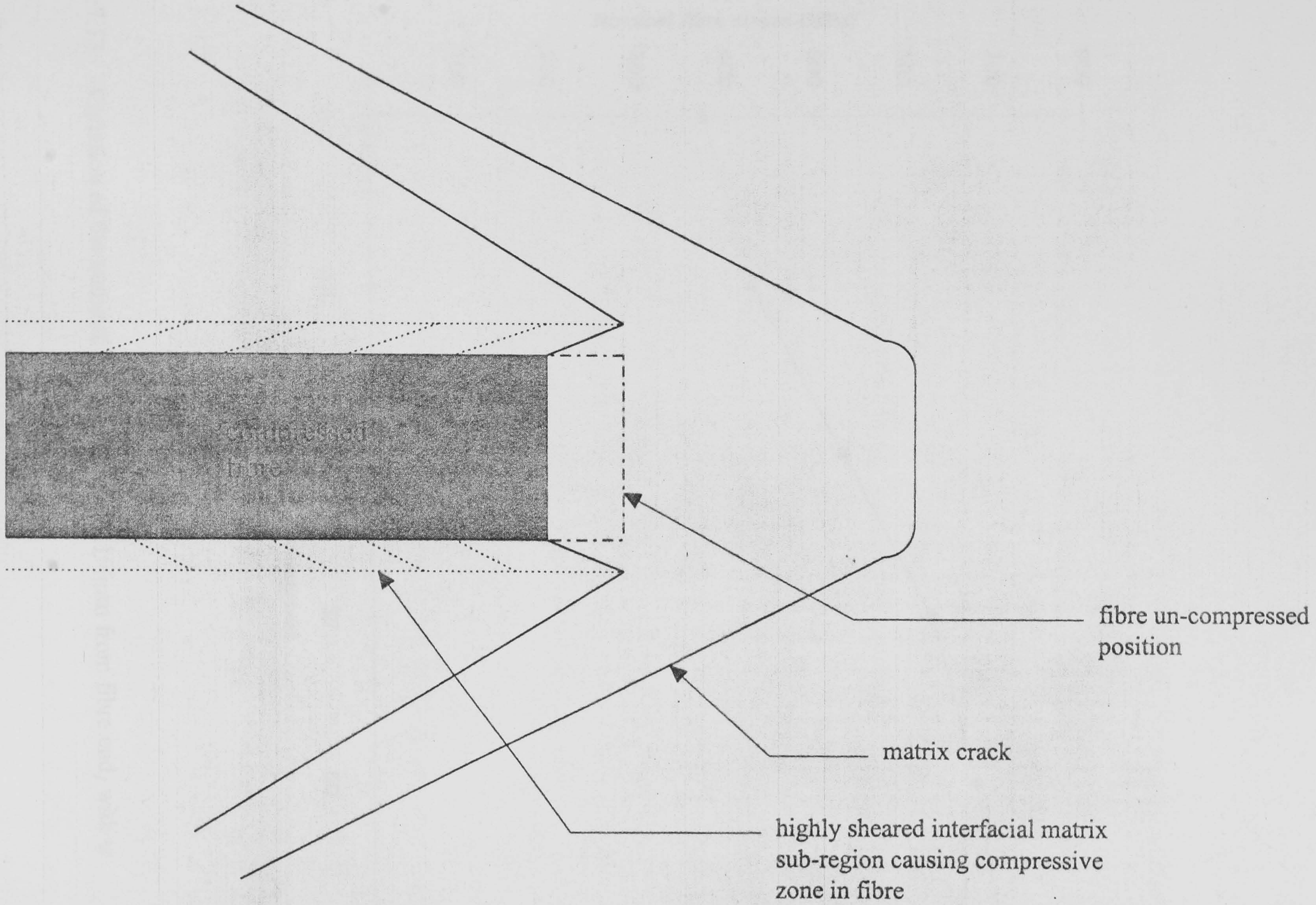

Fig. 7.11 Illustration of how compressive zones in the fibre ends are formed by virtue of the permanent shear in the matrix sub-region, induced under $\psi=0^{\circ}$ regime

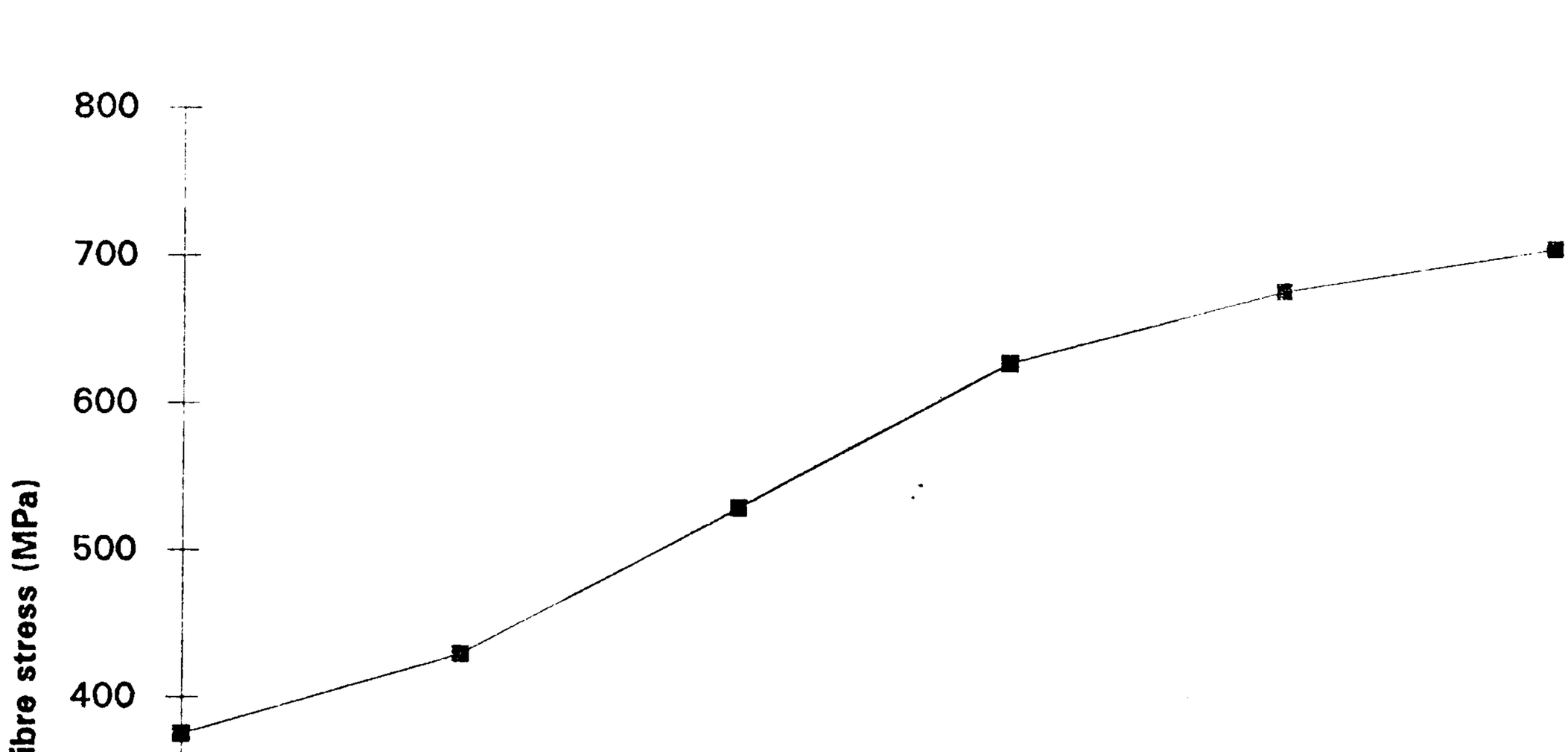

Fig. 7.12 Variation of the nominal stress in the fibre (100μm from fibre end) with ψ

Chapter 8

Interfacial Failure Mode Comparative Study

8.1 Introduction

The analysis of interfacial failure, thus far, has concentrated on the micro-mechanical considerations of the problem. More specifically, attention has been given to the causes and mechanisms of the various Modes of failure, whether they be by a propagating interface crack (Mode β) or by a propagating matrix crack (Mode γ) or simply by interfacial yielding (Mode α). Also the factors that characterise and influence the failure modes have been investigated, such as the coefficient of friction across the interface crack and the pressure-dependency of yielding in the matrix.

However, the *overall* influence of these failure modes as regards the composite specimen as a whole have not been considered. Designers are interested in the *global* properties of the composite and how they will be influenced by the inducement of cracks or localised yielding during service. The relevance of the failure modes with respect to global composite behaviour is a subject not well understood; however, such considerations form the bridge between micro-mechanical analyses and macro-mechanical composite performance.

This chapter is concerned with the critical comparison of the failure modes and their importance as regards global composite behaviour.

8.2 The Failure Modes

Fig. 8.1-2 present the fibre stress profiles for a single fibre composite specimen loaded in tension, undergoing β and γ Modes of interfacial failure, respectively. The Mode β Ω-shape profile consists of an initial linear region, a smooth transition zone and an elastic take-up curve, which correspond to frictional stress transfer across the interface

crack, the crack tip plastic zone and elastically-bonded regions, respectively. The Mode γ S-shape profile consists of an S-shaped take-up curve followed by the elastically bonded portion, where the steepness of the S-shape being proportional to the crack geometry. As has been previously shown, these take-up curves may be considered to be the "fingerprints" of the Mode β and Mode γ failure modes since they indirectly reveal the prevalent failure mode in a composite during a given loading history.

In examining the profiles with regard to the efficiency of reinforcement, it becomes evident that as the mode β interface crack propagates, it leaves behind a region of fibre which reinforces the matrix through a frictional stress transfer mechanism. The linear portion of the fibre stress profile lengthens in tandem with the propagating crack and consequently the reinforcement capability of the fibre is not eliminated but merely reduced. On the contrary, on propagation of a Mode γ matrix crack, the fibre stress take-up profile drops to zero and the S-shape is observed to move forward leaving behind it an unloaded portion of increasing size. Hence in Mode γ, fibre reinforcement capability is being diminished to a comparatively greater extent than in Mode β. Effectively, the stress transfer length increases at a larger rate under a Mode γ failure regime than with mode β.

In order to evaluate the relative fibre reinforcement capability reduction, a *comparative* analysis of the impact of the failure modes on the global properties of the composite specimen is necessary. One of the most important global properties for design purposes is the composite modulus of elasticity, E_c.

8.3 Global Composite Properties

There is a wide range of test data available for the mechanical behaviour of full composites under various forms of loading, particularly uniaxial tensile stress-strain data [1,54]. To date, the majority of testing has been with regard to ascertaining the

effects of *macroscopic* parameters on the composite properties such as the fibre volume fraction, presence of interfacial coupling agents and environmental moisture.

However, the problem with stress-strain curves obtained for a variety of composites is that the source of any non-linearity demonstrated is not apparent. It may be due to the non-linearity in the matrix response, or the initiation of localised interface or matrix cracking, or a combination. In short, the *direct* and *explicit* influence of a given failure mode on the global response of the composite is, as yet, indeterminate.

In order to ascertain the influence of the interfacial failure mode progression on the composite modulus, the stress-strain responses of the composite specimens based on the FE data have been plotted, Fig. 8.3. The graph presents response profiles for the carbon fibre system undergoing Mode β and γ failure. The linear-elastic profile is that derived from the analysis of Chapter 4 in which the restricting assumptions yield a theoretical profile, from which the 'real' profiles deviate on account of the various failure mechanisms. The measure of global stress used is the sectional stress on the composite averaged over the fibre radius, $\sigma_z|_r$. A measure of stress averaged in this manner ensures applicability of the modulus-reduction evaluation to the case of multi-fibre systems where the same mode of failure is likely to occur at a number of fibre end locations. Qualitative evaluations of composite response based on profiles derived in this manner are primarily valid in a comparative context, since the *nominal* composite specimen responses will, to a limited extent, be dependent on specific specimen dimensions. It was established that the effective modulus was insensitive to model dimensions larger than the current model dimensions, since the *effective zone* of fibre reinforcement (or effective volume fraction [1,17]) was smaller than the selected model dimensions. It is immediately clear from Fig. 8.3 that Mode β type failure has, by a significant factor, less influence on the stress-strain response of the composite than Mode γ.

The composite modulus, E_c, may then be plotted as a function of the composite strain, Fig. 8.4, by application of the following equation:

$$E_c(\varepsilon) = \frac{d}{d\varepsilon}\ (\sigma_z|_r) \tag{8.1}$$

The LE profile, by definition, grossly overestimates the composite modulus for all levels of strain, since the composite is supporting abnormally high levels of elastic strain energy. The substantial deterioration of E_c in the presence of a Mode γ crack is emphasized, when compared with the Mode β modulus profile. The reduction in efficiency may be quantified with reference to Fig. 8.4. At 0.5% level of strain, the composite with Mode β has sustained a 5% reduction in modulus whereas with Mode γ a 35% reduction is resultant. This disparity in modulus reduction is particularly of importance in the 0 - 1% applied strain range, since this may be regarded as the service loading range that a composite component is likely to be subjected to. Within this range, Mode γ interfacial failure is far more destructive to the composite modulus than Mode β.

8.4 Controlling Modes of Failure

From the comparative analysis of the two chief interfacial failure modes, it is evident that Mode γ is more damaging than Mode β, the former leading to a substantially greater reduction in global composite modulus over the applied strain range. Thus it is desirable to promote interface cracks rather than matrix cracks, given that crack initiation is an inevitable occurrence during the interfacial failure process. This is because with an interface crack, there is substantial frictional stress transfer as well as crack containment within the interfacial zone, factors both of which maintain high reinforcement efficiency of the fibre during Mode β failure. However, encouraging cracks to propagate along the interface requires the absence of a strong interface, which would otherwise drive the cracks into the matrix. Thus we reach the counter-intuitive conclusion that increasing the interfacial bond strength is detrimental to the composite modulus, and hence to composite performance. This is not quite true, since a weak interface would also lead to the weak transverse strength of the composite. So

there is a trade-off between axial global modulus and transverse strength, when reducing the interfacial bond strength.

The interfacial strength may be controlled by means of coupling agents such as fibre coatings or sizings and decoupling agents [1]. Fibre coatings and sizings generally tend to increase the bond strength, i.e. the interfacial fracture toughness, and decoupling agents tend to weaken the interface. Designing the interfacial bond strength with a view to balancing all the global properties of the composite is a complex task that is specific to the composite system as well as to the intended application.

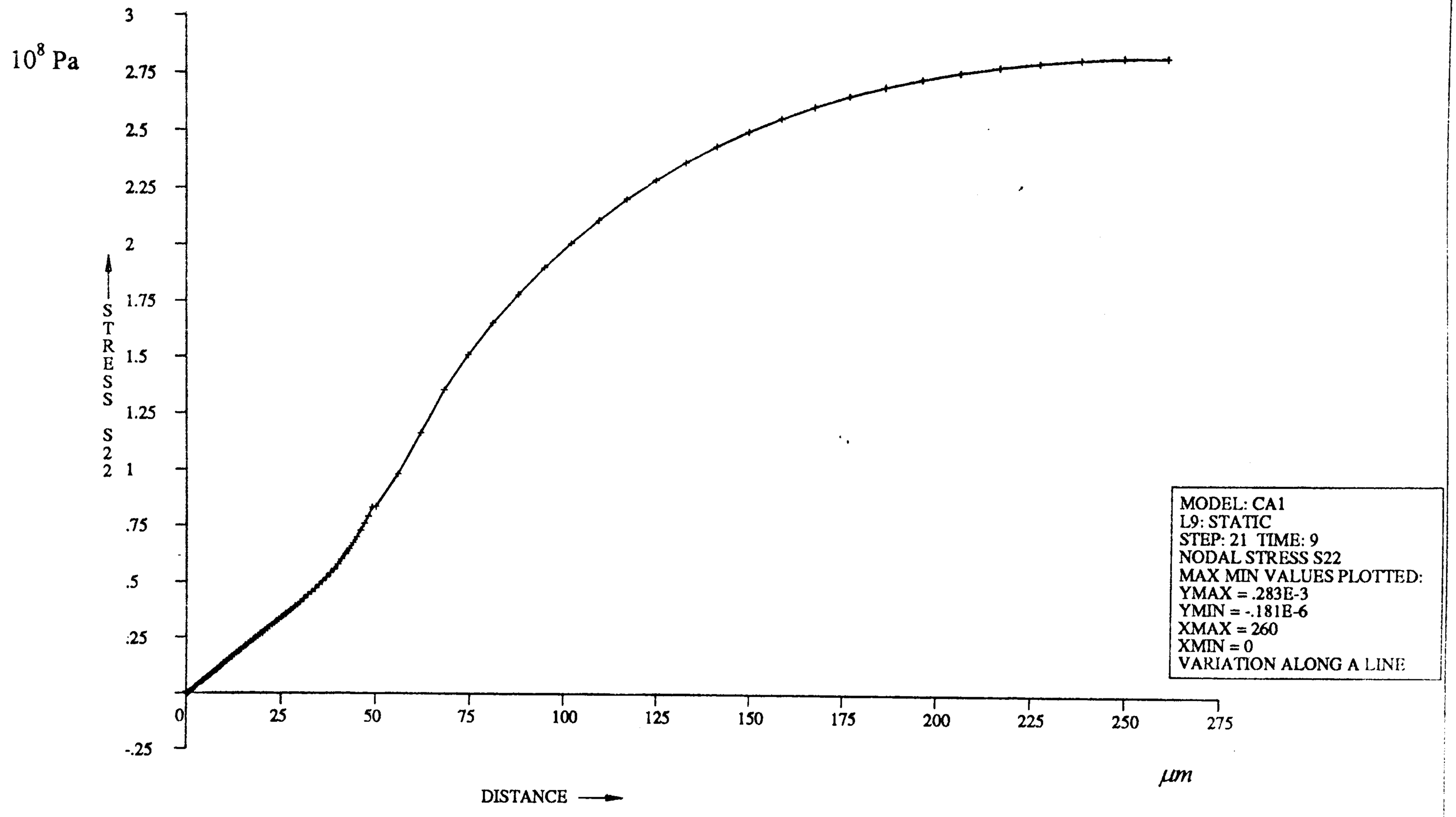

Fig. 8.1 Fibre stress distribution induced during Mode β interfacial failure

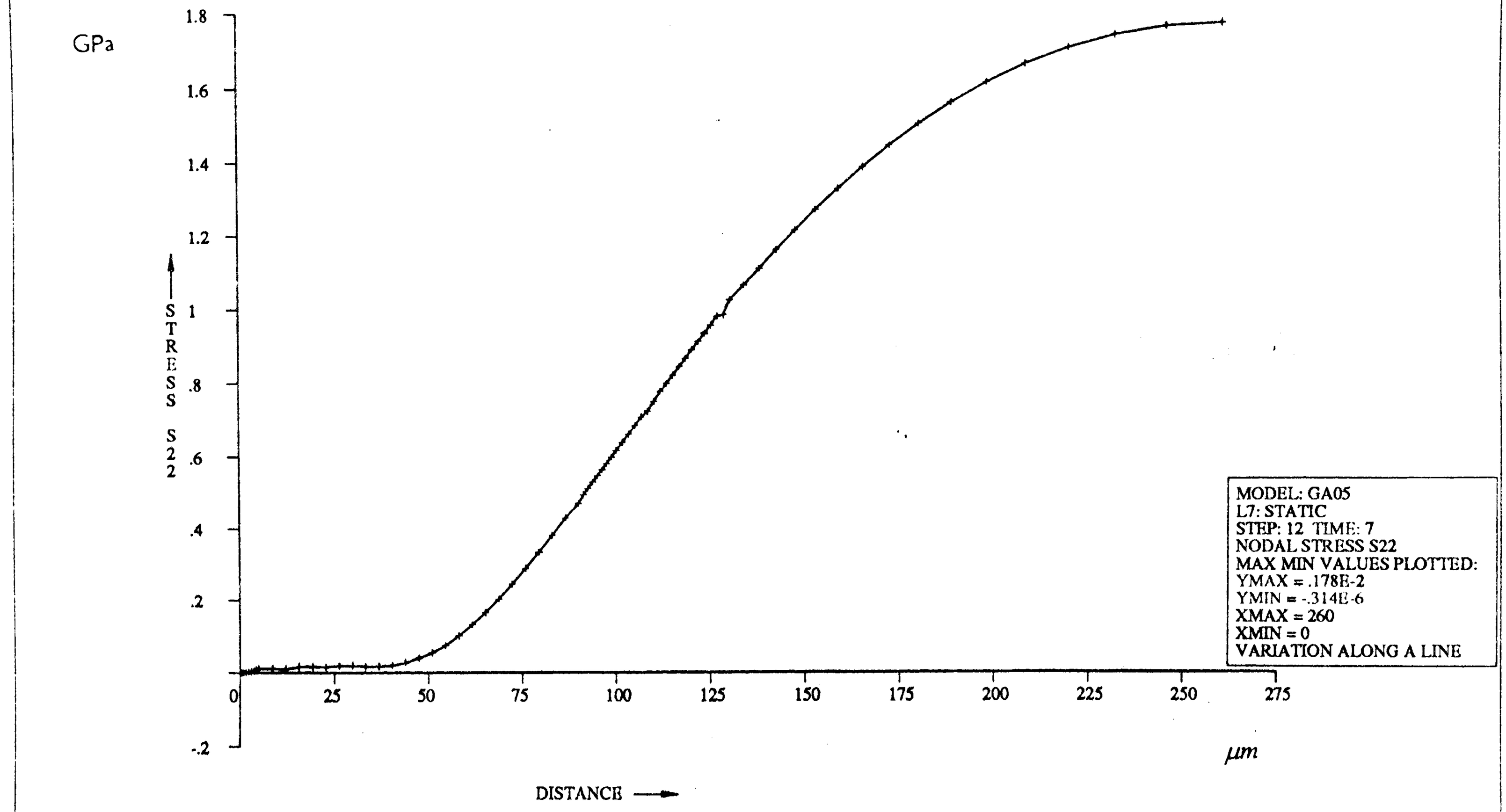

Fig. 8.2 Fibre stress distribution induced during Mode γ interfacial failure

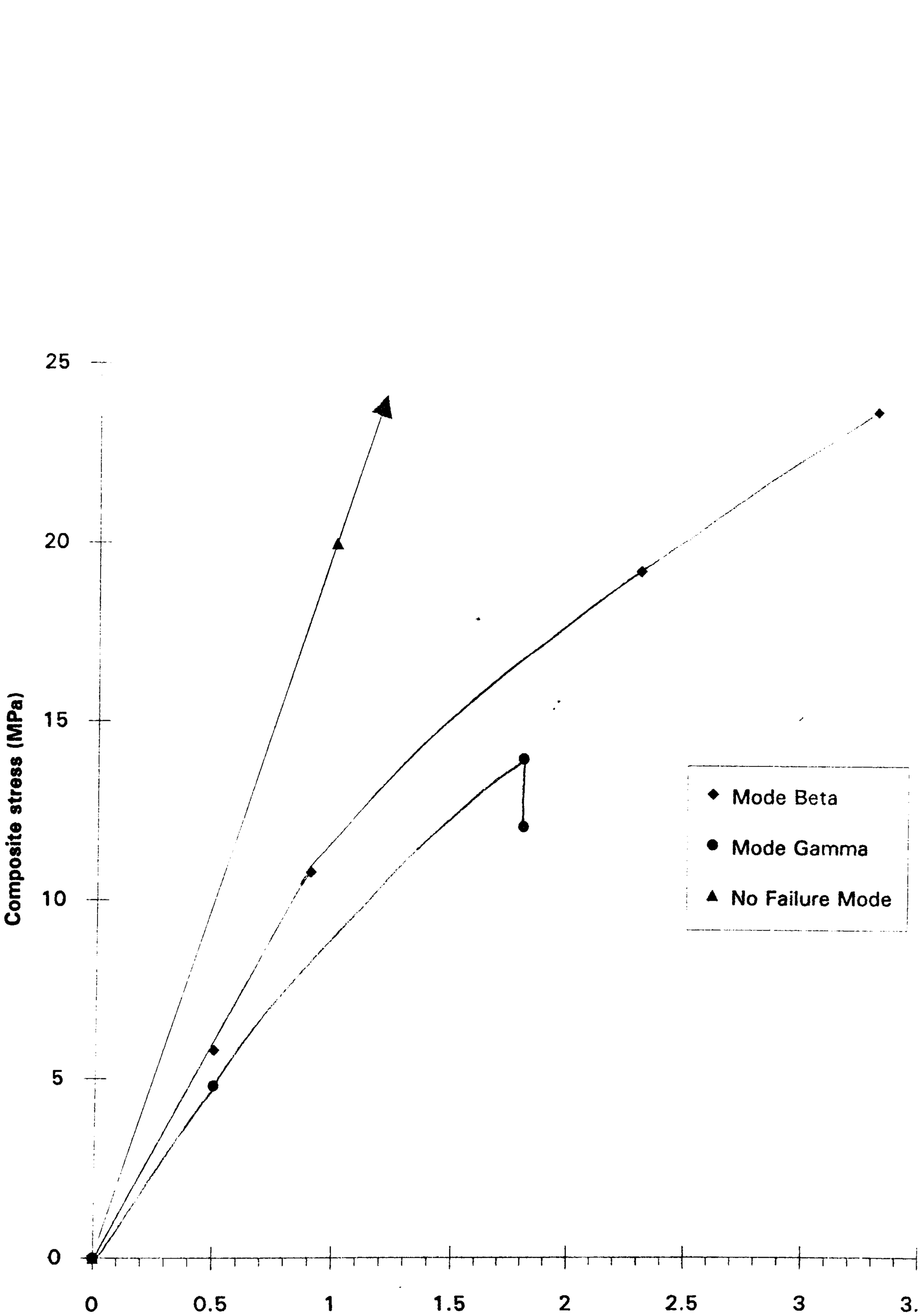

Fig. 8.3 FE-predicted stress-strain response of overall composite under Mode β, Mode γ and no failure regimes

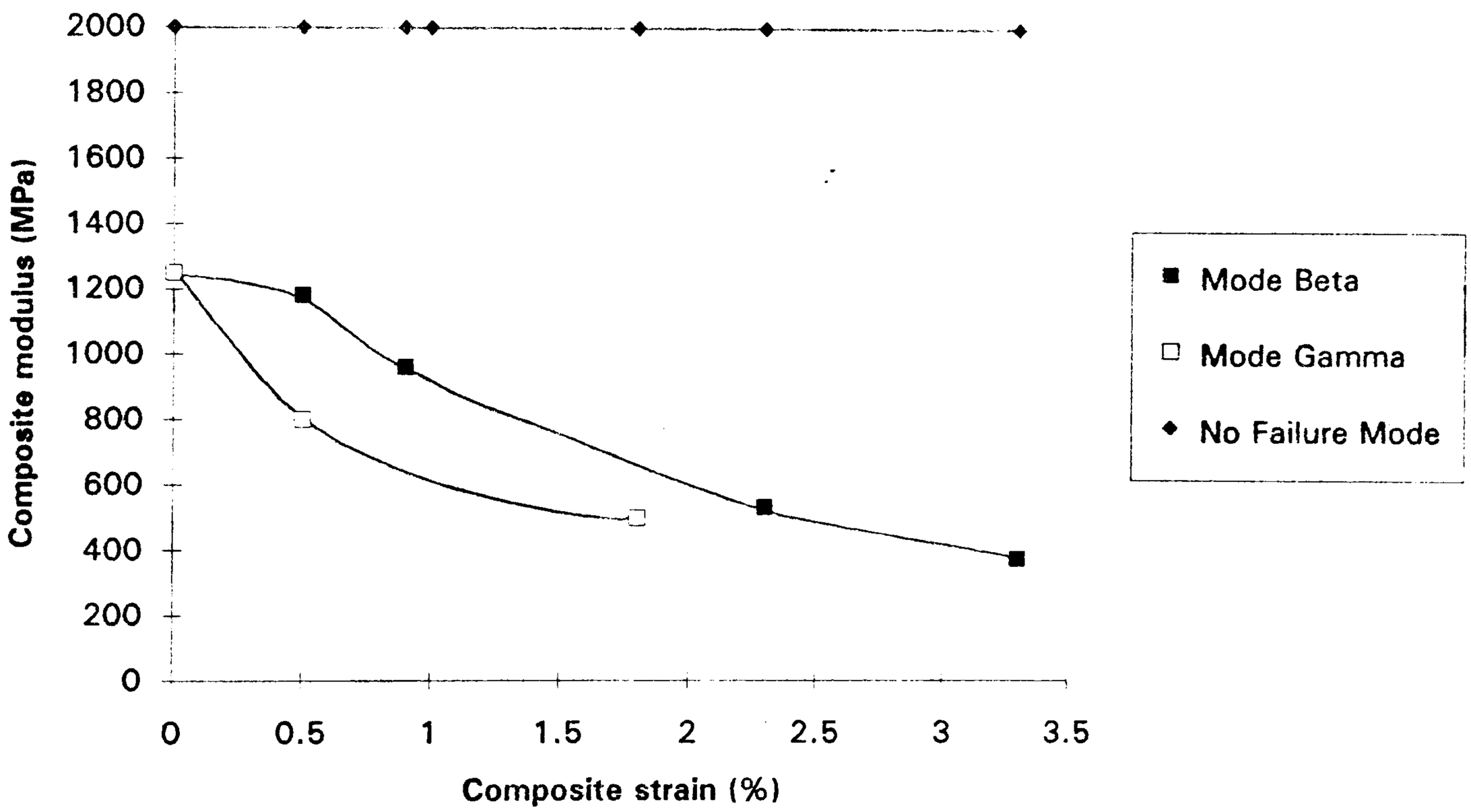

Fig. 8.4 FE-derived modulus profiles for composite under Mode β, Mode γ and no failure regimes

Chapter 9

Interfacial Failure in Multi-Fibre Systems

9.1 Introduction

The primary source of interfacial failure in long fibre composite systems is the failure induced during the *spontaneous fracture* of one of the loaded fibres. During the loading program on the composite, the inducement of fibre fracture and consequent damage zone is likely to initiate successive fractures in adjacent fibres, which would then lead to catastrophic failure of the lamina as a whole. The effects of fibre ends and the associated interfacial failure induced at these locations are of secondary importance, due to the inherent low fibre-end density in long fibre composite systems. In the consideration of interfacial failure in short fibre composites, the representative volume element (RVE) of the system is that of a single short fibre surrounded by a finite volume of matrix, refer Fig. 1.2(a). In addition to being axisymmetric, the system has the advantage of being simpler to analyse. This is, however, not the case for long fibre composite systems in which a fibre has fractured, where the RVE now includes portions of the surrounding fibres, refer Fig. 1.2(b). These surrounding fibres play a key role in reinforcement during the fracture of any given fibre, since the load borne by the fractured fibre is *re-distributed* to the surrounding intact fibres.

9.2 Fracture in Multi-Fibre Composites

If a long-fibre unidirectional lamina is subjected to incremental tensile loading, the axial stress is initially uniform along the length of the fibres. When the applied loading is gradually incremented, there will come a point at which the fracture stress will be reached at a weak location in the fibre. The fracture strength variation over the length of any given sample of fibres is given by the Weibull cumulative probability distribution function [55]. Fracture may occur at a random location in the fibre and the probability of fracture has been found to be proportional to the length of fibre. The

situation is fundamentally different to that of failure in short fibre composites in the sense that the fracture of long fibres and the ensuing interfacial failure is essentially a dynamic process, so any static FE analysis of such a phenomenon will be, by definition, quasi-static. The spontaneous fracture of a fibre will cause the formation of a penny-shaped crack as well as a consequent redistribution in the load being carried by the adjacent intact fibres. This load redistribution will manifest itself as a *stress amplification* in the adjacent fibres near the location of the fracture. Figs. 9.1-2 show both Mode β and γ type failure that would be induced following spontaneous fibre fracture.

The reasons for why a spontaneous fibre fracture may be globally catastrophic for the composite lamina are two-fold. First, there is the marginal weakening of the lamina as fewer fibres are now carrying the load. More importantly, however, is the additional localised stress amplification in the adjacent fibres which will lead to the increase in the probability of successive fibre fractures. Cumulative weakening of the lamina will consequently occur with further successive fibre fractures until its reinforcement capability is completely diminished, thus representing global failure of the lamina.

Of primary interest in the analysis presented in this chapter, are the precise mechanisms involved and the modes of interfacial failure induced at the location of a fibre fracture. By modelling this process in accordance with the Progressional Approach, the post-fracture redistribution of stress in the surrounding intact fibres may be obtained. Also, an understanding of the influence of various modes of interfacial failure on global lamina strength may be gained. By measuring the predicted stress amplification factors (SAF) in these adjacent intact fibres, it is possible to infer relative probabilities as regards successive fractures in the lamina.

9.3 Experimental Data at QMW

The composite specimen that was tested at QMW consisted of seven pre-treated M40B-3K-40B carbon fibres, supplied by Soficar (Toray) Industries, in parallel planar

alignment, Fig. 9.3. The inter-fibre distance was 8μm. The fibres were 6.6 μm in diameter and had a standard level of oxidative surface pre-treatment. The epoxy resin was the LY-HY 5052 Ciba Geigy used in previous studies. Full specimen fabrication details are given in [56].

In a similar manner as with the single fibre specimen testing, the multi-fibre composite was subjected to incremental tensile loading, and the fibre stress distributions were measured along the length of all seven fibres for various levels of applied strain., by Galiotis *et al.*. The technique used for measurement was the recently developed remote laser Raman microscopy (ReRaM) [10,56], which utilizes flexible fibre-optic cables for laser delivery and receiving to and from the measurement probe. This permits operation of the micro-probe in multi-angle positions thus facilitating the testing of a variety of composite specimen geometries.

Monitoring of the fibre stress distributions was performed throughout the incremental tensile loading program. When one of the fibres was observed to fracture, fibre stress measurements were taken with reference to the location of the fracture. Thus distributions of stress in all seven fibres were obtained pre- and post-fracture, with the measurement datum as the fibre fracture location. From these distributions, SAF calculations were made. Comparisons with the FE predictions produced in the current analysis were made and inferences made as to the interfacial failure modes in operation at each stage.

9.4 Finite Element Analyses

The 3D FE model (Fig. 9.4) represents one octant of the composite specimen due to the existence of three orthogonal planes of symmetry in the model geometry, (refer Fig. 9.3). On each of these planes of symmetry in the FE model, appropriate boundary conditions were applied to all constituent nodes to prevent displacements in the associated normal directions. A cross-section of the mesh is shown in Fig. 9.5 in which may be depicted the quarter-section of the central fibre and the three half-

sections of the adjacent fibres. A higher level of mesh refinement in the region of the central fibre has been employed in expectation of high stress and strain gradients that will be induced following central fibre fracture. The mesh consists of approximately 14,200 8-noded brick elements and the length of the model was 600μm. The fibre was modelled as transversely isotropic and the matrix as elasto-plastic (relaxed modulus), and the material properties of fibre and matrix are as given in Table 6.1.

The non-linear loading history consisted of four separate load steps. The two initial load steps were identical to the thermal pre-load and tensile load steps used in the previous single fibre analyses. Hence, a uniform temperature drop of 50 ^{o}C was applied to all nodes in the model, followed by a uniform displacement (equivalent to an applied strain of 0.3%) in the axial direction, imposed on nodal points lying on the end face of the model. The third load step allowed spontaneous fracture of the central fibre and the consequent initiation of a penny-shaped crack. In order to simulate this fracture event, the boundary condition on nodes on the end of the central fibre were removed in this load step thus freeing the fracturing surface. The fibre end was thus permitted to recoil to an unloaded state during this load step, with the exception of the shearing effect of the surrounding matrix acting on the fibre. The concluding load step was a straightforward increase in the applied strain on the composite to 0.5%, in order to correlate results with the experimental data.

In view of the excessively large plastic strains that will be shown to be induced in the current analysis, the analysis was repeated for the case of a fractionally larger transverse crack being inititiated during the fibre fracture load step. The simulation of this event required that the boundary constraint was additionally removed on nodes falling within a 0.5μm radial zone adjacent to the fibre fracture, as shown in Fig. 9.6. This secondary analysis was performed in order to more fully ascertain the nature of the local interfacial failure phenomenon.

9.5 Results and Conclusions

The deformed mesh is presented in Fig. 9.7 showing the matrix contraction due to the thermal cooling of the composite post-fabrication. The contour map of axial stress shows compressive stresses induced in the fibres that are larger in the exterior fibres, Fig. 9.8. This is because the exterior fibres have greater exposure to the contracting matrix and are thus put into a higher level of compression, thereby 'shielding' the inner fibres which consequently sustain lower stresses than their exterior counterparts. However, the value of fibre stress does not exceed 120MPa which is significantly lower than the thermal stress induced in the single fibre specimens of previous analyses. This is due to the fact that there are now seven fibres resisting the thermal contraction of the matrix, and also due to the absence of finite volumes of matrix at the fibre end faces, which otherwise serve to reinforce the contraction, as in the case of single fibre specimens. A low plastic strain of 10% is sustained in the matrix, as shown in the contour map of von Mises strain of Fig. 9.9, and occurs in locations of maximum shear induced at the interface. It should be noted that the dilatational component of the stress tensor is compressive throughout the matrix, hence suppressing possible rupture of thermally-induced yielding matrix. This result was also obtained in the thermal stage of the single fibre analyses (refer Section 6.3.1).

A subsequent uniform applied strain of 0.3% induces uniform stresses throughout all the fibres, as shown in the contour map of axial stress of Fig. 9.10. There are no strain concentrations in the system, due to the absence of geometrical discontinuities and also due to the intactness of the interface along all the fibres during these initial load steps. Since the tensile stress in the fibres is now approximately equal to the lower bound of the fracture stress range (1.3GPa), the central fibre was permitted to fracture in the following load step.

Once fracture and subsequent recoil of the fibre end occurred, the resultant stress state in the fibres is shown in Fig. 9.11. The fractured fibre end sustains a minimal level of stress with gradually increasing stress along the fibre further away from the location of the fibre fracture. Also, the corresponding stress amplification in the adjacent fibre

near the fibre fracture location is clearly visible, Fig. 9.12. Fibre stress profiles are presented for the three adjacent fibres as well as for the central fractured fibre itself, in Figs. 9.13-16.

9.6 Limitations of the Analysis

During the release of elastic strain energy by the fibre post-fracture, the fibre is observed to recoil as shown in the deformed mesh, Fig. 9.17. In doing so, excessive interfacial matrix yielding is induced over a large portion of the fibre length. Examination of the von Mises strain map reveals an unacceptable maximum strain value of 1130% in the vicinity of the fibre fracture, Fig. 9.18. This result is invalid since it violates criterion III (see section 2.4), and inevitable due to the fact that there is *no* allowance for crack propagation *consequent upon* the high plastic strains induced during the analysis. This is due to the absence of a crack propagation criterion in the current analysis. It should be noted that an FE predicted value of gross plastic strain in excess of 50%, in a small-strain analysis such as this, is indicative of the inducement of severly warped mesh elements, which consequently produce inaccurate results. The subsequent load step in which the applied strain on the composite is incremented to 0.5% serves only to worsen the severe non-linearity in the system, as shown by the sharp increase in von Mises strain in the profiles of Fig. 9.19.

A quasi-static consideration of the physical fracture process will be useful in appreciating the importance of crack propagation during fibre fracture. At the instant fracture occurs and a penny-shaped crack is created, an element of matrix located at the crack tip would be momentarily subjected to a high strain. Once the fractured fibre end begins to recoil, relieving itself of elastic strain energy, the matrix element is subjected to increasingly higher levels of strain. Because of the high *strain rate* involved in this process, the actual stress-strain response of the matrix will be that of profile A, the instantaneous modulus in Fig. 9.20, and not of profile B, the relaxed modulus [44-45]. Parenthetically we note that profile A is approximately linear elastic, but with an upper bound on the stress level that is permissable before brittle

fracture of the matrix occurs. Hence profile A only describes the matrix response for the fracture stage of the interfacial failure process. Profile B, is valid for all other stages pre- and post-fracture, as has been assumed in the single fibre elasto-plastic analyses. The matrix element subjected to such a high strain rate will hence fracture in a brittle manner at a relatively early stage of the fibre recoil, and matrix yielding would consequently be suppressed. The preferred failure mode is likely to be that of a matrix crack rather than an interface crack, due to the fact that the fibres in this system are pre-treated. This fibre pre-treatment increases the interfacial fracture toughness hence 'driving' the crack into the matrix. Upon completion of the fractured fibre's recoil, it is expected that a large area of brittle fracture in the form of a Mode γ matrix crack will have been created in the system, in a manner as shown in Fig. 9.2.

Since the current analysis does not include progressive matrix fracture driven by fibre recoil, the matrix is only able to yield to impossibly high values of plastic strain thus predicting incorrect solutions, as has been shown in the current analysis. However, what may be said with a high degree of certainty, is that the interfacial failure process induced during spontaneous fibre fracture is *primarily Mode γ*, with the manifestation of Mode α being minimal.

The current analysis is a quasi-static analysis of an essentially dynamic process, with the induced matrix crack being driven by fibre end recoil, and travelling at high velocity during its formation. In contrast, the fibre-end debonding stage of the interfacial failure process for short fibres is also considered to be instantaneous (See Section 6.3.2), but is several orders of magnitude less explosive than the fibre fracture event considered here, due to the lower strain energy release associated with the fibre end debonding. With reference to the message file that was produced during the numerical solution by ABAQUS, it was found that a matrix plastic strain of 70% was predicted at a fibre recoil increment of 30% of the complete recoil distance. That is to say the surrounding matrix would already have fractured even before the fractured fibre had recoiled 30% of its stress relieving distance.

The FE predicted SAF values in the adjacent fibres, based on the stresses in the profiles of Figs. 9.14-16, were calculated to be 1.13 for the first-adjacent fibre, and 1.01 for the second and third fibres. These values were found to remain unchanged when the applied strain was subsequently incremented to 0.5%. The SAF calculated from the experimental fibre stress profiles for an applied strain of 0.5% was found to be 1.20 for an inter-fibre distance of 8μm [56]. The FE value underestimates the experimental SAF due to the excessive interfacial yielding and suppression of matrix crack formation. This is because the large shearing effect of the recoiling fibre is being absorbed by the abnormally compliant matrix and *not* being fully transferred, via brittle crack propagation, to the adjacent fibres. Hence the yielding matrix is effectively 'shielding' the adjacent fibres from the higher stress amplification post-fracture, that would otherwise normally exist.

In the analysis involving the initiation of a fractionally larger penny-shaped crack, the deformed mesh of the recoiled fibre shows large local shear in the matrix elements near the crack tip. The peak von Mises strain at the crack tip was found to be substantially lower than before at 500%, Fig. 9.21. The fibre stress profiles, however, were found to be very similar with those induced in the case of the smaller crack. This suggests that although a larger matrix crack significantly lowers the local strain concentration, its dimensions are still insufficient to represent the real equilibrium solution. The lowering of the strain with crack length indicates the requirement of additional matrix crack growth, as a result of excessive plastic strain at the crack tip (with the matrix elastic response as given by profile A). A more exhaustive analysis of this phenomenon would entail the use of a crack extension criterion dependent on the maximum stress induced at the crack tip, to be evaluated at each increment of the fibre recoil process. Hence matrix crack growth would occur simultaneously with, and be driven by, fibre recoil, as occurs in the real dynamic process.

9.7 Global Lamina Failure Mechanisms

It may be extrapolated that once a matrix crack has formed at a given fracture location, the probability of successive fractures in surrounding fibres will increase as the matrix crack propagates and encounters intact fibres. It is conceivable that the crack could be arrested or blunted by an adjacent fibre thereby causing the crack to deflect out of its original direction and propagate along the interface of the fibre. Experimental observations to support these type of failure mechanisms have been made using polarized light micrograph investigations by other authors [57]. It was found that tensile-loaded multi-fibre composites specimens, similar to the pre-treated fibre system in the current analysis, reveal an alignment of fractures induced in adjacent fibres, upon the fracture of a given primary fibre. This alignment of successive fibre fractures was found to overrule the influence of randomly distributed fractures occuring due to the Weibull variation in strength over fibre length [55]. On the contrary, composite specimens consisting untreated fibres were found to possess minimal alignment in fibre fractures (i.e. random), as well as large areas of Mode β-type interface cracking. These observations may be explained by the fibre surface pre-treatment effectively increasing the interface bond strength which consequently drives the crack into the matrix, on fracture of a given fibre. This leads to higher SAF's consequent upon the propagating matrix crack, which results in a higher alignment of adjacent fibre fractures. However, for the untreated fibres where the interface strength is low, interface cracks are formed during fracture and the associated stress distribution in the adjacent fibres causes successive fractures, but at a distance from the original fracture plane [57].

Thus the counter-intuitive conclusion is reached that fibre-matrix bond strengthening through specific fibre surface pre-treatments, or coupling agents, is damaging to the global strength of the composite lamina. Recently, toughness-reducing fibre coatings have been developed which promote the initiation of interface cracks on fibre fracture and also the deflection of approaching matrix cracks at the interface, which consequently increase the toughness of the composite as a whole [58].

A mechanism, which has been found in the current investigation to produce lower SAF's, is to allow localised yielding in the vicinity of the fibre fracture to occur, thus shielding the adjacent fibres from high SAF's and reducing the probability of successive fibre fractures. This will inevitably require the addition of a third material phase, or interlayer, whose high strain-rate response is fairly compliant, unlike that of the matrix material, which behaves linear-elastically. Such design would lead to the *containment* of the interfacial failure zone induced upon fibre fracture and would consequently prevent large-scale deterioration in the global composite reinforcement efficiency.

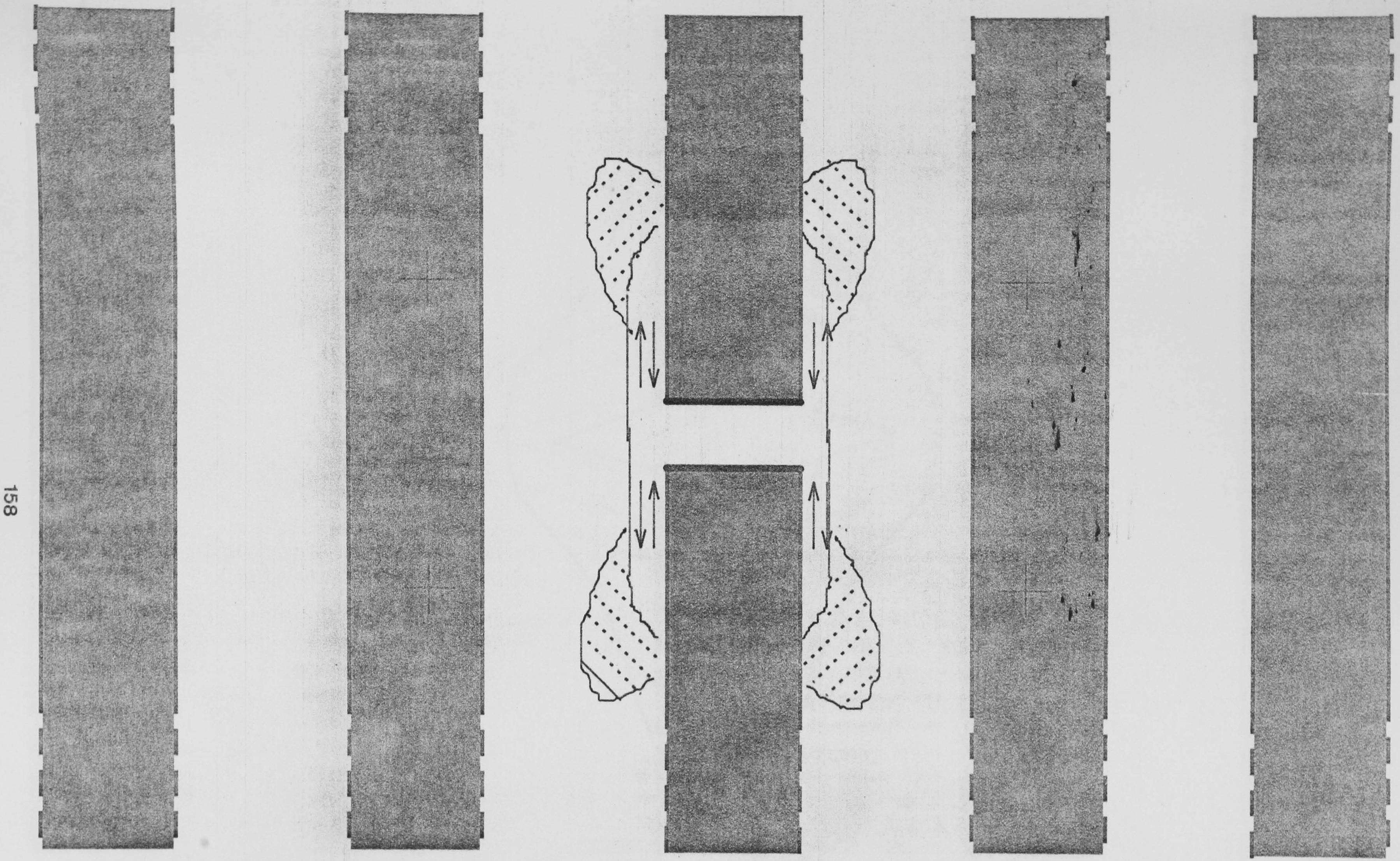

Fig. 9.1 Illustration of failure mode consequent upon fibre fracture (Mode β type)

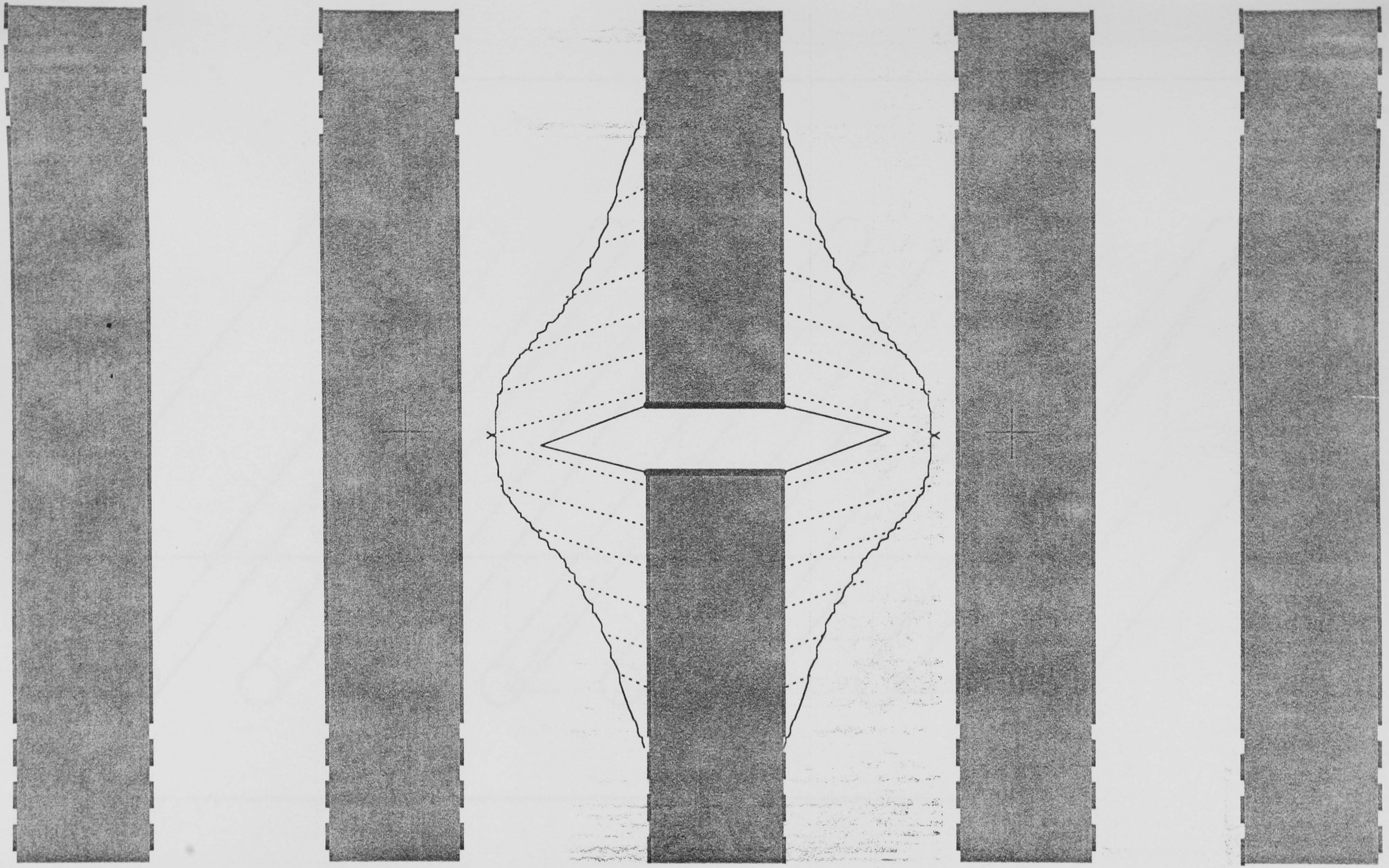

Fig. 9.2 Illustration of failure mode consequent upon fibre fracture (Mode γ type)

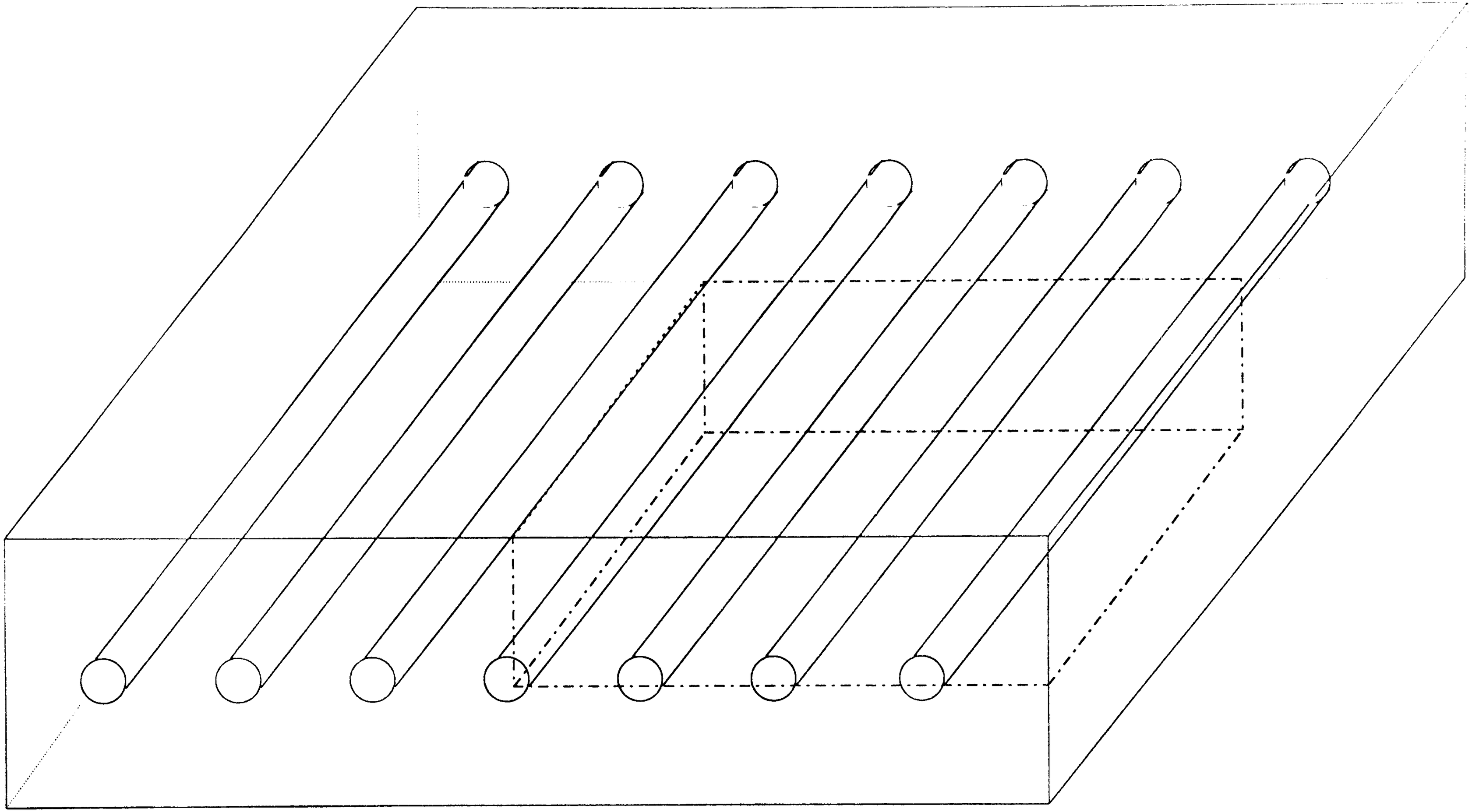

Fig. 9.3 Composite specimen of 7 long fibres in planar array; the octant symmetric section is indicated (dashed lines)

MODEL : 3D

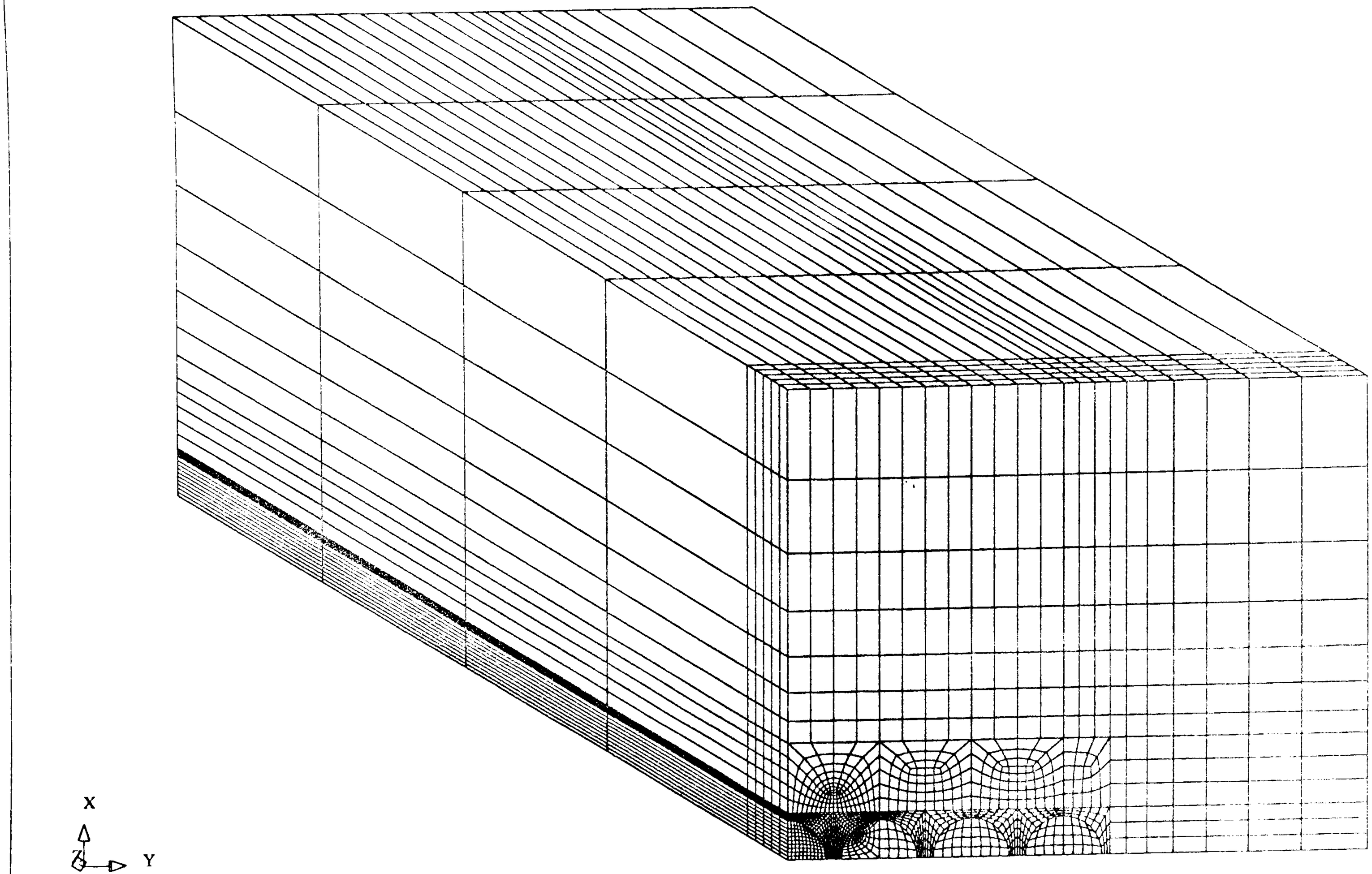

Fig. 9.4 FE mesh of 3D multi-fibre model

MODEL : 3D

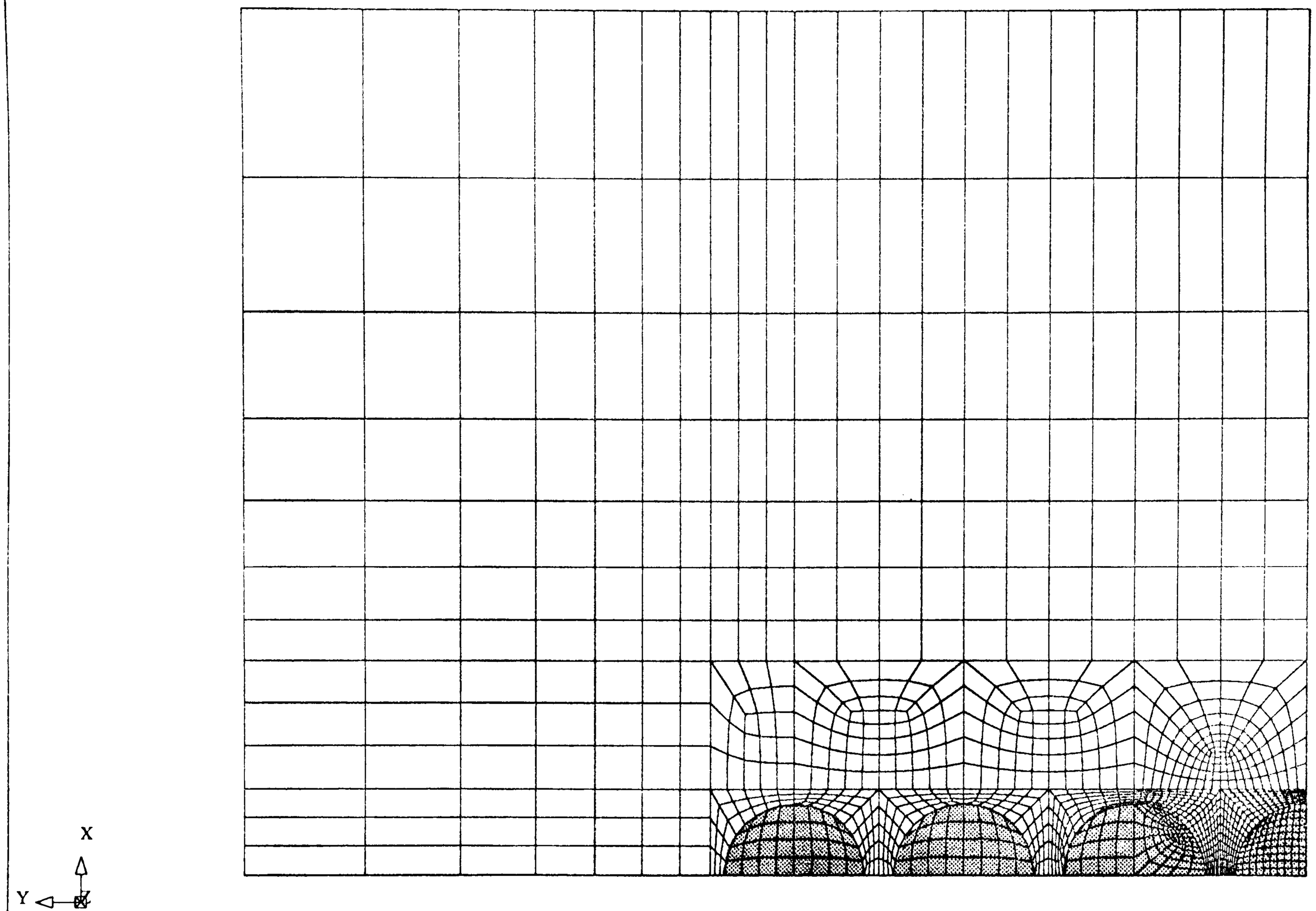

Fig. 9.5 2D section through mesh showing mesh refinement near central fibre

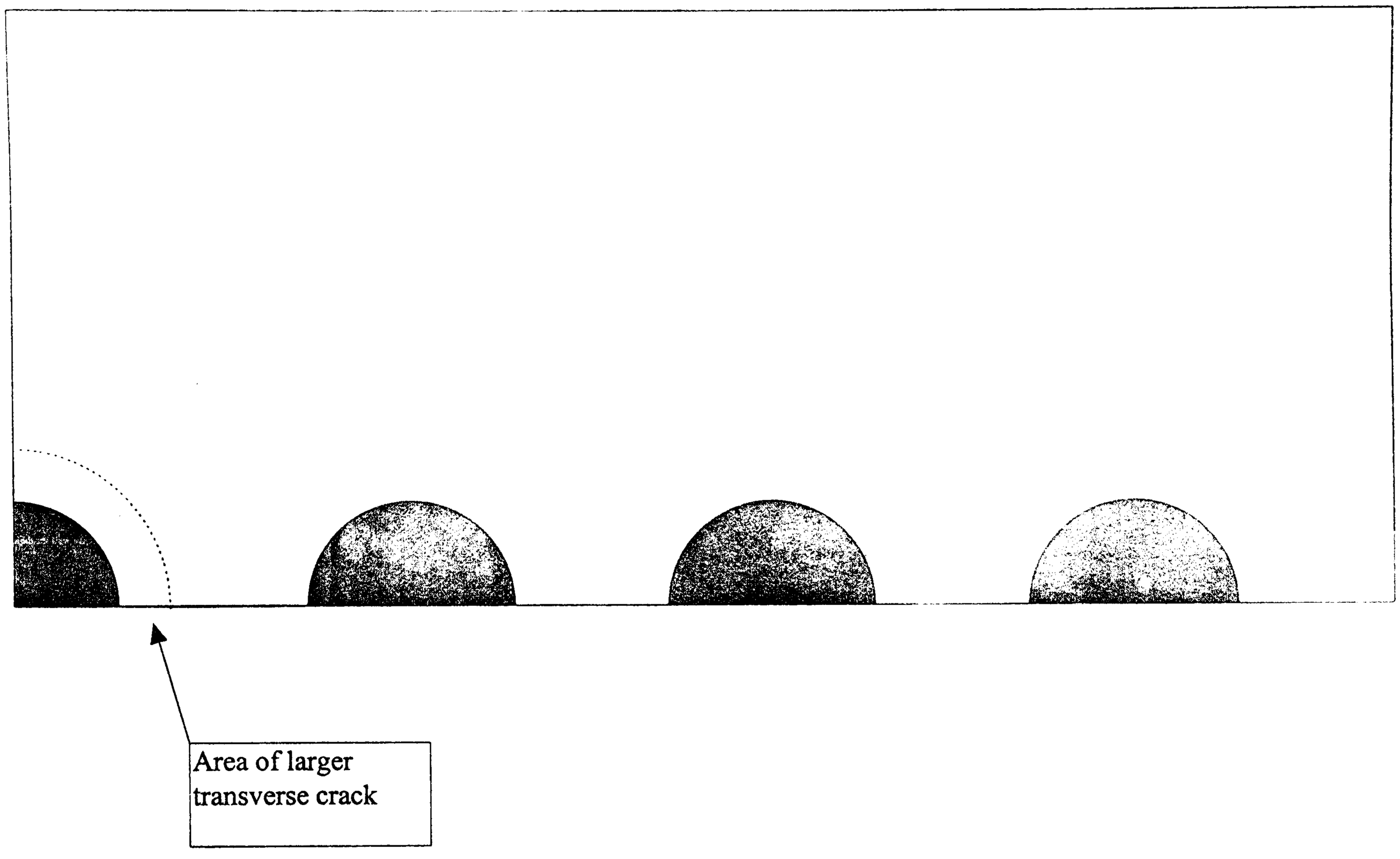

Fig. 9.6 Illustration of area of transverse crack growth consequent upon fibre fracture

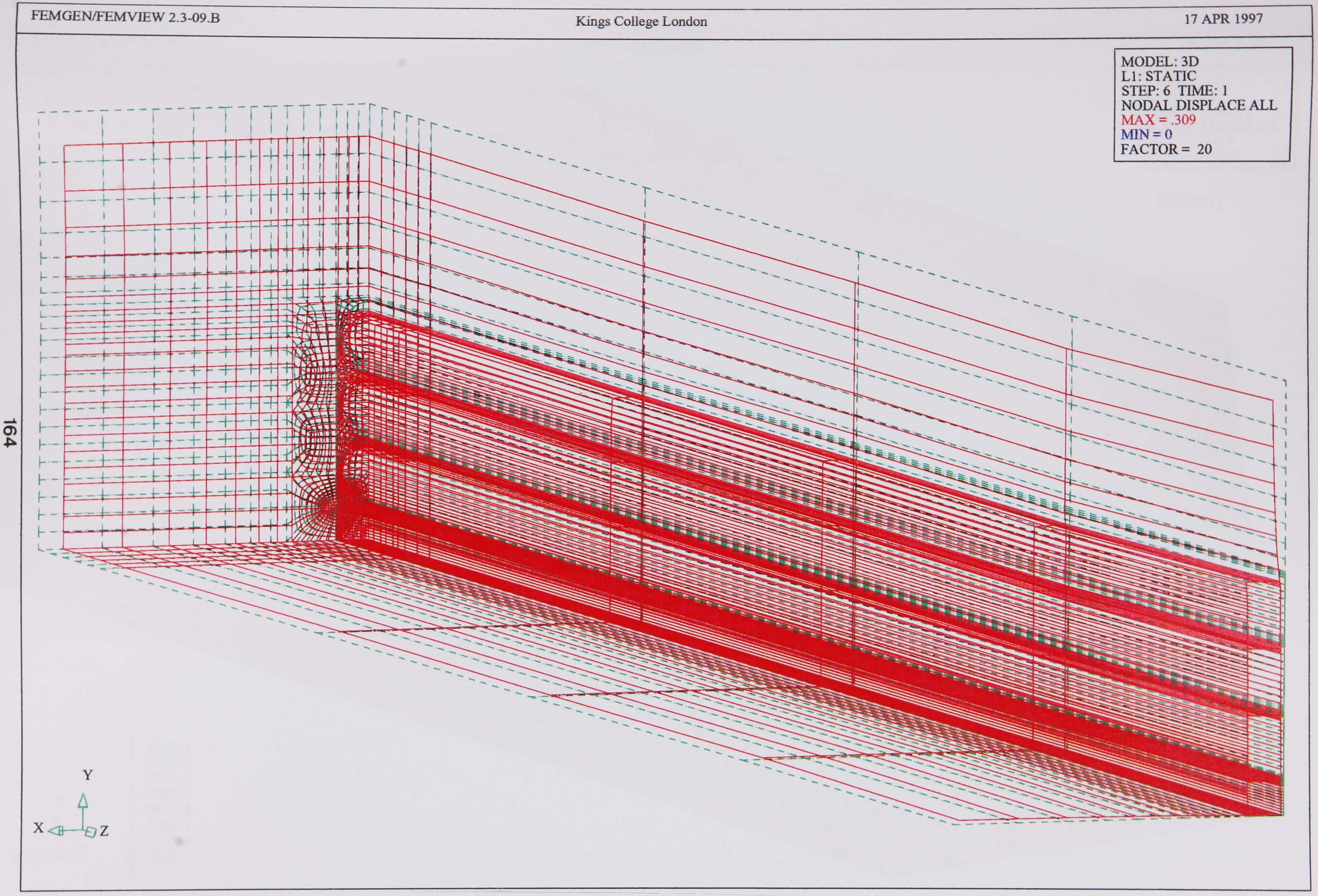

Fig. 9.7 Deformed mesh (solid lines) due to thermal contraction

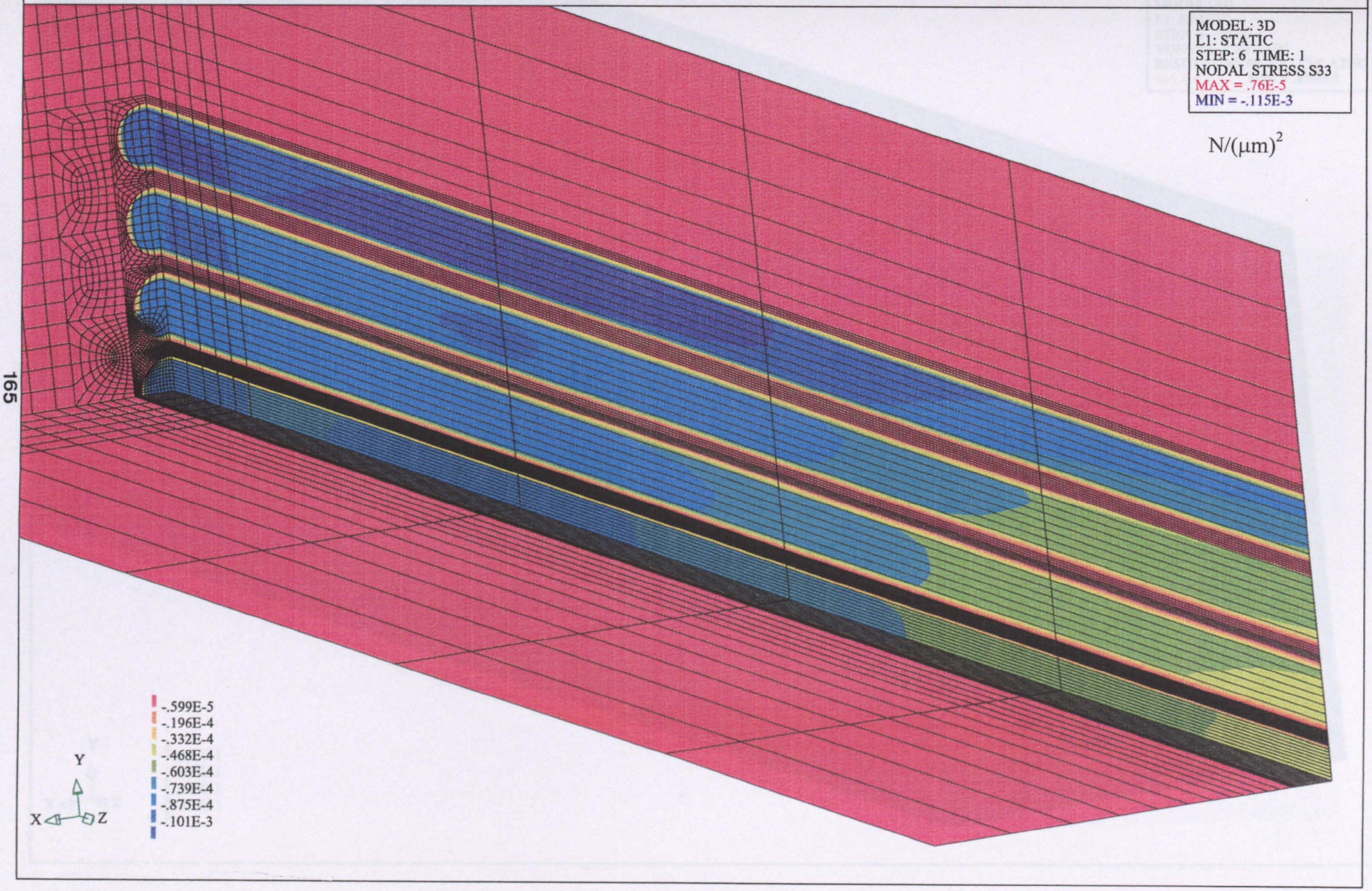

Fig. 9.8 Axial stress contour map due to thermal contraction

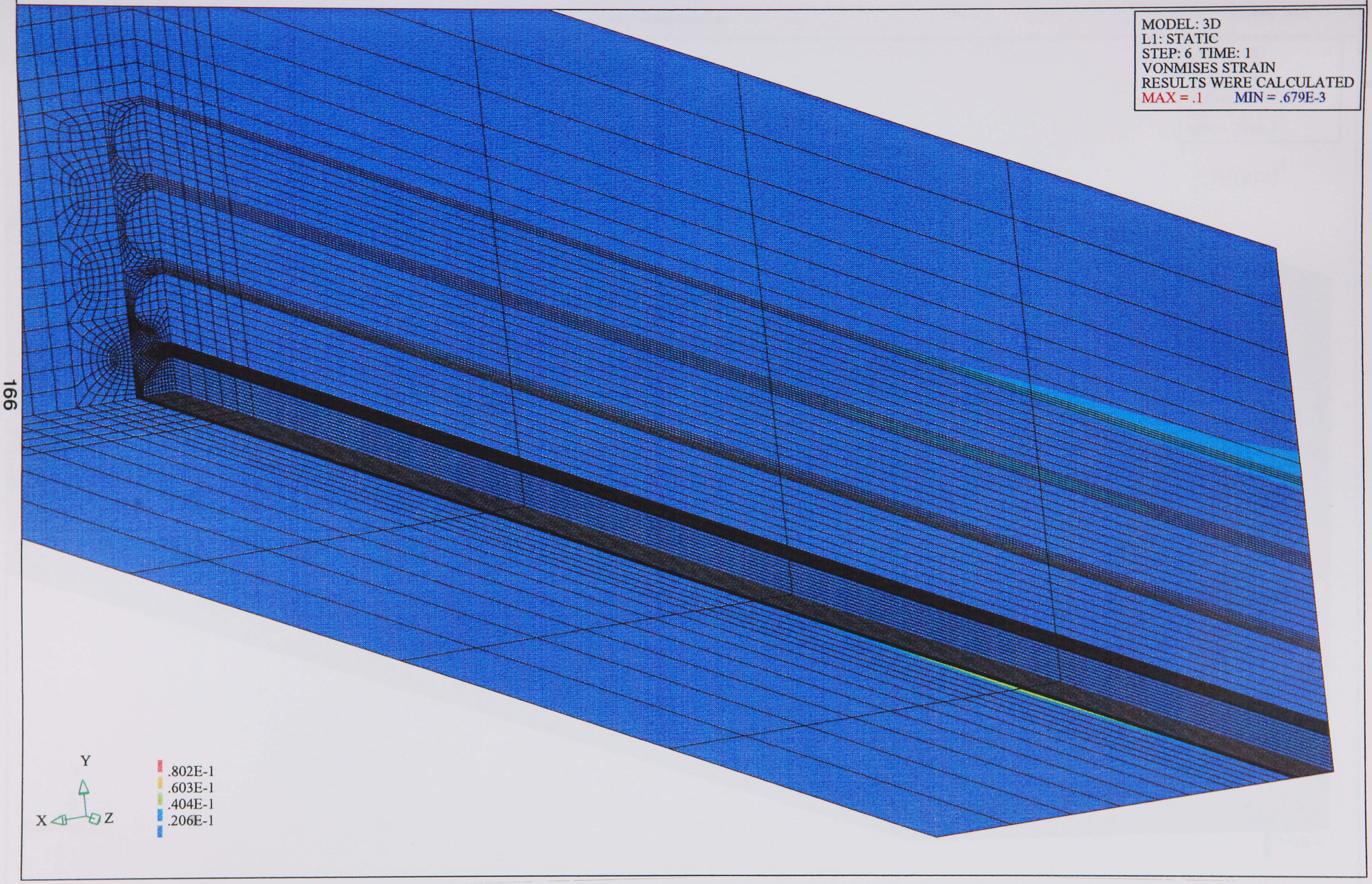

Fig. 9.9 von Mises strain map due to thermal contraction

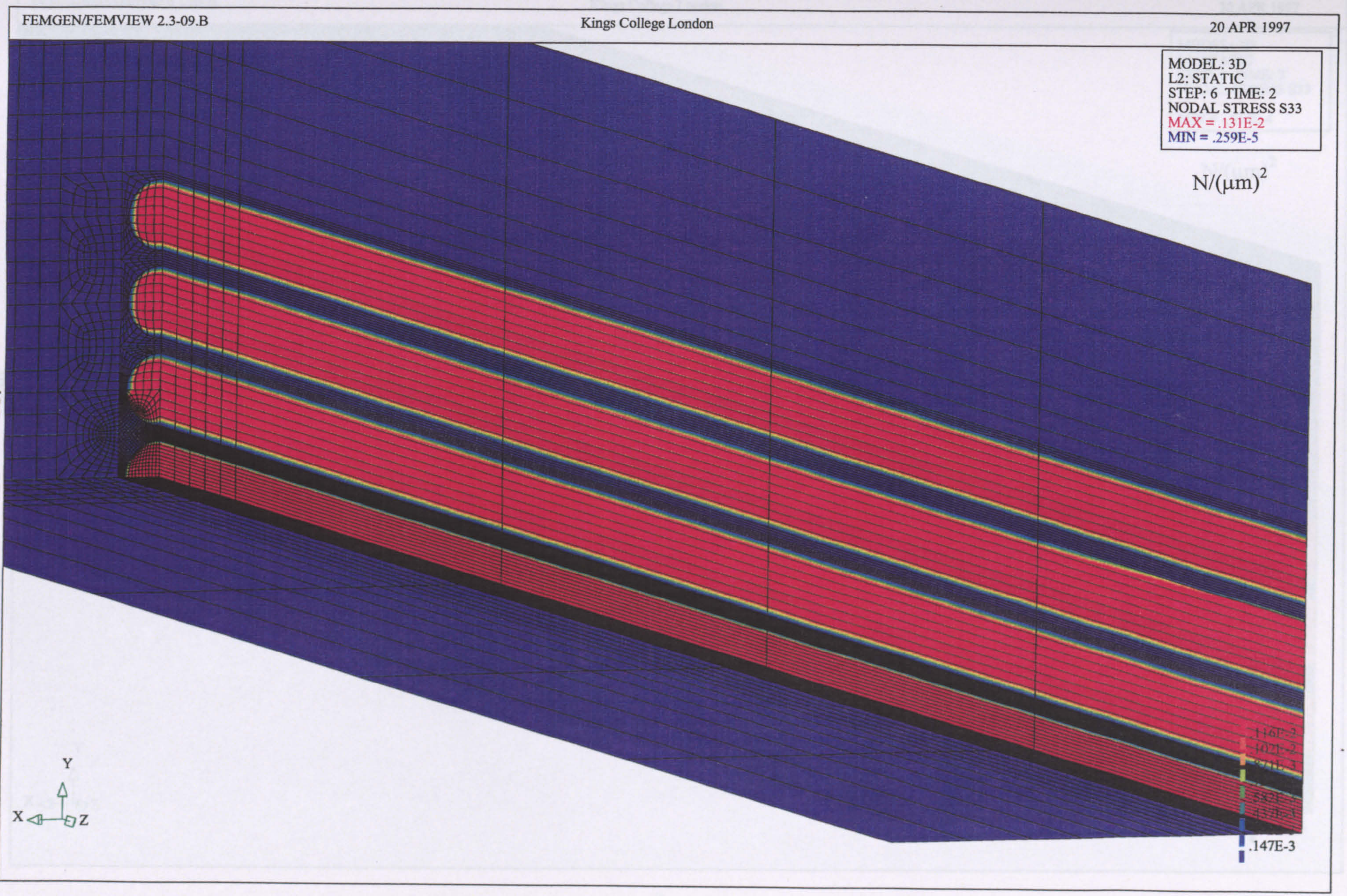

Fig. 9.10 Axial stress map due to uniform tensile loading

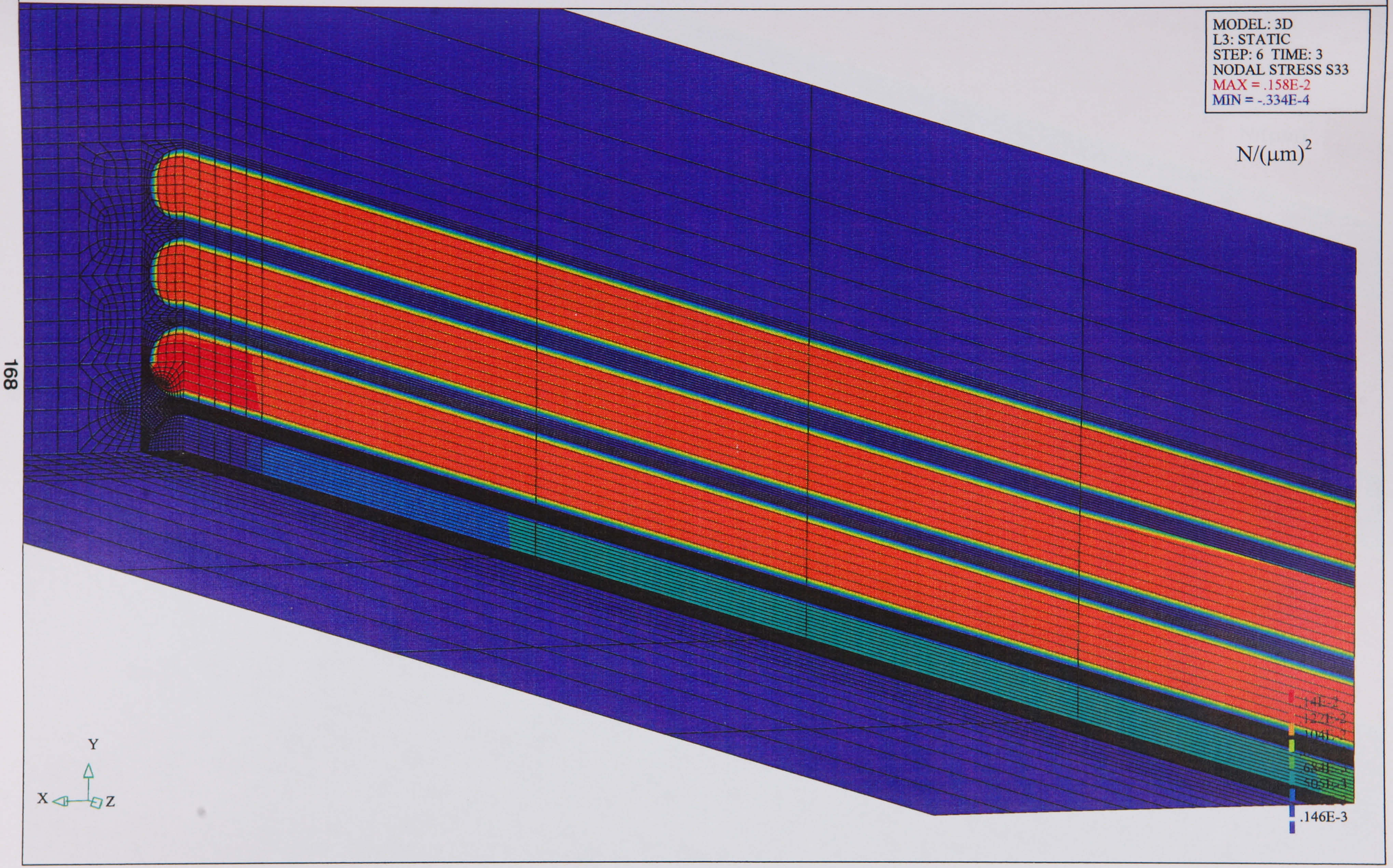

Fig. 9.11 Axial stress map after fracture of central fibre

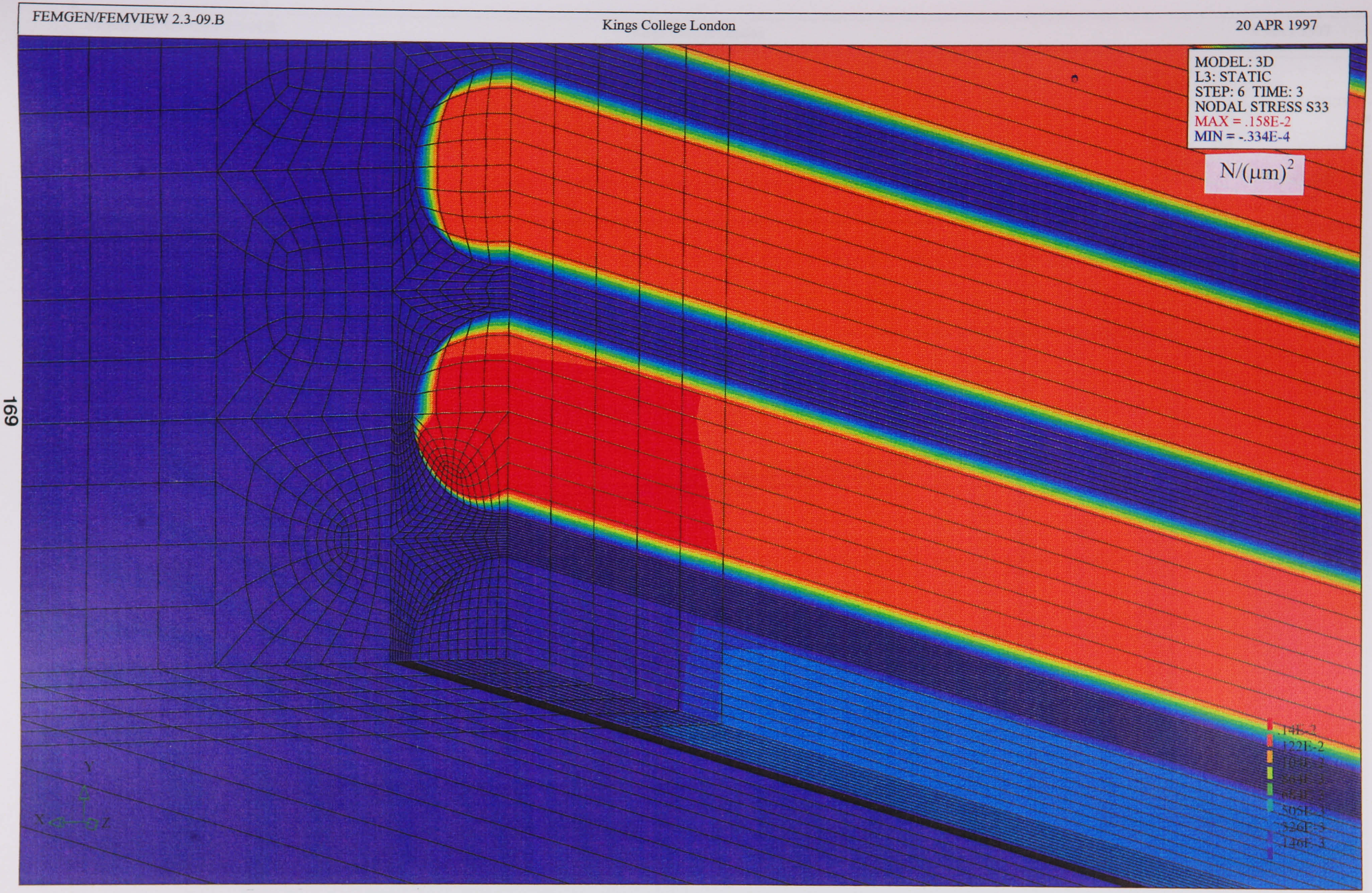

Fig. 9.12 Axial stress map highlighting stress amplification in first adjacent fibre

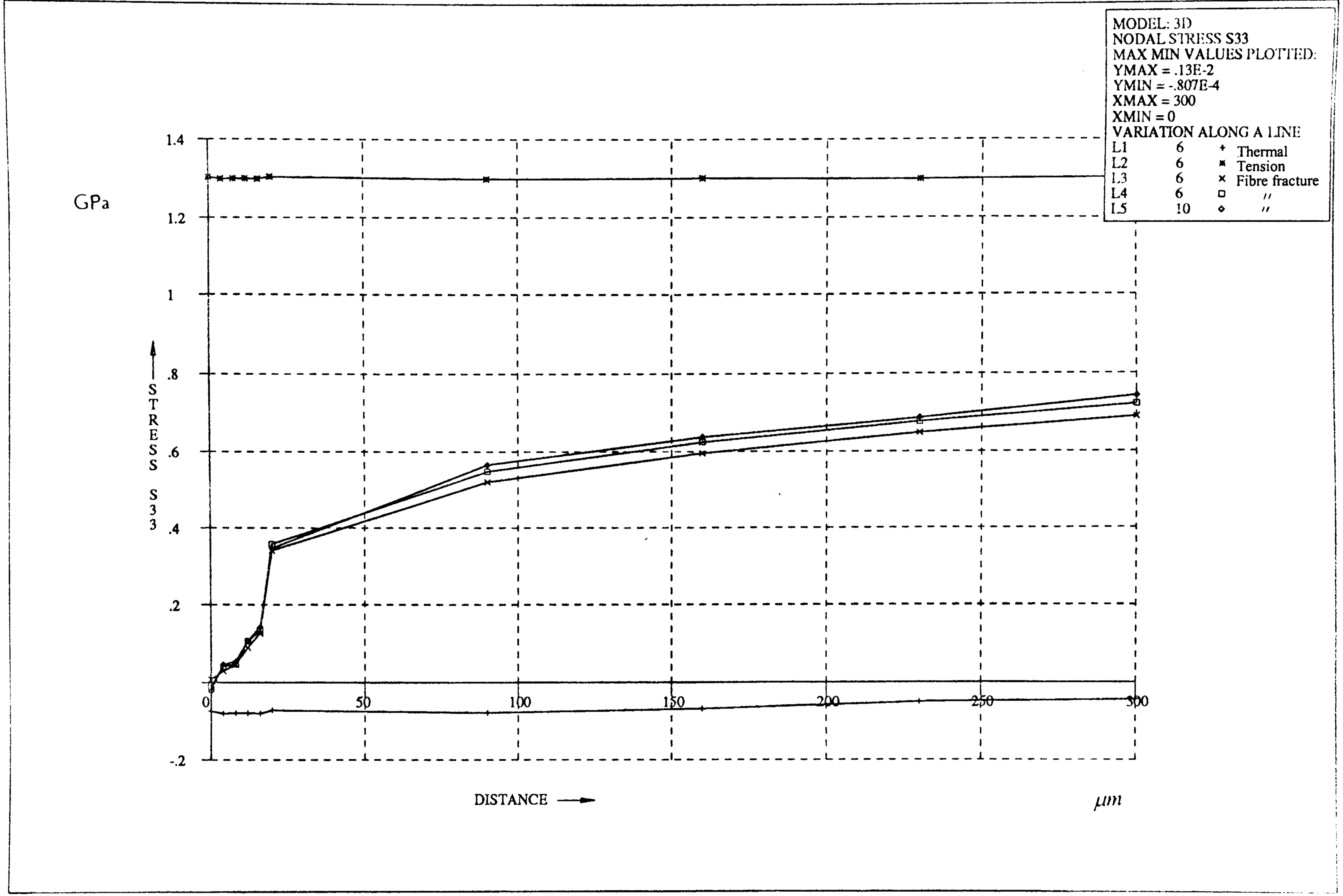

Fig. 9.13 Fibre stress distributions along central fibre for all stages of loading history

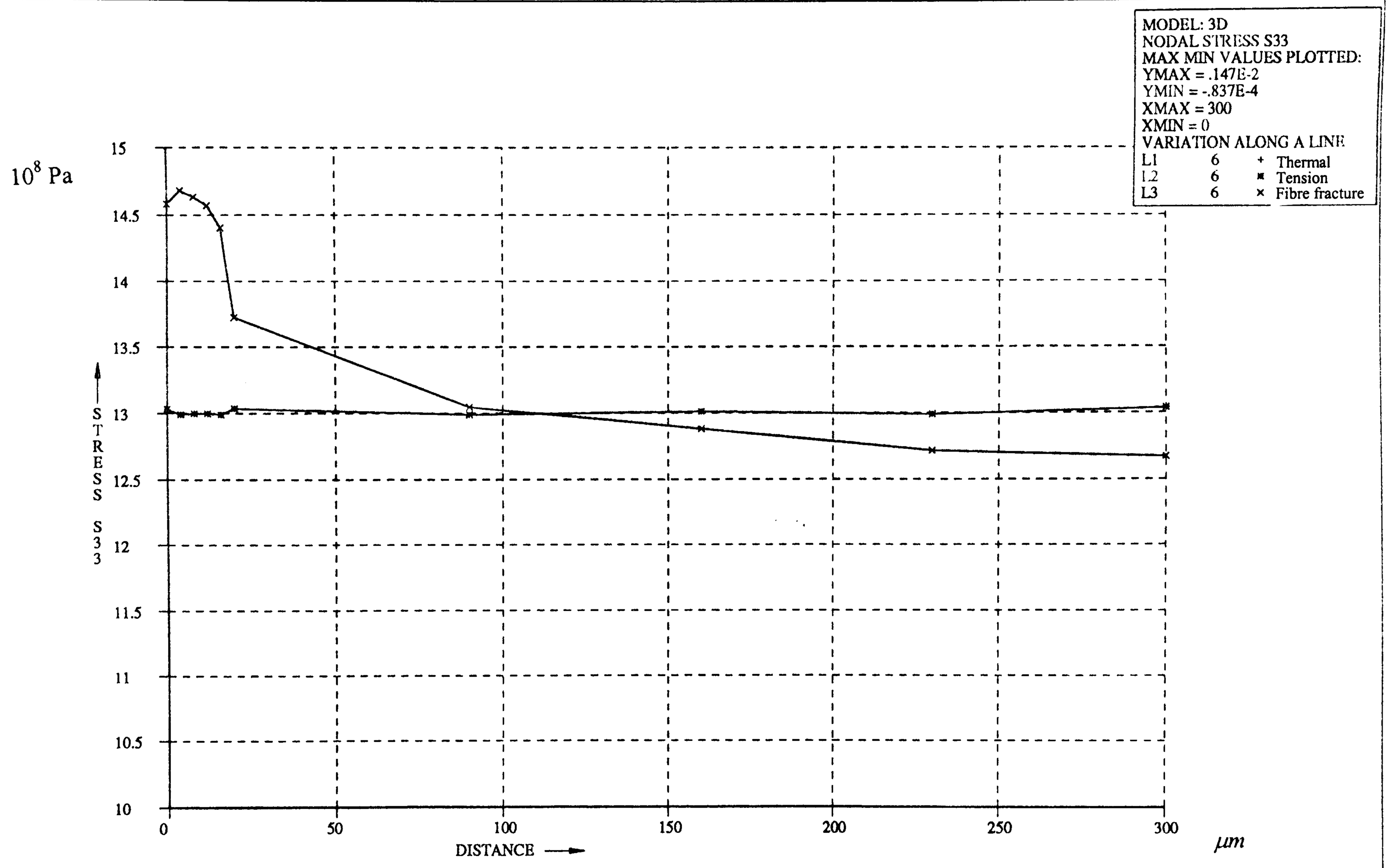

Fig. 9.14 Fibre stress distributions along first adjacent fibre for all stages of loading history

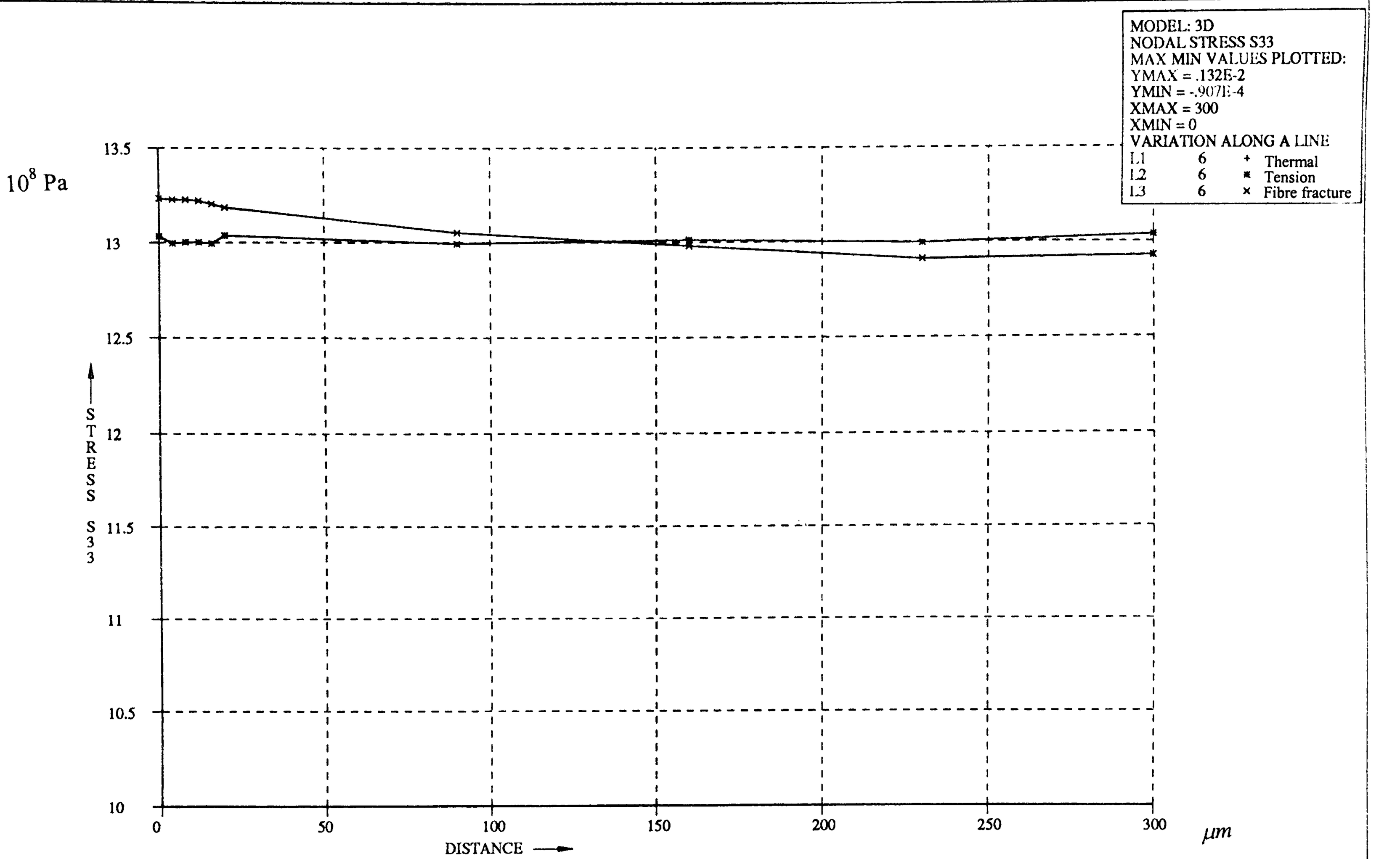

Fig. 9.15 Fibre stress distributions along second adjacent fibre for all stages of loading history

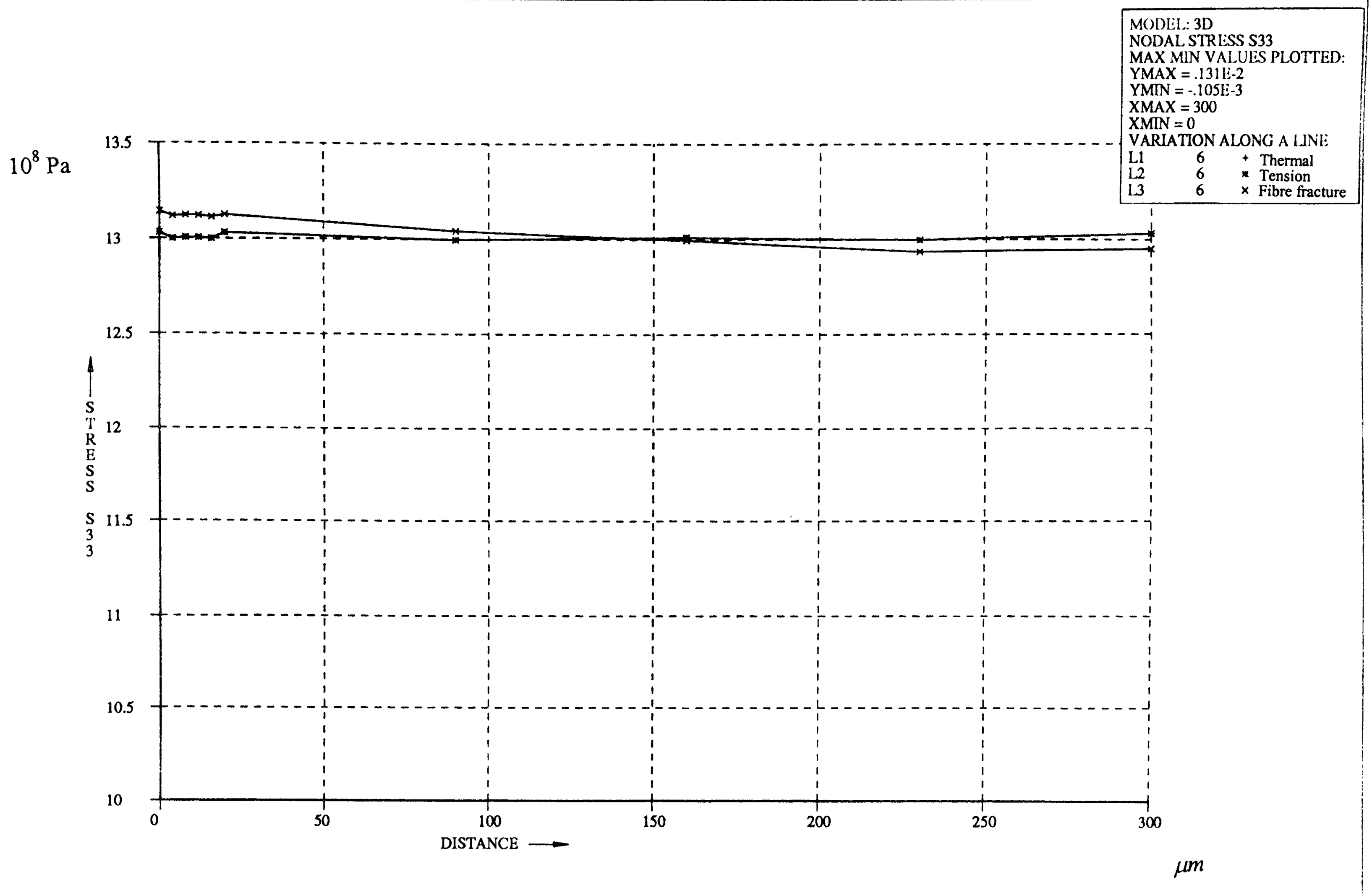

Fig. 9.16 Fibre stress distributions along third adjacent fibre for all stages of loading history

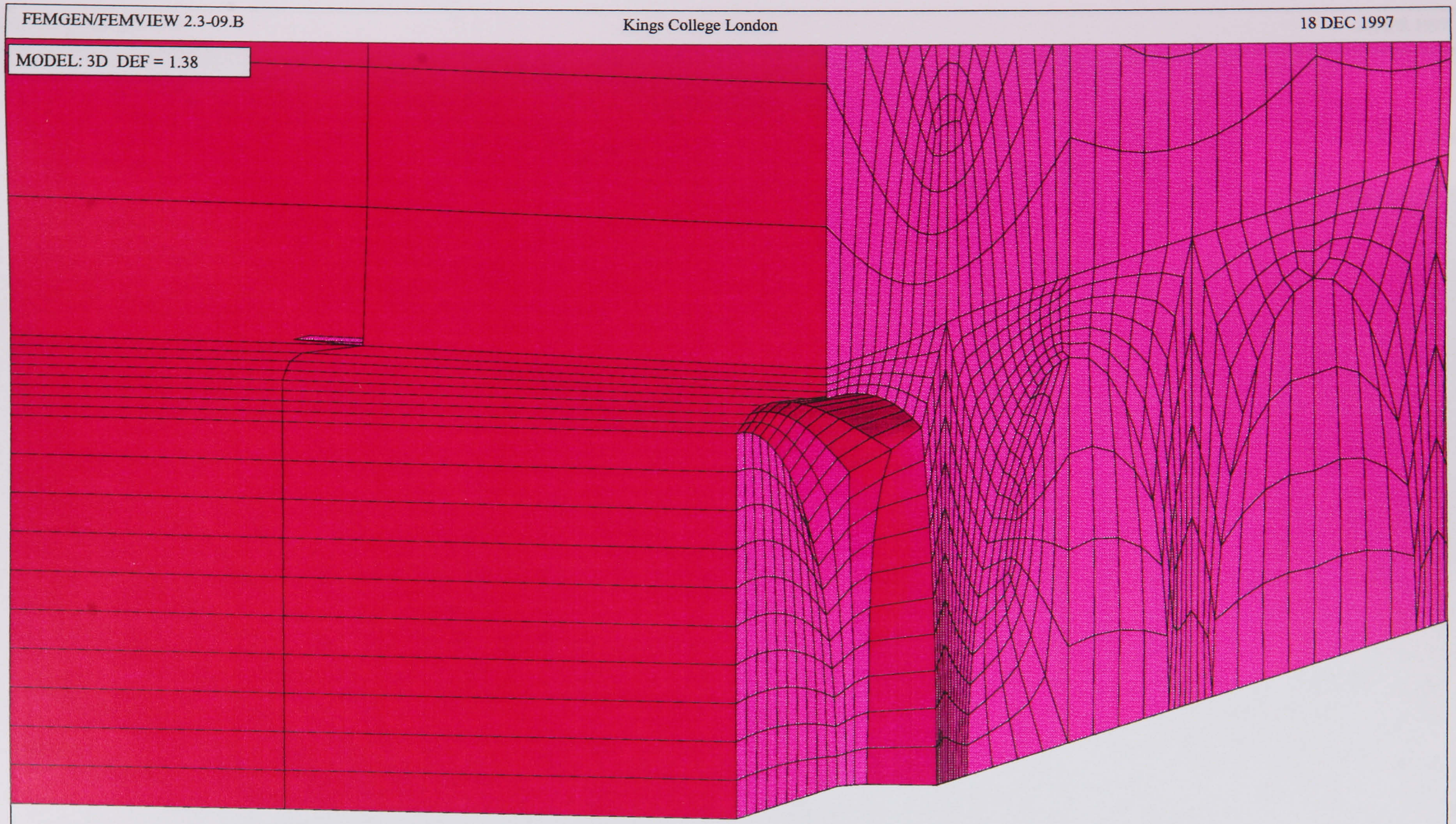

Fig. 9.17 Deformed mesh showing fractured fibre recoil and localised shearing in the adjacent matrix

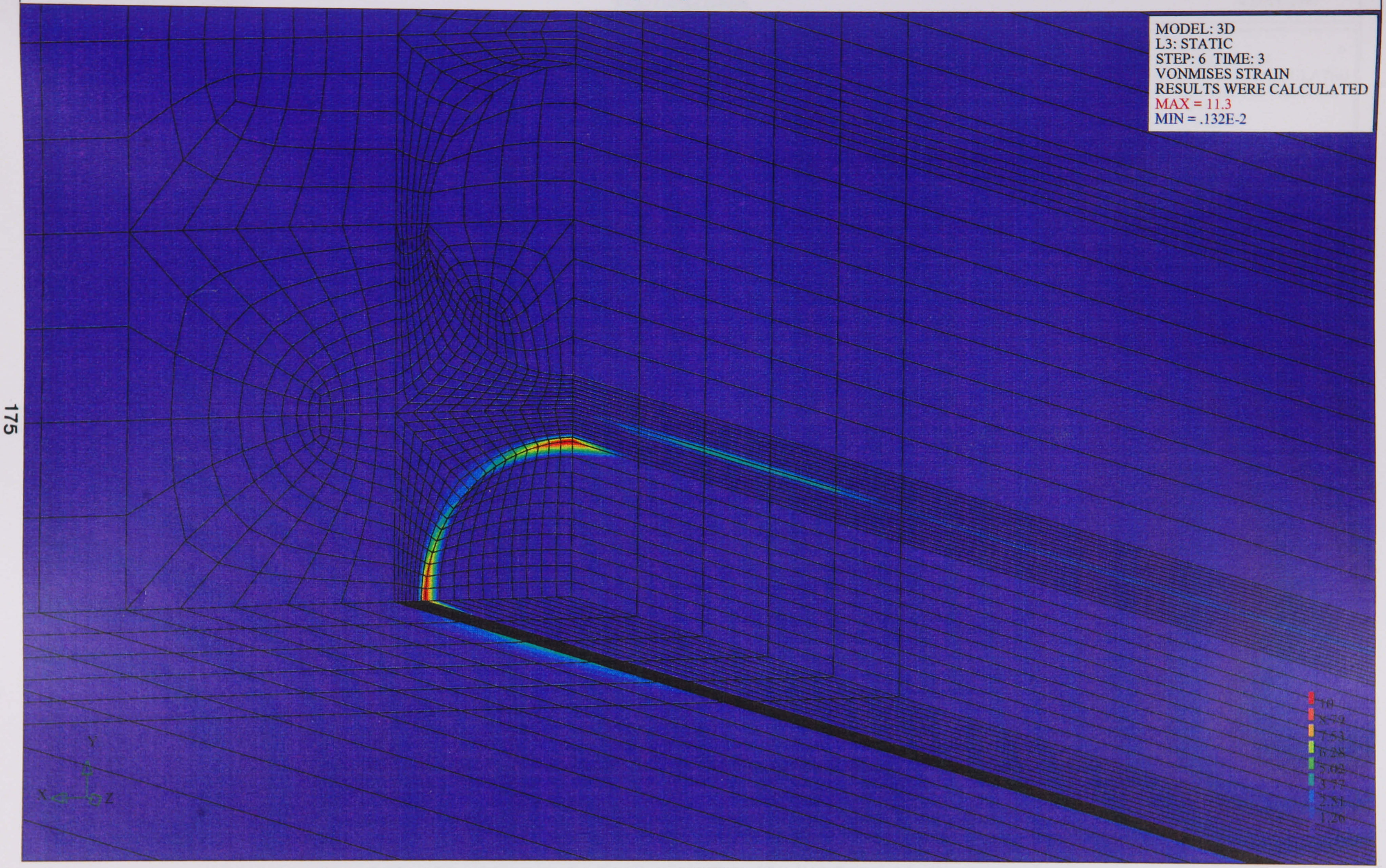

Fig. 9.18 von Mises strain map highlighting gross strain concentration in fracture zone

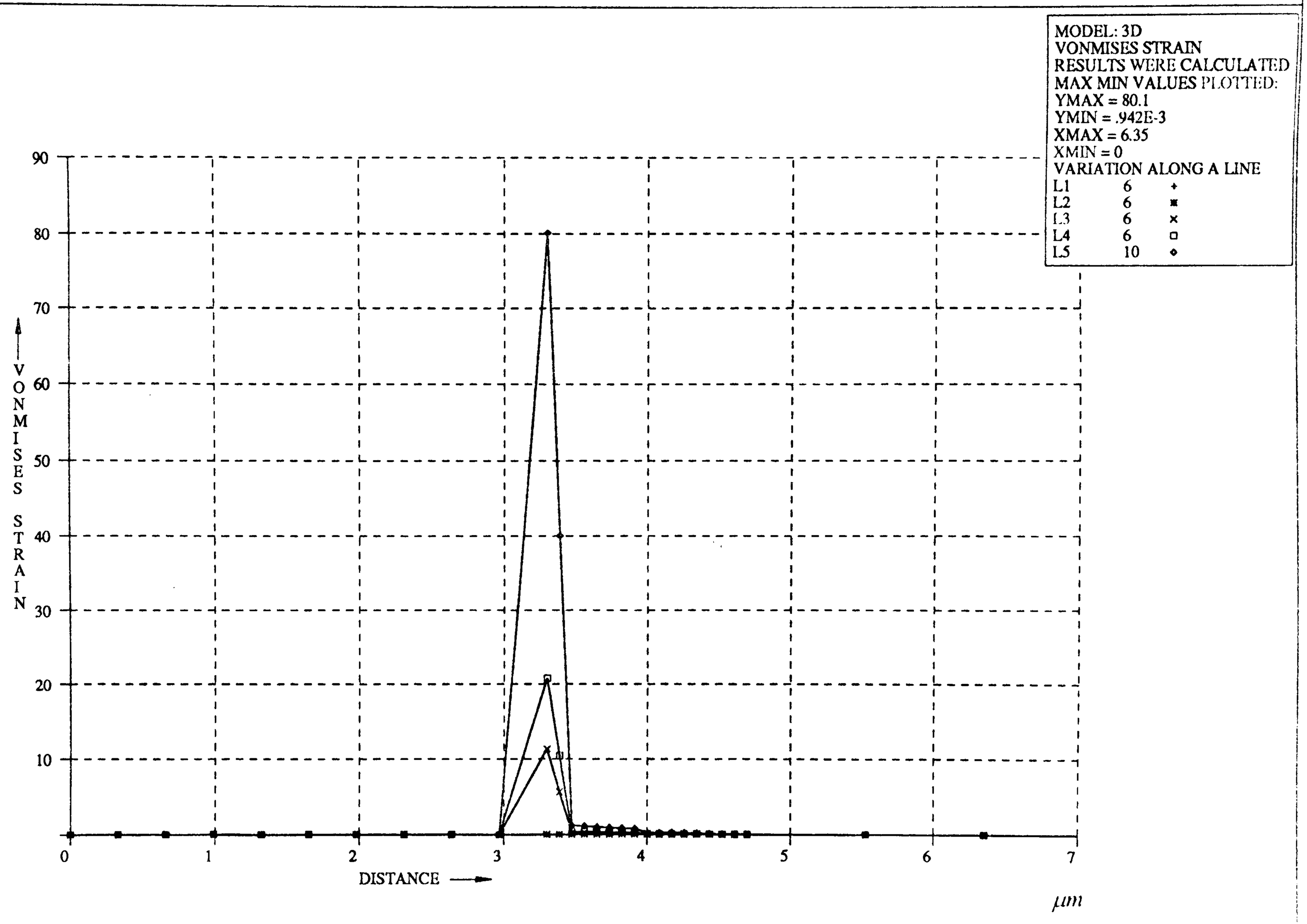

Fig. 9.19 Von Mises strain distribution along Y-axis of model indicating strain concentration

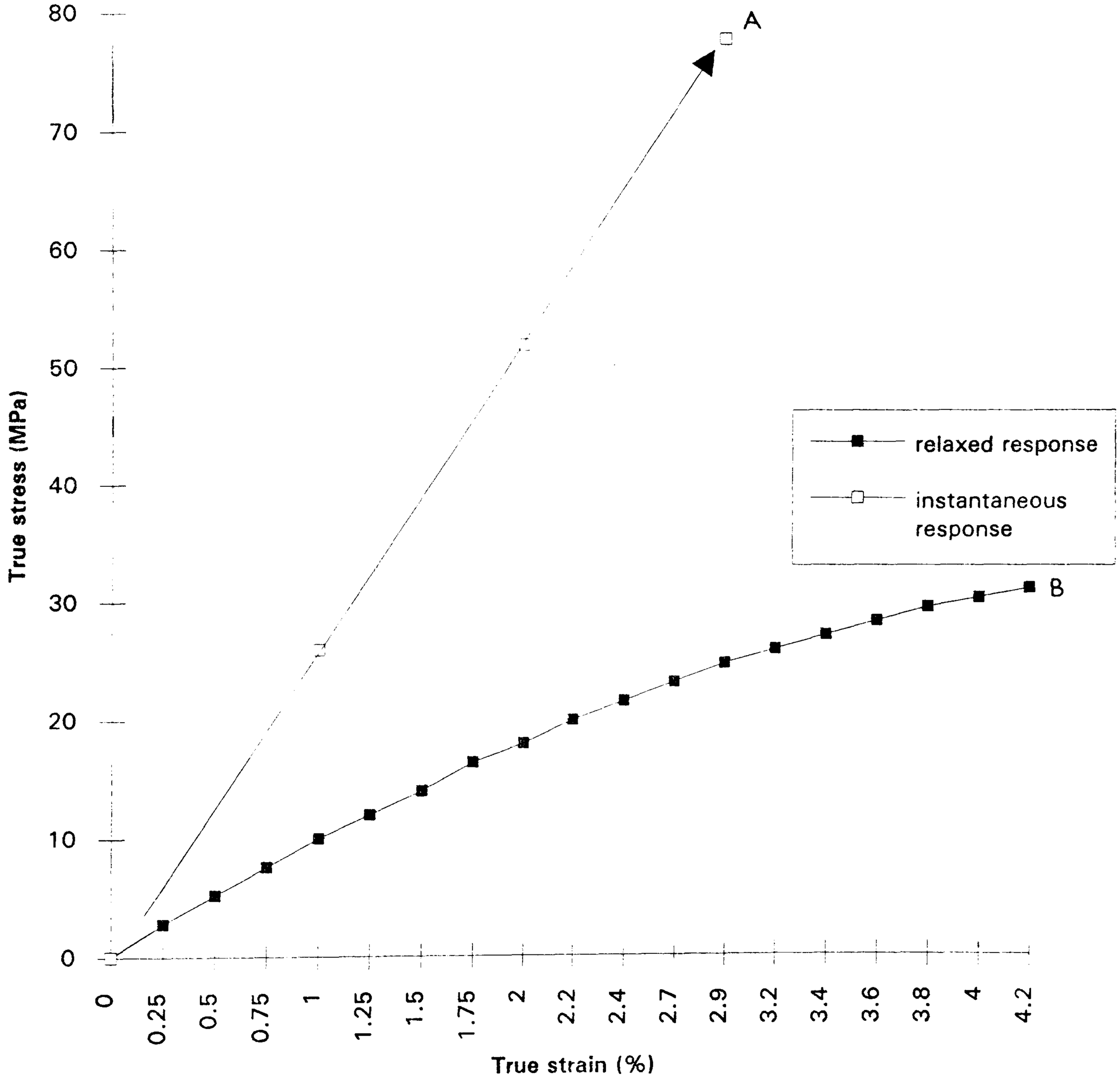

Fig. 9.20 Instantaneous and relaxed stress-strain response of epoxy matrix

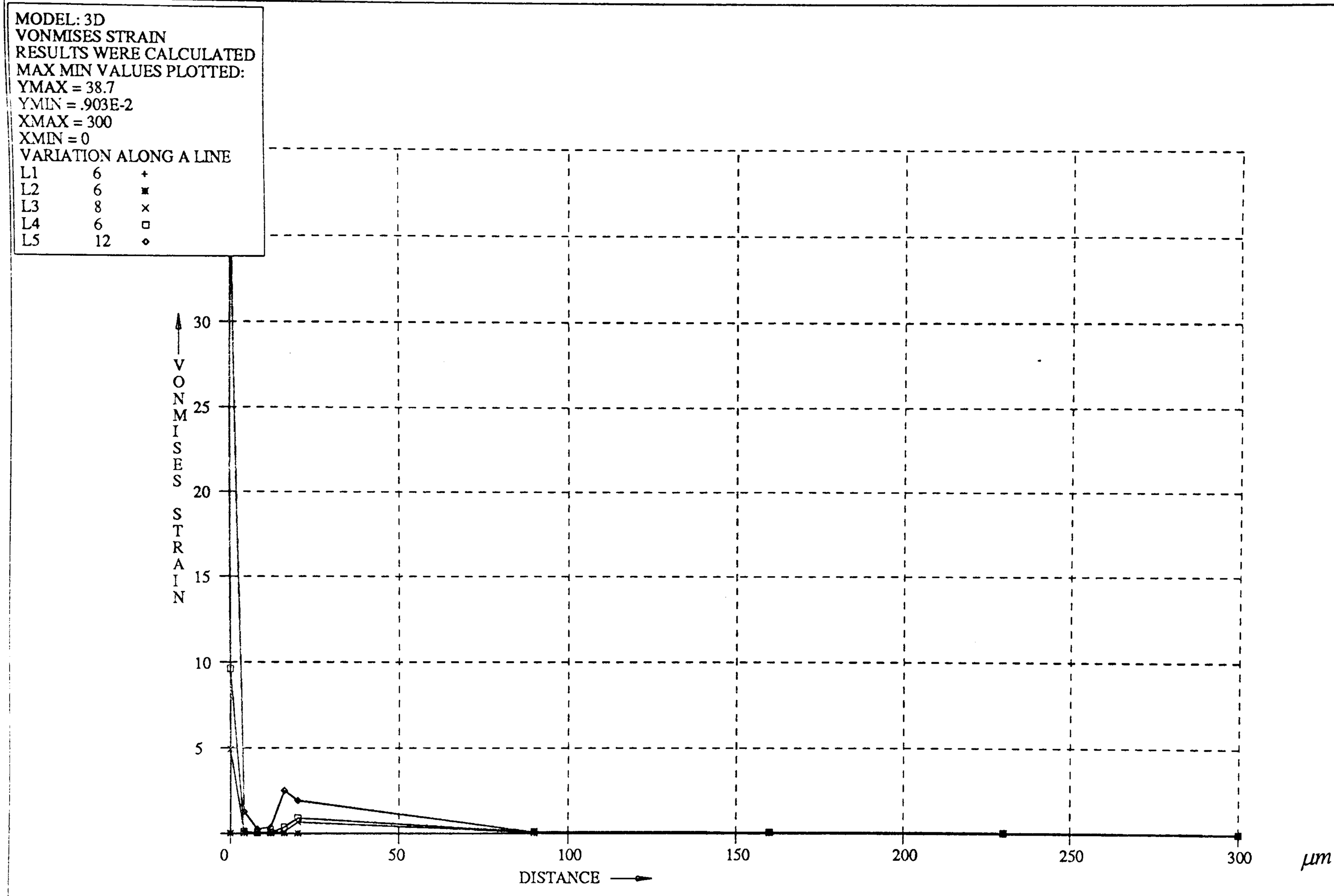

Fig. 9.21 Von Mises strain distributions along Z-axis for larger transverse crack model

Chapter 10

Conclusions and Future Research

10.1 Conclusions

The *Progressional Approach* for the analysis of interfacial failure, developed in this research, is intended to be rigorous and comprehensive in that the process is considered to consist of a series of discrete stages and account is taken of the various systemic non-linearities. The chief sources of non-linearity are matrix plasticity and the inducement of matrix or interface cracks together with the associated frictional stress transfer. FE analyses based on the Progressional Approach are more realistic in that the complex failure mechanisms have been incorporated.

Finite element analyses of various single and multi-fibre composite systems undergoing specific modes of interfacial failure were performed in accordance with the Progressional Approach. The predicted fibre stress distributions characteristic of a given mode of failure were obtained and correlation was made with LRS data, for various levels of applied loading.

The modelling of the initial thermal loading on the composite predicted compression in the fibres and minor localised yielding in the interfacial matrix. The thermal yielding was concluded to be inconsequential on account of the dilatational strain being compressive and thus suppressing possible ductile rupture of the yielding matrix.

Kevlar-49 fibres undergo extensive fibre end fibrillation in which the material properties vary non-uniformly throughout the fibrillated zone. This effect was found to be responsible for exclusively yielding at the interface, Mode α, as the prevalent interfacial failure mode for applied strain levels below 1%. Modes of failure involving interface fracture were concluded to be suppressed until applied strain levels in excess of 1%, where the localised yield strain exceeded the ductile fracture strain.

Carbon fibre systems fail by the initiation and propagation of cracks either into the matrix (Mode γ), or along the interface (Mode β) depending on the condition of the interface. It was found that Modes β and γ possess Ω-shaped and S-shaped fibre stress profiles, respectively. These were established to be their characteristic 'fingerprints' in that they reveal the prevalent failure mode during the loading sequence on the given composite specimen. Mode β involved significant frictional stress transfer across the cracked interface in which a high coefficient of friction estimated to be 0.8-0.9 was found to exist. For Mode γ, the propagation of matrix cracks led to the inducement of a more pronounced S-shape. Also for this mode, the pressure-dependency of matrix yield was found to influence the fibre stress take-up profiles significantly.

In comparing the effect of the two interfacial failure modes on the global composite modulus, Mode γ was found to be substantially more detrimental than Mode β. It was concluded that reinforcement efficiency was compromised by a factor of up to 35% during the inducement and propagation of matrix cracks.

For the case of spontaneous fibre fracture in continuous multi-fibre systems, substantial fibre stress redistribution in the surrounding intact fibres was found to occur post-fracture. Stress amplification factors of 1.13 were obtained in the immediately adjacent fibres. The analysis demonstrated the importance of matrix cracking as the chief form of failure consequent upon fibre fracture, as opposed to gross matrix yielding in the fracture zone.

10.2 Future Research

10.2.1 Systems incorporating interlayers

The Progressional Approach may be applied to a single short-fibre systems in which there exists an *interlayer* between the fibre and matrix. The interlayer, either in the form of a fibre coating or a fibre sizing, may be modelled using material properties to represent the variety of coatings commonly employed. Such analyses would provide an insight as to favourable material properties for the interlayer that would lead to the

maintenance of high levels of fibre reinforcement efficiency during the interfacial failure process. It is likely that a favourable mode of failure could be localised yielding in the interlayer during the early stages of failure, followed by the initiation and propagation of interface cracks contained within the interlayer region. Hence the interlayer may be beneficial in the containment of interfacial failure during the loading sequence.

10.2.2 Inter-Laminar Failure in Composite Laminates

The Progressional Approach may be extended to the case of a full composite laminate subjected to incremental tensile loading. This may be considered the most important application of the approach commercially, since both intra-laminar and inter-laminar failure modes and their complex interaction would be the focus of the analysis. A common laminate is that of a $0/90^{\circ}$ crossply laminate in which adjacent laminae are mutually perpendicular, as shown in Fig. 1.1. It has been established that for a crossply laminate subjected to tensile loading, matrix cracking in the transverse plies *precedes* successive fibre fractures and matrix cracking in the axial plies [59]. The Progressional Approach should be able to predict the likely sequence of events and the interfacial failure consequent to these intra-laminar mechanisms. Hence the influence of these events on the *inter-laminar* stresses and consequent *delamination* failure will be ascertained. Thus, intra-laminar failure would be demonstrated to be the root stage of the inter-laminar failure process.

The model may also be used to establish the scale of deterioration of the global composite modulus with interfacial failure and subsequent delamination. Hence, examination may also be made of the validity of the various assumptions made in the analytical calculation of the laminate modulus. These include the assumption of linear-elasticity of the constituent lamina moduli, those used in the calculation of the transverse lamina moduli (Halpin-Tsai expression) [60], and the Kirchhoff assumptions employed in the evaluation of the global laminate modulus [61].

APPENDIX A Laser Raman Spectroscopy Experimental Measurement

The Materials Department at QMW have, over the past decade, conducted numerous investigations into application of the high resolution stress measurement technique of LRS. Various single and multi-fibre composite specimens of a variety of systems have been tested, particularly under a program of incremental tensile loading. For each test, the axial stress or strain distributions along the length of the embedded fibre were obtained for various levels of applied strain. This measurement technique relies on the fact that the Raman frequency of the atomic vibrations of crystalline reinforcing fibres, such as aramid or carbon, is a function of the axial stress in the fibre at that location [14].

The experimental set-up is given in Fig. A.1. The composite specimen was placed in the mechanical tester and the Raman measurement probe translated on a specially designed rig next to the specimen. Flexible fibre optic cables connected the probe to both the laser and spectrometer which delivered and received the laser beam, respectively.

Raman spectra were obtained using the 514.5nm (green) beam of an Ar-ion laser as the excitation wavelength. The laser beam was directed through a series of mirrors to a modified Nikon microscope which was used to focus the laser beam onto a 1μm spot on the fibre via an objective lens. The 180^{o} backscattered beam was collected by the same microscope and focused on the entrance slit of a SPEX 1877 triple monochromator spectrometer. Finally, the dispersed light from the spectrometer was directed to a Wright Instruments charge-coupled device (CCD) detector, employed as the photon detecting system, and the Raman spectrum was recorded on a PC for specific wavelength windows.

All frequency peak values were derived by applying Lorentzian fitting routines to the raw data obtained from the CCD detector. Unique Raman frequency versus fibre stress calibration curves, produced for each type of fibre, were used to convert the

measured Raman frequency to an axial stress or strain distribution along the length of the fibre.

Examples of raw fibre stress data along the length of the fibre is shown for a Kevlar-49/epoxy system for four applied strains, Fig. A.2, and also for a high-modulus carbon/epoxy system at two levels of applied strain, Fig. A.3. A slight kink in the carbon take-up profiles is observable when comparing the carbon with the Kevlar profiles. This corresponds to an exclusively yielding interfacial failure mechanism in the Kevlar system as contrasted with a primarily interfacial cracking mechanism for the carbon system.

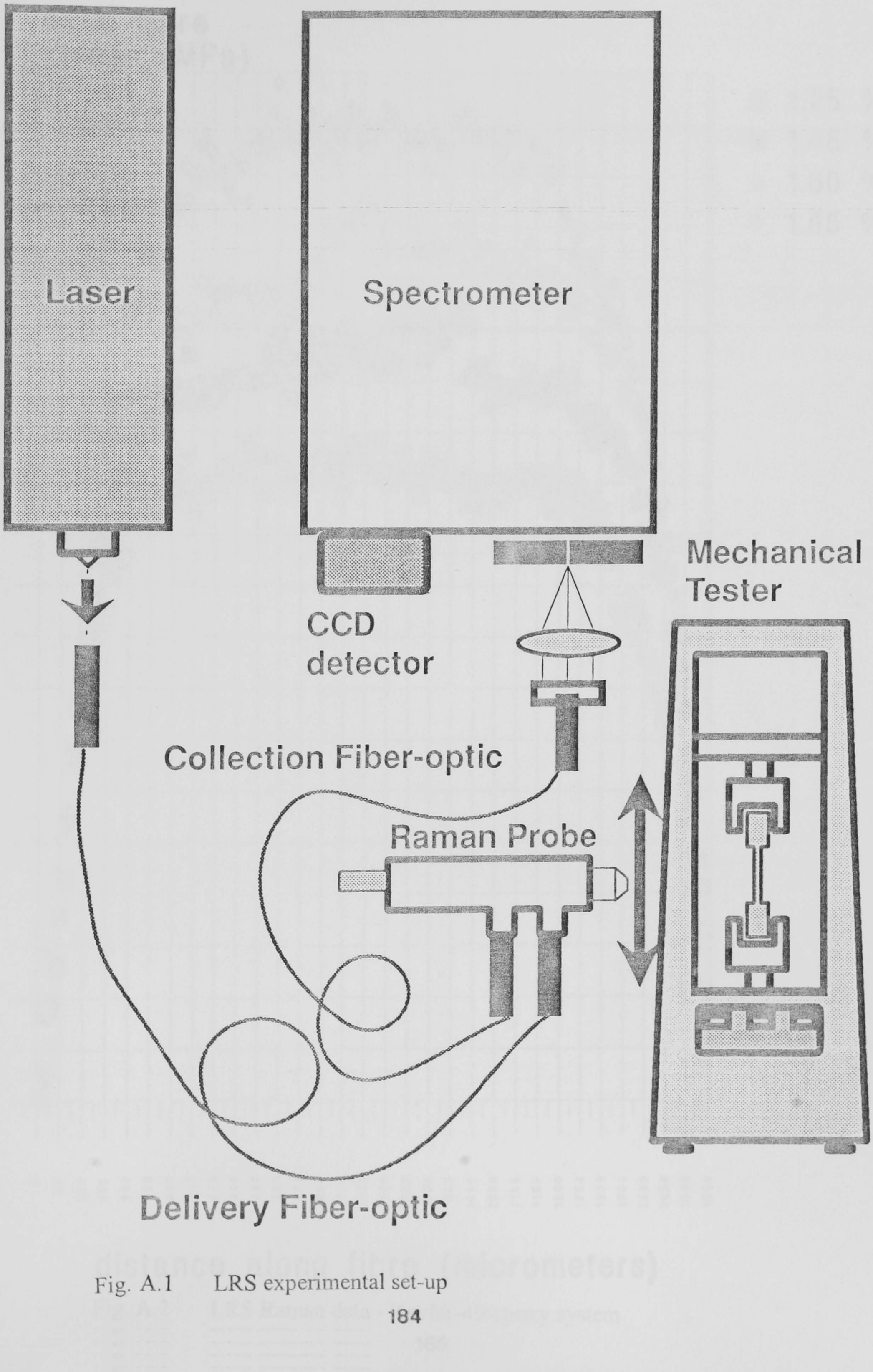

Fig. A.1 LRS experimental set-up

Kevlar-49 Raman data II (1995)

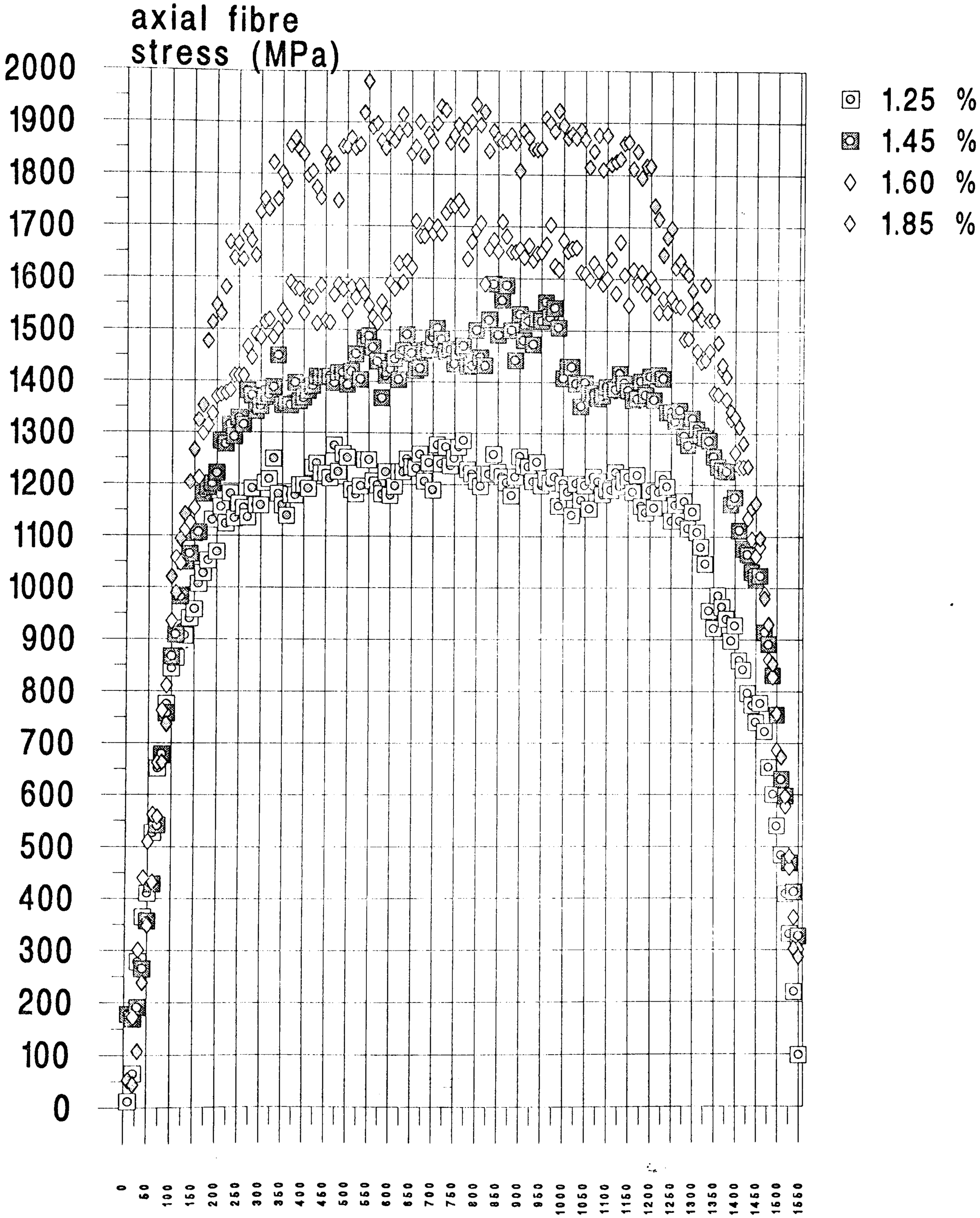

Fig. A.2 LRS Raman data - Kevlar-49/epoxy system

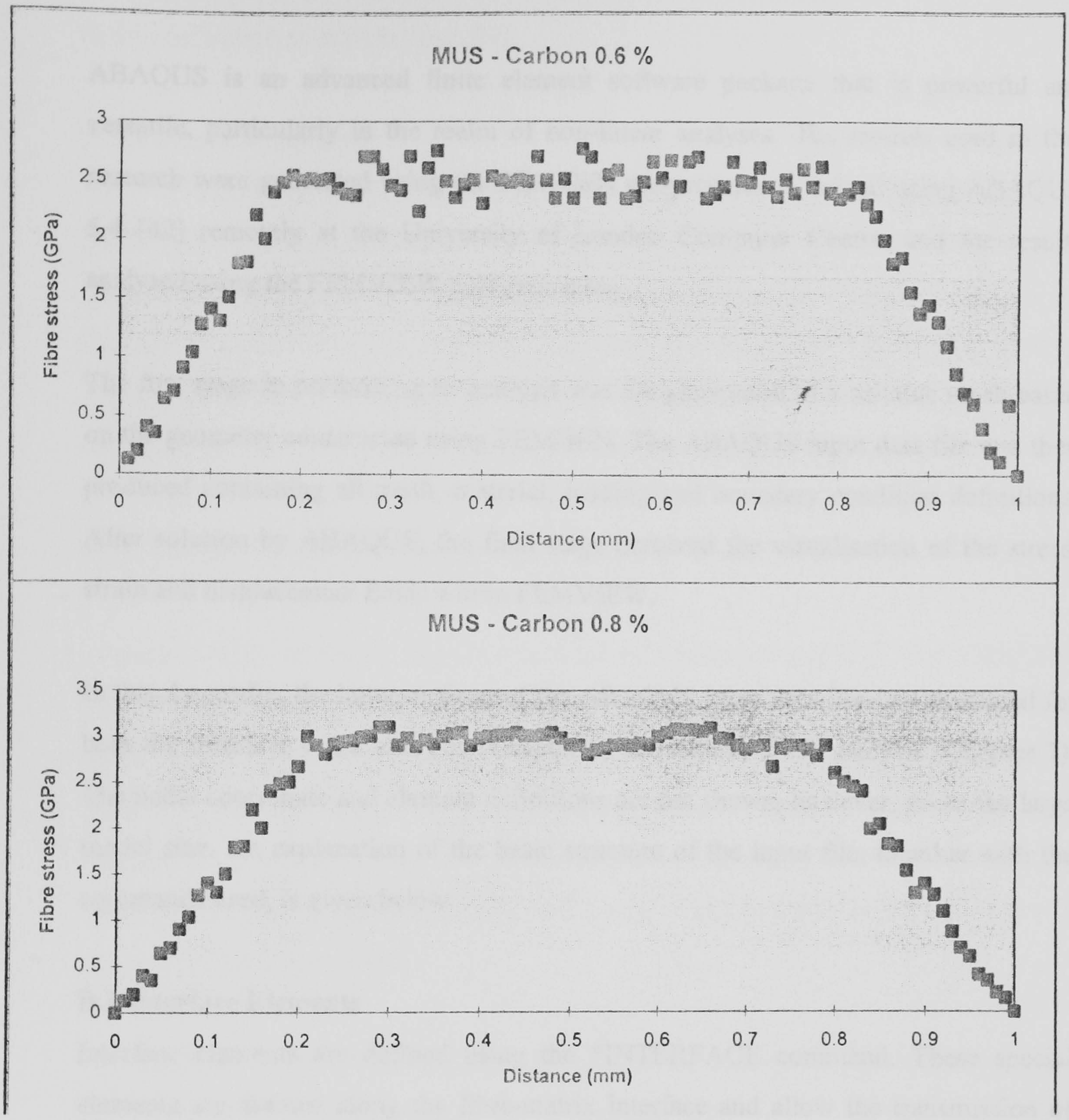

Fig. A.3 LRS Raman data - Carbon/epoxy system

APPENDIX B ABAQUS and Solution Methodology

ABAQUS is an advanced finite element software package that is powerful and versatile, particularly in the realm of non-linear analyses. The models used in this research were generated using the FEMGEN pre-processsor, solved using ABAQUS 5.4 [42] remotely at the University of London Computer Centre, and the results analysed using the FEMVIEW post-processor.

The first stage in performing an analysis was the generation of a suitable mesh based on the geometry constructed using FEMGEN. The ABAQUS input data file was then produced containing all mesh, material, loading and boundary condition definitions. After solution by ABAQUS, the final stage involved the visualisation of the stress, strain and displacement fields within FEMVIEW.

In this Appendix, the latter sections of the ABAQUS input data files are presented for both the interface crack analysis (Chapter 6) and matrix crack analysis (Chapter 7). The nodal coordinate and element definitions are not shown, however, given the large model size. An explanation of the basic structure of the input file, together with the commands used, is given below.

B.1 Interface Elements

Interface elements are defined using the *INTERFACE command. These special elements are defined along the fibre-matrix interface and allow the transmission of normal stresses if the surfaces are in contact. A Fortran program is also presented, after the input data files, which allowed the automatic definition of interface elements for use in the ABAQUS input files. The advantage of the program was the efficient creation of multiple interface elements which were produced from a Fortran input file containing only the interfacial nodes.

The interface is defined as being perfectly bonded at the beginning of the analysis using the *BOND SURFACE command. Addition of the *FRICTION command then

allows the transmission of shear stresses across the interface post-fracture, according to the coefficient of friction specified.

B.2 Material Properties

The *MATERIAL command contains the *ELASTIC and thermal expansion coefficient data. The ENGINEERING CONSTANTS option of *ELASTIC allows the definition of an orthotropic material requiring nine independent elastic constants. In the case of carbon and Kevlar fibres, their transverse isotropy is represented by five independent elastic constants. The order of the nine moduli in the *ELASTIC command is:

E11 , E22 , E33 , ν12 , ν13 , ν23 , G12 , G13 , G23

where E11=E33, ν12=ν23, and G12=G23 for transverse isotropy in the 1-3 coordinate plane. The moduli are expressed in units of $N/(\mu m)^2$. The thermal expansion coefficients are then defined in the *EXPANSION command. For the isotropic matrix definition, only the elastic modulus and Poisson ratio are required in the ISO option of *ELASTIC. The plastic behaviour of the matrix is defined by *PLASTIC where the stress-strain curve is represented digitised using values of stress at various levels of the plastic strain increment.

The *SOLID SECTION command defines the allocation of the various material property definitions to the various parts of the structure.

B.3 Loading History

The loading history consists of a series of load-steps which, in a progressive manner, modify the stress/strain fields in the model induced by the previous load step. The solution procedure in ABAQUS is controlled using an automatic incrementation scheme in which a given load-step is divided up into a number of increments. Numerous iterations are performed for each increment until an equilibrium solution is converged to within the tolerance specified. Depending on the rate of convergence, the incrementation scheme will select smaller or larger increments, as necessary, thus

optimising computation time. The tolerance on the nodal force residuals may be changed from the 0.5% default value using the *CONTROLS command in the load-step definition.

Each load-step starts and ends with *STEP and *END STEP, respectively. The STATIC command indicates that the analysis is static and the values given show the starting, maximum and minimum increment sizes that may be employed during the incrementation scheme. The RESULTS OUTPUT CONTROL section formats the output files generated during the solution procedure.

The thermal load is applied to all nodes in the model using the *TEMPERATURE command together with the value of the temperature change. Tensile load steps are prescribed using *BOUNDARY, in which the magnitude of the displacement (in μm) is specified. Cracks are initiated along previously defined interfaces using the *DEBOND and *CRACK GROWTH commands. Within these commands are specified the rate of crack growth throughout the load-step as well as the location and size of the crack. *J-INTEGRAL evaluates the SERR at the crack tip using a specified number of contours and crack propagation direction.

The *BOUNDARY command applies the boundary condition to all nodes on the plane of symmetry at the centre of the model which allows no axial displacement. For the simulation of spontaneous fibre fracture during the multi-fibre analysis, the boundary condition is removed non-linearly over the load step on nodes on the fracture surface of the fibre.

```
*** Carbon fibre - Progressional Approach : Interface crack analysis ***
***
*INTERFACE,ELSET=CRACK
*BOND SURFACE
*FRICTION,LAGRANGE
0.9
**********************
** SET DEFINITIONS *
**********************
**
*ELSET, ELSET=PHY1
S24      ,S29      ,S6       ,S30      ,S2       ,S4       ,S5       ,S3       ,
S7       ,S10      ,S1       ,S9       ,S19      ,S20      ,S21      ,S22      ,
S27      ,S28      ,S31      ,S32      ,S36      ,S8       ,S14      ,S12      ,
S13      ,S16      ,S26      ,S37      ,S38      ,
*ELSET, ELSET=PHY2
S18      ,S25      ,S11      ,S15      ,S17      ,S23      ,S33      ,S34      ,
S35      ,S39      ,
*ELSET, ELSET=ALL
PHY1     ,PHY2     ,
*ELSET, ELSET=CA1
ALL
**
***************************
** PROPERTY DEFINITIONS *
***************************
**
*SOLID SECTION, ELSET=PHY1       ,MATERIAL=M2
*SOLID SECTION, ELSET=PHY2       ,MATERIAL=M1
**
***************************
** MATERIAL DEFINITIONS *
***************************
**
*MATERIAL, NAME=M1
*DENSITY
  1.000000    ,
*ELASTIC,TYPE=ENGINEERING CONSTANTS
0.020    ,0.392    ,0.020    ,0.030    ,0.270    ,0.030    ,0.012    ,0.008    ,
0.012
*EXPANSION,TYPE=ORTHO
 2.5E-5   , -0.250E-6   , 2.5E-5
*MATERIAL, NAME=M2
*DENSITY
  1.000000    ,
*ELASTIC, TYPE=ISO
102.0E-05,0.360    ,0.000
*PLASTIC
120.0E-07,0.
250.0E-07,.0035
310.0E-07,.0116
*EXPANSION,TYPE=ISO
 5.8E-5
**
***************************
** KINEMATIC CONSTRAINTS *
***************************
**
*NSET, NSET=XAXIS
  764  790  816  842  868  894  920  946  971  996 1021 1046 1071 1097 1123 1149
 1175 2803 2804 2805
*BOUNDARY
XAXIS    ,    2,    2
**
*************************************************
** HISTORY DEFINITION ...                       *
*************************************************
**
*************************
**INITIAL THERMAL LOADING
*************************
```

```
**
*STEP,INC=200
*STATIC
0.1 , 1.0 , 0
*TEMPERATURE
ALLNODE , -50
*****************************
** RESULTS OUTPUT CONTROL *
*****************************
**
** ASCII OUTPUT FORMAT SELECTED
**
*FILE FORMAT, ASCII
**
*EL PRINT,ELSET=S35,FREQ=201,POSITION=AVERAGED AT NODES
S,E
*NODE PRINT,NSET=XAXIS,FREQ=201
U
*EL FILE,FREQ=201,POSITION=AVERAGED AT NODES
S,E
*NODE FILE,FREQ=201
U
*END STEP
**
*****************************************************
**INCREMENTAL "Yield-Max" APPLIED DISPLACEMENT
*****************************************************
*STEP, INC=200
*STATIC
0.1  , 1.0  ,0
*NSET, NSET=SIDE
 1532 1548 1564 1580 1596 1612 1628 1644 1660 1676 1692 1708 1724 1740 1756 1772
 1788 1804 1821 1838 1855 1872 1889 1906 1923 1940 1957 1974 1991 2008 2025
*BOUNDARY
SIDE    ,    2,    2,  -0.4
*BOUNDARY
XAXIS   ,    2,    2
*END STEP
*****************************************************
**INITIATE CRACK AT FIBRE CORNER
*****************************************************
*STEP, INC=200
*STATIC
0.1  , 1.0  ,0
*DEBOND,ELSET=CRACK
0,1.0
0.33,0.67
0.67,0.33
1.0,0
*NSET,NSET=REF
2162,3233
*CRACK GROWTH,NSET=REF,TIME TOLERANCE=0.1
0,0
0.33,1.3
*****************************************************
*NSET,NSET=ENTIP
2154,3594
*J-INTEGRAL,FREQ=201,CONTOURS=4
0,1
ENTIP
*NSET,NSET=INTIP
2767,3231
*J-INTEGRAL,FREQ=201,CONTOURS=4
1,0
INTIP
*END STEP
*****************************************************
**FULLY DEBOND FIBRE END
*****************************************************
*STEP, INC=200
*STATIC
0.1  , 1.0  ,0
*DEBOND,ELSET=CRACK
```

```
0,1.0
0.33,0.67
0.67,0.33
1.0,0
*NSET,NSET=END
2154,3594
*CRACK GROWTH,NSET=END,TIME TOLERANCE=0.1
0,0
0.33,2.27
*END STEP
**
**********************************************
**********************************************
** APPLIED STRAIN - REF:  0.4 % + 4 micron crack **
**********************************************
*STEP, INC=200
*STATIC
0.1  , 1.0  ,0
*DEBOND,ELSET=CRACK
0,1.0
0.33,0.67
0.67,0.33
1.0,0
*NSET,NSET=END
2154,3594
*CRACK GROWTH,NSET=END,TIME TOLERANCE=0.1
0,0
0.33,4
*END STEP
**********************************************
*STEP, INC=200
*STATIC
0.1  , 1.0  ,0
*NSET, NSET=SIDE
 1532 1548 1564 1580 1596 1612 1628 1644 1660 1676 1692 1708 1724 1740 1756 1772
 1788 1804 1821 1838 1855 1872 1889 1906 1923 1940 1957 1974 1991 2008 2025
*BOUNDARY
SIDE    ,    2,    2,  -1.3
*BOUNDARY
XAXIS   ,     2,     2
*END STEP
**********************************************
**********************************************
** APPLIED STRAIN - REF:  0.6 % + 15 micron crack **
**********************************************
*STEP, INC=200
*STATIC
0.1  , 1.0  ,0
*DEBOND,ELSET=CRACK
0,1.0
0.33,0.67
0.67,0.33
1.0,0
*NSET,NSET=END
2154,3594
*CRACK GROWTH,NSET=END,TIME TOLERANCE=0.1
0,0
0.33,15
*END STEP
**********************************************
*STEP, INC=200
*STATIC
0.1  , 1.0  ,0
*NSET, NSET=SIDE
 1532 1548 1564 1580 1596 1612 1628 1644 1660 1676 1692 1708 1724 1740 1756 1772
 1788 1804 1821 1838 1855 1872 1889 1906 1923 1940 1957 1974 1991 2008 2025
*BOUNDARY
SIDE    ,    2,    2,  -4.0
*BOUNDARY
XAXIS   ,     2,     2
*END STEP
**********************************************
**********************************************
```

```
** APPLIED STRAIN - REF:  0.8 % + 25 micron crack **
*****************************************************
*STEP, INC=200
*STATIC
0.1   , 1.0   ,0
*DEBOND,ELSET=CRACK
0,1.0
0.33,0.67
0.67,0.33
1.0,0
*NSET,NSET=END
2154,3594
*CRACK GROWTH,NSET=END,TIME TOLERANCE=0.1
0,0
0.33,25
*END STEP
*****************************************************
*STEP, INC=200
*STATIC
0.1   , 1.0   ,0
*NSET, NSET=SIDE
 1532 1548 1564 1580 1596 1612 1628 1644 1660 1676 1692 1708 1724 1740 1756 1772
 1788 1804 1821 1838 1855 1872 1889 1906 1923 1940 1957 1974 1991 2008 2025
*BOUNDARY
SIDE     ,    2,    2,  -6.0
*BOUNDARY
XAXIS    ,     2,     2
*END STEP
*****************************************************
.
:
```

```
*** Carbon fibre - Progressional Approach : Matrix crack analysis ***

***
*INTERFACE,ELSET=CRACK
*BOND SURFACE
**********************
** SET DEFINITIONS *
**********************
**
*ELSET, ELSET=PHY1
S24      ,S29      ,S2       ,S4       ,S5       ,S3       ,S7       ,S1       ,
S9       ,S19      ,S20      ,S21      ,S22      ,S27      ,S28      ,S31      ,
S32      ,S36      ,S37      ,S6       ,S8       ,S10      ,S14      ,S30      ,
S12      ,S34      ,S13      ,S38      ,S40      ,S41      ,
*ELSET, ELSET=PHY2
S18      ,S25      ,S11      ,S15      ,S17      ,S23      ,S33      ,S35      ,
S39      ,S16      ,S26      ,
*ELSET, ELSET=ALL
PHY1     ,PHY2     ,
*ELSET, ELSET=GA05
ALL
**
**************************
** PROPERTY DEFINITIONS *
**************************
**
*SOLID SECTION, ELSET=PHY1      ,MATERIAL=M2
*SOLID SECTION, ELSET=PHY2      ,MATERIAL=M1
**
**
**************************
** MATERIAL DEFINITIONS *
**************************
**
*MATERIAL, NAME=M1
*DENSITY
  1.000000    ,
*ELASTIC,TYPE=ENGINEERING CONSTANTS
0.020    ,0.392    ,0.020    ,0.030    ,0.270    ,0.030    ,0.012    ,0.008    ,
0.012
*EXPANSION,TYPE=ORTHO
 2.5E-5   , -0.250E-6   , 2.5E-5
*MATERIAL, NAME=M2
*DENSITY
  1.000000    ,
*ELASTIC, TYPE=ISO
102.0E-05,0.360     ,0.000
*PLASTIC
120.0E-07,0.
250.0E-07,.0035
310.0E-07,.0116
*EXPANSION,TYPE=ISO
 5.8E-5
**
**************************
** KINEMATIC CONSTRAINTS *
**************************
**
*NSET, NSET=XAXIS
  217   234   251   268   285   302   319   336   352   368   384   400   416 1254 1255 1256
 1766 1767 1768 1769 1770 1771 1772
*BOUNDARY
XAXIS    ,     2,     2
**
*****************************************
** HISTORY DEFINITION ...               *
*****************************************
**
**************************
**INITIAL THERMAL LOADING
**************************
**
```

```
*STEP,INC=200
*STATIC
0.1 , 1.0 , 0
*TEMPERATURE
ALLNODE , -50
*****************************
** RESULTS OUTPUT CONTROL *
*****************************
**
** ASCII OUTPUT FORMAT SELECTED
**
*FILE FORMAT, ASCII
**
*EL PRINT,FREQ=201,POSITION=AVERAGED AT NODES
S,E
*NODE PRINT,FREQ=201
U
*EL FILE,FREQ=201,POSITION=AVERAGED AT NODES
S,E
*NODE FILE,FREQ=201
U
*END STEP
**
*********************************************
**INCREMENTAL "Yield-Max" APPLIED DISPLACEMENT
*********************************************
*STEP, INC=200
*STATIC
0.1  , 1.0  ,0
*NSET, NSET=SIDE
  757  765  773  781  789  797  805  813  821  829  837  845  853  861  870  879
  888  897  906  915  924  933  942  951  960  969  978  987  996 1005 1014 1023
 1032 1041 1050 1059 1068 1077 1086 1095 1104 1113 1122 1131
*BOUNDARY
SIDE    ,    2,    2,  -0.4
*BOUNDARY
XAXIS   ,    2,    2
*END STEP
*********************************************
*********************************************
**INITIATE CRACK-20 (Fully debonds fibre end)
*********************************************
*STEP, INC=200
*STATIC
0.1  , 1.0  ,0
*CONTROLS,PARAMETERS=FIELD,FIELD=DISPLACEMENT
0.01,0.1,,,
*DEBOND,ELSET=CRACK
0,1.0
0.33,0.67
0.67,0.33
1.0,0
*NSET,NSET=REF
1478,2687
*CRACK GROWTH,NSET=REF,TIME TOLERANCE=0.1
0,0
0.33,20
*END STEP
**
*********************************************
*************************
** APPLIED STRAIN = 1 % **
*************************
*STEP,INC=200
*STATIC
0.1 , 1.0 , 0
*NSET, NSET=SIDE
  757  765  773  781  789  797  805  813  821  829  837  845  853  861  870  879
  888  897  906  915  924  933  942  951  960  969  978  987  996 1005 1014 1023
 1032 1041 1050 1059 1068 1077 1086 1095 1104 1113 1122 1131
*BOUNDARY
SIDE    ,    2,    2,-3.0000000
*BOUNDARY
```

```
XAXIS    ,     2,     2
*END STEP
**
**********************************************
** INCREMENTAL CRACK PROPAGATION **
**********************************
**
*STEP, INC=200
*STATIC
0.1   , 1.0   ,0
*CONTROLS,PARAMETERS=FIELD,FIELD=DISPLACEMENT
0.01,0.1,,,
*DEBOND,ELSET=CRACK
0,1.0
0.33,0.67
0.67,0.33
1.0,0
*NSET,NSET=REF
1478,2687
*CRACK GROWTH,NSET=REF,TIME TOLERANCE=0.1
0,0
0.33,40
*END STEP
**
**********************************************
**
*STEP, INC=200
*STATIC
0.1   , 1.0   ,0
*CONTROLS,PARAMETERS=FIELD,FIELD=DISPLACEMENT
0.01,0.1,,,
*DEBOND,ELSET=CRACK
0,1.0
0.33,0.67
0.67,0.33
1.0,0
*NSET,NSET=REF
1478,2687
*CRACK GROWTH,NSET=REF,TIME TOLERANCE=0.1
0,0
0.33,60
*END STEP
**
**********************************************
**
*STEP, INC=200
*STATIC
0.1   , 1.0   ,0
*CONTROLS,PARAMETERS=FIELD,FIELD=DISPLACEMENT
0.01,0.1,,,
*DEBOND,ELSET=CRACK
0,1.0
0.33,0.67
0.67,0.33
1.0,0
*NSET,NSET=REF
1478,2687
*CRACK GROWTH,NSET=REF,TIME TOLERANCE=0.1
0,0
0.33,90
*END STEP
**
**********************************************
```

*** Fortran Program to create interface elements from
the fibre and matrix nodes on the interface.

```
C       ************************************************
C       PROGRAM TO DEFINE 2-D LINEAR INTERFACE ELEMENTS IN
C       ABAQUS DECK-INPUT FILE.....................
C       BY RAJAT B. NATH.....................APRIL 1996
C       ************************************************

        PROGRAM INTER
        INTEGER F(1:1000),M(1:1000),I,EMAX,E
        OPEN (8,FILE="INTERIN")
        OPEN (9,FILE="INTEROUT")
        E=9000
        READ (UNIT=8,FMT=*) EMAX
        DO 20,I=1,EMAX,1
        READ (UNIT=8,FMT=*) F(I)
20      CONTINUE
        DO 30,I=1,EMAX,1
        READ (UNIT=8,FMT=*) M(I)
30      CONTINUE
        DO 40,I=1,(EMAX-1),1
        WRITE (UNIT=9,FMT=*) E,",",F(I),",",F(I+1),",",M(I),",",M(I+1)
        E=E+1
40      CONTINUE
        END

C       ************************************************
C       STRUCTURE OF INPUT FILE "INTERIN":
C       INTEGER REPRESENTING NUMBER OF NODE-PAIRS ON INTERFACE
C       LIST OF NODES ON FIBRE (LEFT TO RIGHT)
C       LIST OF NODES ON MATRIX (LEFT TO RIGHT)
C       HOW TO PRODUCE AN OUTPUT FILE "INTEROUT":
C       TYPE: f77 inter.f
C       TYPE: a.out
C       TYPE: cat INTEROUT
C       ************************************************
```

APPENDIX C Stress and Strain Tensor Components

The stress tensor may be resolved into two component tensors:

$$\begin{pmatrix} \sigma_{11} & \sigma_{12} & \sigma_{13} \\ \sigma_{21} & \sigma_{22} & \sigma_{23} \\ \sigma_{31} & \sigma_{32} & \sigma_{33} \end{pmatrix} = \begin{pmatrix} \sigma_{11}\text{-}P & \sigma_{12} & \sigma_{13} \\ \sigma_{21} & \sigma_{22}\text{-}P & \sigma_{23} \\ \sigma_{31} & \sigma_{32} & \sigma_{33}\text{-}P \end{pmatrix} + \begin{pmatrix} P & 0 & 0 \\ 0 & P & 0 \\ 0 & 0 & P \end{pmatrix}$$

stress tensor *stress deviator* *stress dilatation*

where $P = {}^{1}/_{3} (\sigma_{11} + \sigma_{12} + \sigma_{13})$

The deviatoric component of stress is also known as the von Mises or distortional component [45].

The dilatational component of stress is also known as the spherical, octahedral-normal, volumetric or bulk component [62,63]. Further, the negative value of dilatational component may sometimes be referred to as the hydrostatic component.

The strain tensor may also be resolved as:

$$\begin{pmatrix} \varepsilon_{11} & \varepsilon_{12} & \varepsilon_{13} \\ \varepsilon_{21} & \varepsilon_{22} & \varepsilon_{23} \\ \varepsilon_{31} & \varepsilon_{32} & \varepsilon_{33} \end{pmatrix} = \begin{pmatrix} \varepsilon_{11}\text{-}D & \varepsilon_{12} & \varepsilon_{13} \\ \varepsilon_{21} & \varepsilon_{22}\text{-}D & \varepsilon_{23} \\ \varepsilon_{31} & \varepsilon_{32} & \varepsilon_{33}\text{-}D \end{pmatrix} + \begin{pmatrix} D & 0 & 0 \\ 0 & D & 0 \\ 0 & 0 & D \end{pmatrix}$$

strain tensor *strain deviator* *strain dilatation*

where $D = {}^{1}/_{3} (\varepsilon_{11} + \varepsilon_{12} + \varepsilon_{13})$

The deviatoric components of stress or strain represents a distortion of a given element of material independent of the volumetric change. The dilatational components represent the volumetric change in shape of the element isolated from the general state of stress. The plastic behaviour of solids is a primary function of the deviatoric components and *normally* independent of the dilatational components.

APPENDIX D Fibre End Fibrillation Models

In the 1-D FEFM, account is taken of the material property variation in the *z* direction. We may consider an infinitesimally thin elemental cylinder within the fibrillated zone (Fig. D.1), with a mean radius r_{cyl} and thickness *dz*. The cylinder is assumed to contain a mixture of fibre uniformly interspersed with matrix, where v_f and v_m are the respective volume fractions. The volume of fibre in the cylinder is equal to the volume of the fibre in the un-fibrillated fibre, radius r_f. Thus the fibre volume fraction is given by

$$v_f = (A_f\, dz) / (A_{cyl}\, dz)$$

where A_{cyl} and A_f are the cross-sectional areas of the cylinder and un-fibrillated fibre, respectively. The fibre is considered to be transversely isotropic and linear elastic, and the matrix to be isotropic and non-linear elasto-plastic. Following a rule of mixtures argument, the effective tensile modulus of the cylinder is a weighted average of those of the fibre and matrix, given by

$$E_{cyl}(\varepsilon) = E_f . v_f + E_m(\varepsilon) . (1\text{-}v_f)$$

where E_{cyl} is the cylinder tensile modulus in a given coordinate direction, E_f is the fibre tensile modulus in the same coordinate direction, E_m is the matrix tensile modulus (independent of coordinate direction since isotropic) and ε is the given level of strain.

Substituting for v_f, we have:

$$E_{cyl}(\varepsilon) = E_f . \{A_f / A_{cyl}\} + E_m(\varepsilon) . (1 - \{A_f / A_{cyl}\})$$

Which simplifies to yield:

$$E_{cyl}(\varepsilon) = E_f . \{r_f / r_{cyl}\}^2 + E_m(\varepsilon) . (1 - \{r_f / r_{cyl}\}^2)$$

Similarly, for the shear moduli, we have the corresponding expression:

$$G_{cyl}(\varepsilon) = G_f . \{r_f / r_{cyl}\}^2 + G_m(\varepsilon) . (1 - \{r_f / r_{cyl}\}^2)$$

where G_{cyl} is the cylinder shear modulus in a coordinate plane, G_f is the fibre shear modulus in a coordinate plane and G_m is the matrix shear modulus.

Since the second term in each equation is always much smaller than the first term, over the range of strain considered, we may ignore the non-linearity of the matrix stress-strain curve with negligible error. Thus the equations simplify to yield:

$$E_{cyl} = E_f . \{r_f / r_{cyl}\}^2 + E_m . (1 - \{r_f / r_{cyl}\}^2)$$
$$G_{cyl} = G_f . \{r_f / r_{cyl}\}^2 + G_m . (1 - \{r_f / r_{cyl}\}^2) \qquad (D.1)$$

Both equations define the variation for the elastic moduli in all coordinate directions, since the fibrillated zone is transversely isotropic due to the influence of the fibre. Hence, the elastic moduli of a given cylinder are solely functions of axial coordinate, z, along the fibrillated zone, since as z decreases, r_{cyl} increases linearly. When $r_f = r_{cyl}$ the equations reduce to the desired result of the fibre elastic moduli.

In the *2-D FEFM*, we consider that the material properties vary in both the axial and radial directions. It is probable that towards the axis of the fibrillated zone, penetration of the matrix becomes progressively more difficult. Hence the extent of fibril dilution by the matrix will be maximum at the periphery of any given cylinder, and minimum at the axis. Thus, the material in the peripheral region of the fibrillated zone will have lower elastic moduli than that nearer the axis. It is assumed that the variation of material properties is linear with respect to the radial axis coordinate, and further, that the elastic moduli on the axis of the zone are three times their corresponding values at the periphery. The average value of the radially varying tensile elastic modulus of a given elemental cylinder, $E_{cr}(r)$, is equal to E_{cyl}. Hence, we have

$$E_{cr}(r) = ar + b$$

where a and b are coefficients determined by the boundary conditions:

$$E_{cr}(0) = 1.5\ E_{cyl} \quad ; \quad E_{cr}(r_{cyl}) = 0.5\ E_{cyl}$$

Solving for a and b, we have for the tensile and shear moduli variations within the cylinder

$$E_{cr}(r) = E_{cyl}\ \{3/2 - r/r_{cyl}\}$$
$$G_{cr}(r) = G_{cyl}\ \{3/2 - r/r_{cyl}\} \qquad (D.2)$$

where E_{cyl} and G_{cyl} are given by equations (D.1).

The four cylinder discretisation of the fibrillated zone according to the 1D-FEFM is shown in Fig. D.2, where the material properties M1, M2 SURF1-SURF4 represent those of the fibre, matrix and the four cylinders, respectively.

The five by four ring discretisation of the fibrillated zone according to the 2D-FEFM is shown in Fig. D.3, where the material properties PA through to SE represent those of the twenty rings.

The ABAQUS input data file portion containing the definition of the various moduli for cylinders and rings, for both 1D-FEFM and 2D-FEFM analyses, is presented after the figures. The syntax of the *ELASTIC command for transverse isotropy is:

E11 , E22 , E33 , ν12 , ν13 , ν23 , G12 , G13 , G23

The moduli are expressed in units of $N/(\mu m)^2$.

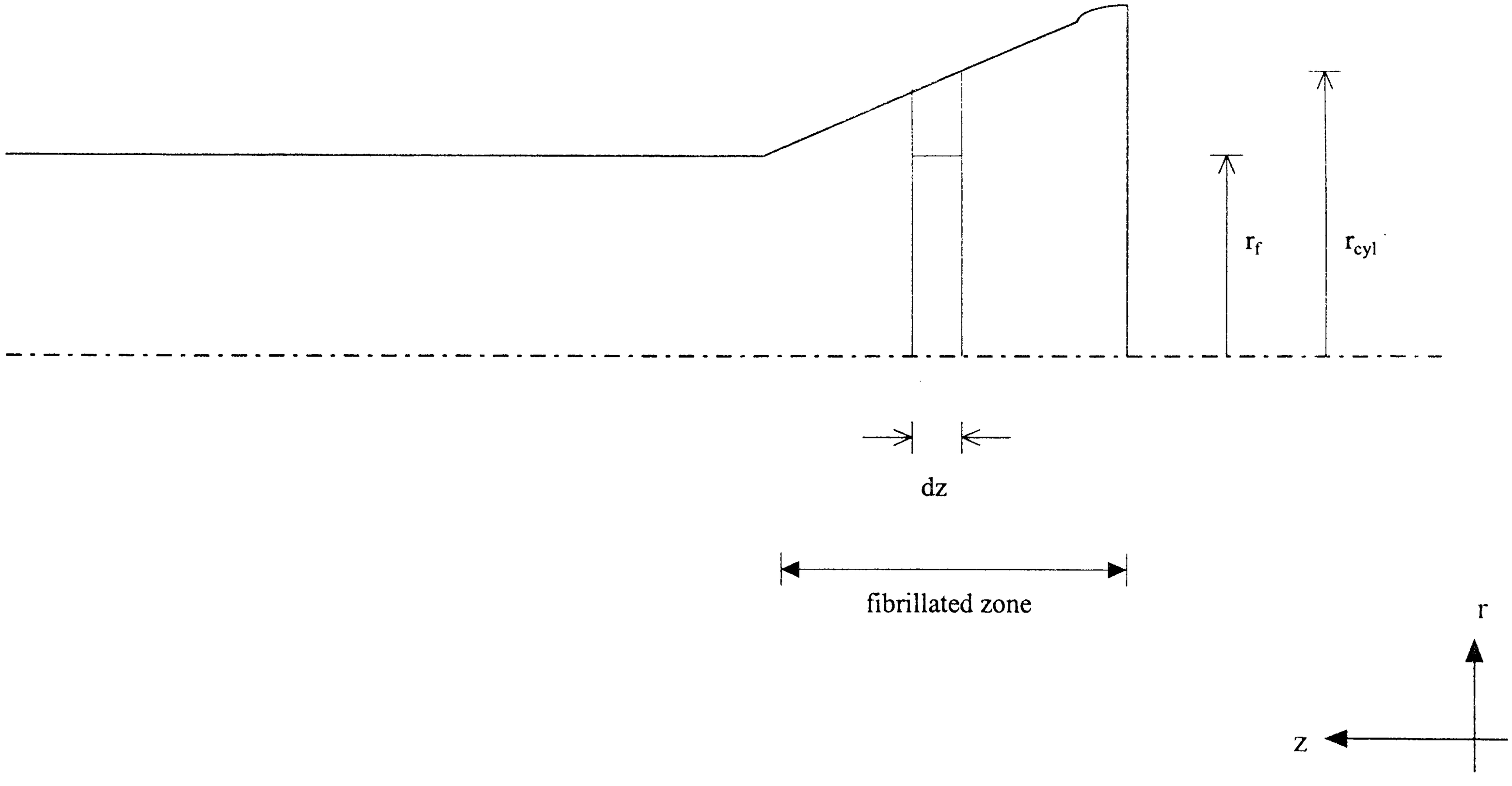

Fig. D.1 Geometry of fibrillated zone

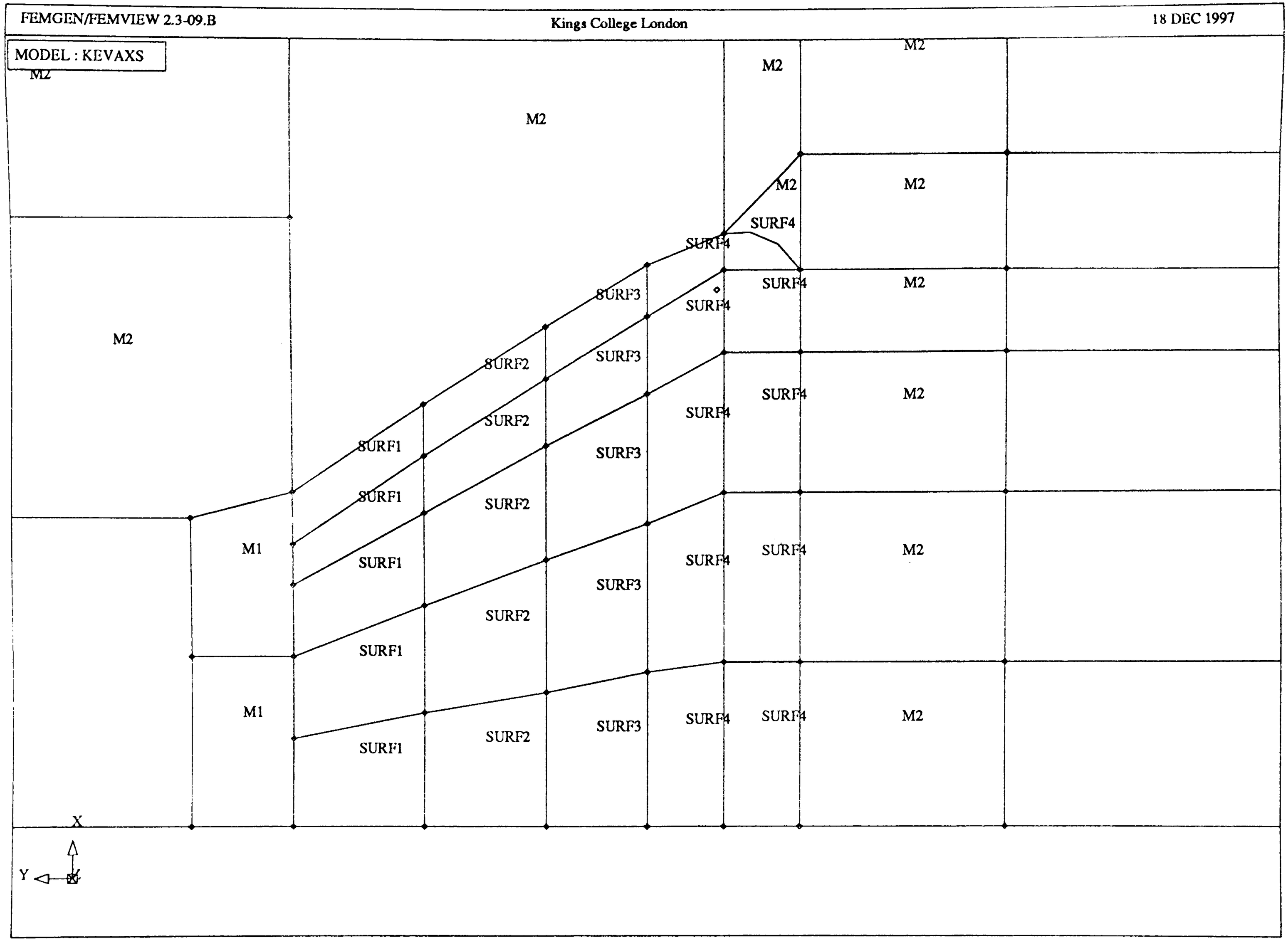

Fig. D.2 Discretisation of fibrillated zone according to 1-D FEFM model

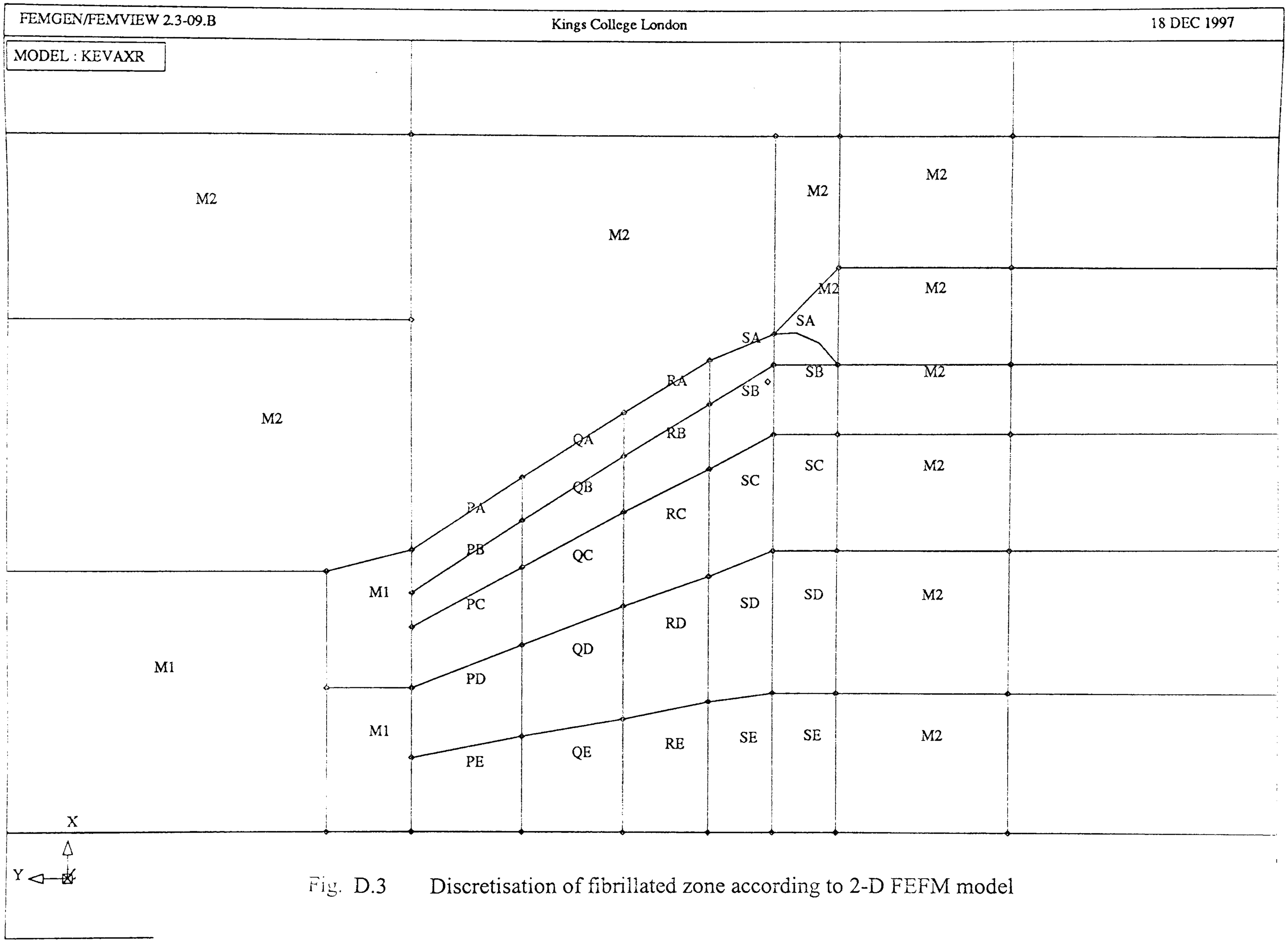

Fig. D.3 Discretisation of fibrillated zone according to 2-D FEFM model

```
***  Kevlar 49 : 1-D Fibrillated Fibre End Model = AXIAL variation   ***

**********
**********
*MATERIAL, NAME=SURF1
*DENSITY
  1.000000     ,
*ELASTIC,TYPE=ENGINEERING CONSTANTS
0.015    ,0.083    ,0.015    ,0.330    ,0.400    ,0.330    ,0.005    ,0.0005    ,
0.005
*EXPANSION,TYPE=ORTHO
4.14E-5   , -5.20E-6   , 4.14E-5
*MATERIAL, NAME=SURF2
*DENSITY
  1.000000     ,
*ELASTIC,TYPE=ENGINEERING CONSTANTS
0.010    ,0.053    ,0.010    ,0.330    ,0.400    ,0.330    ,0.003    ,0.0007    ,
0.003
*EXPANSION,TYPE=ORTHO
4.14E-5   , -5.20E-6   , 4.14E-5
*MATERIAL, NAME=SURF3
*DENSITY
  1.000000     ,
*ELASTIC,TYPE=ENGINEERING CONSTANTS
0.009    ,0.041    ,0.009    ,0.330    ,0.400    ,0.330    ,0.003    ,0.0007    ,
0.003
*EXPANSION,TYPE=ORTHO
4.14E-5   , -5.20E-6   , 4.14E-5
*MATERIAL, NAME=SURF4
*DENSITY
  1.000000     ,
*ELASTIC,TYPE=ENGINEERING CONSTANTS
0.007    ,0.034    ,0.007    ,0.330    ,0.400    ,0.330    ,0.002    ,0.0008    ,
0.002
*EXPANSION,TYPE=ORTHO
 4.14E-5   , -5.20E-6   , 4.14E-5
**
**********
**********


***  Kevlar 49 : 2-D Fibrillated Fibre End Model = AXIAL & RADIAL variation   *


**********
*MATERIAL, NAME=PA
*DENSITY
  1.000000     ,
*ELASTIC,TYPE=ENGINEERING CONSTANTS
0.009    ,0.047    ,0.009    ,0.330    ,0.400    ,0.330    ,0.003    ,0.0005    ,
0.003
*EXPANSION,TYPE=ORTHO
4.14E-5   , -5.20E-6   , 4.14E-5
*MATERIAL, NAME=PB
*DENSITY
  1.000000     ,
*ELASTIC,TYPE=ENGINEERING CONSTANTS
0.010    ,0.056    ,0.010    ,0.330    ,0.400    ,0.330    ,0.003    ,0.0005    ,
0.003
*EXPANSION,TYPE=ORTHO
4.14E-5   , -5.20E-6   , 4.14E-5
*MATERIAL, NAME=PC
*DENSITY
  1.000000     ,
*ELASTIC,TYPE=ENGINEERING CONSTANTS
0.013    ,0.074    ,0.013    ,0.330    ,0.400    ,0.330    ,0.004    ,0.0005    ,
0.004
*EXPANSION,TYPE=ORTHO
4.14E-5   , -5.20E-6   , 4.14E-5
*MATERIAL, NAME=PD
*DENSITY
```

```
  1.000000    ,
*ELASTIC,TYPE=ENGINEERING CONSTANTS
0.017   ,0.094   ,0.017   ,0.330   ,0.400   ,0.330   ,0.005   ,0.0005   ,
0.005
*EXPANSION,TYPE=ORTHO
4.14E-5  , -5.20E-6  , 4.14E-5
*MATERIAL, NAME=PE
*DENSITY
  1.000000    ,
*ELASTIC,TYPE=ENGINEERING CONSTANTS
0.021   ,0.114   ,0.021   ,0.330   ,0.400   ,0.330   ,0.007   ,0.0005   ,
0.007
*EXPANSION,TYPE=ORTHO
4.14E-5  , -5.20E-6  , 4.14E-5
*MATERIAL, NAME=QA
*DENSITY
  1.000000    ,
*ELASTIC,TYPE=ENGINEERING CONSTANTS
0.006   ,0.030   ,0.006   ,0.330   ,0.400   ,0.330   ,0.002   ,0.0007   ,
0.002
*EXPANSION,TYPE=ORTHO
4.14E-5  , -5.20E-6  , 4.14E-5
*MATERIAL, NAME=QB
*DENSITY
  1.000000    ,
*ELASTIC,TYPE=ENGINEERING CONSTANTS
0.007   ,0.036   ,0.007   ,0.330   ,0.400   ,0.330   ,0.002   ,0.0007   ,
0.002
*EXPANSION,TYPE=ORTHO
4.14E-5  , -5.20E-6  , 4.14E-5
*MATERIAL, NAME=QC
*DENSITY
  1.000000    ,
*ELASTIC,TYPE=ENGINEERING CONSTANTS
0.009   ,0.047   ,0.009   ,0.330   ,0.400   ,0.330   ,0.003   ,0.0007   ,
0.003
*EXPANSION,TYPE=ORTHO
4.14E-5  , -5.20E-6  , 4.14E-5
*MATERIAL, NAME=QD
*DENSITY
  1.000000    ,
*ELASTIC,TYPE=ENGINEERING CONSTANTS
0.012   ,0.060   ,0.012   ,0.330   ,0.400   ,0.330   ,0.004   ,0.0007   ,
0.004
*EXPANSION,TYPE=ORTHO
4.14E-5  , -5.20E-6  , 4.14E-5
*MATERIAL, NAME=QE
*DENSITY
  1.000000    ,
*ELASTIC,TYPE=ENGINEERING CONSTANTS
0.014   ,0.073   ,0.014   ,0.330   ,0.400   ,0.330   ,0.005   ,0.0007   ,
0.005
*EXPANSION,TYPE=ORTHO
4.14E-5  , -5.20E-6  , 4.14E-5
*MATERIAL, NAME=RA
*DENSITY
  1.000000    ,
*ELASTIC,TYPE=ENGINEERING CONSTANTS
0.005   ,0.023   ,0.005   ,0.330   ,0.400   ,0.330   ,0.0017   ,0.0007   ,
0.0017
*EXPANSION,TYPE=ORTHO
4.14E-5  , -5.20E-6  , 4.14E-5
*MATERIAL, NAME=RB
*DENSITY
  1.000000    ,
*ELASTIC,TYPE=ENGINEERING CONSTANTS
0.006   ,0.028   ,0.006   ,0.330   ,0.400   ,0.330   ,0.002   ,0.0007   ,
0.002
*EXPANSION,TYPE=ORTHO
4.14E-5  , -5.20E-6  , 4.14E-5
*MATERIAL, NAME=RC
*DENSITY
  1.000000    ,
```

```
*ELASTIC,TYPE=ENGINEERING CONSTANTS
0.008   ,0.036   ,0.008   ,0.330   ,0.400   ,0.330   ,0.003   ,0.0007   ,
0.003
*EXPANSION,TYPE=ORTHO
4.14E-5  , -5.20E-6  , 4.14E-5
*MATERIAL, NAME=RD
*DENSITY
  1.000000    ,
*ELASTIC,TYPE=ENGINEERING CONSTANTS
0.010   ,0.046   ,0.010   ,0.330   ,0.400   ,0.330   ,0.003   ,0.0007   ,
0.003
*EXPANSION,TYPE=ORTHO
4.14E-5  , -5.20E-6  , 4.14E-5
*MATERIAL, NAME=RE
*DENSITY
  1.000000    ,
*ELASTIC,TYPE=ENGINEERING CONSTANTS
0.012   ,0.056   ,0.012   ,0.330   ,0.400   ,0.330   ,0.004   ,0.0007   ,
0.004
*EXPANSION,TYPE=ORTHO
4.14E-5  , -5.20E-6  , 4.14E-5
*MATERIAL, NAME=SA
*DENSITY
  1.000000    ,
*ELASTIC,TYPE=ENGINEERING CONSTANTS
0.004   ,0.019   ,0.004   ,0.330   ,0.400   ,0.330   ,0.0015   ,0.0008   ,
0.0015
*EXPANSION,TYPE=ORTHO
4.14E-5  , -5.20E-6  , 4.14E-5
*MATERIAL, NAME=SB
*DENSITY
  1.000000    ,
*ELASTIC,TYPE=ENGINEERING CONSTANTS
0.005   ,0.023   ,0.005   ,0.330   ,0.400   ,0.330   ,0.0018   ,0.0008   ,
0.0018
*EXPANSION,TYPE=ORTHO
4.14E-5  , -5.20E-6  , 4.14E-5
*MATERIAL, NAME=SC
*DENSITY
  1.000000    ,
*ELASTIC,TYPE=ENGINEERING CONSTANTS
0.007   ,0.030   ,0.007   ,0.330   ,0.400   ,0.330   ,0.002   ,0.0008   ,
0.002
*EXPANSION,TYPE=ORTHO
4.14E-5  , -5.20E-6  , 4.14E-5
*MATERIAL, NAME=SD
*DENSITY
  1.000000    ,
*ELASTIC,TYPE=ENGINEERING CONSTANTS
0.009   ,0.038   ,0.009   ,0.330   ,0.400   ,0.330   ,0.003   ,0.0008   ,
0.003
*EXPANSION,TYPE=ORTHO
4.14E-5  , -5.20E-6  , 4.14E-5
*MATERIAL, NAME=SE
*DENSITY
  1.000000    ,
*ELASTIC,TYPE=ENGINEERING CONSTANTS
0.010   ,0.047   ,0.010   ,0.330   ,0.400   ,0.330   ,0.003   ,0.0008   ,
0.003
*EXPANSION,TYPE=ORTHO
 4.14E-5  , -5.20E-6  , 4.14E-5
**
**********
**********
```

APPENDIX E Pressure Dependent Yield

In plasticity theory, the von Mises cylinder is commonly used to represent the yield surface in three-dimensional principal stress space as shown in Fig. E.1 [65]. The cylinder is oriented with its axis equally inclined to the principal stress axes, coinciding with the hydrostatic line, and has radius $\sqrt{2}.G^{yield}$. If the stress state within the body falls within the yield surface, then linear-elastic behaviour will prevail. However, when the stress state falls on the yield surface, the onset of plasticity takes place. One of the basic postulates of classical plasticity theory is that yielding is independent of the dilatational stress component and thus a function of only the deviatoric stress [45]. This results in the von Mises yield surface cylinder having its axis coincident with the hydrostatic line, where, irrespective of the value of the dilatational stress, the yield stress will be constant.

Polymer matrices (as well as granular materials) exhibit pressure dependent yield where the yield stress is a linear function of the dilatational stress. Thus the yield surface, attributed to Drucker and Prager [64], is conical and is also orientated with its axis coincident with the hydrostatic line, Fig. E.1. The cone angle, ψ, is known as the pressure dependent yield angle (or friction angle for granular materials), since it defines the magnitude of the dependency of the yield stress on the dilatational stress component. Hence the larger the dilatational stress, the larger will be the corresponding yield stress.

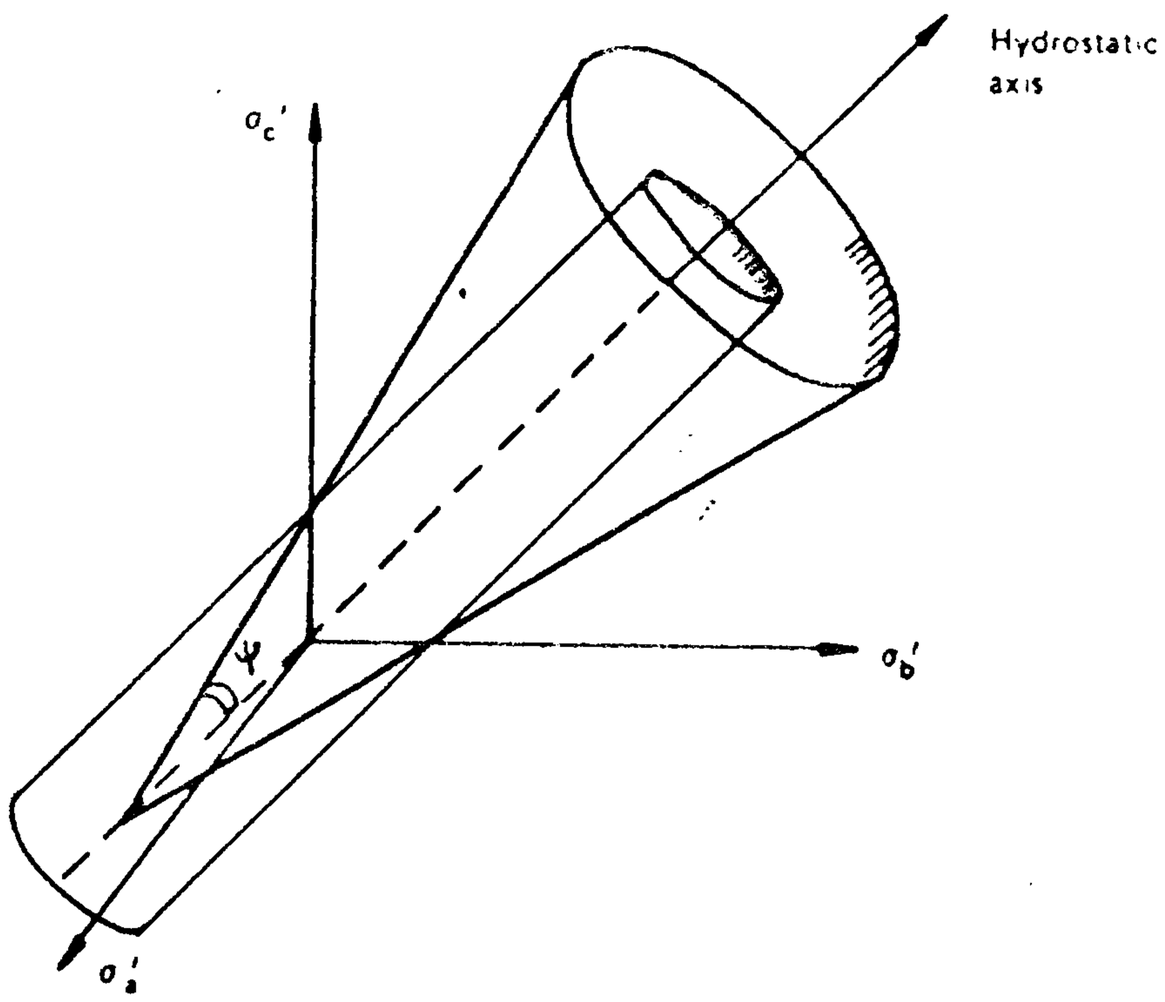

Fig. E.1 von Mises and Drucker-Prager yield surfaces

References

1. Hull, D. & Clyne, T.W. (1996), An Introduction to Composite Materials, *Cambridge University Press*.
2. Theocaris, P.S. (1979), The Effect of the Boundary Interphase on the Thermomechanical Behaviour of Composites Reinforced with Short Fibres, *J. Fibre Sci. and Tech.* **12**, 421.
3. Nath, R.B., Fenner, D.N., & Galiotis, C. (1996), Finite Element modelling of Interfacial Failure in Model Carbon fibre-epoxy Composites, *J. Mat. Sci.*, **31**, 2879.
4. Nath, R.B., Fenner, D.N., & Galiotis, C. (1996), Elasto-plastic Finite Element Modelling of Interfacial Failure in Model Kevlar 49 Fibre-epoxy Composites, *J. Composites,* **27A**, 821.
5. Nath, R.B., Fenner, D.N., & Galiotis, C. (1995), Finite Element Modelling of Interfacial Failure in Carbon Fibre-Epoxy Composites, *3rd International Conference on Deformation and Fracture of Composites,* The Institute of Materials, London, 606.
6. Nath, R.B., Fenner, D.N., & Galiotis, C. (1996), Progression of Interfacial Failure in Kevlar-49 & Carbon Fibre Composites: Elasto-Plastic Finite Element Analysis, *Seventh European Conference on Composite Materials,* The Institute of Materials, London, **I**, 27.
7. Nath, R.B., Fenner, D.N., & Galiotis, C. (1998), The Progressional Approach to Interfacial Failure in Composites: Interface Cracks, *in press*.
8. Jahankhani, H. & Galiotis, C. (1991), Interfacial Shear Stress Distribution in Model Composites, Part 1: A Kevlar 49 Fibre in an Epoxy Matrix, *J. Comp. Mat.*, **25**, 609.
9. Guild, F.J., Vlattas, C. & Galiotis, C. (1994), Modelling of Stress Transfer in Fibre Composites, *J. Comp. Sci. & Tech.*, **50**, 319.
10. Paipetis, A. & Galiotis, C. (1996), Effect of Fibre Sizing on the Stress Transfer Efficiency in Carbon/Epoxy Model Composites, *J. Composites*, **27A**, 755.

11. Sato, N., Kurauchi, T., Sato, S. & Kamigaito, O (1988), Reinforcing Mechanism by Small Diameter Fibre in Short Fibre Composite, *J. Comp. Mat.*, **22**, 850.
12. Busschen, A.ten & Selvadurai, A.P.S. (1995), Mechanics of Segmentation of an Embedded Fibre, Part I: Experimental Investigations, *J. Applied Mechanics*, **62**, 87.
13. Melanitis, N., Galiotis, C., Tetlow, P.L. & Davies, C.K.L. (1992), Interfacial Shear Stress Distribution in Model Composites, Part 2: Fragmentation Studies on Carbon Fibre/Epoxy Systems, *J. Comp. Mat.*, **26**, 574.
14. Galiotis, C. (1993), A Study of Mechanisms of Stress Transfer in Continuous- and Discontinuous-Fibre Model Composites by Laser Raman Spectroscopy, *J. Comp. Sci. Tech.*, **48**, 15.
15. Melanitis, N. & Galiotis, C. (1993), Interfacial Micromechanics in Model Composites using Laser Raman Spectroscopy, *Proc. Royal Society London*, Series A, **40**, 79.
16. Cox, H.L. (1952) The Elasticity and Strength of Paper and Other Fibrous Materials, *British Journal of Applied Physics*, **3**, 72.
17. Dow, N.F. (1963) Study of Stresses Near a Discontinuity in a Filament Reinforced Composite Metal, *Rep. R63SD61, Space Sciences Lab., General Electric*.
18. Whitney, W. & Drzal, L.T. (1987), Axisymmetric Stress Distribution Around an Isolated Fibre Fragment, *Toughened Composites, ASTM STP 937*, 179.
19. McCartney, L.N. (1989), New Theoretical Model of Stress Transfer Between Fibre and Matrix in a Uni-Axially Fibre Reinforced Composite, *Proc. Royal Society London*, Series A, **425**, 215.
20. Netravali, A.N., Henstenburg, R.B., Phoenix, S.L. & Swhwartz, P. (1989), Interfacial Shear Stength Studies using the Single Filament Composite Test (Part I), Polymer Composites, **10**, 226.
21. Piggott, M.R. (1980), Load Bearing Fibre Composites, Oxford: Pergamon Press.
22. Harlin, G. & Willis, J.R. (1988), The Influence of Crack Size on the Ductile-Brittle Transition, *Proc. Royal Society London*, Series A, **415**, 197.
23. Broek, D. (1989), The Practical Use of Fracture mechanics, Kluwer Academic Publishers.

24. Cook, R.D. (1995), Finite Element Modelling for Stress Analysis, *John Wiley and Sons Inc.,* London.
25. Termonia, Y. (1987), Theoretical Study of Stress Transfer in Single Fibre Composites, *J. Mat. Sci.,* **22**, 504.
26. Berthelot, J-M., Cupcic, A. & Brou, K.A. (1993), Stress Distribution and Effective Young's Modulus of Unidirectional Discontinuous Fibre Composites, *J. Comp. Mat.,* **27**, 1391.
27. Fan, C.F. & Hsu, S.L. (1992), A Study of Stress Distribution in Model Composites by using Finite Element Analysis. I: End Effects, *J. Polymer Science, B: Polymer Physics,* **30**, 603.
28. Liou, W.J. (1997), Stress Distributions of Short Fibre Composite Materials, *Computers and Structures*, **62**, 999.
29. Busschen, A.ten & Selvadurai, A.P.S. (1995), Mechanics of Segmentation of an Embedded Fibre, Part II: Computational Modelling and Comparisons, *J. Applied Mechanics*, **62**, 98.
30. Brockmuller, K.M., Bernhardi, O. & Maier, M (1995), Determination of Fracture Stress and Strain of Highly Oriented Short Fibre-Reinforced Composites Using a Fracture Mechanics-Based Iterative Finite Element Method, *J. Mat. Sci.*, **30**, 481.
31. Levy, A. & Papazian, J.M. (1991), Elastoplastic Finite Element Analysis of Short-Fibre-Reinforced SiC/Al Composites: Effects of Thermal Treatment, *Acta Metall. Mater.*, **39**, 2255.
32. Shi, N., Wilner, B. & Arsenault, R.J. (1992), An FEM Study of the Plastic Deformation Process of Whisker Reinforced SiC/Al Composites, *Acta Metall. Mater.*, **40**, 2841.
33. Tripathi, D., Chen, F. & Jones, F.R. (1996), A Comprehensive Model To Predict the Stress Fields in a Single Fibre Composite, *J. Comp. Mat.*, **30**, 1514.
34. Ho, H. & Drzal, L.T. (1995), Non-Linear Numerical Study of The Single-Fibre Fragmentation Test. Part II: A Parametric Study, *J. Comp. Eng.*, **5**, 1245.
35. King, T.R., Blackketter, D.M., Walrath, D.E. & Adams, D.F. (1992), Micromechanics of the Shear Strength of Carbon Fibre/Epoxy Matrix Composites: The Influence of the Matrix and Interface Strengths, *J. Comp. Mat.*, **26**, 558.

36. Wang, S.J., Baptiste, D., Bompard, Ph. & François, D. (1991) Microscopic Failure Mechanisms of an Unidirectional Glass Fibre Composite, *J. Fatigue Fract. Engng. Struct.*, **4**, 391.
37. Nedele, M.R. & Wisnom, M.R. (1994), Three-dimensional Finite Element Analysis of the Stress Concentration at a Single Fibre Break, *J. Comp. Sci. & Tech.*, **51**, 517.
38. Sastry, A.M. & Phoenix, S.L. (1994), Shielding and Magnification of Loads in Elastic, Unidirectional Composites, *SAMPE Journal*, **30**, 61.
39. Hedgepeth, J.M. & van Dyke, P. (1967), Local Stress Concentration in Imperfect Filamentary Composite Materials, *J. Comp. Mat.*, **1**, 294.
40. Xu, S. & Weitsman, Y. (1996), Three-dimensional Effects in Fibre-reinforced Composites Under Compression, *J. Comp. Sci. & Tech.*, **56**, 1113.
41. Plazek, D. & In-Chul, C. (1991), The Evolution of The Viscoelastic Retardation Spectrum During the Development of an Epoxy Resin Network, *J. Polymers Sci., B: Polymer Physics,* **29**, 17.
42. ABAQUS 5.4 (1996), Hibbitt, Karlsson & Sorensen, USA.
43. Hutchings, I.M. (1992), Tribology, *Edward Arnold*, UK.
44. McCrum, N.G., Buckley, C.P. & Bucknall, C.B. (1988), Principles of Polymer Engineering, *Oxford University Press*, UK.
45. Shames, I.H. & Cozzarelli, F.A. (1992), Elastic and Inelastic Stress Analysis, *Prentice-Hall International*, USA.
46. Peijs, T., Schellens, H.J. & Govaert, L.E. (1996), A Micromechanical Approach to Time Dependent Failure of Composite Materials, Progress in Durability Analysis of Composite Systems, *Balkema*.
47. Rice, J.R. (1968), A Path Independent Integral and the Approximate Analysis of Strain Concentration by Notches and Cracks, *J. Appl. Mech.*, 379.
48. Barsoum, R.S. (1976) On The use of Isoparametric Finite Elements in Linear Fracture Mechanics, *Int. J. Num. Meth. Eng.*, **10**, 25.
49. Barsoum, R.S. (1977) Triangular Quarter-point Element as Elastic and Perfectly-Plastic Crack Tip Elements, *Int. J. Num. Meth. Eng.*, **11**, 85.
50. Irwin, G.R., (1957), Analysis of Stresses and Strains Near the End of a Crack Traversing a Plate, *J. Appl. Mech.*, **24**, 361.

51. Rice, J.R. & Rosengren, G.F. (1968), Plain Strain Deformation Near a Crack Tip in a Power-law Hardening Material, *J. Mech. Phys. Solids*, **16**, 1.
52. O'Dowd, N.P., Shih, C.F. & Stout, M.G. (1992), Test Geometries for Measuring Interfacial Fracture Toughness, *Int. J. Solids Structures*, **29**, 571.
53. O'Dowd, N.P., Stout, M.G. & Shih, C.F. (1992), Fracture Toughness of Alumina-niobium Interfaces: Experiments and Analyses, *Philosophical Mag. A*, **66**, 1037.
54. Theocaris, P.S., Papanicolaou, G.C. & Kontou, E.A. (1982), The Effect of Filler-volume Fraction and Strain Rate on the Tensile Properties of Iron-epoxy Particulate Composites, *J. Reinf. Plas. and Comp.* **1**, 206.
55. Weibull, W. (1951), A Statistical Distribution Function of Wide Applicability, *J. Appl. Mech.*, **18**, 293.
56. Chohan, V. & Galiotis, C. (1996), Interfacial Measurements and Fracture Characteristics of 2D Microcomposites Using Remote Laser Raman Microscopy, *J. Comp.*, **27A**, 881.
57. Van Den Heuvel, P.W.J, Van Der Bruggen, Y.J.W. & Peijs, T. (1996), Failure Phenomena in Multi-fibre Model Composites: Part 1. An Experimental Investigation into the Influence of Fibre Spacing and Fibre-matrix Adhesion, *J. Comp.*, **27A**, 855.
58. Lowden, R.A. (1993), Fibre Coatings and the Mechanical Properties of a Continuous Fibre-reinforced SiC Matrix Composite, Designing Ceramic Interfaces II, *Comm. of Europe. Comm.*, Lux., 157.
59. McCartney, L.N. (1992), Theory of Stress Transfer in a 0/90/0° Cross-ply Laminate Containing a Parallel Array of Transverse Cracks, *J. Mech. Phys. Sol.*, **40**, 27.
60. Halpin, J.C. & Tsai, S.W. (1967), Environmental Factors in Composite Design, *Air Force Materials Laboratory Technical Report*, AFML-TR-67-423.
61. Chou, T.W. & Kelly, A. (1980), Mechanical Properties of Composites, *Ann. Rev. Mater. Sci.*, **10**, 229.
62. Filonenko-Borodich, M. (1965), Theory of Elasticity, *Dover Publications*, USA.
63. Timoshenko, S.P. & Goodier, J.N. (1970), Theory of Elasticity, *McGraw-Hill.*
64. Britto, A.M. & Gunn, M.J. (1987), Critical State Soil Mechanics Via Finite Elements, *Ellis Horwood.*

BIBL. LONDIN. UNIV.